Generation of intermediate-depth earthquakes and the fate of subduction fluids

Insights from mantle wedge seismicity and case studies in the Western Hellenic subduction zone

Felix Halpaap

Thesis for the degree of Philosophiae Doctor (PhD)
University of Bergen, Norway
2019

UNIVERSITY OF BERGEN

2019 Generation of intermediate-depth earthquakes and the fate of subduction fluids • Felix Halpaap

Generation of intermediate-depth earthquakes and the fate of subduction fluids

Insights from mantle wedge seismicity and case studies in the Western Hellenic subduction zone

Felix Halpaap

Thesis for the degree of Philosophiae Doctor (PhD)
at the University of Bergen

Date of defense: 07.06.2019

Year: 2019
Title: Generation of intermediate-depth earthquakes and the fate of subduction fluids

Name: Felix Halpaap
Print: Skipnes Kommunikasjon / University of Bergen

Preface

This dissertation for the degree of philosophiae doctor (PhD) has been submitted to the Department of Earth Science at the University of Bergen. The research in this thesis was part of the project "Subduction zone Water and Metamorphism: a Modeling and Imaging Study" (SWaMMIS, reference number 231354), which was supported by the Research Council of Norway (RCN).

Research was conducted mainly in the Geodynamics Group at the Department of Earth Science, University of Bergen, under supervision of Prof. Stéphane Rondenay, and co-supervision by Prof. Lars Ottemöller and Prof. Henk Keers. The candidate enrolled at the university in October 2014, was admitted to the PhD program in April 2015 and submitted the thesis in February 2019.

Between September and December 2015, Prof. Qinya Liu hosted the candidate during a research stay funded through an RCN personal overseas research grant at the Physics Department at the University of Toronto. In October 2016, Prof. Saskia Goes hosted the candidate at the Department of Earth Science and Engineering at Imperial College London.

As a member of the Norwegian Research School for Dynamics and Evolution of Earth and Planets (DEEP), the candidate received additional funding for participation in external courses and the annual DEEP conference. The Open Access Publication fund at the University of Bergen covered 50 % of the article publication charge (APC) of paper I (application ref. 353), and 100 % of the APC for paper II (ref. 645).

Acknowledgements

Time has come to wrap up the PhD and reflect on these exciting years. I am thankful for the opportunities that I have been offered: My first stay in Bergen in the fall of 2013 for a research internship at UiB, which would not have been possible without the contact between my master thesis advisor, Florian Bleibinhaus, to the person that would later be my principal PhD advisor: Stéphane Rondenay. When first coming to Bergen, I experienced the seismology group at UiB as incredibly positive, which made it an easy choice to try to come back for a PhD in 2014. I could not be happier that the last years worked out the way they did. Thank you, Stéphane, for being unmatchable motivational and positive in every meeting, for coming up with exciting scientific questions, for your time to share knowledge and always give constructive feedback on research and writing, and for the freedom that you have given me to explore science in the last years. Thank you also to Lars Ottemöller, co-advisor in my PhD, who was a great match to complement my advisory team with his expertise in local earthquake processing, including development and maintenance of the Seisan analysis software. Finding an open door to both Stéphane's and Lars's office at any time, and getting just the right help to solve the challenges that came up was incredibly helpful.

Regarding the seismology group, I would also like to thank Henk Keers (2nd co-advisor) for his advice especially on tomography, Øyvind Nattvik for IT support, Mareile Anderson and Linda Emdal for administrative support, and Kathrin Spieker, Jan Michalek, Florian Millet, Marte Strømme, Hasbi Ash Shiddiqi, Thomas Theunissen, Andrea Demuth and Berit Marie Storheim for sharing their knowledge in seismology and processing, and for the field work we conducted together on the Lofoten islands, at mount Mannen and in Western Norway. With Jan and Hasbi, I have had great office mates whom I could ask for advice in seismology, with whom I could chat, and who contributed to a great working environment.

The findings that I present in this thesis would not have not been reached without the help of a few more people whom I would like to thank: Saskia Goes for letting me visit her group in London, for her interest in the mantle wedge seismicity, and for

enabling the collaboration with her group, including Alexander Perrin, to produce the thermal-petrologic models that became a critical piece of evidence in our paper.

Working on the PhD, learning and teaching would not have been as fun without the countless trips into the mountains, coffee breaks, and visits to the pubs in Bergen. For all these activities, I would like to thank a number of great friends for feeling at home in Bergen, for sharing lunch, dinner, and drinks, for being great mates in the field (especially in Norway and Brazil), and for scientific advice and discussions: Sebastian (especially for anything related to geodynamics, for making music together, and for mountain biking); Johannes (especially for his expertise in Western Norwegian geology), Kathrin (especially for guidance in the PhD and discussions in seismology), Björn (especially for skiing), Casey (especially for being a great flat mate and organizer for Friday beers), Gauti (especially for his expertise in palynology when needed, and Geosport), Florian (especially for discussions on seismology), Guillaume (especially for discussions on the Aegean and skiing), Hongliang (especially for discussions on fluid flow), Alistair (especially for realizing many skiing trips), and Sven (especially for Geosports).

I would like to thank my parents for their support all along the way. Finally, Ingvild, thank you for putting up with my varying schedule, motivation for chores, and moods during the PhD work – it would have been incomparable without you.

Abstract

The occurrence of intermediate depth earthquakes at 50-300 km depth in subduction zones is puzzling, because high temperatures and pressures at these depths do not allow standard brittle failure. Instead, two main candidate mechanisms have been proposed: dehydration embrittlement and localized thermal shear runaway. It is highly debated which of these two mechanisms is the dominant one, and how the two mechanisms may combine to explain the different styles of seismicity observed in the various parts of subduction systems. While dehydration embrittlement requires that hydrated minerals undergo a phase transition to provide a free fluid phase, shear runaway may occur under dry conditions but within restricted pressure-temperature conditions. These different premises should allow the mechanisms to be distinguishable based on the thermal-petrologic conditions under which earthquakes occur, as these conditions vary significantly between different parts of the subduction system. However, the resolution of seismic images and standard hypocenter solutions do not usually allow earthquakes to be robustly located in relation to the discontinuities outlining the different domains of the subduction system (e.g., subduction interface and slab Moho).

This thesis provides new insight into what generates intermediate depth earthquakes. The work is divided in three parts: (I) a traveltime tomography study, which recovers the outline of the subducting crust and the location of earthquakes in the Western Hellenic subduction zone, (II) a combined seismological-geodynamic investigation, which links intraslab earthquakes to the little-known phenomenon of mantle wedge seismicity, and (III) the development of a new method that helps constrain earthquake locations relative to subduction discontinuities.

Part I investigates the south-to-north transition from oceanic to continental subduction in the Western Hellenic subduction zone. The goal is to see how this transition affects fluid release and related seismicity along strike. Although the northern and southern trenches are offset, seismicity and tomographic images show a smooth transition between slab retreat and slab convergence from south to north. Relocated hypocenters outline a single-planed Wadati-Benioff Zone with significant along-strike

variability, including an abrupt termination toward the transition to continental subduction. Seismic anomalies point to fluid-related metamorphism in three parts of the system: eclogitization of the crust near 90 km depth, subarc melting of the mantle below the volcanic arc, and large-scale silica enrichment in the lower part of the overriding crust.

Part II examines the cause of mantle wedge seismicity clusters, and why the subducting crust updip of these clusters is aseismic. Newly detected and relocated earthquakes, focal mechanisms, and thermal-petrologic models reveal that earthquakes effectively track the flow of fluids from their slab source at >80 km depth to their sink at shallow (<40 km) depth. Between source and sink, the fluids flow updip under a sealed plate interface, facilitating intraslab earthquakes. In some locations, the seal breaks and fluids escape through vents into the mantle wedge, thereby reducing the fluid supply and seismicity updip in the slab. The vents themselves may represent nucleation sites for larger damaging earthquakes.

Part III develops a new seismic processing workflow to enhance and analyze secondary phases of local earthquakes. Secondary phases include seismic wave reflections and conversions that provide information on the earthquake location relative to the discontinuities. The workflow comprises rotation, alignment, bandpass- and polarization-filtering, optimized sorting and plotting of three-component seismograms in station gathers, followed by a comparison with theoretical arrival times of relevant phases. Each station gather exhibits on average two to three secondary arrivals, some of which independently confirm earthquake sources in the mantle wedge and on the plate interface.

Taken together, the three parts of the thesis shed new light into how a cold slab undergoes metamorphism and releases water with depth – two processes that cause melting below the arc, establish pathways for fluid-induced earthquakes in the system, and contribute to chemical enrichment of the lower crust and mantle wedge.

List of publications

Paper I

Felix Halpaap, Stéphane Rondenay, Lars Ottemöller, Seismicity, 2018. **Deformation and Metamorphism in the Western Hellenic Subduction Zone - New Constraints from Tomography**, *Journal of Geophysical Research: Solid Earth* **123**, 4. doi: http://dx.doi.org/10.1002/2017JB015154.

Paper II

Felix Halpaap, Stéphane Rondenay, Alexander Perrin, Saskia Goes, Lars Ottemöller, Håkon Austrheim, Robert Shaw, Thomas Eeken, 2019. **Earthquakes track subduction fluids from slab source to mantle wedge sink**, *Science Advances*, in press.

Paper III

Felix Halpaap, Stéphane Rondenay, Qinya Liu, Florian Millet, Lars Ottemöller. **Toward waveform-based characterization of slab earthquakes**, *to be submitted to Journal of Geophysical Research: Solid Earth*.

Contents

1 Introduction

The physics of shallow earthquakes, which occur due to brittle shear failure of a rock or stick-slip friction on preexisting faults, are relatively well understood (*Green II and Houston*, 1995). These shallow earthquakes mostly occur down to a depth of 30 km within areas with a standard geothermal gradient, and somewhat deeper within subduction zones. However, earthquakes can be recorded down to a depth of approximately 650 km to 700 km in subduction zone environments (with 680 km regarded as the reliable maximum, e.g., *Frohlich*, 2006; *Stark and Frohlich*, 1985; *Ye et al.*, 2016), where pressurized fluids can have an effect on the failing mechanisms.

1.1 Intermediate-depth earthquakes

About one quarter of all earthquakes worldwide occur at intermediate depth (50 km to 300 km). With very few exceptions (e.g., at Gibraltar, and Vrancea in Romania), these intermediate-depth earthquakes appear in active subduction zone environments where they can cause severe damage (*Frohlich*, 2006). An example is the M=7.8 Chillán earthquake in Chile in 1939, which occurred at 80 km to 100 km depth and caused approximately 28 000 fatalities (*Beck et al.*, 1998).

From experimental and modeling studies reviewed by *Lay* (1994) and *Poli and Schmidt* (2002), it is known that water contained inside the subducting plate plays an important role for mineral reactions in subduction zones and that most of it is released before the lithospheric material reaches 300 km depth. A bimodal distribution of the global occurrence of earthquakes versus depth suggests that different mechanisms apply to intermediate-depth earthquakes (50 km to 300 km) and deep-focus earthquakes ($>$ 300 km depth; e.g., *Green II and Houston*, 1995; *Jung et al.*, 2004). It can safely be said that water modulates, if not even triggers seismic events in subduction zones, but there is still no consensus as to what is the main mechanism for intraslab intermediate-depth seismicity.

1.1.1 Dehydration reactions

Oceanic crust contains up to 5–6 wt% H_2O in different forms (*Schmidt and Poli*, 1998). First, it is present in the pore spaces in sediments, from where it is mostly squeezed out after burial at up to 15 km depth (*Hacker et al.*, 2003), while residual fluid trapped in pores may persist to larger depths (*Bostock*, 2013). Second, it is contained as part of the crystal structure in several minerals, of which the most important in mafic rocks (such as oceanic crust) are lawsonite, zoisite, chloritoid, and talc, as well as chlorite (dehydration ca. at 800 °C), and serpentine (dehydration at ca. 600 °C) in peridotites (see Fig. 1.1, *Poli and Schmidt*, 2002). Upon subduction, the slab is dehydrated in both gradual and stepwise manners due to the different mineral reactions that occur when each of the minerals mentioned above reach phase transition conditions. These dehydration reactions occur at different depths depending on the thermal properties of a given slab, with most of the dehydration taking place between 70 km to 300 km (*Schmidt and Poli*, 1998).

Two important parameters which strongly influence seismic activity and its depth inside subduction zones are the velocity of the subducting plate and its age. The faster and older (hence also colder and thicker) the subducting crust is, the deeper seismic activity stretches into the slab due to delayed mineral reactions. An example of fast subduction of old crust is Tonga, where the 109 Ma old Pacific plate subducts below the Australian plate at 165 mm/yr (*Syracuse et al.*, 2010). On the opposite end of the spectrum is the Cascadia subduction zone, where the young (7 Ma) Juan de Fuca plate dives below North America at 35–45 mm/yr (*DeMets et al.*, 1994), which causes the slab to heat up faster. In the Tonga-Kermadec system, abundant intraslab seismicity can be recorded down to depths greater than 600 km (*Frohlich*, 2006) while very few intraslab earthquakes below ca. 70 km are present in the Cascadia subduction zone (e.g., *McCrory et al.*, 2012).

1.1.2 Candidate mechanisms

Two main candidate mechanism for intermediate-depth seismicity are currently discussed in the literature, and further mechanisms have been proposed. These two mechanisms are **dehydration embrittlement** (e.g., *Jung et al.*, 2004; *Kirby et al.*, 1996) and **self-localizing thermal runaway** (e.g., *John et al.*, 2009; *Kaus and Podladchikov*, 2006; *Kelemen and Hirth*, 2007). Further mechanisms include transformational faulting and anticrack formation (e.g., *Green II and Houston*, 1995; *Kirby et al.*, 1996).

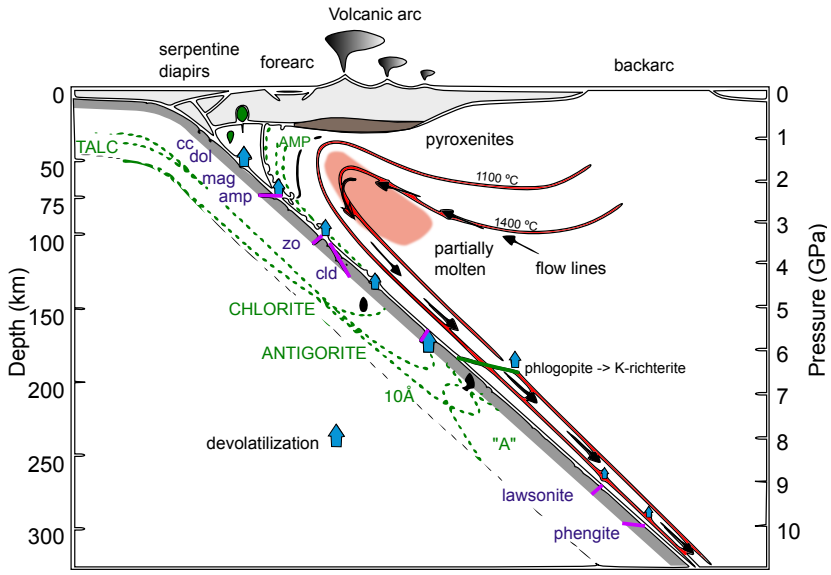

Figure 1.1: Schematic cross section of a subduction zone with important geothermal isolines and phase transitions, showing dehydration reactions. Mineral abbreviations: A: phase A; amp: amphibolite, cc: calcite; cld: chloritoid; dol: dolomite; mag: magnesite; zo: zoisite; 10Å: 10 Å-phase. Labels in capital letters mark phase stability boundaries in peridotite. Modified, with permission from *Poli and Schmidt* (2002).

Evidence for either of the main mechanisms is contributed by a wide range of research covering about 15 orders of magnitude in scale, including laboratory experiments in geochemistry, petrology, and rock physics; mapping and field studies in petrology and (structural) geology; imaging and monitoring studies in geophysics; and numerical modeling in geodynamics. The works of *Frohlich* (2006); *Green II and Houston* (1995) provide thorough overviews of such research, while *Hasegawa and Nakajima* (2017) recently reviewed the observational seismic evidence on intermediate-depth seismicity.

Dehydration embrittlement is a process in which the volume change connected with the dehydration of a water-bearing mineral under differential stress results in the formation of a fault in which ultrafine grains of the reaction product are concentrated. The process is observed at a wide range of pressures (P), temperatures (T) and at both negative and positive volume changes in laboratory experiments (*Jung et al.*, 2004). These experiments suggest that the mechanism is viable to cause earthquakes down to 400 km depth. Limitations regarding the suitability of this processes to explain the earthquakes in the lower layer of a double seismic zone inside slabs have been discussed, as this would require significant amounts of water down to 40 km depth inside

the subducting lithosphere (e.g., *Faccenda et al.*, 2009; *Jung et al.*, 2004). While the term "dehydration embrittlement" in its original sense refers only to seismic failure in vicinity to the dehydration reaction (as defined above), it is now often used in a wider sense that refers to all fluid-modulated embrittlement of rock related to dehydration fluids. In this wider sense, dehydration fluid may have migrated over any distance within the slab before causing seismic failure (c.f. *Hasegawa and Nakajima*, 2017). Within the subducting crust, seismic low-velocity zones point to the presence of considerable amounts of water, both in mineral-bound form (e.g., *Rondenay et al.*, 2008), and as free-fluid phase in ultra-low velocity zones (e.g., *Shiina et al.*, 2017; *Song et al.*, 2009).

John et al. (2009) describe the process of self-localizing thermal runaway, or shear-localization, which allows failure of rock in the absence of a free fluid phase at depths greater than 70 km by thermal runaway. In this process, ductile deformation causes heating of a shear zone, which is weakened by the increased temperature and thus leads to further release of differential stress. The feedback between heating and deformation can lead to local melting of the rock, which cools into a glassy material referred to as pseudotachylite. In some locations where rocks have been educted from large depths, pseudotachylites are unique evidence of paleo-earthquakes at intermediate depth. Locations where these type of rocks can be found in outcrops include Holsnøy (Western Norway, *Austrheim and Boundy*, 1994), Cape Corse (Corsica, French Mediterranean, *Andersen et al.*, 2014; *Austrheim and Andersen*, 2004), and Monviso (Italian Alps, *Angiboust et al.*, 2011). These field observations have guided research on self-localizing thermal runaway, which *Kelemen and Hirth* (2007) and *John et al.* (2009) have constrained in numerical models. There is also seismic evidence pointing to localized thermal runaway, as for example reported by *Prieto et al.* (2013), who found that high stress drops and low radiation efficiency for intermediate-depth earthquakes signify large energy dissipation due to shear heating. The two main intermediate-depth faulting mechanisms described above are possibly related to, and further constrained by, anticrack formation (*Green II and Houston*, 1995) and localized eclogitization of dry metastable rocks (*Austrheim and Boundy*, 1994).

Defining the exact location in the slab where earthquake-promoting processes occur is a challenge. These processes include localized dehydration and mineral transformations (especially eclogitization), as well as the migration of fluids. The difficulty stems from the wide range of pressures and temperatures over which the mineral transformation reactions occur, and their critical dependence on the supply and composition of fluids. In low temperature slabs, eclogitization can take place down to ca. 70–120 km

(2.4-3.5 GPa), while in high temperature slabs such as Cascadia, all eclogitization may be completed at 40 km depth. However, field outcrops such as those found on Holsnøy (*Kühn et al.*, 2000) show that even at ca. 60 km burial depth and 700 °C, eclogitization affects the rock volume in a highly heterogeneous fashion, with the eclogite/rock-ratio ranging from 10–50 %. On Holsnøy, blocks of lower grade granulite of several tens of meters in size are distributed in a matrix of eclogite, even though *P-T* conditions reached at depth were beyond those required for eclogitization. A related hypothesis is that earthquakes may also influence or enhance metamorphism by fracturing the rock and thus increasing the surface for mineral reactions, as suggested by *Austrheim and Boundy* (1994); *Austrheim et al.* (2017); and *Jamtveit et al.* (2018). These authors report that shear zones, including pseudotachylites, are mostly found in eclogite zones, which might indicate a possible feedback between deformation, temperature and metamorphism.

The occurrence of intermediate-depth earthquakes varies considerably between different subduction zones and between the various parts of subduction systems. To understand the earthquake's mechanism, we need to gain a better understanding of the premises and processes that promote their generation, including subduction properties such as slab stress field, slab structure, age, mineralogical composition, subduction velocity, type (oceanic/continental) of the subducting crust, and fluid content (e.g., *Hacker et al.*, 2003). As for all shallow earthquakes, we expect the stress field to be the driving force behind any deformation. But while all active subduction zones exhibit a stress field that forces deformation, only a subset of these subduction zones feature widespread seismicity (e.g., Izu-Bonin) while others are largely aseismic at depth (e.g., a large part of Cascadia). Even within the seismically active subduction zones, the occurrence of earthquakes is limited to certain parts of the system. These seismically active regions can be limited along subduction strike (e.g., in the subducting Juan de Fuca plate in Cascadia, *Wells et al.*, 2002), subduction depth (e.g., Cascadia: 60–80 km, *McCrory et al.*, 2012, New Zealand: 250 km, *Eberhart-Phillips et al.*, 2013) or depth below the subduction interface, where two layers of earthquakes often mark double seismic zones (*Brudzinski et al.*, 2007; *Wei et al.*, 2017; *Yamasaki*, 2003). Together, the evidence suggests that seismic and aseismic areas are likely defined by a combination of parameters, including, but not limited to, the thermal-petrologic conditions (*Abers et al.*, 2013; *Wei et al.*, 2017), stress field, and pore fluid distribution. To better understand these parameters, it should be possible to match the boundaries between seismic and aseismic areas with measurable changes in the seismic parameters (e.g., seismic velocities, density, anisotropy etc.). Resolving and deciphering these changes and how

they relate to seismic failure can help us better constrain the earthquake mechanisms by placing lower and upper bounds on key parameters including temperature, pressure, composition, pore pressure, and fluid content.

1.1.3 Imaging metamorphism and intermediate-depth earthquakes in subduction zones

Geophysical methods, in particular seismology, have improved our understanding of seismicity in various subduction zones. To pinpoint the exact location of hypocenters in relation to large-scale discontinuities and/or local changes in seismic parameters, geophysics relies on advances in high-resolution imaging, earthquake source monitoring, and improved instrumentation. Images of seismic properties can be obtained with a wide variety of methods that excel at resolving different features. Listed here from larger to smaller scale, seismic imaging methods include: global-scale (waveform)-tomography, teleseismic tomography, surface wave tomography, traditional receiver function (RF) studies, local earthquake tomography, RF migration studies, large-scale active-source reflection surveys. The limitations of each method can be overcome by combining the results of several methods, or inverting jointly for some parameters such as the seismic velocities or density. The following overview on imaging studies focuses on seismological methods, while there are some other geophysical imaging methods that have been successful in imaging the relevant depth range of 30–200 km. These include magnetotelluric surveys that recover electric resistivity (e.g., *McGary et al.*, 2014; *Wannamaker et al.*, 2014), and to a limited degree gravity surveys that recover density (e.g., *Lücke and Arroyo*, 2015).

In the last two decades, the number of studies that have imaged subduction systems in targeted high-resolution studies has greatly increased. Previously, assumptions on the slab shape at depths between 40 km to 200 km were mostly based on hypocenter locations outlining the Wadati-Benioff Zone. Due to the lack of high-resolution images, the earthquake's relation to the subducting crust could often not be satisfyingly established. With the advent of dense temporary broadband deployments and improved imaging methods, we now know that intermediate-depth seismicity occurs within the subducting crust and mantle, and that the distribution of earthquakes changes along strike and subduction depth of slabs. Subducting oceanic crust has an average thickness of about 6 km to 8 km - a scalelength that not every method can resolve.

Methods that have proven successful at imaging the subducting crust at depths

ranging 30–200 km are local earthquake tomography (e.g., *Nakajima et al.*, 2009; *Zhang et al.*, 2004), very large-scale reflection seismic surveys (*The Ancorp Working Group et al.*, 1999) and the migration of receiver functions based on the generalized Radon transform (GRT, *Bostock et al.*, 2001; *Rondenay et al.*, 2001; *Shragge et al.*, 2001). The receiver function method is better at imaging sharp boundaries than seismic tomography. It excels at 2-D imaging of the subducting crust, but to recover information about structural variations along-strike the subduction zone, other 3-D RF methods or tomography are needed. The 2-D GRT-RF method and local earthquake tomography have been used in a range of studies, each resulting in remarkable catalogs of comparable images. Images of the subducting crust based on 2-D RF migration are available for subduction zones including Alaska (*Rondenay et al.*, 2008, 2010), Cascadia (*Abers et al.*, 2009; *Nicholson et al.*, 2005; *Rondenay et al.*, 2001), Japan (*Kawakatsu and Watada*, 2007; *Kumar and Kawakatsu*, 2011), Costa Rica and Nicaragua (*MacKenzie et al.*, 2010), Mexico (*Kim et al.*, 2012), and the Hellenic Subduction zone in Greece (*Pearce et al.*, 2012; *Suckale et al.*, 2009). Tomographic images based on local seismicity, with only some of them showing a dipping low-velocity layer, have been obtained for instance in Alaska (*Eberhart-Phillips et al.*, 2006), Cascadia (*Ramachandran and Hyndman*, 2012; *Savard et al.*, 2018), Costa Rica (*Dinc et al.*, 2010), Japan (*Hayashida et al.*, 2012; *Hirose et al.*, 2008; *Nakajima et al.*, 2009; *Zhang et al.*, 2004), Lesser Antilles (*Paulatto et al.*, 2017), Nicaragua (*Syracuse et al.*, 2008), and New Zealand (*Eberhart-Phillips and Reyners*, 1999, 2009; *Eberhart-Phillips et al.*, 2013; *Reyners et al.*, 2006). Very large-scale reflection surveys like ANCORP are even superior in 2-D resolution of the subducting crust, but they are prohibitively more costly. For this reason, only *The Ancorp Working Group et al.* (1999) have imaged subducting crust down to about 100 km depth with this method, in Chile.

Several of these studies have found that intermediate-depth earthquakes in subduction zones do not only occur in the subducting crust, but also below, in the subducting mantle (e.g., *Abers et al.*, 2013; *The Ancorp Working Group et al.*, 1999). *Abers et al.* (2013) found that intermediate-depth earthquakes are limited to the subducting mantle in warmer, younger subduction zones such as Cascadia, but that the mantle probably needs to be hydrated. In old and thus comparably cold subducting slabs, earthquakes also occur throughout the subducting crust, but increasingly close to the subducting Moho with increasing depth. *Abers et al.* (2013) argue that owing to faster subduction rates with a quicker increase in pressure, cold slabs pass through the dehydration window quicker than warm slabs. Along this cold P-T path, the net volume change of rock and fluid upon metamorphism is positive, while along the warm P-T path, the

net volume change is negative. They ascertain that only a positive net volume change, however, leads to an increase in pore pressure that drives dehydration embrittlement and causes earthquakes in cold slabs. Dehydration along various P-T paths is explicitly observable in subduction zones with double seismic zones, in which the separation distance between the two seismically active planes is a function of plate age (*Brudzinski et al.*, 2007). However, hydration of the slab mantle to a depth of 40 km below the slab's surface is required to explain the lower plane of seismicity, and the processes that lead to such deep hydration need to be understood. A common hypothesis is that crustal-scale bending faults that form just before the subducting plate enters the trench are able to transport enough water into the slab (*Faccenda et al.*, 2009; *Ranero et al.*, 2003; *Shillington et al.*, 2015). Alternatively, fluid may be supplied to this part of the slab once its upper layers start dehydrating. In the depth range where dehydration occurs, slabs unbend, which creates a layer of tectonic under-pressure in the slab's core. This layer attracts fluid which then preferentially migrates updip within the layer (*Faccenda et al.*, 2012).

Seismology provides strong evidence that dehydration embrittlement in its original sense (i.e., mineral dehydration directly triggering seismic failure) is found in so-called seismic belts. Seismic belts have primarily been identified in Tonga and E Japan (*Kita et al.*, 2006, 2010; *Wei et al.*, 2017). They are regions within the upper seismic plane of a double seismic zone that exhibit higher seismicity rates than the slab above and below, and whose location matches well temperatures of about 500 °C (*Wei et al.*, 2017). At these conditions, the oceanic crust's blueschist facies rock undergo dehydration and transform into dry eclogite - a transformation beyond which no more crustal earthquakes are observed (*van Keken et al.*, 2012). However, not all intermediate-depth earthquakes can be inferred to occur at specific temperatures like these, and many extraordinary observations suggest that multiple mechanisms may be acting in different parts of the system, or interact with one another. Such extraordinary observations at intermediate-depth include seismicity between the planes of a double seismic zone (*Kita and Ferrand*, 2018; *Nakajima et al.*, 2013), triple seismic zones (*Kawakatsu and Seno*, 1983; *Nakajima et al.*, 2009; *Wang*, 2002), earthquakes in the mantle wedge (*Chang et al.*, 2017; *Davey and Ristau*, 2011; *Laigle et al.*, 2013; *Uchida et al.*, 2010), earthquakes in inactive subduction zones such as Gibraltar and Romania, highly active earthquake nests such as Vrancea, Hindu Kush and Bucaramanga (*Prieto et al.*, 2012), and mantle earthquakes deep within collision belts (e.g., *Wang et al.*, 2016).

Standard catalog locations of intermediate-depth earthquakes are usually not accurate enough to place hypocenters unequivocally above, in, or below the subducting crust. This difficulty is tackled from two angles; by installing target-oriented temporary networks and applying advanced earthquake location methods. These methods include earthquake location based on probabilistic approaches (e.g., *Lomax et al.*, 2009), 3-D traveltime tomography with earthquake relocation to reduce the effect of structural heterogeneity (e.g., *Thurber*, 1983), the double-difference technique to reduce relative location errors within seismicity clusters (*Waldhauser and Ellsworth*, 2000), and combinations of these methods. Precise locations of slab seismicity are available for a number of regions, including Alaska (*Li et al.*, 2013), Cascadia (*Cassidy and Waldhauser*, 2002), New Zealand (*Eberhart-Phillips and Reyners*, 2012), Nicaragua (*Kyriakopoulos et al.*, 2015; *Syracuse et al.*, 2008), and Japan (e.g., *Hasegawa et al.*, 2009; *Uchida et al.*, 2010, and citations therein). Still, even in these locations an additional difficulty arises from the interpretation of what feature represents the subducting crust in the images, and how it relates to seismicity. The subducting crust is often assumed to appear as dipping low-velocity layer imaged in all GRT-RF and some local earthquake tomography studies. This assumption, however, is not definite, as the LVL might only represent for instance a fluid-rich upper layer within the subducting crust, plus a sediment layer, or a serpentine layer above the slab (*Bostock*, 2013). This additional problem has not been entirely addressed, but advances have been made in locations such as Japan, where source and receiver coverage for seismic imaging outshine any other location worldwide (*Hasegawa et al.*, 2009).

In this thesis, I address the challenges concerning slab structure and earthquake locations in a new way in terms of region, dataset, and methodologies. Deep seismicity in the Western Hellenic Subduction Zone in Greece has not been characterized at the level of detail that is available for other subduction zones, but the deployment of several dense temporary arrays and permanent networks now offers unprecedented data coverage of the region. To these data, I apply a repertoire of methods including template-matching based earthquake detection, traveltime tomography, double-difference relocation, and integration with high-resolution 2-D GRT images. The Hellenic subduction zone is well-suited as a natural laboratory for cold subduction zones owing to large variations in subduction parameters along strike, comprehensive historical earthquake catalogs and field studies, good onshore accessibility of the forearc, and recent efforts in imaging and monitoring from temporary and permanent seismic networks.

1.2 Research questions and objectives

The main body of this thesis comprises three parts, for which I summarize the main research questions and objectives in this section. The central research question that I probe is:

> What causes intermediate-depth earthquakes?

A wide range of research has attempted to answer this question (see section 1.1.2 above), and two main candidate mechanisms have been developed: dehydration embrittlement and localized thermal runaway. However, it is not clear whether one mechanism dominates over the other, whether the two mechanisms can operate concurrently, and whether they may be coupled.

To better understand which of the mechanisms may be acting in parts of the subduction system, I approach the main question from the viewpoint of an observational seismologist and pose these additional, complementary questions (1–3 below).

1. Where do intraslab earthquakes occur relative to the main discontinuities (e.g., slab Moho, subduction interface) and the expected phase transitions for different subduction environments?

In the first part, I focus on this question within the Western Hellenic subduction zone (WHSZ). The motivation to focus on the WHSZ is two-fold. First, in the last decade, there has been a tremendous upgrade in seismic monitoring capability through deployment of temporary networks and additional permanent stations in the region. Second, the deep seismicity and structure of the WHSZ are not yet well resolved. The objectives in this first part are:

1.1 to obtain a comprehensive and accurate catalog of earthquakes, waveforms, and arrival picks,

1.2 to obtain 3-D models of seismic P-velocity and P-to-S velocity ratio (Vp/Vs-ratio),

1.3 to map the transition between oceanic and continental subduction, the subduction interface, and the slab Moho from the velocity models, hypocenters and other data (e.g., published receiver function cross sections).

One unexpected result of the first part was that deep earthquakes do not only occur in the slab, but also in confined clusters within the mantle wedge and on the interface. Such observations were unknown a decade ago (*Hacker et al.*, 2003), and only three

authors had described similar features until 2013 (*Davey and Ristau*, 2011; *Laigle et al.*, 2013; *Uchida et al.*, 2010). Motivated by the peculiarity of these clusters, the next question naturally arose:

2. What causes earthquakes in the mantle wedge?

In the second part, I evaluate three potential processes that may produce mantle wedge earthquakes, and discuss what these sites teach us on intermediate-depth earthquakes in general. The three potential processes include (a) ruptures within exotic material (e.g., piled seamounts, plume underplating) of distinct composition and high viscosity in the mantle wedge (*Laigle et al.*, 2013; *Uchida et al.*, 2010), (b) serpentine dehydration embrittlement (*Davey and Ristau*, 2011), and (c) pulses of fluids released from the plate interface (*Nakajima and Uchida*, 2018; *Paulatto et al.*, 2017). To help discriminate these different processes, I pursue the following objectives:

2.1 to analyze whether there are systematic differences between earthquakes in the wedge, on the interface, and in the slab,

2.2 to constrain the location of dehydration reactions in the WHSZ, and check whether mantle wedge earthquakes are related to these reactions both in the WHSZ and globally,

2.3 to probe whether clusters of mantle wedge seismicity show time-dependent behavior.

Comments and reviews on the second paper revealed that mantle wedge seismicity is a controversial topic. The controversy stems from the fact that mantle wedge seismicity is generally rare and only resolved by some high-resolution studies. Meanwhile, for Greece, since the integration of hypocenters and structure required me to push the analyses to the limit of their resolution, some room was left to debate with regards to the exact source region of these earthquakes. To reduce this uncertainty, I propose next to obtain independent evidence for earthquake origins in the mantle wedge and other source regions (i.e., subduction interface, subducting crust and slab mantle). This is expressed in the last research question:

3. Can we discern between earthquakes from different source regions in the subduction system based on their waveforms?

In this last part, I address the question by focusing on the following objectives:

3.1 implement a workflow to synthesize seismic waveforms and arrival times of earthquakes within a complex subduction zone model,

3.2 implement a scheme to adequately process and compare observed seismic waveforms of microearthquakes,

3.3 evaluate waveform characteristics, and determine whether these help distinguish between earthquakes originating in different parts of the system.

In the following sections of this thesis's first chapter, I introduce the main study area which is the WHSZ, the dataset that comes from multiple seismic networks in the region, and the methods that I apply to these data. Research into the questions listed above was a collaborative effort, and findings were presented in contributions at scientific meetings that are listed at the end of the chapter. The second chapter contains three scientific papers in which I focus on each of the research questions, in the order 1–3 as listed above. The last chapter synthesizes the main findings from chapter 2 and concludes with an outlook on open research topics.

1.3 Study area: The Western Hellenic Subduction Zone [1]

The Hellenic arc bends around the west and south of Greece, from the heel of Italy, around the Aegean toward southern Turkey along a 1300-km-long trench (see inset map in Fig. 1.2). The large-scale setting is the collision between the African plate to the south, the Eurasian plate to the north and the Arabian plate to the east. At the intersection sit the smaller Adriatic, Aegean and Anatolian plates. Considering plate motions relative to the large Eurasian plate, the Aegean plate moves southwestward, overriding the Ionian lithosphere of the African plate to the south and the Adriatic microplate to the west (*McKenzie*, 1972). The Aegean plate also rotates counter-clockwise together with the Anatolian plate due to the northward advance of the Arabian plate (*Flerit et al.*, 2004; *Reilinger et al.*, 2006). At the same time, the African plate moves northward at $\approx$2 mm/yr. The overall result is the Hellenic Subduction Zone.

The western portion of the system is referred to as the Western Hellenic subduction zone (WHSZ) and extends for 400 km along Greece's west coast (see Fig. 1.2). The WHSZ is home to large variations in subduction properties along strike, including subduction rate, trench retreat, occurrence of deep seismicity, and overriding plate extension. These variations are related, either directly or indirectly, to a change in convergence regime from the subduction of oceanic crust in the south to continental crust

[1] This section consolidates the introduction to the study area from paper I, section 1 (Introduction) and section 2.1 (Structure of the Western Hellenic Subduction Zone). A survey of seismic imaging and seismicity studies in the area can be found in paper I, sections 2.2 and 2.3, but is not included here.

in the north. Of these variations, the rate of subduction is perhaps the most easy to explain – oceanic crust is less buoyant and therefore subducts at a faster rate than the more buoyant continental crust to the north. What causes the other subduction properties to vary, on the other hand, is less well understood. To gain better insight into the processes that affect subduction properties, we need to better characterize not only what is happening in the regions of oceanic and continental subduction, but also the transition from one regime to the other.

In the south, the oceanic crust of the Ionian sea consists of 6 km to 8 km of crystalline crust overlain by up to 6 km of sediments (*Bohnhoff et al.*, 2001; *Kokinou et al.*, 2005, 2006; *Pearce et al.*, 2012). Measurements of magnetic remanence across the Ionian sea yield model ages of 220 Ma to 230 Ma (*Speranza et al.*, 2012), making it one of the oldest preserved sea floors worldwide. While the southern portion of the WHSZ exhibits the classical features of a subduction zone, the northern portion proved more elusive until the last decade, when new seismic images clarified the situation. Indeed, with the northern portion not featuring any intermediate-depth seismicity, there was no evidence that active subduction was taking place until high-resolution scattered wave images by *Pearce et al.* (2012) showed ongoing subduction of thick continental crust of the Adriatic plate beneath northern Greece. The basement crust of this Adriatic plate has a thickness of 19 km to 30 km, with a progressive thinning toward the Corfu margin, and is covered by a 7 km-thick carbonate platform (*Finetti and Del Ben*, 2005). The dichotomy between south and north results in a southern oceanic slab that is three to four times more negatively buoyant than the continental slab to the north, and a current trench retreat of $\approx$35 mm/yr in the south compared to the 4 mm/yr to 10 mm/yr in the north (*Royden and Papanikolaou*, 2011; *Vassilakis et al.*, 2011).

Given the presence of active subduction along the entire WHSZ, what happens at the transition from oceanic (south) to continental (north) subduction? Abundant surface observations yield a detailed picture of the top of the system. The subduction trench is offset horizontally by 140 km at the Kephalonia Transform Fault (KTF), with faster rollback of the oceanic slab causing a south-westward displacement of the trench in the southern segment (*Royden and Papanikolaou*, 2011). The KTF is a dextral fault along which strong strike-slip earthquakes have occurred in the past (*Karastathis et al.*, 2015; *Sachpazi et al.*, 2000; *Shaw and Jackson*, 2010) – most recently the 2015 M_w=6.5 Lefkada earthquake (*Melgar et al.*, 2017) and, just to the south, the 2018 M_w=6.8 Zakynthos earthquake (*Christos et al.*, 2018).

Over the past 1-4 Myr, the KTF has connected to the North Anatolian fault system

through the so-called Central Hellenic Shear Zone (CHSZ, *Papanikolaou and Royden*, 2007; *Royden and Papanikolaou*, 2011). While this has split the Aegean plate into a more active extensional backarc domain in the south than in the north, differential motion between the southern and northern segments is not concentrated at the KTF. Instead, it is distributed over the entire CHSZ, which is up to 100 km wide (see, e.g., *Papanikolaou and Royden*, 2007; *Royden and Papanikolaou*, 2011; *Vassilakis et al.*, 2011). The CHSZ comprises a region of immature strike-slip faulting, spanning from the Corinth rift to the Northern Gulf of Evia. It remains unclear whether shear deformation in the region is driven from the east by the Anatolian plate, or from below by differential slab retreat. The slab top on either sides of the fault appears to be vertically offset by less than 20 km in the 50–80 km depth range, suggesting an effective rollback of only 70 km in that part of the system (*Pearce et al.*, 2012). At the edge of the extensional domain, the Corinth rift is undergoing rapid extension at a rate of 10 mm/yr to 16 mm/yr, making it one of the youngest and fastest spreading rift basins on Earth (*Nixon et al.*, 2016). The crust there is extensionally thinned, with thicknesses ranging from 25 km beneath the eastern Corinth rift, to 45 km below the central Hellenides mountains (*Zelt et al.*, 2005).

The current Hellenic volcanic arc starts just south of the Corinth rift, on the Methana peninsula, and extends for 500 km toward western Turkey. The arc includes the islands of Milos-Antimilos, Santorini, Kos-Nisyros and is Pliocene to modern in age (*Rizzo et al.*, 2016). It is not clear why there is no volcanic activity beyond Milos though, given that deep seismicity extends 150 km farther north along the strike of the WHSZ, suggesting that the slab dehydrates over that region. Based on a correlation between the distribution of volcanic rocks and the location of slab tears imaged by mantle tomography, *Pe-Piper and Piper* (2007) suggest that the current volcanism occurs due to advection of lithospheric mantle and melting associated with slab tearing.

How the patterns of deformation and the location of volcanoes translate from the surface to the state of the system at greater depth is not yet resolved. Intermediate-depth seismicity appears to terminate rather abruptly beneath the northeastern extension of the KTF (see, e.g., *Hatzfeld and Martin*, 1992), but it is unclear whether this termination is due to a simple change in composition of the subducted slab or to a change in the stress field associated with slab tearing, either along-strike or beneath the KTF (e.g., *Piromallo and Morelli*, 2003; *Royden and Papanikolaou*, 2011; *Spakman et al.*, 1988). Seismic studies carried out until now have not been able to image directly the oceanic-to-continental transition, either due to limited resolution or insufficient data coverage.

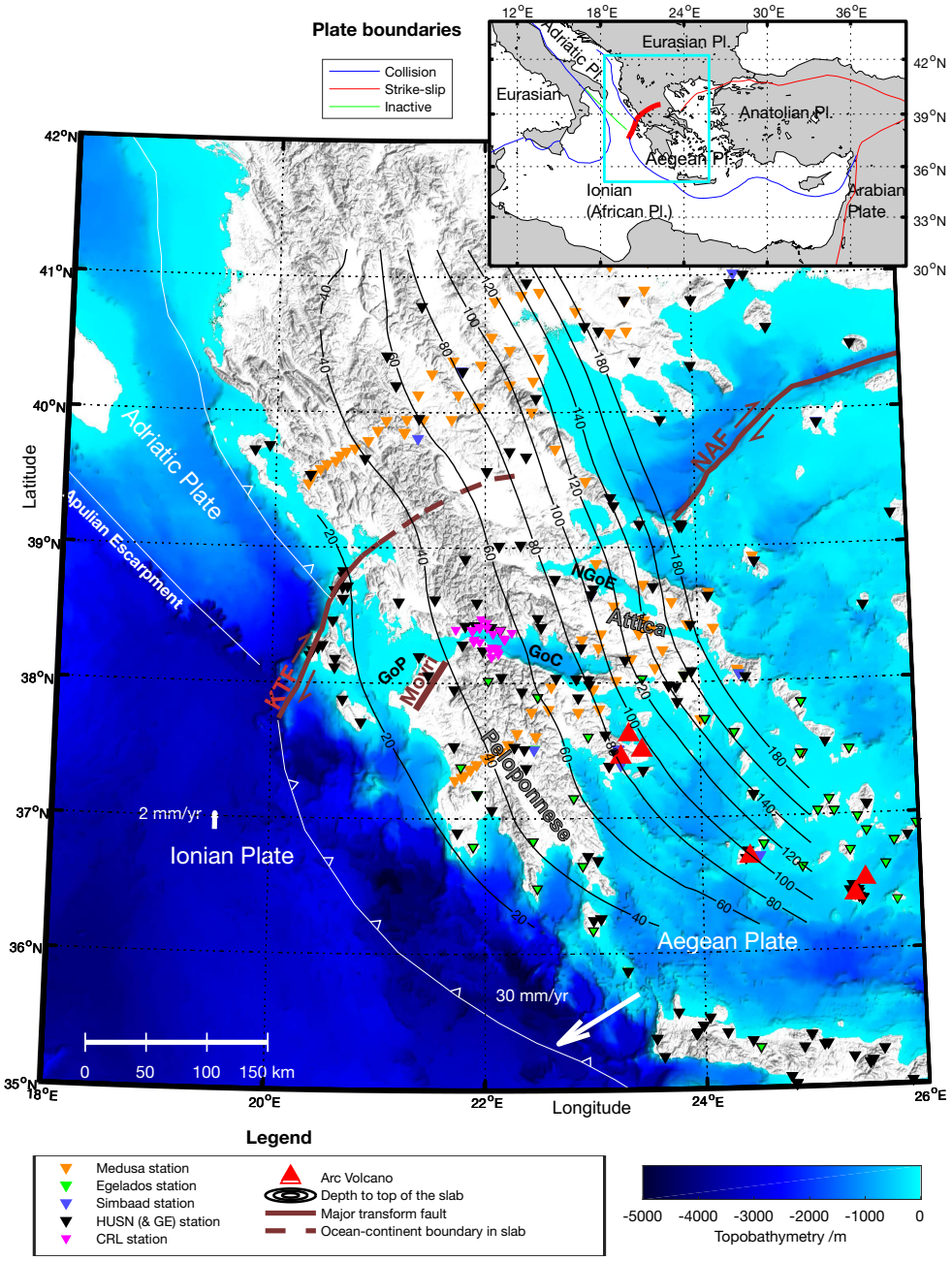

Figure 1.2: Map of mainland Greece, showing major tectonic features and seismic deployments. The inset map depicts the plate configuration in the region and the region zoomed into in the large map. Abbreviations used in the map: KTF: Kephalonia Transform Fault, NAF: North Anatolian Fault; GoC: Gulf of Corinth, GoP: Gulf of Patras, NGoE: Northern Gulf of Evia, HUSN: Hellenic unified seismic network, GE: Geofon global seismic network, CRL: Corinth rift laboratory.

1.4 Data and methods

The research in this thesis is based on a broad repertoire of passive seismic data and methods. In this section, I give a short overview of the seismic experiments and networks that contribute to the dataset, and of the tools and computer codes that I employed in the analyses.

The Hellenic subduction zone has long been a research playground of geoscientists from Europe and North America. In 2006 – 2009, a team of scientists carried out the "Multidisciplinary Experiment for Dynamic Understanding of Subduction under the Aegean" (MEDUSA, *Rondenay*, 2006). It consisted of two dense lines of 40 broadband seismometers each striking in the approximate direction of the slab's dip. Each line used the same set of seismometers that were deployed for about 1.5 years, with the first line placed across the Peloponnese-Attica region in central Greece from 2006–2007 and the second line across northern Greece from 2008–2009.

With their narrow shape, the deployments were primarily designed for receiver function analysis. High-resolution images using the data have been published by *Suckale et al.* (2009), *Pearce et al.* (2012), and *Sachpazi et al.* (2016), while the system's anisotropy structure has been resolved by *Olive et al.* (2014) and consolidated by *Evangelidis* (2017). The distribution of stations, however, is not ideal for local earthquake monitoring that this thesis focuses on. Furthermore, permanent stations in the region did not typically save continuous waveform data prior to 2008, and earthquake detection capabilities were limited until the inception of the Hellenic Unified Seismic Network (HUSN) in 2008. Fortunately, two other temporary projects were operating in the region during overlapping time periods, which greatly improved station coverage. These projects are "Exploring the Geodynamics of Subducted Lithosphere Using an Amphibian Deployment of Seismographs" (Egelados, *Friederich and Meier*, 2008) and "Seismic Imaging of the Mantle Beneath the Anatolian-Aegean Domain" (Simbaad, *Paul et al.*, 2013), for which data is publicly available through the Federation of Digital Seismograph Networks (FDSN). While Egelados covered the Hellenic subduction zone from the Peloponnese to Crete and the Turkish coast, Simbaad consisted of one main profile across West-Central Anatolia with backbone stations around the Aegean. I do not use all the data of the Egelados and Simbaad experiments, but instead focus mainly on the Peloponnese-Attica region, which comprised 20 Egelados stations and 5 Simbaad stations.

During the course of my research, data availability in the region increased further

with the establishment of a dedicated node for the European Integrated Data Archive (EIDA) at the National Observatory of Athens (NOA). Since 2016, the number of usable stations from several Greek seismic monitoring networks has been constantly increasing. These permanent networks include short-period and broadband sensors operated by NOA (1997), the University of Athens (2008), the University of Patras (2000), and the University of Thessaloniki (1981). In addition to the Greek networks, a consortium of French institutions runs a permanent seismic network for near-fault observations around the Gulf of Corinth. This observatory, called the "Corinth Rift Laboratory" (2013), has also been generating large volumes of publicly available data.

In my work, I use seismic data from each of these networks, in particular for the dataset processed in paper II. The expanded coverage afforded by these recently-established networks has allowed me to produce a new improved catalog of deep earthquakes for the region. This catalog is based on both newly detected earthquakes and previous catalogs - including catalogs published by the International Seismological Centre (ISC, 2017) and NOA (2018). The latter also contains a database of moment tensors.

To process these data, I rely on a repertoire of tools that are implemented in mostly open-source software packages. Below, I give an overview of these tools by listing the methods, the computer code in which they are implemented, their capabilities, and the type of input and output data:

1. Seisan seismological analysis software (*Havskov and Ottemöller*, 1999) is used for routine processing of earthquake data, including database management, arrival time picking, location of earthquakes and many additional tasks. With these capabilities, the software and its databases form the backbone of seismological analyses in all chapters of this thesis. For some tasks, Seisan relies on tools that were developed independently, but are now integrated into the analysis package. In the context of methods applied in this thesis, three tools are especially important:

    a) Hypocenter program (*Lienert and Havskov*, 1995), included in the Seisan software, is employed for the location of earthquakes. The program can use absolute arrival times of a wide range of seismic phases at local, regional and teleseismic distances to find an optimal earthquake origin (including time and location). It computes these parameters via an iterative least-squares inversion of arrival times, where residuals are calculated for each phase in a given 1-D velocity model. The program provides a first hypocenter solution

for all earthquakes processed in papers I and II.

b) FocMec program (*Snoke et al.*, 1984), included in the Seisan software, is employed for solving focal mechanisms. The program relies on picked polarities of P- and S-waves to find focal mechanism solutions. It can also use the amplitude ratios of P- and S-waves to converge toward, and better constrain, an optimal solution. I use this method to obtain focal mechanism solutions in paper II.

c) Velest code (*Kissling et al.*, 1994), included in the Seisan software, is employed for constraining a 1-D velocity model for local earthquake relocation, and as an initial model for 3-D tomography studies. The code solves the coupled problem of earthquake origins and 1-D velocity structure through iterative least-squares inversion of absolute first-arrival times of P- and S-waves. An optimal solution is obtained by evaluating the misfit between observed arrival times and computed arrival times for a 1-D velocity model.

2. Simul-family of codes is employed for 3-D local earthquake traveltime tomography (versions SimulPS12 and SimulR16: *Bleibinhaus and Gebrande*, 2006; *Bleibinhaus and Hilberg*, 2012; *Bleibinhaus et al.*, 2003; *Eberhart-Phillips*, 1990; *Thurber*, 1983). This type of tomography relies on absolute arrival time measurements of P- and S-waves, from either earthquakes or controlled sources. It uses primarily arrival times of first arriving waves, but can also use reflected and/or refracted phases. The method uses an iterative, linearized least-squares inversion scheme which produces staggered updates of velocity models (P-velocity and Vp/Vs-ratio) and individual earthquake hypocenters. I use this method in paper I to obtain 3-D models of P-velocity and Vp/Vs-ratio.

3. HypoDD code is employed for high-resolution relative relocation of earthquakes based on the double-difference method (*Waldhauser*, 2012; *Waldhauser and Ellsworth*, 2000). This method relies on measurements of both absolute arrival times and differential traveltimes measured at each station for earthquake pairs (i.e., sets of two earthquakes that are located close to one another). Differential traveltimes can be obtained both from a catalog of arrival time picks, or from cross-correlating waveforms within each earthquake pair. A chain of event pairs is then constructed and the traveltime measurements are iteratively inverted for the hypocenter locations. The algorithm can substantially reduce the uncertainty of earthquake locations relative to one another. Although early implementations assumed a 1-D background velocity model, the latest version (2.1) allows raypaths

to be computed in a 3-D background model, further reducing relative location uncertainties. I use the method to improve the location of earthquakes both in papers I and II.

4. Obspy Python toolbox for seismology (*Beyreuther et al.*, 2010) is employed for the implementation of robust, object-oriented processing workflows. The toolbox can handle a wide variety of tasks in seismology, and I employ it in particular for downloading and archiving of waveform data in connection with Seisan, and the processing of continuous waveform data in paper II.

5. EQCorrscan software package (*Chamberlain et al.*, 2017) is employed for template matching, detection and automatic picking of newly detected earthquakes (relies on Obspy functionality and is integrated with the Seisan databases). I use this tool to substantially expand the dataset of deep earthquakes in Greece, especially by adding small-magnitude events that previous analyses did not detect. Additionally, I employ, improve, and parallelize its functions to calculate differential traveltimes from cross-correlating waveforms, which I then use in HypoDD (see 3.).

6. Gismo toolbox is employed for seismic data analysis in an object-oriented environment in Matlab (*Reyes and West*, 2011; *Thompson and Reyes*, 2017). With its waveform and correlation toolboxes, Gismo is a powerful tool for the analysis of repeating and near-repeating earthquakes with similar waveforms. It accesses the Seisan databases to load earthquake data (origin, picks, amplitudes etc.) and waveforms, which can then be analyzed and compared with a range of functions. I use this tool primarily for the analysis of secondary phases in paper III.

7. Specfem2D spectral element modeling code (see, e.g., *Komatitsch*, 2005) is employed for the accurate simulation of seismic wave propagation in complex media. At its core, Specfem2D solves the weak form of the seismic wave equation on a spectral element mesh in the time domain. It allows complexities such as topography at the free surface, internal discontinuities, anisotropy, (an- / poro-) elasticity, and any lateral variations in elastic parameters and density. The spectral element mesh consists of quadrilateral elements and can be created either with an internal mesher, or with more advanced external meshing tools (described in the next point). Arbitrary source and receiver geometries can then be used to initiate and record wave propagation within this mesh. I use this method to obtain synthetic seismograms within a 2-D subduction zone model in paper III.

8. Trelis meshing software (`https://www.csimsoft.com/trelis`, the commercial version of the former Cubit software) is employed for the creation of a mesh of quadrilateral elements for wave propagation simulations in Specfem. Compared to the Specfem-internal meshers, Trelis allows the meshing of complex geometries and offers a graphical user interface for quality control of the mesh. I use this mesher to construct the subduction zone model on which I run wave simulations in paper III.
9. FM3D multistage fast marching code is employed for the computation of multiphase arrival times in complex 3-D layered models (*de Kool et al.*, 2006; *Rawlinson and Sambridge*, 2004). The code solves the eikonal equation through finite differences in a layered 3-D domain with heterogeneous velocity distribution. I use the code to obtain traveltimes of direct, converted, and reflected phases of deep earthquakes in a 3-D velocity-discontinuity model of the WHSZ in paper III.

1.5 Contributions at scientific meetings

Halpaap, Felix; Rondenay, Stéphane[2]; Ottemöller, Lars. Fluid release and seismicity at a transition between oceanic and continental subduction. *Exploring new frontiers in fluids processes in subduction zones*; 2018-06-25 - 2018-06-28, Leibnitz, Austria.

Halpaap, Felix; Rondenay, Stéphane; Ottemöller, Lars. Slab Seismicity, Metamorphism and Deformation Associated with a Transition from Oceanic to Continental Subduction in Western Greece (Oral). *AOGS Annual Meeting*; 2018-06-07 - 2018-06-07, Honolulu, Hawaii, United States of America.

Halpaap, Felix; Rondenay, Stéphane; Ottemöller, Lars. Slab Seismicity, Metamorphism and Deformation Associated with a Transition from Oceanic to Continental Subduction in Western Greece (Poster). *American Geophysical Union Fall Meeting*; 2017-12-11 - 2017-12-15, New Orleans, Louisiana, United States of America.

[2]The name of the presenting author is underlined if they are not listed as the first author.

Rondenay, Stéphane; McGary, R. Shane; Halpaap, Felix; Goes, Saskia; Perrin, Alexander; Wang, Hongliang; Huismans, Ritske; Ottemöller, Lars (Oral). Seismic probing of hydration and dehydration reactions in subduction zones. *European Geosciences Union General Assembly*; 2017-04-24, Vienna, Austria.

Halpaap, Felix; Rondenay, Stéphane; Ottemöller, Lars. Intermediate Depth Seismicity in the Western Hellenic Subduction Zone: Constraints from Tomography and Double-Difference Relocation (Oral). *Subduction Interface Processes Annual Meeting*; 2017-04-18 - 2017-04-21, Castelldefels, Spain.

Halpaap, Felix; Rondenay, Stéphane; Ottemöller, Lars. Slab seismicity in Greece: Constraints from tomography and double-difference relocation (Poster). *European Geoscience Union General Assembly*; 2016-04-17 - 2016-04-22, Vienna, Austria.

Halpaap, Felix; Rondenay, Stéphane; Ottemöller, Lars. Slab Seismicity in the Western Hellenic Subduction Zone: Constraints from Tomography and Double-Difference Relocation (Poster). *American Geophysical Union Fall Meeting*; 2016-12-12 - 2016-12-16, San Francisco, California, United States of America.

Halpaap, Felix; Ottemöller, Lars; Rondenay, Stéphane. Velocity Structure and Seismicity along the Western Hellenic Subduction Zone (Poster). *Gordon Research Conference: Interior of the Earth*; 2015-06-06 - 2015-06-12, Mount Holyoke, Massachusetts, United States of America.

References cited in the introduction

Abers, G. A., L. S. Mackenzie, S. Rondenay, Z. Zhang, A. G. Wech, and K. C. Creager (2009), Imaging the source region of Cascadia tremor and intermediate-depth earthquakes, *Geology*, *37*(12), 1119–1122, doi:10.1130/G30143A.1.

Abers, G. A., J. Nakajima, P. E. van Keken, S. Kita, and B. R. Hacker (2013), Thermal–petrological controls on the location of earthquakes within subducting plates, *Earth and Planetary Science Letters*, *369-370*, 178–187, doi:10.1016/j.epsl.2013.03.022.

Andersen, T. B., H. Austrheim, N. Deseta, P. Silkoset, and L. D. Ashwal (2014), Large subduction earthquakes along the fossil Moho in Alpine Corsica, *Geology*, *42*(5), 395–398, doi:10.1130/G35345.1.

Angiboust, S., P. Agard, H. Raimbourg, P. Yamato, and B. Huet (2011), Subduction interface processes recorded by eclogite-facies shear zones (Monviso, W. Alps), *Lithos*, *127*(1-2), 222–238, doi:10.1016/j.lithos.2011.09.004.

Aristotle University of Thessaloniki Seismological Network (1981), Permanent Regional Seismological Network operated by the Aristotle University of Thessaloniki, International Federation of Digital Seismograph Networks. Other/Seismic Network, doi:10.7914/SN/HT.

Austrheim, H., and T. B. Andersen (2004), Pseudotachylytes from Corsica: Fossil earthquakes from a subduction complex, *Terra Nova*, *16*(4), 193–197, doi:10.1111/j.1365-3121.2004.00551.x.

Austrheim, H., and T. M. Boundy (1994), Pseudotachylytes Generated During Seismic Faulting and Eclogitization of the Deep Crust, *Science*, *265*, 82–83.

Austrheim, H., K. G. Dunkel, O. Plümper, B. Ildefonse, Y. Liu, and B. Jamtveit (2017), Fragmentation of wall rock garnets during deep crustal earthquakes, *Science Advances*, *3*, doi:10.1126/sciadv.1602067.

Beck, S., S. Barrientos, E. Kausel, and M. Reyes (1998), Source characteristics of historic earthquakes along the central Chile subduction zone, *Journal of South American Earth Sciences*, *11*(2), 115–129.

Beyreuther, M., R. Barsch, L. Krischer, T. Megies, Y. Behr, and J. Wassermann (2010), ObsPy: A Python toolbox for seismology, *Seismological Research Letters*, *81*(3), 530–533, doi:10.1785/gssrl.81.3.530.

Bleibinhaus, F., and H. Gebrande (2006), Crustal structure of the Eastern Alps along the TRANSALP profile from wide-angle seismic tomography, *Tectonophysics*, *414*(1-4),

51–69, doi:10.1016/j.tecto.2005.10.028.

Bleibinhaus, F., and S. Hilberg (2012), Shape and structure of the Salzach Valley, Austria, from seismic traveltime tomography and full waveform inversion, *Geophysical Journal International*, *189*(3), 1701–1716, doi:10.1111/j.1365-246X.2012.05447.x.

Bleibinhaus, F., D. Stich, M. Simon, and H. Gebrande (2003), New results from amplitude preserving prestack depth migration of the Münchberg/Vogtland segment of the MVE deep seismic survey, *Journal of Geodynamics*, *35*, 33–43.

Bohnhoff, M., J. Makris, D. Papanikolaou, and G. Stavrakakis (2001), Crustal investigations of the Hellenic subduction zone using wide aperture seismic data, *Tectonophysics*, *343*, 239–262.

Bostock, M. G. (2013), The Moho in subduction zones, *Tectonophysics*, *609*, 547–557, doi:10.1016/j.tecto.2012.07.007.

Bostock, M. G., S. Rondenay, and J. Shragge (2001), Multiparameter two-dimensional inversion of scattered teleseismic body waves 1. Theory for oblique incidence, *Journal of Geophysical Research*, *106*(12), 30,771–30,782.

Brudzinski, M. R., C. H. Thurber, B. R. Hacker, and E. R. Engdahl (2007), Global Prevalence of Double Benioff Zones, *Science*, *316*(5830), 1472–1474, doi:10.1126/science.1139204.

Cassidy, J. F., and F. Waldhauser (2002), Precise relocations of slab seismicity in the northern Cascadia subduction zone, in *The Cascadia Subduction Zone and Related Subduction Systems*, edited by S. Kirby, K. Wang, and S. Dunlop, pp. 69–74, USGS, Menlo Park, California.

Chamberlain, C. J., C. J. Hopp, C. M. Boese, E. Warren-Smith, D. Chambers, S. X. Chu, K. Michailos, and J. Townend (2017), EQcorrscan: Repeating and near-repeating earthquake detection and analysis in Python, *Seismological Research Letters*, doi:10.1785/0220170151.

Chang, Y., L. M. Warren, and G. A. Prieto (2017), Precise locations for intermediate-depth earthquakes in the Cauca Cluster, Colombia, *Bulletin of the Seismological Society of America*, *107*(6), 2649–2663, doi:10.1785/0120170127.

Christos, K., K. Kyriaki, L. Vasilios, M. Konstantia, M. Basil, M. Konstantinos, P. Christos, Rovithis Emmanouil, S. Thomas, and T. Nikolaos (2018), S. Ionian sea earthquake M 6.8 on 25/10/2018, *Tech. rep.*, Ministry of Infrastructures and Transportation, Thessaloniki.

Corinth Rift Laboratory Team And RESIF Datacenter (2013), CL - Corinth Rift Laboratory Seismological Network (CRLNET), doi:https://doi.org/10.15778/resif.cl.

Davey, F. J., and J. Ristau (2011), Fore-arc mantle wedge seismicity under northeast New Zealand, *Tectonophysics*, *509*(3-4), 272–279, doi:10.1016/j.tecto.2011.06.017.

de Kool, M., N. Rawlinson, and M. Sambridge (2006), A practical grid-based method for tracking multiple refraction and reflection phases in three-dimensional heterogeneous media, *Geophysical Journal International*, *167*(1), 253–270, doi:10.1111/j.1365-246X.2006.03078.x.

DeMets, C., R. G. Gordon, D. F. Argus, and S. Stein (1994), Effect of recent revisions to the geomagnetic reversal time scale on estimates of current plate motions, *Geophysical Research Letters*, *21*(20), 2191, doi:10.1029/94GL02118.

Dinc, A. N., I. Koulakov, M. Thorwart, W. Rabbel, E. R. Flueh, I. Arroyo, W. Taylor, and G. Alvarado (2010), Local earthquake tomography of central Costa Rica: Transition from seamount to ridge subduction, *Geophysical Journal International*, *183*(1), 286–302, doi:10.1111/j.1365-246X.2010.04717.x.

Eberhart-Phillips, D. (1990), Three-dimensional P and S velocity structure in the Coalinga region, California, *Journal of Geophysical Research*, *95*(B10), 15,343–15,363, doi:10.1029/JB095iB10p15343.

Eberhart-Phillips, D., and M. Reyners (1999), Plate interface properties in the northeast Hikurangi subduction zone, New Zealand, from converted seismic waves, *Geophysical Research Letters*, *26*(16), 2565–2568, doi:10.1029/1999GL900567.

Eberhart-Phillips, D., and M. Reyners (2009), Three-dimensional distribution of seismic anisotropy in the Hikurangi subduction zone beneath the central North Island, New Zealand, *Journal of Geophysical Research: Solid Earth*, *114*(6), doi:10.1029/2008JB005947.

Eberhart-Phillips, D., and M. Reyners (2012), Imaging the Hikurangi Plate interface region, with improved local-earthquake tomography, *Geophysical Journal International*, *190*(2), 1221–1242, doi:10.1111/j.1365-246X.2012.05553.x.

Eberhart-Phillips, D., D. H. Christensen, T. M. Brocher, R. Hansen, N. A. Ruppert, P. J. Haeussler, and G. A. Abers (2006), Imaging the transition from Aleutian subduction to Yakutat collision in central Alaska , with local earthquakes and active source data, *Journal of Geophysical Research*, *111*, doi:10.1029/2005JB004240.

Eberhart-Phillips, D., M. Reyners, M. Faccenda, and J. Naliboff (2013), Along-strike variation in subducting plate seismicity and mantle wedge attenuation related to fluid release beneath the North Island, New Zealand, *Physics of the Earth and Planetary Interiors*, *225*, 12–27, doi:10.1016/j.pepi.2013.10.002.

Evangelidis, C. (2017), Seismic anisotropy in the Hellenic subduction zone: Effects of slab segmentation and subslab mantle flow, *Earth and Planetary Science Letters*, *480*, 97–106, doi:10.1016/j.epsl.2017.10.003.

Faccenda, M., T. Gerya, and L. Burlini (2009), Deep slab hydration induced by bending-related variations in tectonic pressure, *Nature Geoscience*, *2*(11), 790–793, doi:10.1038/ngeo656.

Faccenda, M., T. V. Gerya, N. S. Mancktelow, and L. Moresi (2012), Fluid flow during slab unbending and dehydration: Implications for intermediate-depth seismicity, slab weakening and deep water recycling, *Geochemistry, Geophysics, Geosystems*, *13*(1), doi:10.1029/2011GC003860.

Finetti, I. R., and A. Del Ben (2005), Crustal Tectono-Stratigraphic Setting of the Adriatic Sea from New CROP Seismic Data, in *Deep Seismic Exploration of the Central Mediterranean and Italy*, edited by I. R. Finelli, 1 ed., chap. 23, Elsevier, Amster-

dam.

Flerit, F., R. Armijo, G. King, and B. Meyer (2004), The mechanical interaction between the propagating North Anatolian Fault and the back-arc extension in the Aegean, *Earth and Planetary Science Letters*, *224*(3-4), 347–362, doi:10.1016/j.epsl.2004.05.028.

Friederich, W., and T. Meier (2008), Temporary Seismic Broadband Network Acquired Data on Hellenic Subduction Zone, *Eos, Transactions American Geophysical Union*, *89*(40), 378, doi:10.1029/2008EO400002.

Frohlich, C. (2006), *Deep Earthquakes*, Cambridge University Press, Cambridge.

Green II, H. W., and H. Houston (1995), The Mechanics of Deep Earthquakes, *Annual Review of Earth and Planetary Sciences*, *23*, 169–213.

Hacker, B. R., S. M. Peacock, G. A. Abers, and S. D. Holloway (2003), Subduction factory 2. Are intermediate-depth earthquakes in subducting slabs linked to metamorphic dehydration reactions?, *Journal of Geophysical Research*, *108*(B1), 2030, doi:10.1029/2001JB001129.

Hasegawa, A., and J. Nakajima (2017), Seismic imaging of slab metamorphism and genesis of intermediate-depth intraslab earthquakes, *Progress in Earth and Planetary Science*, *4*(1), 12, doi:10.1186/s40645-017-0126-9.

Hasegawa, A., J. Nakajima, N. Uchida, T. Okada, D. Zhao, T. Matsuzawa, and N. Umino (2009), Plate subduction, and generation of earthquakes and magmas in Japan as inferred from seismic observations: An overview, *Gondwana Research*, *16*(3-4), 370–400, doi:10.1016/j.gr.2009.03.007.

Hatzfeld, D., and C. Martin (1992), Intermediate depth seismicity in the Aegean defined by teleseismic data, *Earth and Planetary Science Letters*, *113*(1-2), 267–275, doi:10.1016/0012-821X(92)90224-J.

Havskov, J., and L. Ottemöller (1999), SeisAn Earthquake Analysis Software, *Seismological Research Letters*, *70*(5), 532–534.

Hayashida, T., F. Tajima, J. Nakajima, and J. Mori (2012), A three-dimensional seismic wave speed model in southwestern Japan from combined use of waveform modeling and travel-time tomography, *Journal of Geophysical Research B: Solid Earth*, *117*(11), doi:10.1029/2012JB009345.

Hirose, F., J. Nakajima, and A. Hasegawa (2008), Three-dimensional seismic velocity structure and configuration of the Philippine Sea slab in southwestern Japan estimated by double-difference tomography, *Journal of Geophysical Research: Solid Earth*, *113*(9), doi:10.1029/2007JB005274.

International Seismological Centre (2017), On-line Bulletin, *Tech. rep.*, Internatl. Seismol. Cent., Thatcham, United Kingdom, doi:http://doi.org/10.31905/D808B830.

Jamtveit, B., Y. Ben-Zion, F. Renard, and H. Austrheim (2018), Earthquake-induced transformation of the lower crust, *Nature*, *556*(7702), 487–491, doi:10.1038/s41586-018-0045-y.

John, T., S. Medvedev, L. H. Rüpke, T. B. Andersen, Y. Y. Podladchikov, and H. Austrheim (2009), Generation of intermediate-depth earthquakes by self-localizing thermal runaway, *Nature Geoscience*, *2*, 137–140, doi:10.1038/ngeo419.

Jung, H., H. W. Green II, and L. F. Dobrzhinetskaya (2004), Intermediate-depth earthquake faulting by dehydration embrittlement with negative volume change., *Nature*, *428*, 545–549, doi:10.1038/nature02412.

Karastathis, V. K., E. Mouzakiotis, A. Ganas, and G. A. Papadopoulos (2015), High-precision relocation of seismic sequences above a dipping Moho: the case of the January–February 2014 seismic sequence on Cephalonia island (Greece), *Solid Earth*, *6*, 173–184, doi:10.5194/se-6-173-2015.

Kaus, B. J. P., and Y. Y. Podladchikov (2006), Initiation of localized shear zones in vizcoelastoplastic rocks, *Journal of Geophysical Research: Solid Earth*, *111*(B04), doi:10.1029/2005JB003652.

Kawakatsu, H., and T. Seno (1983), Triple seismic zone and the regional variation of seismicity along the northern Honshu arc (Japan)., *Journal of Geophysical Research*, *88*(B5), 4215–4230, doi:10.1029/JB088iB05p04215.

Kawakatsu, H., and S. Watada (2007), Seismic Evidence for Deep-Water Transportation in the Mantle, *Science*, *316*, 1468–1471, doi:10.1126/science.1140855.

Kelemen, P. B., and G. Hirth (2007), A periodic shear-heating mechanism for intermediate-depth earthquakes in the mantle, *Nature*, *446*(7137), 787–790, doi:10.1038/nature05717.

Kim, Y., M. S. Miller, F. D. Pearce, and R. W. Clayton (2012), Seismic imaging of the Cocos plate subduction zone system in central Mexico, *Geochemistry, Geophysics, Geosystems*, *13*(7), doi:10.1029/2012GC004033.

Kirby, S. H., E. Engdahl, and R. Denlinger (1996), Intermediate depth intraslab earthquakes and arc volcanism as physical expressions of crustal and uppermost mantle metamorphism in subducting slabs, in *Subduction from top to bottom*, edited by G. Bebout, D. Scholl, S. Kirby, and J. Platt, pp. 195–214, AGU Geophys. Mono. No. 96.

Kissling, E., W. L. Ellsworth, D. Eberhart-Phillips, and U. Kradolfer (1994), Initial reference models in local earthquake tomography, *Journal of Geophysical Research*, *99*(B10), 19,635–19,646.

Kita, S., and T. P. Ferrand (2018), Physical mechanisms of oceanic mantle earthquakes: Comparison of natural and experimental events, *Scientific Reports*, *8*, doi:10.1038/s41598-018-35290-x.

Kita, S., T. Okada, J. Nakajima, T. Matsuzawa, and A. Hasegawa (2006), Existence of a seismic belt in the upper plane of the double seismic zone extending in the along-arc direction at depths of 70 – 100 km beneath NE Japan, *Geophysical Research Letters*, *33*, doi:10.1029/2006GL028239.

Kita, S., T. Okada, A. Hasegawa, J. Nakajima, and T. Matsuzawa (2010), Anomalous deepening of a seismic belt in the upper-plane of the double seismic zone in the

Paci fi c slab beneath the Hokkaido corner : Possible evidence for thermal shielding caused by subducted forearc crust materials, *Earth and Planetary Science Letters*, *290*, 415–426, doi:10.1016/j.epsl.2009.12.038.

Kokinou, E., E. Kamberis, A. Vafidis, D. Monopolis, G. Ananiadis, and A. Zelilidis (2005), Deep seismic reflection data from offshore Western Greece: A new crustal model for the Ionian Sea, *Journal of Petroleum Geology*, *28*(2), 185–202, doi:10.1111/j.1747-5457.2005.tb00079.x.

Kokinou, E., E. Papadimitriou, V. Karakostas, E. Kamberis, and F. Vallianatos (2006), The Kefalonia Transform Zone (offshore Western Greece) with special emphasis to its prolongation towards the Ionian Abyssal Plain, *Marine Geophysical Researches*, *27*(4), 241–252, doi:10.1007/s11001-006-9005-2.

Komatitsch, D. (2005), The spectral-element method in seismology, *Geophysical Monograph Series*, *157*, 205–227, doi:10.1029/157GM13.

Kühn, A., J. Glodny, H. Austrheim, and A. Råheim (2000), The Caledonian tectono-metamorphic evolution of the Lindås Nappe: Constraints from U-Pb, Sm-Nd and Rb-Sr ages of granitoid dykes, *Norwegian Journal of Geology*, *82*, 45–57.

Kumar, P., and H. Kawakatsu (2011), Imaging the seismic lithosphere-asthenosphere boundary of the oceanic plate, *Geochemistry, Geophysics, Geosystems*, *12*(1), doi:10.1029/2010GC003358.

Kyriakopoulos, C., A. V. Newman, A. M. Thomas, M. Moore-Driskell, and G. T. Farmer (2015), A new seismically constrained subduction interface model for Central America, *Journal*, pp. 5535–5548, doi:10.1002/2014JB011859.

Laigle, M., A. Hirn, M. Sapin, A. Bécel, P. Charvis, E. Flueh, J. Diaz, J. F. Lebrun, A. Gesret, R. Raffaele, A. Galvé, M. Evain, M. Ruiz, H. Kopp, G. Bayrakci, W. Weinzierl, Y. Hello, J. C. Lépine, J. P. Viodé, M. Sachpazi, J. Gallart, E. Kissling, and R. Nicolich (2013), Seismic structure and activity of the north-central Lesser Antilles subduction zone from an integrated approach: Similarities with the Tohoku forearc, *Tectonophysics*, *603*, doi:10.1016/j.tecto.2013.05.043.

Lay, T. (1994), The Fate of Descending Slabs, *Annual Review of Earth and Planetary Sciences*, *22*, 33–61, doi:10.1146/annurev.earth.22.1.33.

Li, J., G. A. Abers, Y. Kim, and D. Christensen (2013), Alaska megathrust 1: Seismicity 43 years after the great 1964 Alaska megathrust earthquake, *Journal of Geophysical Research: Solid Earth*, *118*(9), 4861–4871, doi:10.1002/jgrb.50358.

Lienert, B. R., and J. Havskov (1995), A computer program for locating earthquakes both locally and globally, *Seismological Research Letters*, *66*(5), 26–36, doi:10.1785/gssrl.66.5.26.

Lomax, A., A. Michelini, and A. Curtis (2009), Earthquake Location, Direct, Global-Search Methods, doi:10.1007/978-0-387-30440-3.

Lücke, O. H., and I. G. Arroyo (2015), Density structure and geometry of the Costa Rican subduction zone from 3-D gravity modeling and local earthquake data, *Solid Earth*, *6*(4), 1169–1183, doi:10.5194/se-6-1169-2015.

MacKenzie, L. S., G. A. Abers, S. Rondenay, and K. M. Fischer (2010), Imaging a steeply dipping subducting slab in Southern Central America, *Earth and Planetary Science Letters*, *296*(3-4), 459–468, doi:10.1016/j.epsl.2010.05.033.

McCrory, P. A., J. L. Blair, F. Waldhauser, and D. H. Oppenheimer (2012), Juan de Fuca slab geometry and its relation to Wadati-Benioff zone seismicity, *Journal of Geophysical Research: Solid Earth*, *117*(9), doi:10.1029/2012JB009407.

McGary, R. S., R. L. Evans, P. E. Wannamaker, J. Elsenbeck, and S. Rondenay (2014), Pathway from subducting slab to surface for melt and fluids beneath Mount Rainier., *Nature*, *511*, 338–40, doi:10.1038/nature13493.

McKenzie, D. (1972), Active tectonics of the Mediterranean region, *Geophys. J. R. Astron. Soc.*, *30*, 109–185.

Melgar, D., A. Ganas, J. Geng, C. Liang, E. J. Fielding, and I. Kassaras (2017), Source characteristics of the 2015 Mw 6.5 Lefkada, Greece, strike-slip earthquake, *Journal of Geophysical Research: Solid Earth*, pp. 2260–2273, doi:10.1002/2016JB013452.

Nakajima, J., and N. Uchida (2018), Repeated drainage from megathrusts during episodic slow slip, *Nature Geoscience*, *11*, 351–356, doi:10.1038/s41561-018-0090-z.

Nakajima, J., Y. Tsuji, A. Hasegawa, S. Kita, T. Okada, and T. Matsuzawa (2009), Tomographic imaging of hydrated crust and mantle in the subducting Pacific slab beneath Hokkaido, Japan: Evidence for dehydration embrittlement as a cause of intraslab earthquakes, *Gondwana Research*, *16*(3-4), 470–481, doi:10.1016/j.gr.2008.12.010.

Nakajima, J., N. Uchida, T. Shiina, A. Hasegawa, B. R. Hacker, and S. H. Kirby (2013), Intermediate-depth earthquakes facilitated by eclogitization-related stresses, *Geology*, *41*(6), 659–662, doi:10.1130/G33796.1.

National Observatory of Athens; Institute of Geodynamics (1997), National Observatory of Athens Seismic Network, International Federation of Digital Seismograph Networks. Other/Seismic Network, doi:10.7914/SN/HL.

National Observatory of Athens; Institute of Geodynamics (2018), Database of revised events, http://bbnet.gein.noa.gr/HL/databases/database.

Nicholson, T., M. Bostock, and J. F. Cassidy (2005), New constraints on subduction zone structure in northern Cascadia, *Geophysical Journal International*, *161*(3), 849–859, doi:10.1111/j.1365-246X.2005.02605.x.

Nixon, C. W., L. C. McNeill, J. M. Bull, R. E. Bell, R. L. Gawthorpe, T. J. Henstock, D. Christodoulou, M. Ford, B. Taylor, D. Sakellariou, G. Ferentinos, G. Papatheodorou, M. R. Leeder, R. E. Collier, A. M. Goodliffe, M. Sachpazi, and H. Kranis (2016), Rapid spatiotemporal variations in rift structure during development of the Corinth Rift, central Greece, *Tectonics*, doi:10.1002/2015TC004026.

Olive, J. A., F. Pearce, S. Rondenay, and M. D. Behn (2014), Pronounced zonation of seismic anisotropy in the Western Hellenic subduction zone and its geodynamic significance, *Earth and Planetary Science Letters*, *391*, 100–109, doi:10.1016/j.epsl.

2014.01.029.

Papanikolaou, D. J., and L. H. Royden (2007), Disruption of the Hellenic arc: Late Miocene extensional detachment faults and steep Pliocene-Quaternary normal faults - Or what happened at Corinth?, *Tectonics*, *26*(5), doi:10.1029/2006TC002007.

Paul, A., H. Karabulut, and RESIF (2013), Seismic network XY:SIMBAAD temporary experiment - Backbone of broadband stations. RESIF - Réseau Sismologique et géodésique Français., doi:https://doi.org/10.15778/resif.xy2007.

Paulatto, M., M. Laigle, A. Galve, P. Charvis, M. Sapin, G. Bayrakci, M. Evain, and H. Kopp (2017), Dehydration of subducting slow-spread oceanic lithosphere in the Lesser Antilles, *Nature Communications*, doi:10.1038/ncomms15980.

Pe-Piper, G., and D. J. W. Piper (2007), Neogene backarc volcanism of the Aegean: New insights into the relationship between magmatism and tectonics, *Geological Society of America Special Papers*, *418*(02), 17–31, doi:10.1130/2007.2418(02).

Pearce, F. D., S. Rondenay, M. Sachpazi, M. Charalampakis, and L. H. Royden (2012), Seismic investigation of the transition from continental to oceanic subduction along the western Hellenic subduction Zone, *Journal of Geophysical Research: Solid Earth*, *117*, doi:10.1029/2011JB009023.

Piromallo, C., and A. Morelli (2003), P wave tomography of the mantle under the Alpine-Mediterranean area, *Journal of Geophysical Research*, *108*(B2), doi:10.1029/2002JB001757.

Poli, S., and M. W. Schmidt (2002), Petrology of Subducted Slabs, *Annual Review of Earth and Planetary Sciences*, *30*, 207–235, doi:10.1146/annurev.earth.30.091201.140550.

Prieto, G. A., G. C. Beroza, S. A. Barrett, G. A. López, and M. Florez (2012), Earthquake nests as natural laboratories for the study of intermediate-depth earthquake mechanics, *Tectonophysics*, *570-571*, 42–56, doi:10.1016/j.tecto.2012.07.019.

Prieto, G. a., M. Florez, S. a. Barrett, G. C. Beroza, P. Pedraza, J. F. Blanco, and E. Poveda (2013), Seismic evidence for thermal runaway during intermediate-depth earthquake rupture, *Geophysical Research Letters*, *40*, 6064–6068, doi:10.1002/2013GL058109.

Ramachandran, K., and R. D. Hyndman (2012), The fate of fluids released from subducting slab in northern Cascadia, *Solid Earth*, *3*(1), 121–129, doi:10.5194/se-3-121-2012.

Ranero, C. R., J. P. Morgan, K. McIntosh, and C. Reichert (2003), Bending-related faulting and mantle serpentinization at the Middle America trench., *Nature*, *425*(6956), 367–373, doi:10.1038/nature01961.

Rawlinson, N., and M. Sambridge (2004), Multiple reflection and transmission phases in complex layered media using a multistage fast marching method, *Geophysics*, *69*(5), 1338–1350, doi:10.1190/1.1801950.

Reilinger, R., S. McClusky, P. Vernant, S. Lawrence, S. Ergintav, R. Cakmak, H. Ozener, F. Kadirov, I. Guliev, R. Stepanyan, M. Nadariya, G. Hahubia, S. Mah-

moud, K. Sakr, A. ArRajehi, D. Paradissis, A. Al-Aydrus, M. Prilepin, T. Guseva, E. Evren, A. Dmitrotsa, S. V. Filikov, F. Gomez, R. Al-Ghazzi, and G. Karam (2006), GPS constraints on continental deformation in the Africa-Arabia-Eurasia continental collision zone and implications for the dynamics of plate interactions, *Journal of Geophysical Research: Solid Earth*, *111*(5), doi:10.1029/2005JB004051.

Reyes, C. G., and M. E. West (2011), The Waveform Suite: A Robust Platform for Manipulating Waveforms in MATLAB, *Seismological Research Letters*, *82*(1), 104–110, doi:10.1785/gssrl.

Reyners, M., D. Eberhart-Phillips, G. Stuart, and Y. Nishimura (2006), Imaging subduction from the trench to 300 km depth beneath the central North Island, New Zealand, with Vp and Vp/Vs, *Geophysical Journal International*, *165*(2), 565–583, doi:10.1111/j.1365-246X.2006.02897.x.

Rizzo, A. L., A. Caracausi, V. Chavagnac, P. Nomikou, P. N. Polymenakou, M. Mandalakis, G. Kotoulas, A. Magoulas, A. Castillo, and D. Lampridou (2016), Kolumbo submarine volcano (Greece): An active window into the Aegean subduction system, *Scientific Reports*, *6*(February), 28,013, doi:10.1038/srep28013.

Rondenay, S. (2006), Multi-disciplinary Experiments for Dynamic Understanding of Subduction under the Aegean Sea, International Federation of Digital Seismograph Networks. Other/Seismic Network, doi:10.7914/SN/XS_2006.

Rondenay, S., M. G. Bostock, and J. Shragge (2001), Multiparameter two-dimensional inversion of scattered teleseismic body waves 3. Application to the Cascadia 1993 data set, *Journal of Geophysical Research*, *106*(12), 30,795–30,807.

Rondenay, S., G. A. Abers, and P. E. van Keken (2008), Seismic imaging of subduction zone metamorphism, *Geology*, *36*(4), 275–278, doi:10.1130/G24112A.1.

Rondenay, S., L. G. J. Montési, and G. A. Abers (2010), New geophysical insight into the origin of the Denali volcanic gap, *Geophysical Journal International*, *182*(2), 613–630, doi:10.1111/j.1365-246X.2010.04659.x.

Royden, L. H., and D. J. Papanikolaou (2011), Slab segmentation and late Cenozoic disruption of the Hellenic arc, *Geochemistry, Geophysics, Geosystems*, *12*(3), doi:10.1029/2010GC003280.

Sachpazi, M., A. Hirn, C. Clément, F. Haslinger, M. Laigle, E. Kissling, P. Charvis, Y. Hello, J. C. Lépine, M. Sapin, and J. Ansorge (2000), Western Hellenic subduction and Cephalonia Transform: Local earthquakes and plate transport and strain, *Tectonophysics*, *319*(4), 301–319, doi:10.1016/S0040-1951(99)00300-5.

Sachpazi, M., M. Laigle, M. Charalampakis, J. Diaz, E. Kissling, A. Gesret, A. Becel, E. Flueh, P. Miles, and A. Hirn (2016), Segmented Hellenic slab rollback driving Aegean deformation and seismicity, *Geophysical Research Letters*, pp. 651–658, doi:10.1002/2015GL066818.

Savard, G., M. G. Bostock, and N. I. Christensen (2018), Seismicity, Metamorphism, and Fluid Evolution Across the Northern Cascadia Fore Arc, *Geochemistry, Geophysics, Geosystems*, *19*(6), 1881–1897, doi:10.1029/2017GC007417.

Schmidt, M. W., and S. Poli (1998), Experimentally based water budgets for dehydrating slabs and consequences for arc magma generation, *Earth and Planetary Science Letters*, *163*, 361–379, doi:10.1016/S0012-821X(98)00142-3.

Shaw, B., and J. Jackson (2010), Earthquake mechanisms and active tectonics of the Hellenic subduction zone, *Geophysical Journal International*, *181*(2), 966–984, doi:10.1111/j.1365-246X.2010.04551.x.

Shiina, T., J. Nakajima, T. Matsuzawa, G. Toyokuni, and S. Kita (2017), Depth variations in seismic velocity in the subducting crust: Evidence for fluid-related embrittlement for intermediate-depth earthquakes, *Geophysical Research Letters*, pp. 810–817, doi:10.1002/2016GL071798.

Shillington, D. J., A. Bécel, M. R. Nedimović, H. Kuehn, S. C. Webb, G. A. Abers, K. M. Keranen, J. Li, M. Delescluse, and G. A. Mattei-Salicrup (2015), Link between plate fabric, hydration and subduction zone seismicity in Alaska, *Nature Geoscience*, *8*(December), 961 – 964, doi:10.1038/ngeo2586.

Shragge, J., M. G. Bostock, and S. Rondenay (2001), Multiparameter two-dimensional inversion of scattered teleseismic body waves 2. Numerical examples, *Journal of Geophysical Research*, *106*(12), 30,783–30,793.

Snoke, J. A., J. W. Munsey, A. G. Teague, and G. A. Bollinger (1984), Program for focal mechanism determination by combined use of polarity and SV-P amplitude ratio data, *Earthquake Notes*, *55*(3), 15.

Song, T.-r. A., D. V. Helmberger, M. R. Brudzinski, R. W. Clayton, P. Davis, X. Pérez-campos, and S. K. Singh (2009), Subducting slab ultra-slow velocity layer coincident with silent earthquakes in southern Mexico, *Science*, *502*(April), 502–507, doi:10.1126/science.1167595.

Spakman, W., M. J. R. Wortel, and N. J. Vlaar (1988), The Hellenic Subduction Zone: A tomographic image and its geodynamic implications, *Geophysical Research Letters*, *15*(1), 60–63, doi:10.1029/GL015i001p00060.

Speranza, F., L. Minelli, A. Pignatelli, and M. Chiappini (2012), The Ionian Sea: The oldest in situ ocean fragment of the world?, *Journal of Geophysical Research B: Solid Earth*, *117*(12), doi:10.1029/2012JB009475.

Stark, P. B., and C. Frohlich (1985), The depths of the deepest deep earthquakes, *Journal of Geophysical Research*, *90*(B2), 1859–1869.

Suckale, J., S. Rondenay, M. Sachpazi, M. Charalampakis, A. Hosa, and L. H. Royden (2009), High-resolution seismic imaging of the western Hellenic subduction zone using teleseismic scattered waves, *Geophysical Journal International*, *178*(2), 775–791, doi:10.1111/j.1365-246X.2009.04170.x.

Syracuse, E. M., G. A. Abers, K. Fischer, L. MacKenzie, C. Rychert, M. Protti, V. Gonzalez, and W. Strauch (2008), Seismic tomography and earthquake locations in the Nicaraguan and Costa Rican upper mantle, *Geochemistry, Geophysics, Geosystems*, *9*(7), doi:10.1029/2008GC001963.

Syracuse, E. M., P. E. van Keken, G. A. Abers, D. Suetsugu, C. Bina, T. Inoue, D. A.

Wiens, and M. Jellinek (2010), The global range of subduction zone thermal models, *Physics of the Earth and Planetary Interiors*, *183*, 73–90, doi:10.1016/j.pepi.2010.02.004.

The Ancorp Working Group, O. Oncken, E. Lüschen, J. Mechie, S. Sobolev, A. Schulze, C. Gaedicke, S. Grunewald, J. Bribach, G. Asch, P. Giese, P. Wigger, M. Schmitz, S. Lueth, E. Scheuber, C. Haberland, A. Rietbrock, H. Götze, H. Brasse, R. Patzwahl, G. Chong, H. Wilke, G. González, A. Jensen, M. Araneda, H. Vieytes, G. Behn, E. Martínez, R. Rössling, J. Amador, E. Ricaldi, H. Chumacero, and R. Luterstein (1999), Seismic reflection image revealing offset of Andean subduction-zone earthquake locations into oceanic mantle, *Nature*, *397*(January), 341–344, doi:10.1038/16909.

Thompson, G., and C. Reyes (2017), GISMO - a seismic data analysis toolbox for MATLAB.

Thurber, C. H. (1983), Earthquake locations and three-dimensional crustal structure in the Coyote Lake Area, central California, *Journal of Geophysical Research*, *88*(B10), 8226, doi:10.1029/JB088iB10p08226.

Uchida, N., S. H. Kirby, T. Okada, R. Hino, and A. Hasegawa (2010), Supraslab earthquake clusters above the subduction plate boundary offshore Sanriku, northeastern Japan: Seismogenesis in a graveyard of detached seamounts?, *Journal of Geophysical Research: Solid Earth*, *115*(9), doi:10.1029/2009JB006797.

University of Athens (2008), University of Athens, Seismological Laboratory, International Federation of Digital Seismograph Networks. Other/Seismic Network, doi:10.7914/SN/HA.

University of Patras; Geology Department; Seismological Laboratory (2000), PSLNET, permanent seismic network operated by the University of Patras, Greece, International Federation of Digital Seismograph Networks. Other/Seismic Network, doi:10.7914/SN/HP.

van Keken, P. E., S. Kita, and J. Nakajima (2012), Thermal structure and intermediate-depth seismicity in the Tohoku-Hokkaido subduction zones, *Solid Earth*, *3*(2), 355–364, doi:10.5194/se-3-355-2012.

Vassilakis, E., L. H. Royden, and D. Papanikolaou (2011), Kinematic links between subduction along the Hellenic trench and extension in the Gulf of Corinth, Greece: A multidisciplinary analysis, *Earth and Planetary Science Letters*, *303*(1-2), 108–120, doi:10.1016/j.epsl.2010.12.054.

Waldhauser, F. (2012), User Guide to HypoDD Version 2.1b, *Tech. rep.*, Lamont-Doherty Earth Observatory, Palisades, New York.

Waldhauser, F., and W. L. Ellsworth (2000), A double-difference earthquake location algorithm: Method and application to the northern Hayward fault, California, *Bulletin of the Seismological Society of America*, *6*, 1353–1368.

Wang, K. (2002), Unbending combined with dehydration embrittlement as a cause for double and triple seismic zones, *Geophysical Research Letters*, *29*(18), 36–1–36–4,

doi:10.1029/2002GL015441.

Wang, X., D. Zhao, and J. Li (2016), The 2013 Wyoming upper mantle earthquakes: Tomography and tectonic implications, *Journal of Geophysical Research: Soild Earth*, *121*, 6797–6808, doi:10.1002/2016JB013118.

Wannamaker, P. E., R. L. Evans, P. A. Bedrosian, M. J. Unsworth, V. Maris, and R. S. McGary (2014), Segmentation of plate coupling, fate of subduction fluids, and modes of arc magmatism in Cascadia, inferred from magnetotelluric resistivity, *Geochemistry, Geophysics, Geosystems*, *15*, 4692–4711, doi:10.1002/2015GC00591.

Wei, S. S., D. A. Wiens, P. E. van Keken, and C. Cai (2017), Slab temperature controls on the Tonga double seismic zone and slab mantle dehydration, *Science Advances*, *3*, doi:10.1126/sciadv.1601755.

Wells, R. E., R. J. Blakely, and C. S. Weaver (2002), Cascadia microplate models and within-slab earthquakes, in *The Cascadia Subduction Zone and Related Subduction Systems—Seismic Structure, Intraslab Earthquakes and Processes, and Earthquake Hazards*, edited by S. Kirby, K. Wang, and S. Dunlop, pp. 17–23, U.S. Geological Survey, Menlo Park, California.

Yamasaki, T. (2003), Double seismic zone and dehydration embrittlement of the subducting slab, *Journal of Geophysical Research*, *108*(B4), 2212, doi:10.1029/2002JB001918.

Ye, L., T. Lay, Z. Zhan, H. Kanamori, and J.-l. Hao (2016), The isolated 680 km deep 30 May 2015 MW 7.9 Ogasawara (Bonin) Islands earthquake, *Earth and Planetary Science Letters*, *433*(June 1994), 169–179, doi:10.1016/j.epsl.2015.10.049.

Zelt, B. C., B. Taylor, M. Sachpazi, and A. Hirn (2005), Crustal velocity and Moho structure beneath the Gulf of Corinth, Greece, *Geophysical Journal International*, *162*(1), 257–268, doi:10.1111/j.1365-246X.2005.02640.x.

Zhang, H., C. H. Thurber, D. Shelly, S. Ide, G. C. Beroza, and A. Hasegawa (2004), High-resolution subducting-slab structure beneath northern Honshu, Japan, revealed by double-difference tomography, *Geology*, *32*(4), 361–364, doi:10.1130/G20261.2.

2 Scientific results

Paper I

Seismicity, Deformation and Metamorphism in the Western Hellenic Subduction Zone - New Constraints from Tomography

Felix Halpaap, Stéphane Rondenay, Lars Ottemöller

Department of Earth Science, University of Bergen, Bergen, Norway.

Journal of Geophysical Research: Solid Earth **123 (4)**, 3000-3026 (2018),
doi: 10.1002/2017JB015154

Cover on right hand side: In Halpaap et al. (doi.org/10.1002/2017JB015154): Three-dimensional block model of the subduction interface and seismicity based on the results obtained in this study. The subducting oceanic crust of the Ionian plate is dark blue, while the subducting continental crust of the Adriatic plate is in brown. Variable shading on the interfaces represents relief, with oblique illumination from a light source to the right of the model. The magenta solid lines mark large strike-slip faults, including the Kephalonia Transform Fault and the western tip of the North Anatolian Fault. The magenta dashed line marks the putative boundary between oceanic and continental slabs based on the contrast in seismicity (though apparent changes in the slab's tomographic response could also be used to constrain this boundary, we refrain from doing so as there is a progressive change in resolution associated with the contrast in seismicity between north and south; see Figure 2). Relocated hypocenters are indicated by red spheres, with size corresponding to magnitude. The green spheres are hypocenters projected onto the slab top surface. Red dashed lines indicate the outline of a V-shaped seismic gap believed to be associated with a broad zone of deformation in the oceanic slab. With permission, from: Uri ten Brink, Yehuda Ben-Zion, Martha Savage, Paul Tregoning, André Revil, Doug Schmitt, Michael Walter (eds.), 2018. Volume 123, Issue 4, April 2018. *Journal of Geophysical Research: Solid Earth, 123* (4).

JOURNAL OF GEOPHYSICAL RESEARCH
Solid Earth
AN AGU JOURNAL

JGR

Volume 123 • Issue 4 • April 2018 • Pages 2519–3282

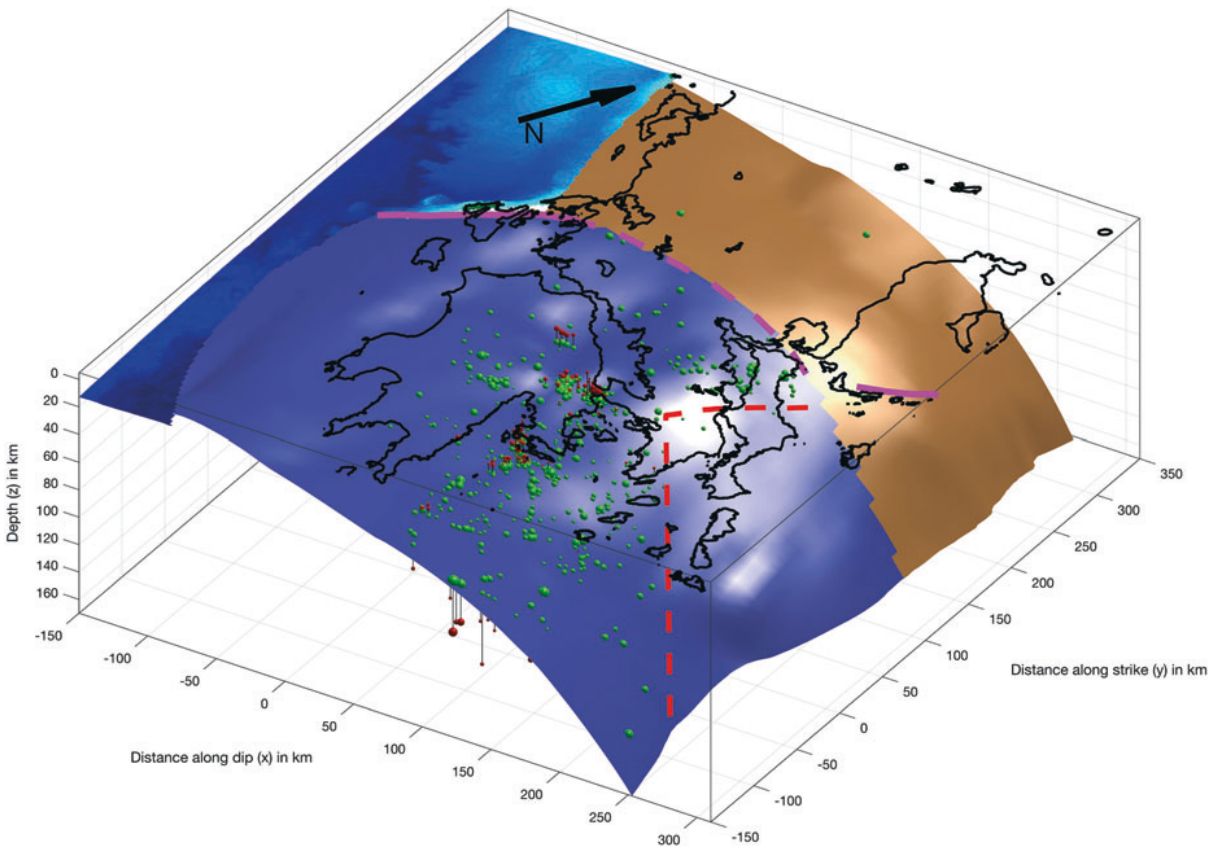

AGU100 ADVANCING EARTH AND SPACE SCIENCE

WILEY

AGU PUBLICATIONS

Journal of Geophysical Research: Solid Earth

RESEARCH ARTICLE
10.1002/2017JB015154

Key Points:
- The oceanic crust subducting below central Greece contains a 10 km thin, single-planed Wadati-Benioff Zone
- Transition between oceanic subduction (south) to continental subduction (north) is smooth rather than a tear
- Mantle wedge corner is relatively dry, but there is abundant silica enrichment above the forearc interface

Supporting Information:
- Supporting Information S1

Correspondence to:
F. Halpaap,
felix.halpaap@uib.no

Citation:
Halpaap, F., Rondenay, S., & Ottemöller, L. (2018). Seismicity, deformation, and metamorphism in the Western Hellenic Subduction Zone: New constraints from tomography. *Journal of Geophysical Research: Solid Earth*, *123*. https://doi.org/10.1002/2017JB015154

Received 27 OCT 2017
Accepted 17 FEB 2018
Accepted article online 23 FEB 2018

Seismicity, Deformation, and Metamorphism in the Western Hellenic Subduction Zone: New Constraints From Tomography

Felix Halpaap[1], **Stéphane Rondenay**[1], **and Lars Ottemöller**[1]

[1]Department of Earth Science, University of Bergen, Bergen, Norway

Abstract The Western Hellenic Subduction Zone is characterized by a transition from oceanic to continental subduction. In the southern oceanic portion of the system, abundant seismicity reaches depths of 100 km to 190 km, while the northern continental portion rarely exhibits deep earthquakes. Our study investigates how this oceanic-continental transition affects fluid release and related seismicity along strike. We present results from local earthquake tomography and double-difference relocation in conjunction with published images based on scattered teleseismic waves. Our tomographic images recover both subducting oceanic and continental crusts as low-velocity layers on top of high-velocity mantle. Although the northern and southern trenches are offset along the Kephalonia Transform Fault, continental and oceanic subducting crusts appear to align at depth. This suggests a smooth transition between slab retreat in the south and slab convergence in the north. Relocated hypocenters outline a single-planed Wadati-Benioff Zone with significant along-strike variability in the south. Seismicity terminates abruptly north of the Kephalonia Transform Fault, likely reflecting the transition from oceanic to continental subducted crust. Near 90 km depth, the low-velocity signature of the subducting crust fades out and the Wadati-Benioff Zone thins and steepens, marking the outline of the basalt-eclogite transition. Subarc melting of the mantle is only observed in the southernmost sector of the oceanic subduction, below the volcanic part of the arc. Beneath the nonvolcanic part, the overriding crust appears to have undergone large-scale silica enrichment. This enrichment is observed as an anomalously low Vp/Vs ratio and requires massive transport of dehydration-derived fluids updip through the subducting crust.

1. Introduction

The Western Hellenic Subduction Zone (WHSZ) is home to large variations in subduction properties along strike, including subduction rate, trench retreat, occurrence of deep seismicity, and overriding plate extension. These variations are related, either directly or indirectly, to a change in convergence regime from the subduction of oceanic crust in the south to continental crust in the north. Of these variations, the rate of subduction is perhaps the most easy to explain—oceanic crust is less buoyant and therefore subducts at a faster rate than the more buoyant continental crust to the north. What causes the other subduction properties to vary, on the other hand, is less well understood. To gain better insight into the processes that affect subduction properties, we need to better characterize not only what is happening in the regions of oceanic and continental subduction but also the transition from one regime to the other.

While the southern portion of the WHSZ exhibits the classical features of a subduction zone, the northern portion proved more elusive until the last decade, when new seismic images clarified the situation. Indeed, with the northern portion not featuring any intermediate depth seismicity, there was no evidence that active subduction was taking place until high-resolution scattered wave images by Pearce et al. (2012) showed ongoing subduction of thick continental crust beneath northern Greece.

Given the presence of active subduction along the entire WHSZ, what happens at the transition from oceanic (south) to continental (north) subduction? Abundant surface observations yield a detailed picture of the top of the system. The subduction trench is discontinuous at the Kephalonia Transform Fault (KTF), with faster rollback of the oceanic slab causing a southwestward displacement of the trench in the southern segment. But the differential motion between the southern and northern segments is not concentrated at the KTF. Instead, it is distributed in an ≈100 km wide zone extending inland from the KTF into the Central Hellenic Shear

AGU Journal of Geophysical Research: Solid Earth 10.1002/2017JB015154

Zone (CHSZ) (see, e.g., Papanikolaou & Royden, 2007; Royden & Papanikolaou, 2011; Vassilakis et al., 2011). In this region, which includes the Gulf of Corinth, deformation occurs along generally E-W striking normal faults that crosscut older trench-parallel structures. How these patterns of deformation are translated from the surface to greater depth is, however, not yet resolved. Intermediate depth seismicity appears to terminate rather abruptly beneath the northeastern extension of the KTF (see, e.g., Hatzfeld & Martin, 1992), but it is unclear whether this termination is due to a simple change in composition of the subducted slab or to a change in the stress field associated with slab tearing, either along strike or beneath the KTF (e.g., Piromallo, 2003; Royden & Papanikolaou, 2011; Spakman et al., 1988). Seismic studies carried out until now have not been able to image directly the oceanic-to-continental transition, either due to limited resolution or insufficient data coverage.

Here we present a set of improved seismic velocity models and earthquake locations that give us new insight into processes that occur in the oceanic and continental subduction portions of the WHSZ, as well as in the transition between the two regimes. After a brief summary of the study area (section 2), we describe the methodologies (section 3) and the data set (section 4) used in our study. The analyses are performed on a new, integrated set of *P* and *S* wave arrival times from local earthquakes recorded at permanent and temporary stations deployed across Greece and neighboring countries. These are inverted with a modified version of the SIMULR16 package (Bleibinhaus, 2003) for local traveltime tomography and with hypoDD 2.1D (Waldhauser, 2012) for earthquake relocations. The results are presented (section 6) and interpreted (section 7) with the goal of better characterizing the transition between oceanic and continental subduction in western Greece and understanding how this transition affects seismicity, the stress field, and fluid processes across the region.

2. Geodynamic Setting

2.1. Structure of the Western Hellenic Subduction Zone

The Hellenic arc bends around the west and south of Greece, from the heel of Italy, around the Aegean toward southern Turkey along a 1,300 km long trench (see inset map in Figure 1). The large-scale setting is the collision between the African plate to the south, the Eurasian plate to the north, and the Arabian plate to the east. At the intersection sit the smaller Adriatic, Aegean, and Anatolian plates. Considering plate motions relative to the large Eurasian plate, the Aegean plate moves southwestward, overriding the Ionian lithosphere of the African plate to the south and the Adriatic microplate to the west (McKenzie, 1972). The Aegean plate also rotates counterclockwise together with the Anatolian plate due to the northward advance of the Arabian plate (Flerit et al., 2004; Reilinger et al., 2006). At the same time, the African plate moves northward at ≈2 mm/yr. The overall result is the Hellenic Subduction Zone.

The western portion of the system, which we have previously defined as the WHSZ, extends for 400 km along Greece's west coast (see Figure 1). It is in the middle of this subsegment that the transition from oceanic to continental subduction occurs. In the south, the oceanic crust of the Ionian sea consists of 6 km to 8 km of crystalline crust overlain by up to 6 km of sediments (Bohnhoff et al., 2001; Kokinou et al., 2005, 2006; Pearce et al., 2012). Measurements of magnetic remanence across the Ionian sea yield model ages of 220 Ma to 230 Ma (Speranza et al., 2012), making it one of the oldest preserved sea floors worldwide. In the north, the basement crust of the Adriatic plate has a thickness of 19 km to 30 km, with a progressive thinning toward the Corfu margin, and is covered by a 7 km thick carbonate platform (Finetti & Del Ben, 2005). This dichotomy results in a southern oceanic slab that is 3 to 4 times more negatively buoyant than the continental slab to the north and a current trench retreat of ≈35 mm/yr in the south compared to the 4 mm/yr to 10 mm/yr in the north (Royden & Papanikolaou, 2011; Vassilakis et al., 2011).

The differential rollback between the Ionian and Adriatic slabs is accommodated by the KTF, a dextral fault along which strong strike-slip earthquakes have occurred in the past (Karastathis et al., 2015; Sachpazi et al., 2000; Shaw & Jackson, 2010). At the KTF, the trench is offset horizontally by 140 km (Royden & Papanikolaou, 2011). However, the slab top on either sides of the fault appears to be vertically offset by less than 20 km in the 50–80 km depth range, suggesting an effective rollback of only 70 km in that part of the system (Pearce et al., 2012). While the trench is well defined south of the KTF, it is mostly covered by sediments and thus lacks a clear bathymetric signature to the north. Instead, the most prominent seafloor feature north of the KTF is the Apulian escarpment, which runs in a northwestern direction and represents the edge of the Adriatic (Apulian) microplate. As such, the Apulian escarpment represents the continuation, past the tip of the KTF, of the boundary between oceanic crust of the Ionian sea and the continental crust of the Adriatic plate

AGU Journal of Geophysical Research: Solid Earth 10.1002/2017JB015154

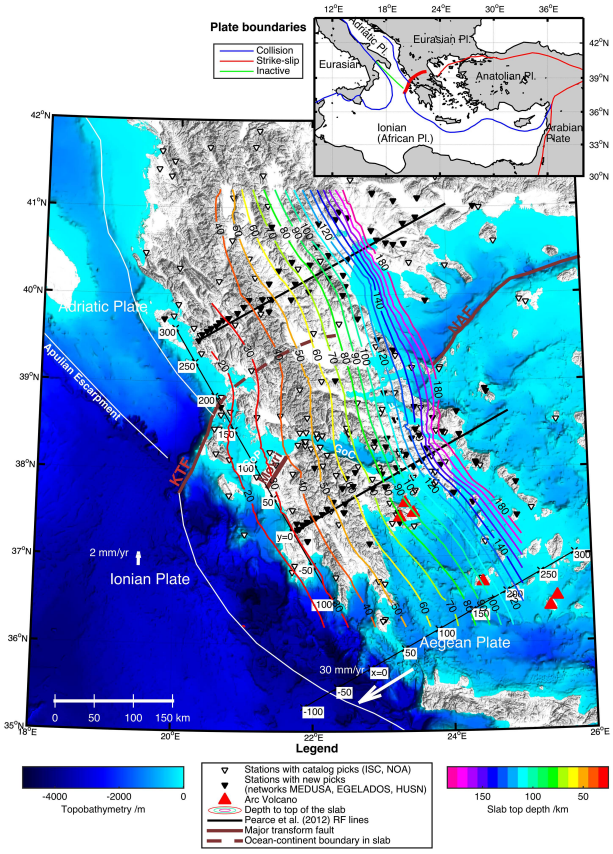

Figure 1. Map of mainland Greece and the Western Hellenic Subduction Zone, showing major geological features and the seismic stations used in this study. The inset shows an overview map of the eastern Mediterranean, with convergent plate boundaries in blue, transform boundaries in red, and inactive boundaries in green. The yellow rectangle in the inset marks the area shown in the main figure. Black numbers on white indicate the local coordinate system used for our analysis, whose origin is located at station XS.S001 and which is rotated by 30° counterclockwise from east (from a point at 39°N, 22°E), such that *x* increases in the direction of subduction dip and *y* increases along the strike of the subduction zone toward NW. See legend for the description of other symbols and lines.

(Finetti & Del Ben, 2005). But unlike the KTF, which is very active seismically, the Apulian escarpment is characterized as a passive margin without significant seismicity (Del Ben et al., 2015; Finetti & Del Ben, 2005).

Over the past 1–4 Myr, the KTF has connected to the North Anatolian Fault system through the so-called Central Hellenic Shear Zone (Papanikolaou & Royden, 2007; Royden & Papanikolaou, 2011). This has split the Aegean plate into a more active extensional backarc domain in the south than in the north. The Central Hellenic Shear Zone comprises a region of immature strike-slip faulting, spanning from the Corinth rift

AGU Journal of Geophysical Research: Solid Earth 10.1002/2017JB015154

to the Northern Gulf of Evia. It remains unclear whether shear deformation in the region is driven from the east by the Anatolian plate or from below by differential slab retreat. At the edge of the extensional domain, the Corinth rift is undergoing rapid extension at a rate of 10 mm/yr to 16 mm/yr, making it one of the youngest and fastest spreading rift basins on Earth (Nixon et al., 2016). The crust there is extensionally thinned, with thicknesses ranging from 25 km beneath the eastern Corinth rift to 45 km below the central Hellenides mountains (Zelt et al., 2005).

While the boundary between Adriatic and Ionian slabs has been fairly well constrained at the surface via direct observations, its structure at depth has been inferred mainly via geodynamic models until now. For example, models of Royden and Papanikolaou (2011) that are based on the age and thickness of accreted sediments suggest that Ionian lithosphere has been subducting since ≈8 Ma below the Peloponnesus, resulting in the subduction of 300 km of Ionian oceanic crust. This implies that the oceanic crust should have reached ≈150 km depth at 260 km horizontal distance from the current trench, assuming a shallow slab dip of 17° steepening to 45° below 90 km depth (based on Papazachos et al., 2000; Pearce et al., 2012; Zhu et al., 2015, and this study). The oceanic-continental plate boundary which subducts at the KTF should thus progressively bend toward the east, as indicated by the red dashed line in Figure 1, to join with the putative boundary of the subducted Ionian crust. At depth, the differential rollback between the two slabs could be accommodated by trench-normal tear, as has been suggested by Govers and Wortel (2005).

In addition to the structural differences described above, the transition from oceanic to continental subduction should also cause variations in the amount of fluid that enters the system. Indeed, there is seismic evidence that the Adriatic plate entering the WHSZ is drier than the Ionian plate (Finetti & Del Ben, 2005; Kokinou et al., 2005). This evidence is based on the detection of bending faults, which play an important role in hydrating the crust and mantle of a slab prior to subduction. For the WHSZ, such bending faults that penetrate the entire crust have been imaged in the Ionian (Kokinou et al., 2005) but not in the Adriatic (Finetti & Del Ben, 2005). This variation in hydration should have an influence on seismicity and magma generation along the WHSZ, something that we investigate in more details with our new models.

The current Hellenic volcanic arc starts just south of the Corinth rift, on the Methana peninsula, and extends for 500 km toward western Turkey. The arc includes the islands of Milos-Antimilos, Santorini, and Kos-Nisyros and is Pliocene to modern in age (Rizzo et al., 2016). It is not clear why there is no volcanic activity beyond Milos though, given that deep seismicity extends 150 km farther north along the strike of the WHSZ, suggesting that the slab dehydrates over that region. Based on a correlation between the distribution of volcanic rocks and the location of slab tears imaged by mantle tomography, Pe-Piper and Piper (2007) suggest that the current volcanism occurs due to advection of lithospheric mantle and melting associated with slab tearing.

2.2. Slab Images

Images of the Hellenic subduction zone at depth have been obtained through a range of seismic methods. These include seismic tomography at continental/mantle scales (e.g., Bijwaard et al., 1998; Koulakov et al., 2009; Piromallo, 2003; Spakman et al., 1988; Zhu et al., 2015) and local scales (Lamara, 2015; Papazachos & Nolet, 1997), receiver function studies (e.g., Gesret et al., 2011; Li et al., 2003; Sachpazi et al., 2016; Sodoudi et al., 2015), inversion of scattered teleseismic waves (e.g., Pearce et al., 2012; Suckale et al., 2009), active-source reflection imaging (e.g., Finetti & Del Ben, 2005; Kokinou et al., 2005, 2006; von Huene et al., 1997; Zelt et al., 2005), and refraction imaging (e.g., Bohnhoff et al., 2001). For a comprehensive overview of seismic studies that have been conducted until now in the region, we refer the reader to Suckale et al. (2009) and Pearce et al. (2012). Here we limit our review to those studies which are directly relevant to understanding the transition from oceanic to continental subduction in the WHSZ.

Tomographic studies have imaged the structure of the Hellenic subduction zone over a wide range of scales. At small scale, local earthquake tomography images the slab as a high-velocity tabular feature that dips gently from the surface down to 140 km depth (Lamara, 2015; Papazachos & Nolet, 1997). At larger scale, regional and teleseismic tomography shows an ≈150 km thick plate dipping at ≈45° between 200 km and 1,200 km depth (Bijwaard et al., 1998; Koulakov et al., 2009; Piromallo, 2003; Spakman et al., 1988; Zhu et al., 2015). While the lower portion of the slab appears fairly continuous across the mantle transition zone and into the lower mantle, the upper-mantle portion is discontinuous in most models beneath western Greece. Spakman et al. (1988) and Wortel and Spakman (2000) have suggested that this gap represents a trench-parallel slab tear which propagates from the north to the south.

AGU Journal of Geophysical Research: Solid Earth 10.1002/2017JB015154

Methods based on teleseismic receiver functions yield higher-resolution images than tomography in the 0–200 km depth range. Two profiles showing the subducted crust beneath southern and northern Greece were obtained by inversion of scattered teleseismic waves recorded at stations of the Multidisciplinary Experiment for Dynamic Understanding of Subduction under the Aegean (MEDUSA) (see black lines in Figure 1; Pearce et al., 2012; Suckale et al., 2009). In the south, the Ionian crust is seen by Pearce et al. (2012) as an 8 km thick low-velocity layer extending from 35 km depth beneath the coast to 90 km depth beneath Attica. In the north, the Adriatic crust is also seen as a low-velocity layer, but it is much thicker (20 km) and extends down to only 70 km depth (as imaged by *S* wave scattering potential $\delta\beta/\beta$). The termination of the low-velocity signature at depth has been interpreted by Suckale et al. (2009) and Pearce et al. (2012) as representing the transformation of crustal rocks into eclogite. Both the southern and northern segments dip at the same angle of 17° toward an azimuth of 60 ± 10°. Based on single-station receiver functions, Gesret et al. (2011) resolved similar dips in the 16° to 18° range but on average more easterly azimuths between 50° and 70°. More recently, a series of receiver function profiles by Sachpazi et al. (2016) revealed that the Ionian slab appears to be segmented into 30 km wide strips that run parallel to the subduction direction. These segments are delimited by vertical offsets of up to 10 km and are believed to be bounded by transform faults inherited from a spreading ridge. The profiles of Sachpazi et al. (2016) also showed a bend in the slab at 60 km depth, which is consistent with the geometry of the Wadati-Benioff Zone (WBZ) beneath the region (Hatzfeld, 1994; Papazachos et al., 2000).

Active source seismic studies yield the highest resolution across the WHSZ, though their depth range is usually limited to the crust and uppermost mantle. These approaches are particularly useful to characterize the slab before it reaches the trench. In the south, offshore surveys carried out in the Ionian sea (Kokinou et al., 2005, 2006) imaged thin oceanic crust entering the trench near the KTF. Near the Mediterranean ridge, another survey by von Huene et al. (1997) produced a 3-D image of what appears to be a mostly sediment-covered seamount. Based on these and other onshore-offshore profiles across Crete (Bohnhoff et al., 2001), the crust entering the trench in the southern part of the WHSZ appears to have an average thickness of 7 km and to be clearly oceanic in nature. In contrast, to the north, offshore profiles across the Adriatic sea have imaged a 19 km to 30 km thick crystalline crust (Del Ben et al., 2015; Finetti & Del Ben, 2005) moving toward the trench. Active source experiments have also been used to constrain the subducted slab at depth—for example, Zelt et al. (2005) identified reflected signals from the top of the slab at 70 km depth beneath the Gulf of Corinth.

2.3. Slab Seismicity

Shallow seismicity is abundant nearly everywhere in Greece, while intermediate depth earthquakes (deeper than 40 km) are confined to the slab. These intermediate depth earthquakes account for ≈30% of earthquakes above magnitude 5 compiled by the International Seismological Centre (2017) since 1960 for the region. In western Greece, large earthquakes of magnitude $M \geq 6$ occur both in the overriding and subducting plates (Durand et al., 2014). Two regions of the overriding plate that are particularly active seismically are the Corinth rift and the KTF. Large earthquakes related to the subducting plate occur both at the subduction interface and at intermediate depth within the slab. Focal mechanisms of regional events are routinely calculated by the National Observatory of Athens (NOA) (Konstantinou et al., 2010) for earthquakes down to magnitude $M_W = 4$. There are also more focused compilations of reviewed focal mechanisms by Shaw and Jackson (2010) and Serpetsidaki et al. (2016). In general, subduction-related earthquakes are thought to result from two main causes in the WHSZ.

1. The slab breaking up, plunging downward, rolling back, and slipping along the interface with the overriding plate (Durand et al., 2014; Papazachos et al., 2000). This sequence of earthquakes includes normal faulting in the slab and thrust faulting along the interface, with both types of faulting occurring in the direction of subduction.
2. Compression parallel to the trench due to the convex shape of the slab, which results in arc-parallel thrusting (Benetatos et al., 2004; Rontogianni et al., 2011).

Earthquake relocation studies have been carried out using increasingly widespread and dense seismic networks. An early investigation by Papazachos et al. (2000) showed a steepening of the WBZ at 70 km depth below the Peloponnesus (Papazachos et al., 2000). Based on the newer earthquake catalogs, (Sachpazi et al., 2016) suggested that intermediate depth earthquakes cluster along slab-parallel lines, possibly denoting inherited transform faults. While these two studies relied on 1-D background velocity models, others used more general treatments based on nonlinear inversion (e.g., Brüstle, 2012) and/or double difference

AGU Journal of Geophysical Research: Solid Earth 10.1002/2017JB015154

(e.g., Galanis et al., 2006; Karakonstantis & Papadimitriou, 2010). Still, none of these studies has yet tackled the high degree of uncertainty related to deep earthquake locations in the WHSZ and their relation to structures imaged by receiver functions.

3. Methods

In this study, we seek to improve earthquake locations and obtain 3-D models of *P* wave velocity and Vp/Vs ratio for the WHSZ. To do so, we adopt a strategy that comprises three stages: (1) 1-D inversion of *P* and *S* wave arrival times, to build a starting model for the tomography; (2) local earthquake tomography, in which we invert *P* and (*S*-*P*) wave arrival times to obtain 3-D velocity models of the subsurface; and (3) double-difference relocation, to increase the accuracy of relative earthquake locations. Even though there exists a scheme that combines stages 2 and 3 (tomoDD; Zhang et al., 2004), we opted for a stepwise approach. This gives us access to improved forward solvers for the tomography and relocation. For the tomography, we use SIMULR16 (Bleibinhaus, 2003), an upgrade of the popular SIMULPS package (Eberhart-Phillips, 1990; Thurber, 1983; Thurber & Eberhart-Phillips, 1999). While the ray tracer of SIMULPS was shown to be accurate for arrays smaller than 50 km × 50 km (Evans et al., 1999), that of SIMULR16 can handle larger arrays such as ours, which is 500 km × 500 km. To obtain relative earthquake locations, we use version 2.1D of the hypoDD double-difference software package (Waldhauser, 2012). The advantage of this version is that it can handle a 3-D background velocity model, in contrast to previous versions which used a 1-D model. This allows us to use directly our resulting 3-D tomographic model to relocate the earthquakes. Below, we describe the three stages of our analysis in more details.

3.1. One-Dimensional Velocity Inversion

In the first stage, we invert our arrival time observations to generate an optimal 1-D velocity model which we then use as a starting model for the 3-D inversion. This is a key step as it has been shown that the results of 3-D traveltime inversion are highly dependent on its starting model, and thus, great care should be placed into determining this model (see, e.g., Kissling et al., 1994). Here we use the program VELEST (Kissling et al., 1994), which inverts *P* and *S* arrival times for 1-D velocity structure and hypocenter coordinates using a damped least squares iterative inversion scheme. VELEST also requires a starting model and an initial parameterization (i.e., number of layers and layer thicknesses), which we set by combining information from various sources in the literature. The crustal part is based on the 1-D model of Haslinger et al. (1999), which was obtained by local earthquake tomography in the Gulf of Arta. Below the base of that model (45 km), we use velocities from the global AK135 model (Kennett et al., 1995). As for the parameterization, we introduce thin layers close to the expected average Moho depth from previous receiver function studies (Sachpazi et al., 2016), so that VELEST can return a sharp velocity increase in that prescribed depth rage. The introduction of low-velocity layers in the initial model is prohibited by VELEST, as such structure would produce 1-D solutions that are more complicated than necessary.

3.2. Local Earthquake Tomography

In the second stage, we use SIMULR16 to iteratively relocate earthquakes and invert for the 3-D Vp and Vp/Vs ratio structure. SIMULR16 employs a linearized damped least squares inversion scheme for perturbing an initial velocity model. A damping parameter is used to control the maximum perturbations per iteration, which is usually determined from an *L* curve test to find the best trade-off between root mean square (RMS) residual and data variance. The inversion is linearized through Fermat's principle, which states that the ray's traveltime is stationary for small changes in the raypath (Bleibinhaus, 2003). And since only small changes of raypath are allowed at each step, the data kernel *G* can also be assumed to remain constant within one iteration. Each iteration updates the model parameters by a perturbation Δm, which includes changes in Vp and Vp/Vs ratio from the previous iteration models as well as station corrections. This perturbation can be expressed as follows:

$$\Delta m = \left(G^T G + \Theta^2 E\right)^{-1} \times \left(G^T \Delta d\right), \tag{1}$$

where *G* is the data kernel, Θ is the damping parameter, *E* is the error matrix, and Δd is the residual between the current model's synthetic traveltimes and the traveltime observations *d*. Hypocenters are relocated after each update of the velocity model by individual least squares inversions for each earthquake. In both layers of inversion, the iterative process is stopped either when a maximum number of iterations is reached (15 for velocity models and 10 for hypocenters) or when an *F* test indicates that no significant improvement in data residuals has occurred from one iteration to the next.

AGU Journal of Geophysical Research: Solid Earth 10.1002/2017JB015154

At each update of the velocity model, raypaths are calculated through a process that combines an artificial ray tracer (ART) and a pseudo bending ray tracer (PB) (as described in Um & Thurber, 1987). Our version of SIMULR16 comprises two improvements that permit the accurate treatment of long raypaths (i.e., greater than 80 km), which have been shown to introduce significant errors in the solution when using the traditional ART-PB approach (Haslinger & Kissling, 2001). First, it includes the modified ray tracer of Bleibinhaus (2003), which improves the ART and includes an iterative segmentation during PB to compute the rays more accurately in very heterogeneous areas. These changes increase computational cost, and they also improve ART-PB's accuracy by more than 1 order of magnitude for distances above 140 km (Bleibinhaus, 2003), which benefits this study since many of our raypaths exceed this distance. Second, we implement a new correction to account for the sphericity of the Earth which, if ignored, can yield traveltime errors of up to 1–2 s for raypaths exceeding 500 km. We chose the "sphere-in-a-box" approach from Theunissen et al. (2018). This approach calculates hypocenters and raypaths in a Cartesian coordinate system where the topography, station locations, and initial hypocenters are converted from latitude, longitude, and depth to the local left-handed Cartesian coordinates *x* (azimuth 60°), *y* (azimuth 330°), and *z* (down) (Theunissen et al., 2018). This way, we can represent the subduction zone and related seismicity in their true geometry. It also lets us build an initial 1-D velocity model that honors the geospherical shape, with an additional adjustment of surface elevations based on the ETOPO1 topography model (Amante & Eakins, 2009).

In terms of parameterization, we use a variable grid spacing and a regridding strategy that help improve the robustness of the final models. The SIMUL family of programs operates on a rectangular grid with variable node spacing where inversion nodes can be turned on or off—with values at off nodes being interpolated (Thurber & Eberhart-Phillips, 1999). This allows to vary the number of nodes as a function of ray coverage (supporting information Figure S1), Fresnel zone size, and expected structure. For example, in our application, we use a smaller node spacing in the crust to better implement the geospherical correction and improve the recovery of the Moho. Nodes are automatically turned off when their derivative weight sum—a measure of ray hits and residual—falls below a certain threshold (usually 10). This helps increase the determination ratio (number of observations versus number of unknowns) and thus the robustness of the inversion. The overall grid spacing is decreased over the course of the inversion to build robust starting models for progressively detailed inversions. A first set of inversions is performed on a coarse grid (12 × 13 × 18 nodes), followed by two additional sets with more refined grids (23 × 23 × 21 and 27 × 27 × 24 nodes; see Figure S1). The final model of each set of inversions serves as the starting model for the next set.

Throughout the various inversion steps, the observations are weighted based on picking errors, event-station offsets, and traveltime residuals. Picking errors are set at a constant value of 0.2 s for all observations (see section 4 for further discussion). In terms of event-station offsets, observations made at offsets ≤100 km receive a weight of 100%; those that are between 100 km and 400 km see a linear weight reduction between 100 and 50%, and those in the 400 km to 900 km range receive between 50 and 25%. Offsets above 900 km are not considered. As for traveltime residuals, full weight is applied to observations that yield residuals <0.6 s. Then the weights are reduced linearly from 100% to 2% for residuals between 0.6 s and 3.0 s and from 2% to 0% for residuals between 3.0 s and 7.0 s. No inversion data are discarded with this weighting strategy, since our preprocessing already gets rid of arrival time picks that yield more than 5 s residuals after initial relocation with a 1-D model.

3.3. Double-Difference Relocation

In the third stage, we improve relative locations of earthquake hypocenters computed in stage 2 by applying the double-difference method of Waldhauser and Ellsworth (2000). Double-difference relocation considers traveltime differences between pairs of nearby earthquakes. Owing to the earthquakes' proximity, one can assume that the raypaths connecting them to a given station are nearly identical except for the short segment separating them and that the velocity is constant over that segment. Given these assumptions, the difference in traveltime between the two events at a given station is only a function of their separation in space, and a precise measure of this separation can be obtained via a quantity called the "double difference," which is expressed as follows (see Waldhauser & Ellsworth, 2000):

$$dr_k^{ij} = \left(t_k^i - t_k^j\right)^{\text{obs}} - \left(t_k^i - t_k^j\right)^{\text{cal}}, \tag{2}$$

where dr_k^{ij} is the double difference at station k for events i and j and t_k^i andt_k^j are the traveltimes of the two events at that station, which are either observed ("obs") or calculated by ray tracing through a background

AGU Journal of Geophysical Research: Solid Earth 10.1002/2017JB015154

velocity model ("calc"). Here we use hypoDD version 2.1D (Waldhauser, 2012) to calculate the raypaths and traveltimes through our resulting 3-D model from stage 2. This yields more accurate traveltime values than the original version of hypoDD, which relies on 1-D background models that cannot address the high level of heterogeneities found in subduction zones. With double differences from multiple stations and events, one then forms a system of equations that can be solved for hypocentral parameters (i.e., perturbations Δx, Δy, Δz, Δt to the initial hypocentral locations that minimize the various double differences). This system of equations can be solved either with a singular value decomposition algorithm for <700 events (threshold for this survey due to 32 bit memory restrictions), which allows accurate error estimation, or with the conjugate gradient algorithm for a larger number of events.

4. Data

The data set used in this study consists of *P* and *S* wave arrival times for earthquakes that occurred beneath the study area. It comprises a combination of our own manual picks from recordings made at temporary/permanent stations and arrivals from reviewed events located by the International Seismological Centre (ISC) and the NOA. We consider only earthquakes that initial estimates place within our inversion domain—a region encompassing all of mainland Greece and the Peloponnesus (Figure S1). We thus start with an initial set of 3,063 earthquakes (see left panels in Figure S2 in supporting information) and follow a quality-control workflow to extract events/data that will ensure robust inversion results. In this section, we describe how we pick/integrate the arrival time data and how we select the high-quality data that we retain for further analysis.

We manually pick arrival times from ISC-listed events recorded between 2006 and 2009 by the MEDUSA network and by available EGELADOS and NOA stations. We pick all deep events with magnitudes $M \geq 3$, but due to the abundance of shallow events, we limit our inversion data set to shallow earthquakes with magnitudes greater than 4. All clearly visible *P* and *S* arrivals are picked in SEISAN (Havskov & Ottemöller, 1999), and a four-level quality rating is applied: (1) *clear impulsive*, (2) *clear emergent*, (3) *unclear emergent*, characterized by significant variations in apparent arrival depending on filter frequencies, and (4) *questionable arrival*, characterized by high noise levels, especially for *S* arrivals. We use these quality ratings to weight our picks in the subsequent relocation and tomographic inversion, that is, by 100%, 50%, 25%, and 12.5%, respectively. If possible, we pick these arrivals without filtering the seismograms, but weaker events often require a filter with corner frequencies between 2 and 15 Hz.

Our data set is supplemented with ISC- and NOA-published arrival times from other stations in Greece and Albania. These new data are selected by applying the following rules: (1) if picked by several agencies, the arrival times of one event at a given station must not differ by more than 1 s; (2) for two arrival times published within that range, we choose the earlier arrival; (3) for three or more arrival times we choose the median value. For a few publicly available permanent stations, we are able to compare our picks to the picks that other agencies sent to the ISC. Comparing absolute differences, we find that these *P* picks ($n = 1,041$) deviate on average by 0.45 s from our picks. Though this deviation may seem large, it is biased by picks associated with noisy events recorded at large offsets. And since these long-offset picks are automatically downweighted by the inversion (see section 3.2), the effective deviation on meaningful picks is in reality a lot smaller.

The robustness of the assembled arrival time picks is assessed through an initial set of hypocenter relocations computed in SEISAN with a standard 1-D background velocity model. At this stage, we use three criteria to further refine the events that will be used for tomographic inversion: (1) azimuthal ray coverage, (2) number of observations, and (3) size and shape of the error ellipse. We do not apply hard limits on each of these selection criteria, as this would restrict our data set to earthquakes located directly below densely instrumented areas. Instead, a more flexible selection helps us retain earthquakes located near the boundaries of the inversion domain, particularly those offshore toward the trench. These events may yield slightly larger hypocentral errors due to one-sided coverage, but they can considerably improve ray coverage in the deeper regions of the tomographic model (Koulakov et al., 2009). In general, we try to avoid earthquakes that yield gaps in azimuthal ray coverage greater than 180° but keep those for which all arrival time residuals were small (< 3 s) and the hypocentral depth estimate appears robust (i.e., resolved with a clear global residual minimum at this depth). This leads to a set of earthquakes with azimuthal coverage gaps that average 102.5°, in which only ≈13% have gaps larger 180°. All retained earthquakes are observed by at least eight stations, with an average of ≈28 stations per earthquake. Hypocentral errors are restricted to under 15 km and 20 km in the horizontal and vertical directions, respectively, and preferably below 10 km in both directions for earthquakes

AGU Journal of Geophysical Research: Solid Earth 10.1002/2017JB015154

that have comprehensive azimuthal coverage. After the event selection has been refined based on the three criteria, we reject arrival time picks that consistently yield data residuals > 5 s after several (usually 8) rounds of relocations and further data winnowing.

The resulting data set contains a total 42,512 picks (29,333 *P* and 13,179 *S* picks) of which 8,646 were picked and weighted in this study. These stem from 1,070 events, which include 104 deep events published by the ISC over the 1990–2006 period, 730 deep events published by NOA since 2008, and 235 ISC-published events observed by the MEDUSA network. Given the multiple sources of data, it is difficult to determine a consistent picking error that is useable to assess hypocenter errors in the subsequent analyses. Errors for our manual picks are on average <0.1 s and 0.2 s for *P* and *S* waves, respectively (i.e., based on Diehl et al., 2002). Thus, we choose the more conservative value of 0.2 s for all our picks to take into account the inclusion of ISC and NOA data. This value is deemed conservative because it is at the upper range of picking errors used in other comparable studies using similar inversion codes (0.03 s to 0.2 s; Eberhart-Phillips & Bannister, 2010; Reyners et al., 2006). Though it is smaller than the average difference of 0.45 s observed between some of our picks and ISC/NOA picks, the downweighting of long-offset observations should reduce this difference to below 0.2 s. Nevertheless, to ensure that we do not misrepresent our uncertainties, we later discuss how doubling this picking error affects hypocenter errors.

5. Resolution

In this study, resolution pertains to both the resulting velocity models and hypocenter locations. For the velocity models, we assess the resolution by conducting checkerboard tests and comparing the inversion results of two independent data subsets. Here we only discuss the checkerboard tests. The inversion results of independent data subsets (one based on our new picks and one based on data published by NOA since 2008) and their comparison to the final model are described in the supporting information (see Figures S4 and S5). This test demonstrates that the recovery of robust velocity features is independent of station setup, hypocenter distribution, and picking source. With regard to hypocenter locations, we measure how errors decrease progressively through the iterative relocation processes described in stages 1–3 of the section 3.

5.1. Checkerboard Tests

With the checkerboard tests, we assess how well an anomaly can be recovered as a function of its size, sharpness, and location within the inversion domain. Since this is the most commonly used resolution test in local earthquake tomography, the community has established standard guidelines. We follow those of Koulakov et al. (2009) whenever they are compatible with SIMULR16's input and output structure. We start by creating a series of models based on our final tomographic model, in which velocities are alternately perturbed by ±5% on grids of progressively decreasing mesh size, from 120 km × 120 km × 120 km to 30 km × 30 km × 30 km. We then calculate synthetic traveltimes from this perturbed velocity model. To these synthetic traveltimes, we add Gaussian-distributed random noise with a standard deviation of 0.2 s, our estimated picking error. Lastly, we invert for velocity structure and hypocenter locations using our final tomographic model without checkerboard perturbations as starting model.

The outcome of our resolution test is shown in Figure 2, where we display inversion results for the smallest grid sizes which recovers the checkerboard structure adequately, that is, 45 km × 45 km × 45 km for *P* velocities and 60 × 60 × 60 km for Vp/Vs ratio. These represent good estimates of the smallest structure we can expect to image robustly beneath western Greece. As shown in the depth slices of Figure 2, the well-resolved volume thins out with depth in regions where earthquake sources become confined to a narrow band. However, the amplitude of the velocity contrasts is recovered accurately down to depths of 80 km.

5.2. Hypocenter Error Estimation

Since each stage of our stepwise inversion approach (1-D inversion, 3-D inversion, and hypoDD) relocates hypocenters, we must start this section by discussing how the location uncertainties are computed in each case. This is important because there are slight differences in how hypocentral errors are calculated at each step. In general, the errors are estimated based on the solution misfit, that is, the traveltime residuals. These residuals include both picking errors and errors associated with unmodeled velocity structure, and there is no simple way to separate these two sources (Lienert & Havskov, 1995). Compared to the 1-D inversion, it is clear that the 3-D inversion reduces significantly the occurrence of unmodeled velocities and thus reduces their effects, while the double-difference scheme attempts to eliminate altogether the influence of the velocity model by computing the relative earthquake locations within clusters.

AGU Journal of Geophysical Research: Solid Earth 10.1002/2017JB015154

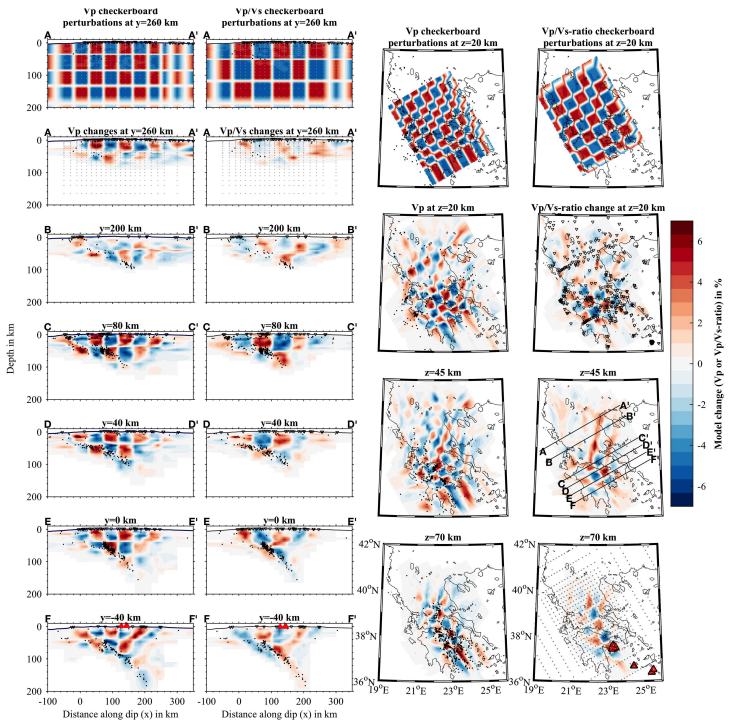

Figure 2. Checkerboard recovery test for *P* velocities and Vp/Vs ratios, shown along cross-sections A to F and at three horizontal depths slices. The uppermost row shows the input perturbations used for the calculation of the synthetic data. The inversion grid shown on cross-section A and depth slice for 70 km (small gray dots) is the same for all other sections. Station and cross-section locations are displayed on the z = 20 km and z = 45 km horizontal depth slices, respectively.

In all steps, the errors are calculated from the outer product of an SVD-derived general inverse operator and the estimated variance

$$e_i^2 = C_{ii} \cdot {\sigma_d}^2, \tag{3}$$

where e_i is the error of the i*th* parameter, C_{ii} is the outer product of an SVD-derived general inverse operator, and ${\sigma_d}^2$ is the data variance. What differs from one stage to the other is how the data variance is estimated. In the 1-D inversion, it is calculated a posteriori from the solution misfit (Lienert & Havskov, 1995)

$${\sigma_d}^2 = \frac{S^2}{(n-m)}, \tag{4}$$

where the solution misfit, S, is the sum of the weighted traveltime residuals, n is the number of observations, and m is the number of degrees of freedom. In the 3-D inversion, the data variance includes an a priori estimate based on the picking error in addition to the solution misfit (based on HYPOINVERSE; see Klein, 2002)

$${\sigma_d}^2 = e_{\mathrm{rd}}^2 + c_{\mathrm{err}} \cdot {\mathrm{rms}_d}^2, \tag{5}$$

where e_{rd} is the picking error, rms_d is the RMS of the weighted data residuals, and c_{err} is a weighting parameter (Klein, 2002) which allows to adjust the influence of errors due to unmodeled velocity structure.

AGU Journal of Geophysical Research: Solid Earth 10.1002/2017JB015154

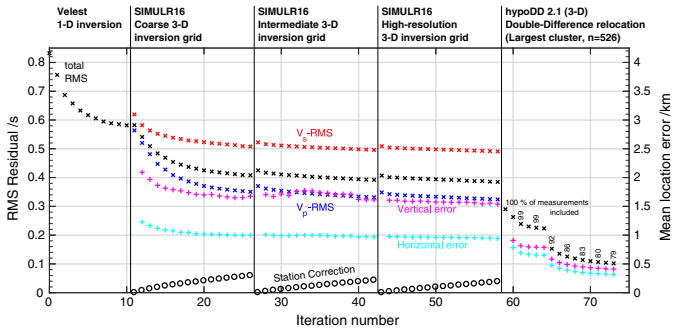

Figure 3. Reduction of root mean square (RMS) traveltime residuals and hypocenter errors for each iteration of 1-D inversion (stage 1), 3-D inversion (stage 2), and double-difference relocation (stage 3). The 3-D inversion is done for three successively denser grids, as discussed in section 3.2. Double-difference results are shown for the largest cluster of seismicity (n = 526 earthquakes) found by hypoDD. The percentages indicate the share of differential traveltimes that are included in each iteration of the hypoDD relocation.

Assuming that the 3-D inversion reduces that influence considerably, we choose a weighting parameter of 0.5 in accordance with Evans et al. (1999). This choice ensures that hypocentral errors still depend on how good the fit to the data is, while preventing reading errors to be mapped into the hypocentral error twice. In hypoDD, the variance is calculated solely based on the RMS of the weighted data residuals for differential traveltimes (Waldhauser & Ellsworth, 2000).

Taking into account these definitions of hypocentral relocation errors, we find that our errors are reduced by approximately an order of magnitude from ≈7 km at the outset of stage 1 to ≈500 m for the best resolved cluster at the end of stage 3 (see Figure 3). The initial error is already quite small owing to our strict selection of well-locatable earthquakes for tomography. From Figure 3, we observe that the errors are reduced by approximately 25% in the 1-D inversion (stage 1), 25% in the three stages of 3-D inversion (stage 2), and a further 50% in the double difference relocation. It is important to note here that the hypocenter catalog obtained at the end of the 3-D inversion provides absolute locations, which allows us to assess where the earthquakes occurred relative to the main structures of the system (e.g., subduction interface, subducted Moho). Double-difference relocation, on the other hand, improves the relative hypocenter accuracy and gives us an idea of the finer structures (e.g., active faults) along which these earthquakes occur.

As described in equation (4), the hypocenter errors calculated in the 3-D inversion depend on an assumed picking error, which we set at 0.2 s based on our manually picked arrivals and previous applications of the SIMULR package (see section 4). But since there are inconsistencies >0.2 s between our manual picks and ISC/NOA picks, we must assess the effects of considering larger picking errors. We find that a doubling of the picking error results in hypocentral errors 1.5–2 times larger than those presented above. At the end of the 3-D inversion, the estimated hypocentral errors for e_{rd} = 0.2 s are 1.5 km in the vertical direction and 1 km in the horizontal direction, which would be doubled to 3.0 km and 2.0 km for e_{rd} = 0.4 s. However, even with these conservative estimates, we should be able to determine where the earthquakes occurred relative to the main structures of the system, which are resolved with a similar degree of resolution by teleseismic scattered wave imaging (Pearce et al., 2012; Suckale et al., 2009).

6. Inversion Results

In this section, we first describe the new 1-D velocity models of the WHSZ generated by our analysis and compare them to our starting 1-D model. Then, we present the 3-D velocity models and relocated hypocenters for western Greece, focusing on the features that are deemed robust based on our resolution tests (see section 5.1 and supporting information).

AGU Journal of Geophysical Research: Solid Earth 10.1002/2017JB015154

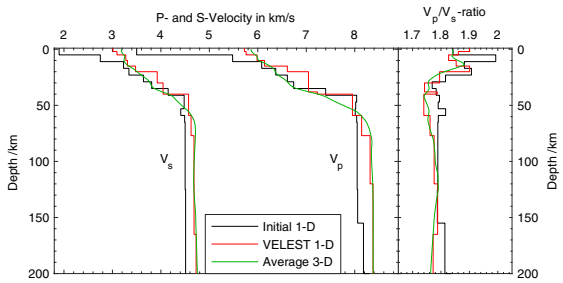

Figure 4. Comparison of 1-D velocity models. "Initial 1-D" denotes the initial model based on the model of Haslinger et al. (1999) for the crust and the AK135 model (Kennett et al., 1995) for depths below 45 km. "VELEST 1-D" is the final model based on the 1-D inversion done with program VELEST (Kissling et al., 1994) in stage 1. "Average 3D" is a 1-D velocity model constructed by taking a depth-averaged model through the final 3-D velocity model obtained at the end of stage 2.

6.1. Velocity Inversion

6.1.1. One-Dimensional Velocity Models

Our analysis workflow generates two new 1-D velocity models for the study area: (i) a layered model obtained by the 1-D inversion in VELEST at stage 1 and (ii) a model calculated by averaging velocities within depth slices through the final 3-D velocity model obtained at stage 2. These new models are plotted in Figure 4, in conjunction with the starting 1-D model that was used for the inversion (see section 3.2). Compared to the starting model, our new layered 1-D velocity model exhibits more pronounced velocity gradients at layer boundaries, especially at 15 km to 20 km and 38 km to 40 km depths, with velocities that are greater in the upper crust and comparable in the lower crust. Velocities in the upper mantle are 3% to 7% higher than those from the AK135 model, something that might be due to the existence of a cold (i.e., fast) dipping slab across a large portion of the imaged volume. For its part, the depth-averaged 1-D model tends to follow more closely the starting model in the crust and the new 1-D layered model in the mantle (with velocities higher than AK135). But in contrast to both the starting and the new 1-D layered models, the depth-averaged model is very smooth, reflecting the fact that it averages over laterally variable structures associated with the subduction system.

6.1.2. Three-Dimensional Velocity Models

The results of our 3-D local earthquake tomography of western Greece are presented as trench-normal vertical sections (A-A′ to F-F′, Figures 5 and 6) and horizontal depth slices (15 to 80 km depth, Figures 7 and 8) through the final Vp and Vp/Vs ratio models (a set of trench-parallel sections is also shown in Figure S6 of the supporting information). The Vp model shows a dichotomy between a low-velocity upper layer representing generally the overriding crust (top layer, 0 km to 40–60 km, Vp< 7.5 km/s) and a high-velocity lower layer representing the mantle (bottom layer, Vp> 7.8 km/s on average). The interface between crust and mantle is not as clear in the Vp/Vs model, but the upper crust exhibits generally higher Vp/Vs ratios (1.85 to 1.95). Five outstanding features of interest in the velocity models are marked with roman numerals I–V in Figures 6–8.

1. A localized thickening of the top layer down to ≈60 km depth within the collision zone, with a rapid thinning to ≈35 km depth on both sides. North of the KTF (cross-sections A and B), this feature appears to be offset by 40 km toward the backarc relative to its southern counterpart (c.f., cross-sections C-F).
2. A low-Vp (7.0–7.8 km/s) layer dipping at 20° toward the NE and extending from 40 km to up to 90 km depth. This low-Vp layer appears most clearly in the center of the imaged domain (sections C-E) but is generally visible in all the cross sections. To the north, the velocity contrast marking the top of the layer becomes less sharp, but the bottom of the layer remains clearly demarcated from the underlying higher-velocity mantle (see, e.g., Figure 6 B). Below the central and southern Peloponnesus (6 E-F), the low-Vp layer appears somewhat interrupted at 60 km depth.

AGU Journal of Geophysical Research: Solid Earth 10.1002/2017JB015154

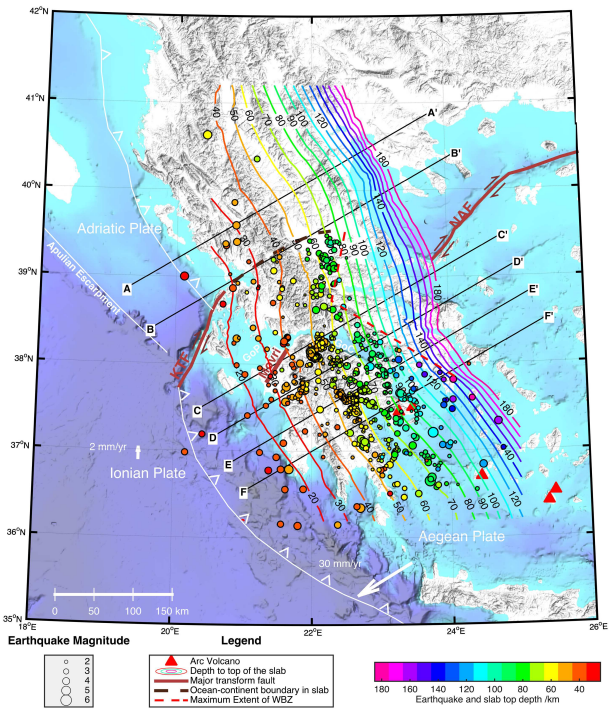

Figure 5. Map of mainland Greece and the Western Hellenic Subduction Zone showing the locations of cross sections and relocated hypocenters. Parallel black lines with labels A-A′ to F-F′ indicate the locations of the cross sections through the final 3-D velocity models shown in Figure 6. Colored circles represent earthquakes with depths greater than 25 km that were relocated in this study. The circles are color coded by depth, and their size is proportional to earthquake magnitude. See legend for the description of other symbols and lines.

3. A high-Vp (8.4 km/s to 8.9 km/s) dipping layer directly underlying the low-Vp dipping layer described in the previous point. This layer is observed from 50 km to 180 km depth and appears to extend beyond the bottom of the imaged volume.
4. A low Vp/Vs ratio anomaly (down to ≈1.64) located mainly in the lower part of the overriding crust, with some excursions into the mantle wedge and upper crust. It stretches 75 km from the suspected plate interface toward the arc and is ≈15 km thick where sharply imaged. The contrast between the anomaly (low Vp/Vs) and the upper crust (high Vp/Vs) is greatest below the northwestern Peloponnesus (Figure 6 C and D).
5. A high Vp/Vs ratio anomaly (up to ≈1.85) located just above the WBZ in the southern sections (C-F). The feature has the largest amplitude in section E, below the central Peloponnesus, and extends all the way to the southern boundary of the study area.

Features VI–VIII are addressed in the description of hypocenters and in section 7.

6.2. Hypocenters

The earthquakes that were relocated beneath the WHSZ as part of this study are shown in Figure 5 (full set in map view), Figure 6 (subsets in cross sections), and Figures 7 and 8 (subsets in horizontal depth slices).

AGU Journal of Geophysical Research: Solid Earth 10.1002/2017JB015154

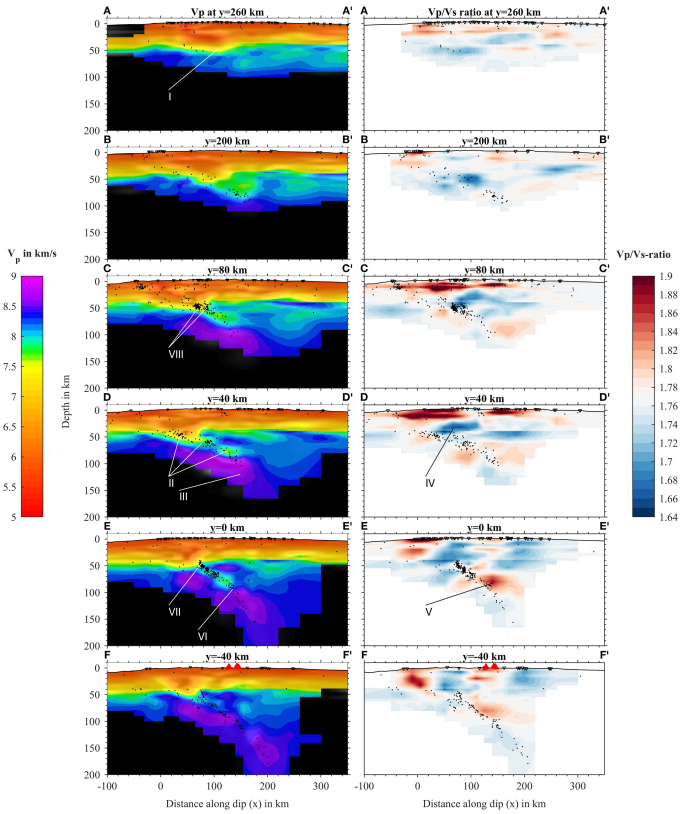

Figure 6. Cross sections through the final 3-D Vp and Vp/Vs ratio models. Locations of the cross sections are indicated in Figure 5, and the reference axes for the coordinate system (*x*,*y*) are shown in Figure 1. Black dots represent relocated hypocenters at two different stages of the analysis: the left column shows hypocenters after double difference relocation (stage 3), whereas the right column shows hypocenters after 3-D inversion of traveltimes (stage 2; see Figure S2 for a further comparison of hypocenters during each stage).

All these maps and cross sections show earthquake locations obtained at the end of stage 3 in our analysis workflow (i.e., double-difference relocation), except for the cross sections in the right column of Figure 6, which shows earthquake locations obtained after stage 2 (3-D inversion). The reason for showing hypocenters from stages 2 and 3 side by side is to assess the improvements associated with double-difference relocation (all incremental differences from before stage 1 to after stage 3 are described in the supporting information, with Figure S2 showing earthquake locations and hypocentral errors from each stage). When comparing the left and right columns of Figure 6 (see also Figure S2), we note that the improvements in relocation due to hypoDD relocation are subtle, that is, the overall hypocenter distribution looks very similar compared to stage 2, but closer inspection reveals that the double-difference relocation tends to collapse clouds of earthquakes into more confined planes of seismicity (likely representative of faults).

AGU Journal of Geophysical Research: Solid Earth 10.1002/2017JB015154

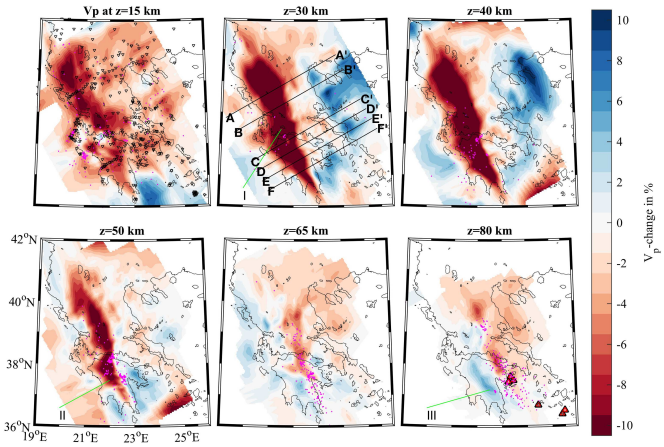

Figure 7. Horizontal depth slices through the final 3-D Vp model with superimposed seismicity. Magenta dots indicate hypocenters relocated by double difference within each depth slice. Black lines mark the locations of the cross sections shown in Figure 6, for comparison. The large, coherent low-velocity feature is interpreted as the subducting crust dipping toward the NE. It is deformed at 38°N, probably due to a higher rate of rollback in the south compared to the north. Here we chose to plot velocity perturbations to highlight imaged structures. For direct comparison with cross sections, depth slices showing absolute *P* velocities are presented in Figure S7 of the supporting information.

From Figures 5 and 6, we note that the relocated earthquakes form a relatively narrow dipping band which follows the expected path of the subducted slab and thus outlines a well-defined WBZ in the southern portion of the system. This WBZ reaches a maximum depth of 185 km in the south, beneath the Cyclade Islands. In this southern part of the model, there is an apparent bend in the WBZ at 80 km, marking a dip increase from 20° above to 60° below (see feature VI in Figure 6). Simultaneously, the WBZ becomes thinner below that bend. Moving northward, the lower end of the WBZ rises progressively to a minimum depth of 60–70 km beneath a region encompassing the Gulf of Corinth and the Northern Gulf of Evia, before it plunges again toward the north, forming a V-shaped gap in deep seismicity (see red dashed line in Figures 5 and 11). Below this central region, the WBZ also appears to migrate slightly toward the backarc from south to north (compare profiles C and B in Figure 6). We observe a possible bend of the WBZ at ~60 km depth in profile C (i.e., shallower than to the south), but this feature is not well constrained due to the limited number of earthquakes outlining the deeper segment of the WBZ. Farther north, the well-defined WBZ disappears almost completely and quite abruptly along a SW-NE line coinciding with cross-section B in Figure 5. Beyond this point, only a handful of intermediate depth events have occurred during the time period of our study.

Within the region where the WBZ is well defined, two earthquake clusters stand out from the general intraslab seismicity. The first cluster is located directly below the southern receiver function migration line (feature VII, in section E of Figure 6). In this cluster, earthquakes form a rough plane that has a dip of ≈60° and extends above the low-velocity layer, between 40 and 60 km depth. There is very little intraslab seismicity trenchward of this cluster. The second cluster is located beneath Leontio in the northern Peloponnesus (feature VIII, in section C of Figure 6). This cluster is more cloud shaped than the first one and appears to be divided into two subclusters. It has a height of 20 km, a width of 30 km, and extends from 40 km to 60 km depth. We also note that it is located near the apex of the V-shaped seismicity gap discussed above (see Figure 5).

7. Discussion

In this section, we interpret our velocity models and relocated earthquakes in conjunction with previous seismic results obtained in the region. We rely particularly on constraints provided by the high-resolution 2-D

Journal of Geophysical Research: Solid Earth 10.1002/2017JB015154

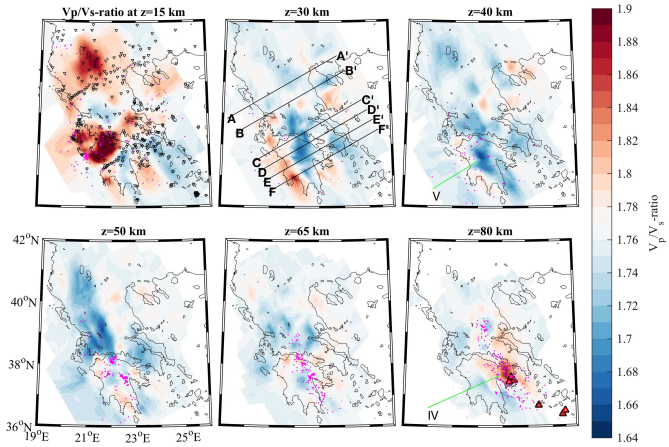

Figure 8. Horizontal depth slices through the final 3-D Vp/Vs ratio model with superimposed seismicity. Magenta dots indicate hypocenters relocated by double difference within each depth slice. Black lines mark the locations of the cross sections shown in Figure 6, for comparison. The high Vp/Vs ratio anomaly centered below the Saronic Gulf at 80 km depth might represent hydrated, partially melted material in the mantle wedge which feeds the overlying volcanic arc (red triangles). Regions of low Vp/Vs ratios occur in the overriding forearc crust (see, e.g., anomaly labeled V), especially to the north of 38°N (at 50 km depth).

images from scattered teleseismic waves, obtained by Suckale et al. (2009) and Pearce et al. (2012) with an inversion technique based on the Generalized Radon Transform (GRT-RF). Side-by-side comparisons and maps integrating the various results are shown in Figures 9–11. Figure 9 shows both the tomographic Vp model and GRT images, which we remigrated with the depth-averaged 1-D velocity model from this study (Figure 4). Compared to the previous images of Pearce et al. (2012), the only change is an upward shift of the slab structure by up to 3 km. From the tomographic models, the GRT-RF images, and from the 3-D receiver function

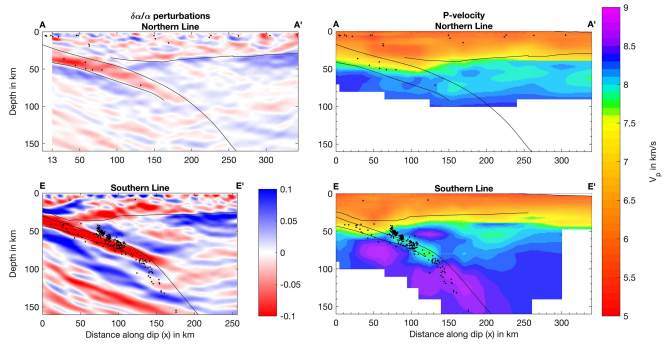

Figure 9. Comparison of Generalized Radon Transform images (Pearce et al., 2012) and tomographic models along the northern and southern lines of the MEDUSA experiment. Only *P* wave scattering potential ($\delta\alpha/\alpha$) and *P* velocities are plotted, together with earthquakes relocated by double difference. The black solid lines indicate the interpreted overriding Moho, slab top, and subducting Moho.

AGU Journal of Geophysical Research: Solid Earth 10.1002/2017JB015154

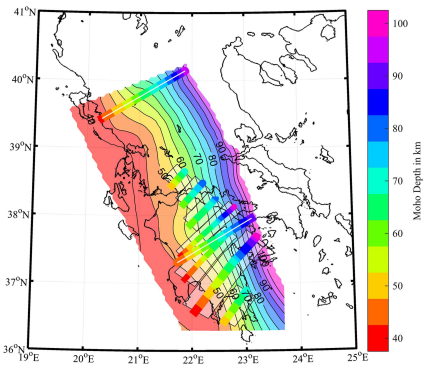

Figure 10. Depth contours of the subducted Moho from 3-D tomography and comparison with previous receiver function studies. The background contours and color map indicate the depth to the subducted Moho from our resulting 3-D Vp model. The light, transparent boxes overlaying the base map show subducted Moho depths from the 3-D receiver function study of Sachpazi et al. (2016), while the boxes with white lines (one in the south and one in the north) show the subducted Moho depth from the Generalized Radon Transform images of Pearce et al. (2012). A comparison of the various results reveals deviations that are generally less than $\pm 5km$, except for a few receiver function profiles from Sachpazi et al. (2016) which show a subducted Moho that is ≈10 km deeper beneath the Gulf of Corinth.

study of Sachpazi et al. (2016), we picked both the subducting Moho and the slab top (where possible). In Figure 10, we show that the new estimate of the subducting Moho fits these studies within approximately 5 km (vertically). Figure 11 depicts a common model of the subduction interface geometry in 3-D. We then interrogate these integrated seismic models to gain new insight into the relationships between the ocean-continent transition and the structure, dynamics, and seismicity of the WHSZ.

7.1. Subducting Crust and Seismicity

We interpret the dipping low-velocity layer observed across our models (Feature II; see section 6) and the GRT profiles as the hydrated, basaltic oceanic crust. We note that the tomographically derived velocities of 7.0 km/s to 7.8 km/s may seem high for hydrated oceanic crust, but they probably represent lower velocities that have been smoothed and smeared by the tomographic inversion. The layer disappears at a maximum depth of 90 km, where the crust likely transforms into eclogite. During eclogitization, the subducting crust loses its velocity contrast in comparison with the underlying subducting mantle and the overlying mantle wedge (Figure 6, features II and V). The apparent termination depth of 90 km is very similar to that found by Pearce et al. (2012) and Sachpazi et al. (2016), where the subducting crust or Moho, respectively, could be imaged to about 100 km depth. Below this depth, earthquake hypocenters occur along a much steeper trend of 60°. This agrees well with the results of Papazachos et al. (2000) where a bend in the WBZ is inferred at 100 km depth. Imaging this bend in the slab structure has proved challenging, as shown by both the weak recovery of velocity contrasts below 90 km in this study and the RF studies of both Pearce et al. (2012) and Sachpazi et al. (2016). The velocity contrast along a steeply dipping slab is hard to recover with RF techniques due to the conflict between the limited aperture of the seismometer arrays and the wide-angle conversions along steeply dipping features (MacKenzie et al., 2010). While Sachpazi et al. (2016) place the slab bend at 60 km depth, Pearce et al. (2012) do not capture any bend in the slab down to the termination of the LVL at 100 km. Although recovery of structures through tomography is also hampered at this depth due to the ray coverage and source distribution (as shown by the checkerboard tests), our images do show a velocity contrast following the steepening trend of the WBZ down to 150 km depth and beyond. This increase in velocity from the mantle wedge to the slab across this trend suggests that we do recover some slab structure reflecting the eclogitized crust below 90 km. Thermal-petrological models predict that the basalt-eclogite transition occurs over a large depth range (van Keken et al., 2012) so we would perhaps expect a more progressive fading of the LVL here. However, imaging a thinning and hydrated subducting crust is challenging when the slab steepens at the same time.

Previous regional and teleseismic tomographic models (Koulakov et al., 2009; Piromallo, 2003; Spakman et al., 1988; Zhu et al., 2015) suggest a general slab dip of 45° below 100 km. This contrasts with our observation of the 60° dip for the deep part of the WBZ. While the thinning and steepening of the WBZ may be due in part to the bending of the slab, it also suggests that seismicity follows a path that is deeper in the slab and oblique to the subduction interface at this depth. This path could follow the phase boundary between blueschist and eclogite, which can result in a thinning of the seismic zone as shown by van Keken et al. (2012). Upon complete eclogitization of the crustal material, there is much less fluid available beyond that depth, which limits the potential occurrence of dehydration embrittlement and associated intermediate depth earthquakes (see Figure 12). The shape of this phase change is a result of the subducting crust being heated from the top; thus, material closer toward the bottom of the subducting crust only reaches the temperatures required for the phase transition at greater depths. It is not perfectly understood why the steepening of the slab occurs at eclogitization depth, but this phenomenon has been observed in many subduction zones and may be related to the sudden density increase at that depth (Klemd et al., 2011). While the thinning of the WBZ occurs over a depth range between 80 km and 180 km in the south, this depth range is much shorter north of the Gulf of Corinth: instead of thinning out, seismicity is more intense at a depth of 90 km. This clustering of the deepest intermediate depth seismicity has been observed in Japan, where Nakajima et al. (2013) postulated

Journal of Geophysical Research: Solid Earth 10.1002/2017JB015154

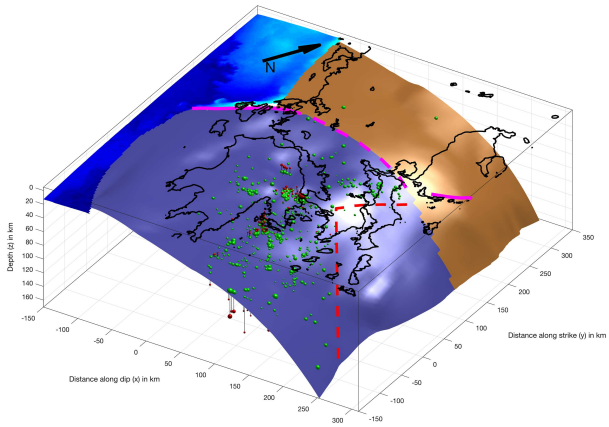

Figure 11. Three-dimensional block model of the subduction interface and seismicity based on the results obtained in this study. The subducting oceanic crust of the Ionian plate is dark blue, while the subducting continental crust of the Adriatic plate is in brown. Variable shading on the interfaces represents relief, with oblique illumination from a light source to the right of the model. The magenta solid lines mark large strike-slip faults, including the Kephalonia Transform Fault and the western tip of the North Anatolian Fault. The magenta dashed line marks the putative boundary between oceanic and continental slabs based on the contrast in seismicity (though apparent changes in the slab's tomographic response could also be used to constrain this boundary, we refrain from doing so as there is a progressive change in resolution associated with the contrast in seismicity between north and south; see Figure 2). Relocated hypocenters are indicated by red spheres, with size corresponding to magnitude. The green spheres are hypocenters projected onto the slab top surface. Red dashed lines indicate the outline of a V-shaped seismic gap believed to be associated with a broad zone of deformation in the oceanic slab.

that the cause may be the differential stresses induced through the volume change which accompany the basalt-eclogite transition. These different styles in the termination of the WBZ across the study region likely show that the thermal state of the subducting crust varies considerably between the south and north.

Earthquakes in this region occur along a thin, single-planed WBZ (instead of a double seismic zone) and are largely restricted to the southern part of the system. Nearly all the earthquakes map directly into the low-velocity subducting crust. Seismicity within the subducting mantle is nearly absent, but a few such events do occur in the south of the imaged domain (Figure 6 cross-section F). In this region south of mainland Greece, biased station coverage might have caused an increase in depth errors. If these are true mantle earthquakes, occurring below the main plane of seismicity within the subducting crust, this second plane would be offset by only ≈12 km. Since double seismic zones are generally expected to have a separation distance of more than 35 km (Brudzinski et al., 2007) for a plate age such as the Ionian of 230 Ma (Speranza et al., 2012), we assume that the WBZ in our study region consists of only one plane of seismicity (equivalent to the upper plane of a double seismic zone).

Along strike of the subduction zone, seismicity decreases abruptly toward the north, along a trench-perpendicular line extending from the KTF toward the backarc (see map of relocated seismicity in Figure 5). Deep earthquakes are nearly absent north of that line. However, there are a few robustly located earthquakes that occur between 40 km and 70 km depth in the Adriatic subducting crust (see the nine earthquakes with depths >40 km observed north of line B-B′ in Figure 5). The existence of these earthquakes lends independent support to mounting evidence that active subduction is currently taking place north of the KTF. As the KTF marks the boundary between drier continental crust in the north and wetter oceanic crust in the south, we can further hypothesize that the difference in composition and metamorphic state of the subducting crusts might be responsible for the aseismicity in the north. The GRT image in Figure 9 A shows

AGU Journal of Geophysical Research: Solid Earth 10.1002/2017JB015154

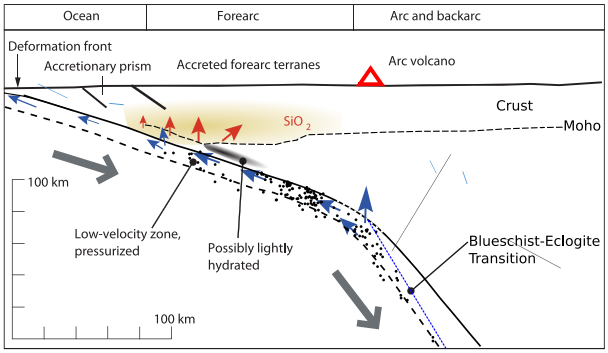

Figure 12. Conceptual model of quartz enrichment in the overriding lower forearc crust in Greece, after the model proposed for Cascadia by Audet and Bürgmann (2014). Compared to Cascadia, the Western Hellenic Subduction Zone is a much colder subduction zone. That means that the subducting crust is dehydrated and transformed to eclogite at larger depths. It also leaves a larger piece of intact, impermeable subduction interface to guide fluid migration to the forearc. Thus, less mantle wedge hydration and more quartz enrichment in the forearc occur.

that the low-velocity layer extends to 90 km depth (as imaged by *P* wave scattering potential), some 20 km below the deepest earthquakes in the north. That could imply that unmetamorphosed crust is stable to depths beyond where earthquakes occur, possibly because there is not enough water to facilitate prograde metamorphism (Austrheim, 1987) and trigger earthquakes.

The two intense clusters of seismicity (Figure 6 features VII and VIII and Figure 9) that stand out above the average WBZ seismicity are striking, because they seem to occur within and up to 15 km above the subducting Ionian crust (see Figure 6 C, E). This would mean that some of these earthquakes occur in the mantle wedge, which is not expected from the current models for intermediate depth seismicity. Even though the mantle wedge is usually assumed aseismic, we note that earthquakes within the mantle wedge have been discussed in Japan (Uchida et al., 2010) and New Zealand (Davey & Ristau, 2011). In Japan, it has been suggested that earthquakes occur in detached, subducted seamounts (Uchida et al., 2010). In New Zealand, it has been hypothesized that earthquakes are associated with the boundary of the serpentine stability field within the mantle wedge (Davey & Ristau, 2011). At this point, we are unable to say whether these clusters indicate one or another of these processes, but the matter is the subject of ongoing work.

7.2. Fluid Flux and Metasomatism

Now that we have established where the dehydration and eclogitization of the slab occur based on our Vp models; we can look into what happens to the released fluids and the effect they have on the composition of the mantle wedge and the forearc crust. To do this, we focus on Vp/Vs images, as these are particularly sensitive to variations in porosity, fluid/melt content, and fluid pressure (Unsworth & Rondenay, 2013).

7.2.1. Evidence for Free Fluids or Melt

High Vp/Vs ratios are indicative of water-rich fluids or melts. We find a high Vp/Vs ratio in one location in the subarc mantle wedge, clearly limited to along the strike of the subduction zone (Figure 6 V). Within this part of the subduction zone, right above the slab at 80 km depth, the Vp/Vs ratio increases to 1.86 from an average of 1.77. This anomaly coincides with the disappearance of the low-velocity subducting crust (II) and the bend of the WBZ (VI) throughout the southern part of the slab. The variable amplitude of this anomaly along strike of the WHSZ suggests that dehydration and fluid flux vary strongly along strike as well. As the Quaternary volcanic arc of the WHSZ does not continue north of where the anomaly appears strongest, we suspect a possible correlation between the amount of slab dehydration and volcanism in this area. However, we do note that active eclogitization reflected in deep earthquake clusters also occurs farther north, which would release

AGU Journal of Geophysical Research: Solid Earth 10.1002/2017JB015154

fluids in areas where we do not image high Vp/Vs anomalies. We do not know what happens to these fluids in the north; they are possibly released at depths where the mantle wedge is too cold to allow melting, but both the hydration of the cold mantle wedge corner and updip migration through the subducting crust are possible scenarios.

7.2.2. Hydration of the Mantle Wedge Corner

Where temperatures are too low for dehydration-derived fluids to fuel melting below the arc, fluids might either hydrate the cold mantle wedge corner or migrate farther updip. During hydration of the cold mantle wedge corner, chlorite and serpentine in particular are formed. These exhibit high anisotropy, low density, low seismic velocities, and high Vp/Vs ratios in comparison to mantle peridotite.

Evidence for serpentinization has been found for the cold corner of the Hellenic mantle wedge (Olive et al., 2014; Sodoudi et al., 2015). But unlike more extreme cases such as Cascadia, where serpentinization is so extensive that it causes an inversion of the Moho seismic impedance contrast (Bostock et al., 2002), the WHSZ exhibits only moderate signs of serpentinization. Indeed, the GRT images of Suckale et al. (2009) and Pearce et al. (2012) found only a small weakening in the Moho's signal above the mantle wedge beneath the Peloponnesus. The pattern of seismic anisotropy within the backarc that Olive et al. (2014) recovered supports at least a thin layer of serpentine at the top of the subducting crust. Our results show low velocities only within the very tip of the mantle wedge when we assume the wedge's location from Pearce et al. (2012; see Figure 9). The resolution of our tomography is likely inferior to the GRT images, and the low velocities could be smeared between the thickened overriding crust and the subducting crust. However, the Vp/Vs ratio shows locally pronounced, low values of 1.65 within the lower overriding crust, stretching into the cold corner of the mantle wedge. These low Vp/Vs ratios are not compatible with a dominant presence of serpentine, and neither is *P* velocities above 8 km/s, which are typical of mantle peridotite. The high velocities thus indicate a rather dry mantle wedge corner. This fits well with a recent estimate of less than 5% mantle wedge hydration for the Hellenic, and many other comparable subduction zones, based on their water budget (Abers et al., 2017).

7.2.3. Silica Enrichment of the Lower Forearc Crust

In our tomographic model, the low Vp/Vs feature (Figure 6 IV) extends from the subduction interface toward the arc, suggesting that the lower crust has been altered by subduction-derived material. With its low bulk Vp/Vs ratio and Poisson's ratio, quartz is the most likely abundant mineral to explain an exceptionally low bulk Vp/Vs ratio over such a large region (Hyndman et al., 2015). This kind of silica enrichment has been proposed based on similar tomographic evidence for the Cascadia subduction zone by Ramachandran and Hyndman (2012). According to the conceptual model of Audet and Bürgmann (2014) and Hyndman et al. (2015), large quantities of quartz (possibly even its β phase) are precipitated in veins in the lower overriding crust by fluids that are derived from the subducting crust and migrate updip. This updip migration path may be particularly favored over migration to the mantle wedge in the case of an undamaged, impermeable interface. Precipitation is thought to occur at the interface between the subducting and overriding crust, which exhibits a higher permeability than the deeper subduction interface below the mantle wedge. A possible field analog has been described by Breeding and Ague (2002) in New Zealand. There, large amounts of quartz have been precipitated in veins in a comparable, now exposed, forearc environment.

How much silica can be transported depends on silica solubility, which is controlled by temperature. An aqueous fluid in equilibrium with quartz-bearing rocks contains more silica at high temperatures than at low temperatures (Manning, 1994). But the source of quartz is uncertain. For Cascadia, Hyndman et al. (2015) suggest that both metamorphosed silt- and sand-rich rocks and metamorphosed basalts might provide soluble quartz. In comparison to unaltered basalt, metamorphosed blueschists can contain modal quartz together with low-silica minerals, according to Peacock (1993).

If the anomalous Vp/Vs ratio in the lower overiding forearc crust does indeed represent a region of silica enrichment, then it would be a considerably larger volume than has been inferred in Cascadia by Audet and Bürgmann (2014), Hyndman et al. (2015), and Ramachandran and Hyndman (2012). In the WHSZ, the low Vp/Vs ratio spans a region of up to 80 km between subduction interface and toward the arc rather than half that size as conceptualized for Cascadia. Requiring dehydration-derived fluids for the silica transport, this large area of quartz deposition in the WHSZ conflicts with the interpretation of little fluid transport to, and little hydration of, the cold mantle wedge corner.

AGU Journal of Geophysical Research: Solid Earth 10.1002/2017JB015154

Two causes might help explain this discrepancy of large amounts of precipitated quartz, but low mantle wedge hydration in the WHSZ (see sketch in Figure 12).

1. The WHSZ possesses an unusually large sedimentary prism, with 8 km of sediments on top of the crystalline oceanic crust, compared to a global average of 3.5 km for accretionary subduction zones (Clift & Vannucchi, 2004). Combined with a larger-than-usual thickness of subducted sediments (1 km compared to a global average of 0.3 km; Syracuse et al., 2010), there is a large source for quartz solution available. This source is notably larger than in the Cascadia subduction zone, where 2 km of sediments lies on top of the subducting plate and 0.4 km of sediments is subducted (Syracuse et al., 2010).
2. Estimates of the amount of hydration in the mantle wedge corner and of silica transport assume only vertical migration of dehydration-derived fluids. In reality, fluids might migrate considerable distances updip within the subducting crust due to an impermeable plate interface. The plate interface might be sealed where it is unaffected by metamorphic reactions that are accompanied by volume changes—particularly the blueschist to eclogite transition. In Cascadia (a hot subduction zone end member with profound mantle wedge hydration), these metamorphic reactions occur at much shallower depths and closer to the cold mantle wedge corner than in the colder WHSZ. The weak, shallow subduction interface could allow fluid migration to the cold mantle wedge in Cascadia. Meanwhile in Greece, fluid migration might be prohibited by an intact seal formed by a low-permeability plate interface reaching down to greater depths. Thus, less mantle wedge hydration but more silica transport might still be compatible.

We thus argue that fluids fluxed from the subducting oceanic crust may have transported silica to the overriding forearc crust of the WHSZ. This might have a strong effect on the rheology of the plate interface: Audet and Bürgmann (2014) showed that short recurrence intervals of episodic tremor and slip correlate with high Vp/Vs ratios in the forearc crust. Based on this relationship, we expect that episodic tremor and slip behavior would exhibit short recurrence intervals in the WHSZ. Future research will need to evaluate this prediction, as no episodic tremor and slip has been observed in the WHSZ to date.

7.3. Transition Between Continental and Oceanic Slab

Both our tomographic images and the relocated hypocenters shed light on the characteristics of the transition between oceanic subduction in the south and continental subduction in the north. These new observations, in conjunction with results from previous imaging studies, suggest that there is a sharp transition in crustal type below the KTF at depth but that the zone in which the slab is deformed due to differential rollback between south and north stretches over an area spanning the whole Central Hellenic Shear Zone (CHSZ). Here we will discuss the likely mechanisms of slab deformation in the WHSZ. We base this discussion in Figure 10, which shows the depth contours of the subduction interface, and Figure 11, which shows the spatial relation between the subduction interface and seismicity in a 3-D model.

7.3.1. Is There a Trench-Parallel Slab Tear?

A trench-parallel slab tear propagating from the north to the south has been suggested by mantle-scale tomography studies, which diffusely imaged an intermittent slab in the north (e.g., Bijwaard et al., 1998; Koulakov et al., 2009; Spakman et al., 1988; Zhu et al., 2015). The disturbance appears at a range of depths: in Spakman et al. (1988), the anomaly is discontinuous at 180 km to 250 km depth, in Koulakov et al. (2009) at 300 km to 500 km depth, and in the EU60 velocity model published by Zhu et al. (2015) at 200 km to 400 km depth. The *P* wave model of Piromallo (2003) does not show a disturbance. Spakman et al. (1988) suggest that the tear reaches the southern Peloponnesus in their model, while the model of Zhu et al. (2015) suggests that the tear affects the slab north of Greece. Based on their tomographic results, Wortel and Spakman (2000) discussed the development of slab detachment and the propagation of trench-parallel tears in the Mediterranean as a necessary consequence of the Tethys closure. They suggest that a slab tear is propagating from the north to the south, which would fit in well with the current understanding of a light, continental crust withstanding subduction in the north and a dense oceanic slab pulling in the south (Royden & Papanikolaou, 2011).

Although our tomographic study does not reach the depths of the inferred tear, we can look into our results to see if any observations are consistent or inconsistent with the presence of such a tear. Hypothetically, the termination of slab seismicity could mark the location where the deeper slab has been detached. Detaching the slab would remove slab pull forces which might be required for intraslab earthquakes. With the disappearance of slab pull, rollback should stop where the slab is detached—which is the case in northern Greece.

AGU Journal of Geophysical Research: Solid Earth 10.1002/2017JB015154

However, the pattern of intermediate depth earthquakes and the geological history of the KTF are not consistent with being directly affected by a trench-parallel slab tear. First, seismicity within the subducting crust up to the KTF is well distributed, while one would expect to find earthquake clusters and swarms in regions where the slab tear is propagating (Meighan et al., 2013). Neither seismicity, focal mechanisms nor a σ_3-axis subparallel to the slab dip (Rontogianni et al., 2011) indicates an anomalous stress field that could be associated with the tip of a slab tear. Second, the proposed location of the tip of the slab tear (Spakman et al., 1988) is not located at the KTF. If tearing was an ongoing process that affected stress and strain in the slab, one would expect a southward migration of shallow deformation simultaneous with the tear propagation. The KTF has been active for the last 8 Myr, so it seems unlikely that shallow deformation has been affected by a southward propagation of a slab tear.

Even though our results cannot directly confirm or refute the hypothesis of a trench-parallel slab tear, a tear is not necessary to explain the observations within the seismically active part of the slab, especially the termination in seismicity across the KTF, which could be due to petrological changes instead.

7.3.2. Is There a Trench-Perpendicular Slab Tear?

A trench-perpendicular, vertical slab tear along the continuation of the KTF has previously been hypothesized based on the trench offset (Govers & Wortel, 2005; Royden & Papanikolaou, 2011; Suckale et al., 2009). Royden and Papanikolaou (2011) suggest that a slab tear is the cause of dextral strike-slip plate movement at the KTF. They attribute the differential plate movement to denser oceanic crust rolling back at a higher rate south of the KTF compared to lighter, more buoyant continental crust resisting rollback in the north. However, our tomographic models do not support a trench-perpendicular slab tear in the upper 100 km, an observation that is consistent with the conclusions of Pearce et al. (2012). Although our relocation study reveals a sharp termination of seismicity in the slab at the KTF, there is no noticeable offset marking a tear between the subducting crust just to the south and the north of the KTF (see the slab top model in Figure 11).

This observation is consistent across our tomographic models, the high-resolution images from 100 km north of the KTF (Pearce et al., 2012), and in the distribution of hypocenters contained in the subducting crusts.

7.3.3. Deformation of the Slab

Based on our observations, it appears that the deformation between subducting oceanic and continental crusts is widely distributed rather than occurring along a discrete fault. There are indeed a number of features in our models that point to a broad zone of deformation within the slab south of the KTF, instead of a vertical tear at the KTF.

First, there is a gradual offset in the position of the subducting crust and hypocenters south and north of the Gulf of Corinth (see slab top model in Figure 11), which implies that the center of deformation in the slab lies about 100 km south of the KTF.

Second, there is a v-shaped gap in deep seismicity below central Greece, which coincides approximately with that offset. Maximum hypocenter depth increases both toward the south and the north of this gap at 38.7°N (see red lines in Figure 11). This gap in seismicity might reflect a change in thermal conditions within the subducting crust due to the widely distributed deformation. One explanation would be that the subducting crust is stretched and thinned across the zone of deformation within the slab below the CHSZ, heating the crust more efficiently. Alternatively, seismicity terminates earlier due to warm mantle material flowing into the mantle wedge in this region, where the overriding crust is extending and thinning, also heating the subducting crust locally. A warmer subducting crust would reach the eclogite facies conditions earlier and thus prohibit the mechanisms enabling intermediate depth earthquakes or at least reduce their occurrence.

Taken together, these observations paint a picture of a slab that is deforming due to the subduction of crusts with different compositions. In contrast to earlier models (Pearce et al., 2012; Royden & Papanikolaou, 2011), the deformation of the slab occurs in a distributed fashion below the CHSZ rather than at the KTF, thus well within the oceanic part of the slab.

7.3.4. Stress Transfer to the Lower Overriding Crust

The location of the CHSZ and the zone of deformation within the slab correlate in their extents, which raises the question whether these two features are linked through coupling between the overriding and subducting crusts. This is especially relevant because the deformation taking place in the CHSZ is not well understood. The CHSZ is home to the largest strike-slip earthquake recorded on mainland Greece—the *M*6.4 Movri event of 2008 (fault plane marked in red in Figures 1 and 5; Gallovič et al., 2009). This earthquake, in which the lower overriding crust below the Movri mountains ruptured (Serpetsidaki et al., 2014), was unexpected

AGU Journal of Geophysical Research: Solid Earth 10.1002/2017JB015154

considering the absence of any comparable event in the historical record (Gallovič et al., 2009). According to Papadopoulos et al. (2010), the fault that ruptured had not been active for at least the last 300 years. The occurrence of a lower-crustal earthquake in the overriding plate, so close to the subduction interface, calls for a closer inspection of current plate-coupling models for the area. These models suggest little to no coupling along the whole interface (Baker et al., 1997; Jackson & McKenzie, 1988; Shaw & Jackson, 2010) or strong coupling limited to the upper 15 km of crust, with a shallow transition toward stable sliding between the ductile lower crust and the slab (Laigle et al., 2002). In the following section, we present evidence to help resolve the mismatch between a large earthquake rupturing the lower crust and the apparent lack of a transmittable force that could cause this earthquake.

There are a number of observations that support the suggestion that deformation in the CHSZ and within the slab is linked.

1. First, GPS data from McClusky et al. (2000) support the theory that the largest dextral shearing movement in the upper plate is realized within the CHSZ rather than at the KTF farther north. This suggests that while some differential plate motion offsets the trenches at Kephalonia, there is a larger force deforming the upper plate farther south.
2. Second, according to Serpetsidaki et al. (2014), the Movri earthquake is associated with an immature fault system with a predominantly dextral strike-slip movement, in line with the northern end of the CHSZ. This immaturity suggests that faulting started only recently, which matches our model of a slab in which deformation has been growing since the onset of differential subduction.
3. Third, although Serpetsidaki et al. (2014) place the Movri earthquake 50 km toward the backarc from the contact zone between overriding and subducting crusts in their model, our tomographic models suggest that the Movri event falls right into the area of thickened crust, where coupling between the crusts would be possible.

These observations all point toward at least some transfer of deformation between the overriding and subducting plates at the scale of the whole crust, and therefore, to a more complex situation occurring at the plate interface.

An updated understanding of the plate interface in the WHSZ is crucial to explain the occurrence of the Movri earthquake in the lower overriding crust. To explain the driving force behind the stress leading to the earthquake, two models have been proposed by Serpetsidaki et al. (2014). One model attributes strain to differential subduction rates, while the other model invokes the North Anatolian Fault as the driving force behind the strain. In the second model, they suggest that the premature fault system could be developing along a shear zone in the uppermost mantle which connects active crustal segments.

Based on the close spatial correlation between the zone of deformation in the slab, the northern part of the CHSZ and the Movri earthquake, we favor the differential slab rollback as the driving force behind stresses leading to the Movri earthquake. We also note that the westward propagation of the North Anatolian Fault into the northern part of the CHSZ might be focused by the deformation affecting both the slab and the CHSZ, possibly aided by the flow in the mantle wedge associated with differential subduction. Both models would not work if the lower crust was too ductile for stress transfer. In summary, our results are consistent with models that allow for partial coupling in the region, but more work is needed to determine the exact nature of this coupling.

8. Conclusions

We present new, high-resolution Vp and Vp/Vs ratio models and relocated hypocenters of the WHSZ. This new information helps us better understand the transition from oceanic subduction in the south of the region to continental subduction in the north, as well as the fate of slab-derived fluids. Our main results can be summarized in three points.

1. Intermediate depth seismicity occurs within a single plane throughout the southern part of the study area and is nearly nonexistent in the northern part, with an abrupt south-to-north transition occurring at the KTF. This change in seismicity appears to mark the boundary between two subducting domains: oceanic in the south and continental in the north and reflects their varying composition and fluid content. Slab dehydration seems to be particularly active in the southern part of the system, below the Peloponnesus,

AGU Journal of Geophysical Research: Solid Earth 10.1002/2017JB015154

where there is evidence for partial melting in the subarc mantle. Despite being nearly aseismic, the subducting continental crust in the north exhibits a low-velocity signature to at least 90 km depth (as imaged by *P* wave scattering potential $\delta\alpha/\alpha$). We interpret this low-velocity signature and seismic quiescence as reflecting an absence of fluids, which inhibits metamorphism and seismicity in a metastable continental subducting crust.

2. The transition between oceanic subduction with more rollback in the south to continental subduction with less rollback in the north is reflected by a smoothly deformed slab rather than a tear in the tomographic images. This slab deformation is accompanied by a gap in deep intraslab seismicity (>60 km depth), probably indicative of a change in thermal regime between south and north. The zone of slab deformation underlies the whole CHSZ and seems to affect the deformation in the overriding Aegean plate. We associate both the dextral strike-slip fault system of the 2008 Movri earthquake (*M*6.4) and the western extension of the North Anatolian Fault with this area of deformation, which is driven by differential subduction.
3. How fluids interact with the mantle wedge and the overriding crust seems to be impacted by the change in subduction style. Beneath the Hellenic arc, in the south, fluids emanating from the subducted oceanic crust appear to migrate directly upward into the mantle wedge, where they trigger partial melting. By contrast, in the central part of the WHSZ, our results suggest that slab-derived fluids might migrate toward the trench below an intact seal at the slab interface until they reach the lower crust of the overriding plate, where they precipitate silica.

Acknowledgments
We thank Maria Sachpazi, Jonny Wu, and the Associate Editor for their thoughtful reviews, which helped clarify and improve the original manuscript. The study was supported by funding from the Research Council of Norway for the project "Subduction zone Water and Metamorphism: A Modelling and Imaging Study" (project 231354). The services of E.J. Farmer Editing and Proofreading were used. Earthquake catalogs and phase arrival data were downloaded from the International Seismological Centre http://www.isc.ac.uk/ and the National Observatory of Athens http://bbnet.gein.noa.gr/HL/. Seismic waveform data from the MEDUSA network and selected stations of the Hellenic Unified Seismic Network are archived at the Incorporated Research Institutions for Seismology (IRIS) Data Management Center (DMC) (http://ds.iris.edu/ds/nodes/dmc) under temporary network code XS (2006–2009) and permanent network code HL, respectively. Waveform data of the EGELADOS stations can be downloaded from the Observatories and Research Facilities for European Seismology (ORFEUS) European Integrated Data Archive (EIDA) (http://www.orfeus-eu.org/data/eida/) under temporary network code Z3 (2005–2007). Shuttle Radar Topography Mission (SRTM) topography data for Figures 1 and 5 were downloaded from the U.S. Geological Survey at https://dds.cr.usgs.gov/srtm/. Bathymetry data in these figures are from the Smith and Sandwell bathymetry database at the Scripps Institution of Oceanography, University of California at San Diego, at http://topex.ucsd.edu/marine_topo/. Maps were created with the m_map Matlab toolbox (https://www.eoas.ubc.ca/~rich/map.html. A catalog of the relocated earthquakes, the tomographic models of *P* velocity and Vp/Vs ratio, the slab top model, and coastlines of Greece (from Wessel & Smith, 1996) are included in the supporting information of this paper. These supporting information are available online and contain a description about how the data sets can be readily displayed in Paraview (Ahrens et al., 2005).

References

Abers, G. A., van Keken, P. E., & Hacker, B. R. (2017). The cold and relatively dry nature of mantle forearcs in subduction zones. *Nature Geoscience*, *10*, 333–337. https://doi.org/10.1038/ngeo2922

Ahrens, J., Geveci, B., & Law, C. (2005). ParaView: An end-user tool for large-data visualization. *Visualization Handbook*, *836*, 717–731. https://doi.org/10.1016/B978-012387582-2/50038-1

Amante, C., & Eakins, B. W. (2009). *ETOPO1 1 arc-minute global relief model: Procedures, data sources and analysis*. Boulder, CO: NOAA Technical Memorandum NESDIS NGDC-24. National Geophysical Data Center

Audet, P., & Bürgmann, R. (2014). Possible control of subduction zone slow-earthquake periodicity by silica enrichment. *Nature*, *510*, 389–392. https://doi.org/10.1038/nature13391

Austrheim, H. (1987). Eclogitization of lower crustal granulites by fluid migration through shear zones. *Earth and Planetary Science Letters*, *81*, 221–232.

Baker, C., Hatzfeld, D., Lyon-Caen, H., Papadimitriou, E., & Rigo, A. (1997). Earthquake mechanisms of the Adriatic Sea and Western Greece: Implications for the oceanic subduction-continental collision transition. *Geophysical Journal International*, *131*(3), 559–594. https://doi.org/10.1111/j.1365-246x.1997.tb06600.x

Benetatos, C., Kiratzi, a., Papazachos, C., & Karakaisis, G. (2004). Focal mechanisms of shallow and intermediate depth earthquakes along the Hellenic Arc. *Journal of Geodynamics*, *37*(2), 253–296. https://doi.org/10.1016/j.jog.2004.02.002

Bijwaard, H., Spakman, W., & Engdahl, E. R. (1998). Closing the gap between regional and global travel time tomography. *Journal of Geophysical Research*, *103*(B12), 30,055–30,078. https://doi.org/10.1029/98JB02467

Bleibinhaus, F. (2003). 3D simultaneous refraction and reflection seismic travel time tomography and application to deep seismic TRANSALP wide-angle data (Doctoral dissertation). München: Ludwig-Maximilians-Universitat Munchen. Retrieved from https://edoc.ub.uni-muenchen.de/1263/

Bohnhoff, M., Makris, J., Papanikolaou, D., & Stavrakakis, G. (2001). Crustal investigations of the Hellenic subduction zone using wide aperture seismic data. *Tectonophysics*, *343*, 239–262.

Bostock, M. G., Hyndman, R. D., Rondenay, S., & Peacock, S. M. (2002). An inverted continental Moho and serpentinization of the forearc mantle. *Nature*, *417*(6888), 536–538. https://doi.org/10.1038/417536a

Breeding, C. M., & Ague, J. J. (2002). Slab-derived fluids and quartz-vein formation in an accretionary prism, Otago Schist, New Zealand. *Geology*, *30*(6), 499–502. https://doi.org/10.1130/0091-7613(2002)030<0499:SDFAQV>2.0.CO;2

Brudzinski, M. R., Thurber, C. H., Hacker, B. R., & Engdahl, E. R. (2007). Global prevalence of double Benioff zones. *Science*, *316*(5830), 1472–1474. https://doi.org/10.1126/science.1139204

Brüstle, A. (2012). Seismicity of the eastern Hellenic subduction zone (Doctoral dissertation). Ruhr-Universität Bochum, Bochum, Germany. Retrieved from https://www-brs.ub.ruhr-uni-bochum.de/netahtml/HSS/Diss/BruestleAndrea/diss.pdf

Clift, P., & Vannucchi, P. (2004). Controls on tectonic accretion versus erosion in subduction zones: Implications for the origin and recycling of the continental crust. *Reviews of Geophysics*, *42*, RG2001. https://doi.org/10.1029/2003RG000127

Davey, F. J., & Ristau, J. (2011). Fore-arc mantle wedge seismicity under northeast New Zealand. *Tectonophysics*, *509*(3-4), 272–279. https://doi.org/10.1016/j.tecto.2011.06.017

Del Ben, A., Mocnik, A., Volpi, V., & Karvelis, P. (2015). Old domains in the South Adria plate and their relationship with the West Hellenic front. *Journal of Geodynamics*, *89*, 15–28. https://doi.org/10.1016/j.jog.2015.06.003

Diehl, T., Kissling, E., & Bormann, P. (2002). Tutorial for consistent phase picking at local to regional distances. In P. Bormann (Ed.), *New manual of seismological observatory practice (NMSOP-2)* (chap. IS 11.4, pp. 1–21). Potsdam: IASPEI, GFZ German Research Centre for Geosciences. https://doi.org/10.2312/GFZ.NMSOP-2_ IS_11.4

Durand, V., Bouchon, M., Floyd, M. A., Theodulidis, N., Marsan, D., Karabulut, H., & Schmittbuhl, J. (2014). Observation of the spread of slow deformation in Greece following the breakup of the slab. *Geophysical Research Letters*, *41*, 7129–7134. https://doi.org/10.1002/2014GL061408

Eberhart-Phillips, D. (1990). Three-dimensional *P* and *S* velocity structure in the Coalinga region, California. *Journal of Geophysical Research*, *95*(B10), 15,343–15,363. https://doi.org/10.1029/JB095iB10p15343

Eberhart-Phillips, D., & Bannister, S. (2010). 3-D imaging of Marlborough, New Zealand, subducted plate and strike-slip fault systems. *Geophysical Journal International*, *182*(1), 73–96. https://doi.org/10.1111/j.1365-246x.2010. 04621.x

AGU Journal of Geophysical Research: Solid Earth 10.1002/2017JB015154

Evans, J. R., Eberhart-Phillips, D., & Thurber, C. H. (1999). User's manual for SIMULPS12 for imaging Vp and Vp/Vs: A derivative of the "Thurber" tomographic inversion SIMUL3 for local earthquakes and explosions. *U.S. Geological Survey Open File Report*, 94–431.

Finetti, I. R., & Del Ben, A. (2005). Crustal tectono-stratigraphic setting of the adriatic sea from new CROP seismic data. In I. R. Finelli (Ed.), *Deep Seismic Exploration of the Central Mediterranean and Italy* (chap. 23). Amsterdam: Elsevier.

Flerit, F., Armijo, R., King, G., & Meyer, B. (2004). The mechanical interaction between the propagating North Anatolian Fault and the back-arc extension in the Aegean. *Earth and Planetary Science Letters*, *224*(3-4), 347–362. https://doi.org/10.1016/j.epsl.2004.05.028

Galanis, O., Papazachos, C., Scordilis, E., & Hatzidimitriou, P. (2006). Improved earthquake locations in Greece using the DD algorithm and a 3D velocity model. In *First European Conference on Earthquake Engineering and Seismology* (810 pp.). Geneva, Switzerland.

Gallovič, F., Zahradník, J., Křížová, D., Plicka, V., Sokos, E., Serpetsidaki, A., & Tselentis, G. A. (2009). From earthquake centroid to spatial-temporal rupture evolution: Mw 6.3 Movri Mountain earthquake, June 8, 2008, Greece. *Geophysical Research Letters*, *36*, L21310. https://doi.org/10.1029/2009GL040283

Gesret, A., Laigle, M., Diaz, J., Sachpazi, M., Charalampakis, M., & Hirn, A. (2011). Slab top dips resolved by teleseismic converted waves in the Hellenic subduction zone. *Geophysical Research Letters*, *38*, L20304. https://doi.org/10.1029/2011GL048996

Govers, R., & Wortel, M. J. R. (2005). Lithosphere tearing at STEP faults: Response to edges of subduction zones. *Earth and Planetary Science Letters*, *236*(1-2), 505–523. https://doi.org/10.1016/j.epsl.2005.03.022

Haslinger, F., & Kissling, E. (2001). Investigating effects of 3-D ray tracing methods in local earthquake tomography. *Physics of the Earth and Planetary Interiors*, *123*(2-4), 103–114. https://doi.org/10.1016/S0031-9201(00) 00204-1

Haslinger, F., Kissling, E., Ansorge, J., Hatzfeld, D., Papadimitriou, E. E., Karakostas, V., et al. (1999). 3D Crustal structure from local earthquake tomography around Gulf of Arta. *Tectonophysics*, *304*, 210–218.

Hatzfeld, D. (1994). On the shape of the subducting slab beneath the Peloponnese, Greece. *Geophysical Research Letters*, *21*(3), 173–176. https://doi.org/10.1029/93GL03079

Hatzfeld, D., & Martin, C. (1992). Intermediate depth seismicity in the Aegean defined by teleseismic data. *Earth and Planetary Science Letters*, *113*(1-2), 267–275. https://doi.org/10.1016/0012-821X(92)90224-J

Havskov, J., & Ottemöller, L. (1999). SeisAn earthquake analysis software. *Seismological Research Letters*, *70*(5), 532–534.

Hyndman, R. D., McCrory, P. A., Wech, A., Kao, H., & Ague, J. (2015). Cascadia subducting plate fluids channelled to fore-arc mantle corner: ETS and silica deposition. *Journal of Geophysical Research: Solid Earth*, *120*, 4344–4358. https://doi.org/10.1002/2015JB011920

International Seismological Centre (2017). *On-line bulletin*. Thatcham, UK: International Seismological Centre. Retrieved from http://www.isc.ac.uk

Jackson, J., & McKenzie, D. (1988). The relationship between plate motions and seismic moment tensors, and the rates of active deformation in the Mediterranean and Middle East. *Geophysical Journal International*, *93*(1), 45–73. https://doi.org/10.1111/j.1365-246x.1988.tb01387.x

Karakonstantis, A., & Papadimitriou, P. (2010). Earthquake relocation in Greece using a unified and homogenized seismological catalogue. *Bulletin of the Geological Society of Greece*, *43*(4), 2043–2052.

Karastathis, V. K., Mouzakiotis, E., Ganas, A., & Papadopoulos, G. A. (2015). High-precision relocation of seismic sequences above a dipping Moho: The case of the January–February 2014 seismic sequence on Cephalonia island (Greece). *Solid Earth*, *6*, 173–184. https://doi.org/10.5194/se-6-173-2015

Kennett, B. L. N., Engdahl, E. R., & Buland, R. (1995). Constraints on seismic velocities in the Earth from traveltimes. *Geophysical Journal International*, *122*, 108–124. https://doi.org/10.1111/j.1365-246x.1995. tb03540.x

Kissling, E., Ellsworth, W. L., Eberhart-Phillips, D., & Kradolfer, U. (1994). Initial reference models in local earthquake tomography. *Journal of Geophysical Research*, *99*(B10), 19,635–19,646.

Klein, F. W. (2002). *User's guide to HYPOINVERSE-2000, a FORTRAN program to solve for earthquake locations and magnitudes*. Menlo Park CA: U.S. Geological Survey Open File Report 02-171.

Klemd, R., John, T., Scherer, E. E., Rondenay, S., & Gao, J. (2011). Changes in dip of subducted slabs at depth: Petrological and geochronological evidence from HP-UHP rocks (Tianshan, NW-China). *Earth and Planetary Science Letters*, *310*(1-2), 9–20. https://doi.org/10.1016/j.epsl.2011.07.022

Kokinou, E., Kamberis, E., Vafidis, A., Monopolis, D., Ananiadis, G., & Zelilidis, A. (2005). Deep seismic reflection data from offshore Western Greece: A new crustal model for the Ionian Sea. *Journal of Petroleum Geology*, *28*(2), 185–202. https://doi.org/10.1111/j.1747-5457.2005.tb00079.x

Kokinou, E., Papadimitriou, E., Karakostas, V., Kamberis, E., & Vallianatos, F. (2006). The Kefalonia Transform Zone (offshore Western Greece) with special emphasis to its prolongation towards the Ionian Abyssal Plain. *Marine Geophysical Researches*, *27*(4), 241–252. https://doi.org/10.1007/s11001-006-9005-2

Konstantinou, K. I., Melis, N. S., & Boukouras, K. (2010). Routine regional moment tensor inversion for earthquakes in the Greek region: The National Observatory of Athens (NOA) database (2001–2006). *Seismological Research Letters*, *81*(5), 750–760. https://doi.org/10.1785/gssrl

Koulakov, I., Kaban, M. K., Tesauro, M., & Cloetingh, S. (2009). P- and S-velocity anomalies in the upper mantle beneath Europe from tomographic inversion of ISC data. *Geophysical Journal International*, *179*(1), 345–366. https://doi.org/10.1111/j.1365-246x.2009.04279.x

Laigle, M., Hirn, A., Sachpazi, M., & Clément, C. (2002). Seismic coupling and structure of the Hellenic subduction zone in the Ionian Islands region. *Earth and Planetary Science Letters*, *200*(3-4), 243–253. https://doi.org/10.1016/S0012-821X(02)00654-4

Lamara, S. (2015). 3D waveform tomography of the Hellenic subduction zone (Doctoral dissertation). Bochum, Germany: Ruhr-Universitat Bochum. Retrieved from http://hss-opus.ub.ruhr-uni-bochum.de/opus4/files/4415/diss.pdf

Li, X., Bock, G., Vafidis, A., Kind, R., Harjes, H. P., Hanka, W., et al. (2003). Receiver function study of the Hellenic subduction zone: Imaging crustal thickness variations and the oceanic Moho of the descending African lithosphere. *Geophysical Journal International*, *155*(2), 733–748. https://doi.org/10.1046/j.1365-246x.2003.02100.x

Lienert, B. R., & Havskov, J. (1995). A computer program for locating earthquakes both locally and globally. *Seismological Research Letters*, *66*(5), 26–36. https://doi.org/10.1785/gssrl.66.5.26

MacKenzie, L. S., Abers, G. A., Rondenay, S., & Fischer, K. M. (2010). Imaging a steeply dipping subducting slab in Southern Central America. *Earth and Planetary Science Letters*, *296*(3-4), 459–468. https://doi.org/10.1016/j.epsl.2010.05.033

Manning, C. E. (1994). The solubility of quartz in H_2O in the lower crust and upper mantle. *Geochimica et Cosmochimica Acta*, *58*(22), 4831–4839.

McClusky, S., Balassanian, S., Barka, A., Demir, C., Ergintav, S., Georgiev, I., et al. (2000). Global Positioning System constraints on plate kinematics and dynamics in the eastern Mediterranean and Caucasus. *Journal of Geophysical Research*, *105*(B3), 5695–5719. https://doi.org/10.1029/1999JB900351

McKenzie, D. (1972). Active tectonics of the Mediterranean region. *Geophysical Journal International*, *30*, 109–185.

Meighan, H. E., Ten Brink, U., & Pulliam, J. (2013). Slab tears and intermediate-depth seismicity. *Geophysical Research Letters*, *40*, 4244–4248. https://doi.org/10.1002/grl.50830

Nakajima, J., Uchida, N., Shiina, T., Hasegawa, A., Hacker, B. R., & Kirby, S. H. (2013). Intermediate-depth earthquakes facilitated by eclogitization-related stresses. *Geology*, *41*(6), 659–662. https://doi.org/10.1130/G33796.1

Nixon, C. W., McNeill, L. C., Bull, J. M., Bell, R. E., Gawthorpe, R. L., Henstock, T. J., et al. (2016). Rapid spatiotemporal variations in rift structure during development of the Corinth Rift, central Greece. *Tectonics*, *35*, 1225–1248. https://doi.org/10.1002/2015TC004026

Olive, J. A., Pearce, F., Rondenay, S., & Behn, M. D. (2014). Pronounced zonation of seismic anisotropy in the Western Hellenic subduction zone and its geodynamic significance. *Earth and Planetary Science Letters*, *391*, 100–109. https://doi.org/10.1016/j.epsl.2014.01.029

Papadopoulos, G. A., Karastathis, V., Kontoes, C., Charalampakis, M., Fokaefs, A., & Papoutsis, I. (2010). Crustal deformation associated with east Mediterranean strike-slip earthquakes: The 8 June 2008 Movri (NW Peloponnese), Greece, earthquake (Mw6.4). *Tectonophysics*, *492*(1-4), 201–212. https://doi.org/10.1016/j.tecto.2010.06.012

Papanikolaou, D. J., & Royden, L. H. (2007). Disruption of the Hellenic arc: Late Miocene extensional detachment faults and steep Pliocene-Quaternary normal faults—Or what happened at Corinth? *Tectonics*, *26*, TC5003. https://doi.org/10.1029/2006TC002007

Papazachos, B. C., Karakostas, V. G., Papazachos, C. B., & Scordilis, E. M. (2000). The geometry of the Wadati-Benioff zone and lithospheric kinematics in the Hellenic arc. *Tectonophysics*, *319*(4), 275–300. https://doi.org/10.1016/S0040-1951(99)00299-1

Papazachos, C., & Nolet, G. (1997). *P* and *S* deep velocity structure of the Hellenic area obtained by robust nonlinear inversion of travel times. *Journal of Geophysical Research*, *102*, 8349–8367. https://doi.org/10.1029/96JB03730

Pe-Piper, G., & Piper, D. J. W. (2007). Neogene backarc volcanism of the Aegean: New insights into the relationship between magmatism and tectonics. *Geological Society of America Special Papers*, *418*(02), 17–31. https://doi.org/10.1130/2007.2418(02)

Peacock, S. M. (1993). The importance of blueschist -> eclogite dehydration reactions in subducting oceanic crust. *Geological Society of America Bulletin*, *105*(5), 684–694. https://doi.org/10.1130/0016-7606(1993)105<0684:TIOBED>2.3.CO;2

Pearce, F. D., Rondenay, S., Sachpazi, M., Charalampakis, M., & Royden, L. H. (2012). Seismic investigation of the transition from continental to oceanic subduction along the western Hellenic subduction Zone. *Journal of Geophysical Research*, *117*, B07306. https://doi.org/10.1029/2011JB009023

Piromallo, C. (2003). *P* wave tomography of the mantle under the Alpine-Mediterranean area. *Journal of Geophysical Research*, *108*(B2), 2065. https://doi.org/10.1029/2002JB001757

Ramachandran, K., & Hyndman, R. D. (2012). The fate of fluids released from subducting slab in northern Cascadia. *Solid Earth*, *3*(1), 121–129. https://doi.org/10.5194/se-3-121-2012

Reilinger, R., McClusky, S., Vernant, P., Lawrence, S., Ergintav, S., Cakmak, R., et al. (2006). GPS constraints on continental deformation in the Africa-Arabia-Eurasia continental collision zone and implications for the dynamics of plate interactions. *Journal of Geophysical Research*, *111*, B05411. https://doi.org/10.1029/2005JB004051

Reyners, M., Eberhart-Phillips, D., Stuart, G., & Nishimura, Y. (2006). Imaging subduction from the trench to 300 km depth beneath the central North Island, New Zealand, with Vp and Vp/Vs. *Geophysical Journal International*, *165*(2), 565–583. https://doi.org/10.1111/j.1365-246x.2006.02897.x

Rizzo, A. L., Caracausi, A., Chavagnac, V., Nomikou, P., Polymenakou, P. N., Mandalakis, M., et al. (2016). Kolumbo submarine volcano (Greece): An active window into the Aegean subduction system. *Scientific Reports*, *6*(February), 28013. https://doi.org/10.1038/srep28013

Rontogianni, S., Konstantinou, N. S., Melis, C. P., & Evangelidis (2011). Slab stress field in the Hellenic subduction zone as inferred from intermediate-depth earthquakes. *Earth, Planets and Space*, *63*(2), 139–144. https://doi.org/10.5047/eps.2010.11.011

Royden, L. H., & Papanikolaou, D. J. (2011). Slab segmentation and late Cenozoic disruption of the Hellenic arc. *Geochemistry, Geophysics, Geosystems*, *12*, Q03010. https://doi.org/10.1029/2010GC003280

Sachpazi, M., Hirn, A., Clément, C., Haslinger, F., Laigle, M., Kissling, E., et al. (2000). Western Hellenic subduction and Cephalonia transform: Local earthquakes and plate transport and strain. *Tectonophysics*, *319*(4), 301–319. https://doi.org/10.1016/S0040-1951(99)00300-5

Sachpazi, M., Laigle, M., Charalampakis, M., Diaz, J., Kissling, E., Gesret, A., et al. (2016). Segmented Hellenic slab rollback driving Aegean deformation and seismicity. *Geophysical Research Letters*, *43*, 651–658. https://doi.org/10.1002/2015GL066818

Serpetsidaki, A., Elias, P., Ilieva, M., Bernard, P., Briole, P., Deschamps, A., et al. (2014). New constraints from seismology and geodesy on the Mw = 6.4 2008 Movri (Greece) earthquake: Evidence for a growing strike-slip fault system. *Geophysical Journal International*, *198*(3), 1373–1386. https://doi.org/10.1093/gji/ggu212

Serpetsidaki, A., Sokos, E., & Tselentis, G.-A. (2016). A ten year moment tensor database for western Greece. *Physics and Chemistry of the Earth, Parts A/B/C*, *95*, 2–9. https://doi.org/10.1016/j.pce.2016.04.007

Shaw, B., & Jackson, J. (2010). Earthquake mechanisms and active tectonics of the Hellenic subduction zone. *Geophysical Journal International*, *181*(2), 966–984. https://doi.org/10.1111/j.1365-246x.2010.04551.x

Sodoudi, F., Brüstle, A., Meier, T., Kind, R., Friederich, W., & Egelados Working Group (2015). Receiver function images of the Hellenic subduction zone and comparison to microseismicity. *Solid Earth*, *6*(1), 135–151. https://doi.org/10.5194/se-6-135-2015

Spakman, W., Wortel, M. J. R., & Vlaar, N. J. (1988). The Hellenic subduction zone: A tomographic image and its geodynamic implications. *Geophysical Research Letters*, *15*(1), 60–63. https://doi.org/10.1029/GL015i001p00060

Speranza, F., Minelli, L., Pignatelli, A., & Chiappini, M. (2012). The Ionian Sea: The oldest in situ ocean fragment of the world? *Journal of Geophysical Research*, *117*, B12101. https://doi.org/10.1029/2012JB009475

Suckale, J., Rondenay, S., Sachpazi, M., Charalampakis, M., Hosa, A., & Royden, L. H. (2009). High-resolution seismic imaging of the western Hellenic subduction zone using teleseismic scattered waves. *Geophysical Journal International*, *178*(2), 775–791. https://doi.org/10.1111/j.1365-246x.2009.04170.x

Syracuse, E. M., van Keken, P. E., Abers, G. A., Suetsugu, D., Bina, C., Inoue, T., et al. (2010). The global range of subduction zone thermal models. *Physics of the Earth and Planetary Interiors*, *183*, 73–90. https://doi.org/10.1016/j.pepi.2010.02.004

Theunissen, T., Chevrot, S., Sylvander, M., Monteiller, V., Calvet, M., Villaseñor, M., et al. (2018). Absolute earthquake locations using 3-D versus 1-D velocity models below a local seismic network: Example from the Pyrenees. *Geophysical Journal International*, *212*, 1806–1828. https://doi.org/10.1093/gji/ggx472

Thurber, C. H. (1983). Earthquake locations and three-dimensional crustal structure in the Coyote Lake Area, central California. *Journal of Geophysical Research*, *88*(B10), 8226–8236. https://doi.org/10.1029/JB088iB10p08226

Thurber, C. H., & Eberhart-Phillips, D. (1999). Local earthquake tomography with flexible gridding. *Computers and Geosciences*, *25*(7), 809–818. https://doi.org/10.1016/S0098-3004(99)00007-2

Uchida, N., Kirby, S. H., Okada, T., Hino, R., & Hasegawa, A. (2010). Supraslab earthquake clusters above the subduction plate boundary offshore Sanriku, northeastern Japan: Seismogenesis in a graveyard of detached seamounts? *Journal of Geophysical Research*, *115*, B09308. https://doi.org/10.1029/2009JB006797

Um, J., & Thurber, C. H. (1987). A fast algorithm for two-point ray tracing. *Bulletin of the Seismological Society of America*, *77*(June), 972–986.

AGU Journal of Geophysical Research: Solid Earth 10.1002/2017JB015154

Unsworth, M., & Rondenay, S. (2013). Mapping the distribution of fluids in the crust and lithospheric mantle utilizing geophysical methods. In M. Unsworth & S. Rondenay (Eds.), *Metasomatism and the chemical transformation of rock, lecture notes in Earth System Sciences* (pp. 535–598). Berlin: Springer-Verlag. https://doi.org/10.1007/978-3-642-28394-9_13

van Keken, P. E., Kita, S., & Nakajima, J. (2012). Thermal structure and intermediate-depth seismicity in the Tohoku-Hokkaido subduction zones. *Solid Earth*, *3*(2), 355–364. https://doi.org/10.5194/se-3-355-2012

Vassilakis, E., Royden, L. H., & Papanikolaou, D. (2011). Kinematic links between subduction along the Hellenic trench and extension in the Gulf of Corinth, Greece: A multidisciplinary analysis. *Earth and Planetary Science Letters*, *303*(1-2), 108–120. https://doi.org/10.1016/j.epsl.2010.12.054

von Huene, R., Reston, T., Kukowski, N., Dehghani, G., & Weinrebe, W. (1997). A subducting seamount beneath the Mediterranean Ridge. *Tectonophysics*, *271*(3-4), 249–261. https://doi.org/10.1016/S0040-1951(96) 00241-7

Waldhauser, F. (2012). *User guide to HypoDD version 2.1b*. Palisades, New York: Lamont-Doherty Earth Observatory.

Waldhauser, F., & Ellsworth, W. L. (2000). A double-difference earthquake location algorithm: Method and application to the northern Hayward fault, California. *Bulletin of the Seismological Society of America*, *6*, 1353–1368.

Wessel, P., & Smith, W. H. F. (1996). A global, self-consistent, hierarchical, high-resolution shoreline. *Journal of Geophysical Research*, *101*(B4), 8741–8743.

Wortel, M. J. R., & Spakman, W. (2000). Subduction and slab detachment in the Mediterranean-Carpathian region. *Science*, *290*(5498), 1910–1917. https://doi.org/10.1126/science.290.5498.1910

Zelt, B. C., Taylor, B., Sachpazi, M., & Hirn, A. (2005). Crustal velocity and Moho structure beneath the Gulf of Corinth, Greece. *Geophysical Journal International*, *162*(1), 257–268. https://doi.org/10.1111/j.1365-246x. 2005.02640.x

Zhang, H., Thurber, C. H., Shelly, D., Ide, S., Beroza, G. C., & Hasegawa, A. (2004). High-resolution subducting-slab structure beneath northern Honshu, Japan, revealed by double-difference tomography. *Geology*, *32*(4), 361–364. https://doi.org/10.1130/G20261.2

Zhu, H., Bozdağ, E., & Tromp, J. (2015). Seismic structure of the European upper mantle based on adjoint tomography. *Geophysical Journal International*, *201*(1), 18–52. https://doi.org/10.1093/gji/ggu492

Confidential manuscript submitted to *JGR-Solid Earth*

Supporting Information for "Seismicity, Deformation and Metamorphism in the Western Hellenic Subduction Zone - New Constraints from Tomography"

Felix Halpaap, Stéphane Rondenay, Lars Ottemöller

[1]Department of Earth Science, University of Bergen, P.O.Box 7803, 5020 Bergen, Norway.

Contents

Additional Supporting Information (Files uploaded separately)

1. DS1: Relocated earthquakes
2. DS2: Tomographic P-velocity and Vp/Vs-ratio models
3. DS3: Slab top surface model
4. DS4: Coastlines of Greece

Introduction

This supporting information contains a series of figures that supplement those shown in the main manuscript. These figures are either discussed in the main manuscript or in the supporting text that follows below. The supporting text includes a detailed description of the hypocenters at each relocation stage, and a discussion of additional resolution tests. Lastly, we provide files containing the resulting velocity models (P-velocity and Vp/Vs-ratio), a complete catalog of earthquake hypocenters, and tables containing geographical data for the slab top surface model and the coastlines of Greece used in all the maps of this paper.

Hypocenters at each relocation stage

Figure S2 shows the hypocenters calculated before and after each of the three relocation stages described in the Methods section of the main paper (Section 3). This information allows us to assess the gains in hypocenter accuracy achieved after each stage. The first column displays all the earthquakes downloaded and evaluated from the ISC catalog (black dots, 1990-2009, M > 3 for depths larger 40 km, M > 4 for depths smaller 40 km) and the NOA catalog (blue dots, 2008-2015, all earthquakes with depths larger 40 km). We plot this initial set of hypocenters without error bars, as formal hypocentral errors are not calculated in a coherent manner until we carry out a quality control on the events and picks (see Section 4 - Data). This quality control winnows the number of events retained for inversion to 1070 (see second column of Figure S2). A large number of events are removed at this stage, in partic-

Corresponding author: F. Halpaap, felix.halpaap@uib.no

Confidential manuscript submitted to *JGR-Solid Earth*

ular in the 40-80 km depth range below the trench and the backarc, and in a band extending 20-50 km beneath the main Wadati-Benioff Zone. After 3-D tomographic inversion, the formal hypocentral errors are reduced considerably, especially for events at the trench, and the Wadati-Benioff Zone becomes narrower and better defined (see third column of Figure S2). Note that at this stage, an additional 5 events are eliminated from the dataset based on their large hypocentral errors. Lastly, the double-difference relocation further sharpens seismicity patterns within individual clusters with precision down to the km-scale, as see for example in the main cluster of seismicity between X=70-110 km in section E-E'(see fourth column of Figure S2).

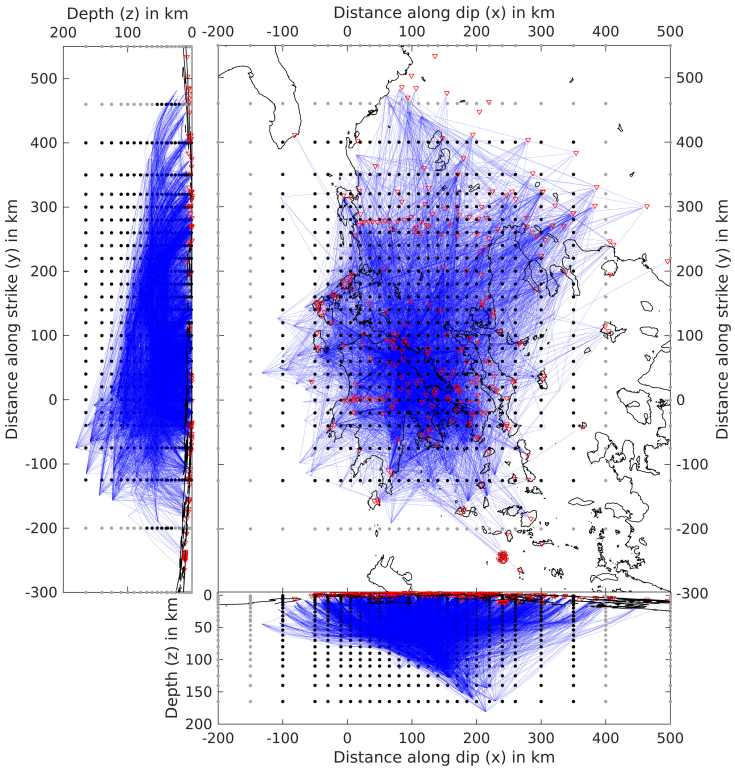

Figure 1. Ray coverage of the FULL-dataset, which was used for the final velocity model. This figure depicts the complete inversion domain, with inversion nodes marked as black dots and predefined interpolation nodes marked in grey. The local coordinate system's location is marked in figure 5 in the main text. Stations are marked as red triangles and inversion nodes as gray dots. Only about one fourth of all rays are plotted for better visualization. The plot includes all rays reaching deeper than 100 km, 20 % of rays >50 km, 10 % of rays >15 km, and 5 % of the shallower rays.

Resolution Test: Inversion of independent data subsets

To assess whether the anomalies that we recover in this study are robust features independent of station setup, hypocenter distribution and picking entity, we conducted tomographic inversions of two independent subsets of data.

We divide the full dataset of arrival time observations (referred to as "FULL" dataset, ray coverage shown in Fig. S1) into two independent subsets:

1. The first subset, referred to as “MEI”, includes out manual time picks for deep and shallow earthquakes that were recorded between 2006-2009 by stations of the MEDUSA and EGELADOS experiments. These are supplemented by picks from the ISC for earthquakes that occurred in the region and were recorded at permanent stations between 1995-2009.
2. The second subset, referred to as “NOA”, comprises arrival times of deep earthquakes (deeper than 35 km) recorded by stations of the Hellenic Unified Seismic Network and published by the National Observatory of Athens (NOA) published since 2008. Here we include picks between 2008-2015.

Due to the difference in station coverage, these datasets differ significantly in terms of earthquake magnitude range and average station-earthquake offset. In the last few years, the Hellenic seismic network has been expanded significantly. Thus, there are more low-magnitude events in the NOA dataset that match the selection criterion regarding the minimum number of observations. For the FULL dataset, the average station-earthquake offset is 151 km, for MEI it is 207 km, and for NOA it is 82 km, while the mean earthquake depth for the three datasets is 54 km, 36 km and 61 km, respectively.

First, we compare the 1-D models output by VELEST for the three datasets (see Fig. S3). The models differ significantly in the crust, with the NOA-dataset yielding systematically higher velocities than the MEI-dataset. This discrepancy is likely due to the difference in ray paths (short for NOA, long for MEI) and event depths (deeper for NOA than MEI) between the two subsets. And it may very well be that neither subset yields an adequate ray coverage to recover crustal velocities accurately. Combining the two subsets in the FULL dataset affords a more comprehensive ray coverage and yields an intermediate 1-D velocity model. Below the Moho, all three datasets recover velocities that are similar.

Second, we compare the 3-D inversion results for the three datasets. These comparisons are shown in Figures S4 and S5. We first note that the five main features that we have identified in the Results Section, and which form the basis of most of our interpretation, are well observed in the independent subsets:

I A thickening of the top layer with low velocities near the collision zone
II A low-Vp layer dipping at 20° toward the NE
III A high-Vp dipping layer directly underlying the low-Vp dipping layer (II)
IV A low Vp/Vs-ratio feature in the lower overriding crust
V A high Vp/Vs-ratio anomaly just above the WBZ in the southern part of the mantle wedge (C - F)

There are, however, a number of notable differences between the models from the two subsets. As in the case of the 1-D inversions, theses differences are associated with the variability in ray coverage between the two subsets: (i) In the northern part of the imaged domain, there is poorer recovery of deep structure below 50 km depth in the NOA-subset; (ii) In the southern part, the dipping LVL is only weakly recovered in the MEI-dataset; and (iii) The overriding crust has systematically higher velocities in the NOA-dataset. Despite these discrepancies, we have confidence in our final model because the five main features are well recovered by both independent subsets.

Data Set S1.

This file "ds01.csv" contains the relocated earthquakes with origin time (year, month, day, hour, minute, second), hypocenters (longitude and latitude in decimal centidegrees, z-coordinate in km, with the z-axis pointing up from the surface) magnitude.

Data Set S2.

File "ds02.vtk" contains the 3-D P-velocity and Vp/Vs-ratio models, with velocities in km/s. The models can be opened for display with the opensource visualization software Paraview [*Ahrens et al.*, 2005], and the file format can be read with appropriate vtk-reader functions in most programming languages. X- and Y-coordinates are supplied in centidegrees (longitude and latitude times 100) so that the aspect ratio of axes does not have to be corrected.

Data Set S3.

File "ds03.csv" contains the point data of the fitted slab top. Points are provided with longitude and latitude values in decimal centidegrees, and z-coordinates in km, with the z-axis pointing up from the surface. To display the slab top surface in Paraview, load "ds03.csv". Apply the "TableToPoints" filter, chosing longitude as X-values, latitude as Y-values and "z(up)" as Z-values. Then apply the "Delaunay2d"-filter to the object output from "TableToPoints".

Data Set S4.

File "ds04.vtk" contains the coastlines of Greece, which can be loaded into Paraview for display on top of the tomographic model. The coastline data are from the global self-consistent, hierarchical, high-resolution shoreline database [GSHHS, *Wessel and Smith*, 1996].

References

Ahrens, J., B. Geveci, and C. Law (2005), ParaView: An end-user tool for large-data visualization, *Visualization Handbook*, *836*, 717–731, doi:10.1016/B978-012387582-2/50038-1.

Haslinger, F., E. Kissling, J. Ansorge, D. Hatzfeld, E. E. Papadimitriou, V. Karakostas, K. C. Makropoulos, H. G. Kahle, and Y. Peter (1999), 3D Crustal structure from local earthquake tomography around Gulf of Arta, *Tectonophysics*, *304*, 210–218.

Kennett, B. L. N., E. R. Engdahl, and R. Buland (1995), Constraints on seismic velocities in the Earth from traveltimes, *Geophys. J. Int*, *122*, 108–124, doi:10.1111/j.1365-246X.1995.tb03540.x.

Wessel, P., and W. H. F. Smith (1996), A global, self-consistent, hierarchical, high-resolution shoreline, *Journal of Geophysical Research*, *101*(B4), 8741–8743.

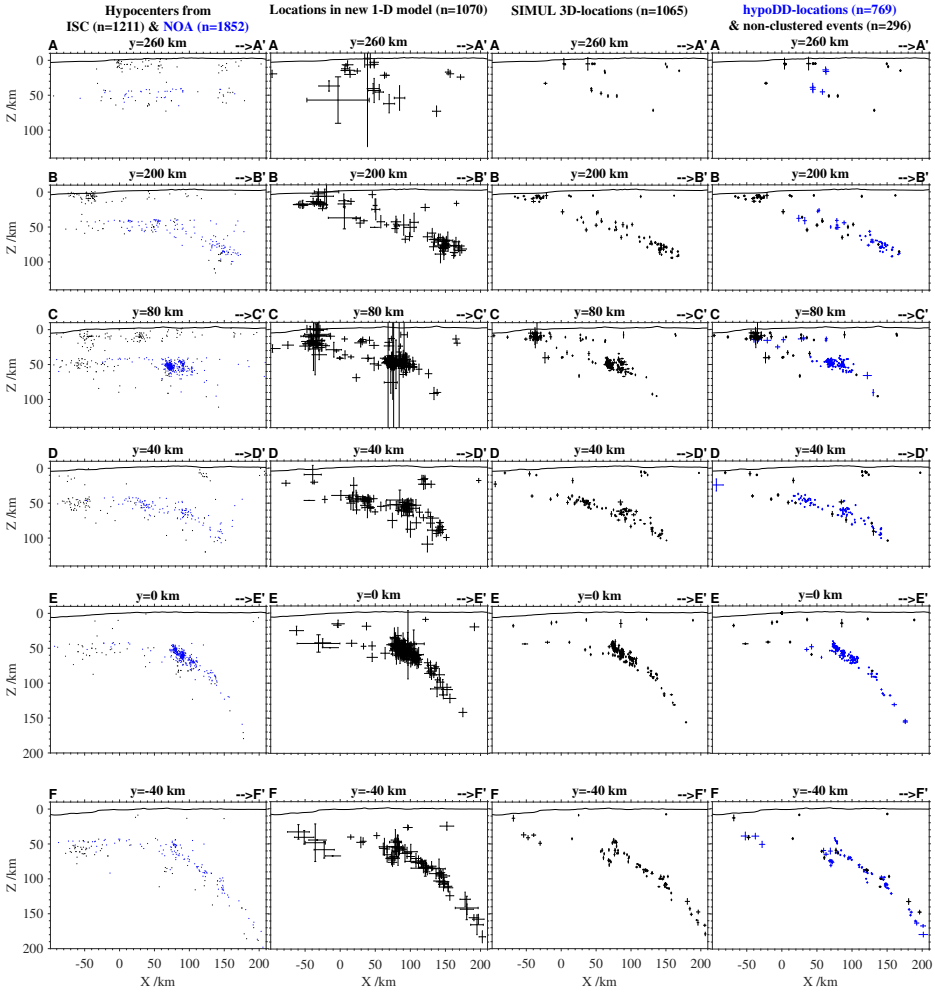

Figure 2. Comparison of hypocenters: (1) from the ISC catalog (black dots) and the NOA catalog (blue dots); 2) after quality control selection based on 1-D joint velocity/hypocenter inversion; 3) after 3-D tomographic inversion; and 4) after double-difference relocation. In the fourth column, blue dots show hypocenters that were deemed part of a deep cluster and thus relocated by double-difference, whereas black dots are isolated hypocenters that remain unchanged from 3-D inversion results. See supplemental text for discussion.

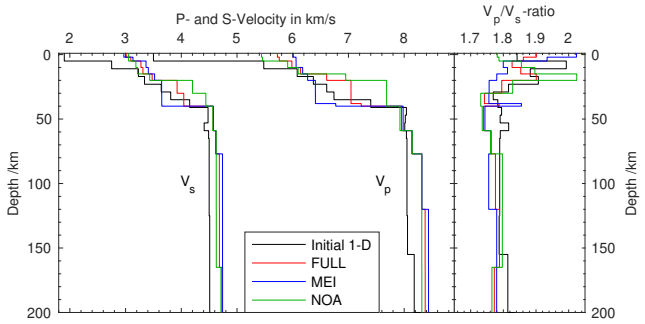

Figure 3. Comparison of 1-D velocity models used for the two independent data subsets MEI and NOA, and for the FULL dataset. "Initial 1-D" denotes the initial model based on the model of *Haslinger et al.* [1999] for the crust and the AK135 model [*Kennett et al.*, 1995] for depths below 45 km.

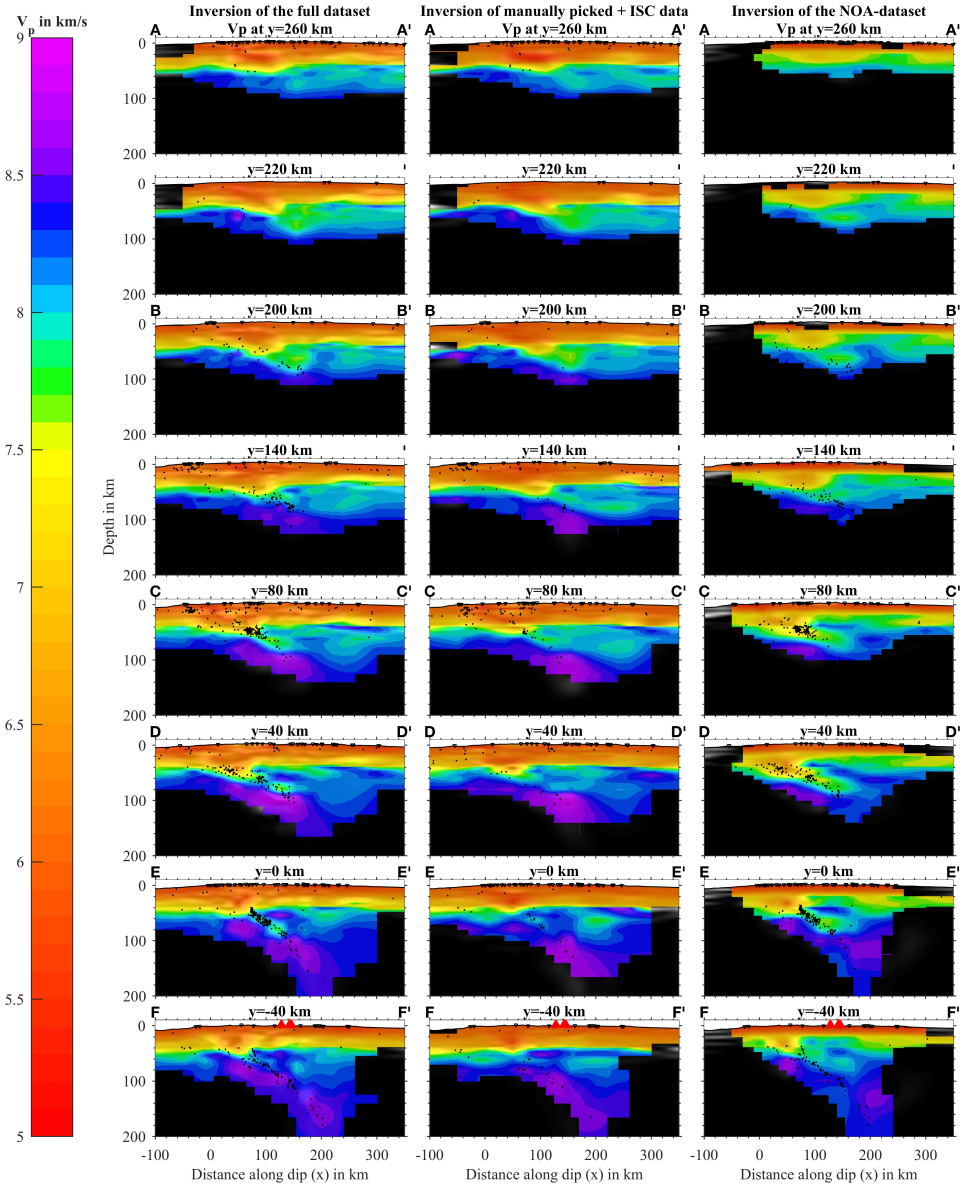

Figure 4. Comparison of 3-D Vp models obtained from the inversion of the FULL dataset and two independent data subsets, MEI and NOA, along eight cross sections (sections A-F, see Fig. S7).

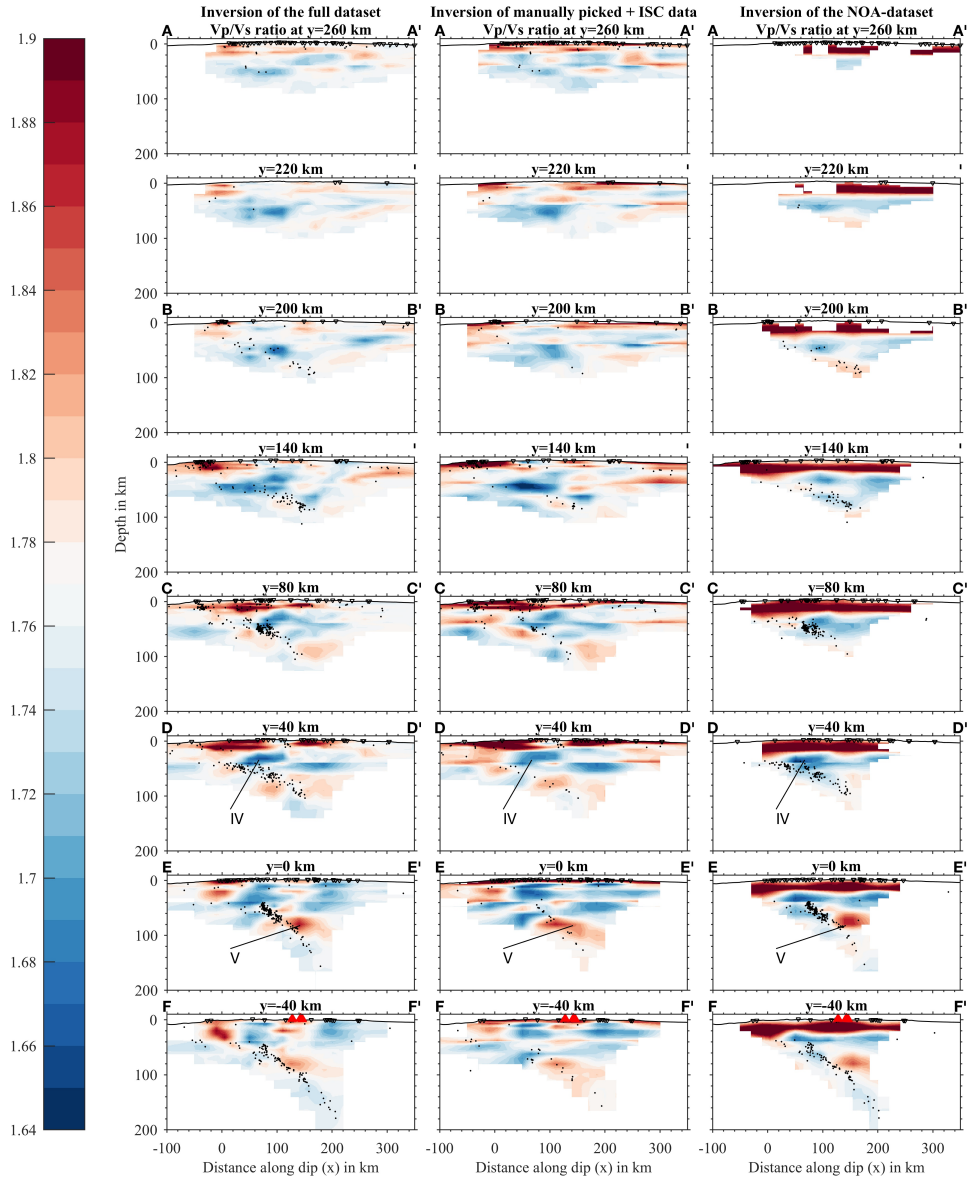

Figure 5. Comparison of 3-D Vp/Vs-ratio models obtained from the inversion of the FULL dataset and two independent data subsets, MEI and NOA, along eight cross sections (sections A-F, see Fig. S7).

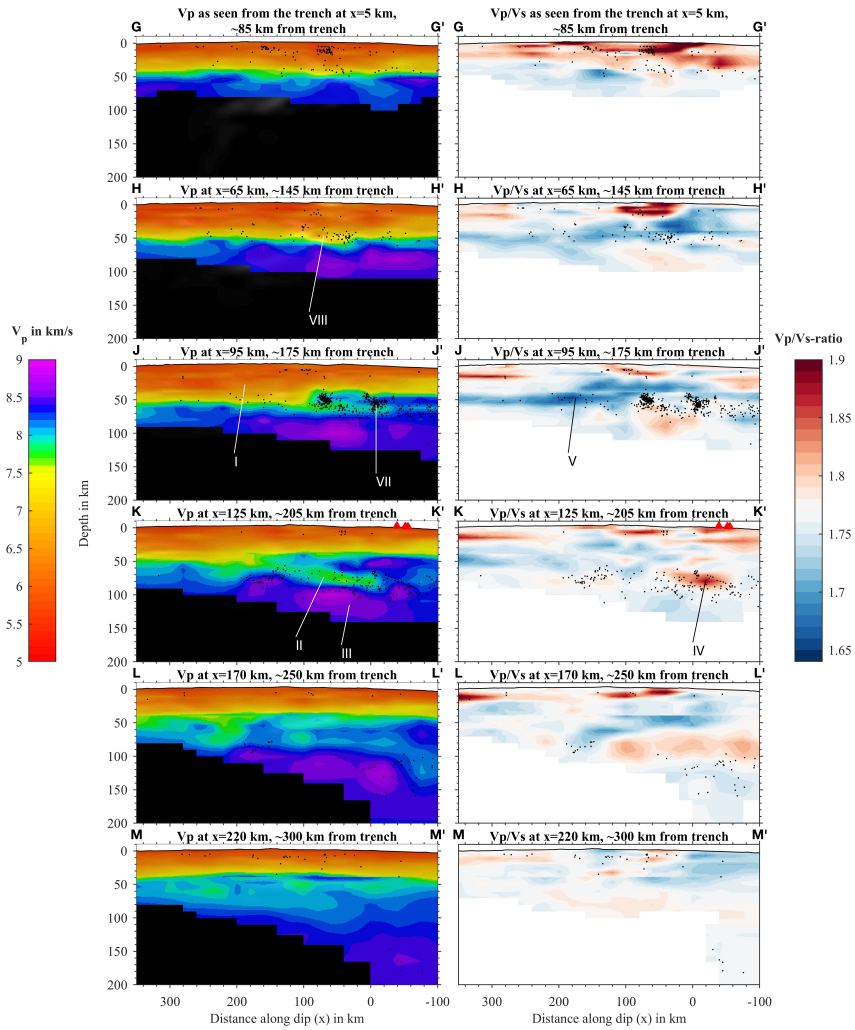

Figure 6. Trench-parallel cross sections through the P-velocity and Vp/Vs-ratio models - as seen from the trench toward the NE. The location of these cross sections G-M are plotted in the upper-right panel of Fig. S7. Roman numerals mark features discussed in sections 6-7 of the main article. Note how the low-velocity subducting crust (II) is well resolved throughout the model, albeit most clearly in the middle of the sections where ray coverage is best. Feature IV, which we interpret as partial melt in the mantle wedge, is clearly limited in its along-strike extent. Meanwhile feature V, which we interpret as silica-enrichment of the lower forearc crust, becomes clearer beyond the northwestern end of region of inferred partial melt. Two earthquake clusters in the mantle wedge (VII) are also clearly limited in their along-strike extent.

Paper II

Earthquakes track subduction fluids from slab source to mantle wedge sink

Felix Halpaap[1], Stéphane Rondenay[1], Alexander Perrin[2], Saskia Goes[2], Lars Ottemöller[1], Håkon Austrheim[3], Robert Shaw[2], Thomas Eeken[2]

[1] Department of Earth Science, University of Bergen, Bergen, Norway.
[2] Department of Earth Science and Engineering, Imperial College London, London, UK.
[3] Physics of Geological Processes (PGP), The Njord Centre, Department of Geosciences, University of Oslo, Oslo, Norway.

Science Advances, in press (2019)

As supplements to the paper, the datasets and data products obtained in this study are deposited in the PANGAEA repository (`www.pangaea.de`) under:

Halpaap, Felix; Rondenay, Stéphane; Perrin, Alexander; Goes, Saskia; Ottemöller, Lars; Austrheim, Håkon; Shaw, Robert; Eeken, Thomas (2018): Western Hellenic Subduction Zone: deep earthquake activity 2000 - 2017, plate interface geometry and thermal model. PANGAEA, https://doi.org/10.1594/PANGAEA.894351.

Science Advances
AAAS

Science Advances
AAAS

wedge (□□, □□), (ii) serpentine dehydration embrittlement (□□), and (iii) pulses of fluids released from the plate interface (□□, □□). Though no consensus has been reached, the similarities between these different clusters both in terms of geometry (localized clouds extending 10-40 km above the slab) and earthquake mechanisms (extensional) point to a common origin. There is an additional shared attribute that has received little attention until now but will be key in the following discussion: in all these regions, the subducting crust directly updip from the mantle wedge earthquakes exhibits a region of diminished seismic activity (Figs. 2 A, 4).

□

□□□□ □□□□□

Our seismic results, in conjunction with thermal-petrologic models constructed specifically for western Greece (see Methods), can help discriminate between the possible causes of mantle wedge earthquakes. First, we can test the serpentine dehydration hypothesis by contrasting the P-T outline of the serpentine-out reaction with the seismicity distribution (Fig. 3). This comparison shows that earthquakes occur in a portion of the system that is much too cold for de-serpentinization to occur. Thus the de-serpentinization hypothesis is not supported by our results. Second, we can also reject the hypothesis of large bodies of exotic material in the mantle wedge, as these would cause velocity perturbations that are not supported by the seismic images (Figs. 2-3), which show a fairly uniform, high-velocity mantle wedge beneath western Greece. Our results point instead to mantle wedge seismicity as being due to fluids released from the subducted slab (□□). They also tell a broader story of fluid transit from source to sink in cold subduction zones (Fig. 5), which we shall now explore further with the aid of our thermal-petrologic models.

The deepest slab earthquakes appear to mark the primary locus of mineral-sourced fluids, associated with the blueschist-eclogite transition in the crust and the antigorite-out reaction in the mantle (□, □□). Our thermal-petrologic models (Fig. 3 B) show that for western Greece these reactions occur at 80-140 km and 80-200 km depth, respectively, with limited sources of fluids present at shallower depths. These reactions occur along isotherms that are oblique to the dip of the slab, matching well the obliquity observed between seismicity and slab structure (Fig. 3 A). Major fluid production and release at this depth is also supported by the tomographically imaged high Vp/Vs-ratio in the overlying subarc mantle wedge (Figs. 2 D, S3, (□□)).

While most fluids escape directly upward into the mantle wedge through a plate interface damaged by metamorphic reactions (□□), some must make their way updip through the slab. This updip flow can occur under an intact plate interface that remains sealed owing to shear-induced grain size reduction (□, □□, □□) and/or along a direction of minimum effective pressure that follows the slab (□□). The latter has been invoked to explain intraslab seismicity (□□, □□), and could produce the zones of weakness required to facilitate rupture in the Hellenic forearc slab updip of 80 km depth□But simply observing intraslab seismicity above 80 km is insufficient to favor such fluid-aided weakening over alternative rupture processes. What establishes fluid as an essential player is the fact that at some locations the seismicity deflects from the slab into the mantle wedge, leaving regions of considerably reduced seismicity updip of the point of deflection. This points to a scenario in which the earthquake-inducing fluids, during their updip migration, encounter a vent at the interface that diverts them into the mantle wedge. The slab

Earthquake Detection

signal-to-noise ratio. The template matching is done with the EQcorrscan 0.2.7 software package (*34*), on the template envelopes filtered between 1.5 – 6.0 Hz. We use the envelopes because they describe any earthquake from a similar source region, as reflected by a distinct separation between P- and S-phases, rather than events with similar mechanism, which would restrict our search to repeating earthquakes. With this approach, we detect another 259 deep events, which are all manually picked and verified for quality control.

Third, we expand our search to earthquakes that occurred over the entire available time span of 2006-2017. To do so, we run the EQcorrscan template-matching software for all stations that were operating during that time in the northeastern Peloponnese and Attica region. We use a suite of templates that comprise the templates and detected events from step 2 (339) plus 255 events from the NOA catalog, for a total of 594 templates. Here, the template matching is done on the waveforms instead of the envelopes. The waveforms are 7-s long (starting 0.2 s before the P- or S-pick) and filtered between 2.5-8.0 Hz. A detection triggers when the median average deviations of the cross-correlation sum across channels is >8, upon which the program picks an arrival on those channels where the highest single-channel cross-correlation exceeds 0.4 in a 0.8-s window around the detection. We retain events with at least six P-picks for manual review. Only events located within 60/+50 km of the profile in Fig. 3 A are retained. This returns an additional 646 events for the 2006-2017 period.

Through the procedure described above, we add 941 events to the catalog of ref. (*16*), which together with the 317 newly verified deep events of the NOA catalog 2016 – 2017 result in a catalog with a total of 2172 events. For the period of 2006 – 2017 this catalog is complete to a magnitude threshold of 1.9 (fig. S5 B), owing mainly to the quality control that allowed us to identify and reject events from the NOA catalog that were located in the upper plate. Within the vicinity of the Tripoli cluster, our detection procedure yields a data subset (plotted in Fig. 3 A) that is complete to a lower magnitude threshold of 1.1, as shown in fig. S5 C.

Earthquake Relocation

To determine precise earthquake hypocenters, we adopt a relocation procedure that comprises three stages: (a) inversion in the 1-D background velocity model obtained in ref. (*16*); (b) inversion in the 3-D background velocity model obtained in ref. (*16*); and (c) relocation with the double-difference (DD) method (*35*). Stages (a) and (b) closely follow the methodology of ref. (*16*), except that here we fix the velocity model to those obtained in that study – i.e., the velocity models are not updated during the relocation. Below, we discuss the outcome of each stage in more detail.

In **stage a)**, we compute earthquake locations by least-squares inversion of P- and S-arrival times in a 1-D model. We perform picking in Seisan (*36*) and the relocation is done with the program Hypocenter (*37*) included in Seisan. For each event, we visually check that picks are correctly assigned and remove picks with residuals larger than 6 s. We estimate absolute location errors from the solution variance (arrival time misfit) as described in refs. (*16*, *37*). The hypocenter solutions obtained at this stage have average location errors of 5.1 km in the horizontal direction and 7.5 km in the vertical direction. The results are used to identify events with deep origin (>35 km depth – taking into account vertical error bars) that will be retained for further processing.

(rather than absolute errors as in stages a and b) through jackknife-resampling of the dataset (*35*, *40*). For this we rerun the double-difference inversion 1000 times with a reduced dataset in which 10 % of the differential arrival times are randomly removed. The errors are then estimated with the general "delete-j" jackknife estimator described in ref. (*40*). We find that, on average, the relative location error is 0.19 km in the horizontal direction and 0.21 km in the vertical direction. The relative errors of earthquakes within ± 50 km of the cross section in Fig. 3 A are shown in fig. S7.

Focal Mechanisms

We calculate focal mechanisms from first motion polarities and select the best solution based on the misfit of amplitude ratios between P- and S-arrivals. This is done using the program FocMec (*41*). The polarities are picked manually on the vertical channel. Solutions are calculated only for events that have at least 10 consistent polarity picks (the average was 23 picks). The amplitude ratios are automatically measured in the frequency domain in Seisan. We adopt a two-step workflow to compute the focal mechanisms. In a first step, we use FocMec to find an approximate solution based exclusively on polarities, searching the parameter space for strike, dip, and rake-values that best fit the polarities. When we find clearly concentrated groups of solutions (i.e., solutions where the P and T axes fall in small, ~1/10 areas of the lower hemisphere projection), we proceed to the second step in which we constrain the solutions further by fitting observed amplitude ratios to theoretical predictions. For these fits, we impose two restrictions to help identify robust solutions: i) the number of amplitude ratios where observation and prediction do not match should not exceed 25 – 50 % of the total number of measurements; and ii) the maximum amplitude ratio error, i.e., the difference between the measured and predicted amplitude ratio, should not exceed 30 – 40 %. We aim to choose these values such that they yield less than ~30 solutions when searching the parameter space in steps of 1 – 2°. In the case where an earthquake has a large number of polarity picks (20), this second step requires us to tolerate more polarity errors than in the first step since we may be fitting more polarities close to the nodal planes. However, we only allow the solutions from step 2 to refine those from step 1, and do not accept solutions that differ markedly between the two steps.

Here, we solve for 81 focal mechanisms with the approach described above. This initial list is complemented with 21 solutions from the literature (see table S2). This results in a catalog of 85 earthquakes with one or more focal mechanism solutions. Figure S4 shows 38 of these focal mechanisms for earthquakes that occurred within section C of Fig. 1 (see also Fig. 3 A).

Thermal and phase stability Modeling

We calculate temperatures for the subduction zone and flow in the mantle wedge (and below the subducting plate) as in Perrin et al. (*42*), by solving the coupled Stokes and energy equations in Boussinesq approximation using the code Fluidity (*43*). We constrain the models by kinematically prescribing the subducting plate, with the plate interface interpreted from the scattered wave image in Fig. 3 A. Beyond the depth to which the image recovers a sharp velocity contrast at the top of the subducting crust, we trace the lower-to-higher (from top to bottom) velocity contrast in the tomographic image in fig. S6 A, which we then extend linearly to depth. At an approximate angle of 45°, this trend agrees well with the dip of the slab imaged in mantle-scale tomography ((*44*), *and references therein)*. The top 10 km of the subducting plate has a set velocity of 35 mm/yr (*13*). Due to the composite temperature- and pressure-dependent dislocation-diffusion creep rheology (all parameters as in Perrin et al.

anisotropy in the Western Hellenic subduction zone and its geodynamic significance. *Earth Planet. Sci. Lett.* **391**, 100–109 (2014).

32. J. Escartín, G. Hirth, B. Evans, Strength of slightly serpentinized peridotites: Implications for the tectonics of oceanic lithosphere. *Geology.* **29**, 1023–1026 (2001).

33. National Observatory of Athens, Database of revised events (2018), (available at http://bbnet.gein.noa.gr/HL/databases/database).

34. C. J. Chamberlain, C. J. Hopp, C. M. Boese, E. Warren-Smith, D. Chambers, S. Chu, X. Shanna X., K. Michailos, J. Townend, EQcorrscan: Repeating and near-repeating earthquake detection and analysis in Python. *Seismol. Res. Lett.* (2017), doi:10.1785/0220170151.

35. F. Waldhauser, W. L. Ellsworth, A double-difference earthquake location algorithm: Method and application to the northern Hayward fault, California. *Bull. Seismol. Soc. Am.* **6**, 1353–1368 (2000).

36. J. Havskov, L. Ottemöller, SeisAn Earthquake Analysis Software. *Seismol. Res. Lett.* **70**, 532–534 (1999).

37. B. R. Lienert, J. Havskov, A computer program for locating earthquakes both locally and globally. *Seismol. Res. Lett.* **66**, 26–36 (1995).

38. F. Bleibinhaus, H. Gebrande, Crustal structure of the Eastern Alps along the TRANSALP profile from wide-angle seismic tomography. *Tectonophysics*. **414**, 51–69 (2006).

39. M. Beyreuther, R. Barsch, L. Krischer, T. Megies, Y. Behr, J. Wassermann, ObsPy: A Python toolbox for seismology. *Seismol. Res. Lett.* **81**, 530–533 (2010).

40. B. W. Tichelaar, L. J. Ruff, How Good Are Our Best Models? *EOS.* **70**, 593, 605–606 (1989).

41. J. A. Snoke, J. W. Munsey, A. G. Teague, G. A. Bollinger, Program for focal mechanism determination by combined use of polarity and SV-P amplitude ratio data. *Earthq. Notes*. **55**, 15 (1984).

42. A. Perrin, S. Goes, J. Prytulak, D. R. Davies, C. Wilson, S. Kramer, Reconciling mantle wedge thermal structure with arc lava thermobarometric determinations in oceanic subduction zones, *Geochemistry, Geophys. Geosystems*. **17**, 4105–4127 (2016).

43. D. R. Davies, C. R. Wilson, S. C. Kramer, Fluidity: A fully unstructured anisotropic adaptive mesh computational modeling framework for geodynamics. *Geochemistry, Geophys. Geosystems*. **12** (2011), doi:10.1029/2011GC003551.

44. H. Zhu, E. Bozd g, J. Tromp, Seismic structure of the European upper mantle based on adjoint tomography. *Geophys. J. Int.* **201**, 18–52 (2015).

45. E. M. Syracuse, P. E. van Keken, G. A. Abers, D. Suetsugu, C. Bina, T. Inoue, D.A. Wiens, M. Jellinek, The global range of subduction zone thermal models. *Phys. Earth Planet. Inter.* **183**, 73–90 (2010).

46. T. J. B. Holland, R. Powell, An internally consistent thermodynamic data set for phases of petrological interest. *J. Metamorph. Geol.* **16**, 309–343 (1998).

47. J. a D. Connolly, Computation of phase equilibria by linear programming: A tool for

Seismol. Res. Lett.

Phys. Chem. Earth, Parts A/B/C

Ann. Geophys.

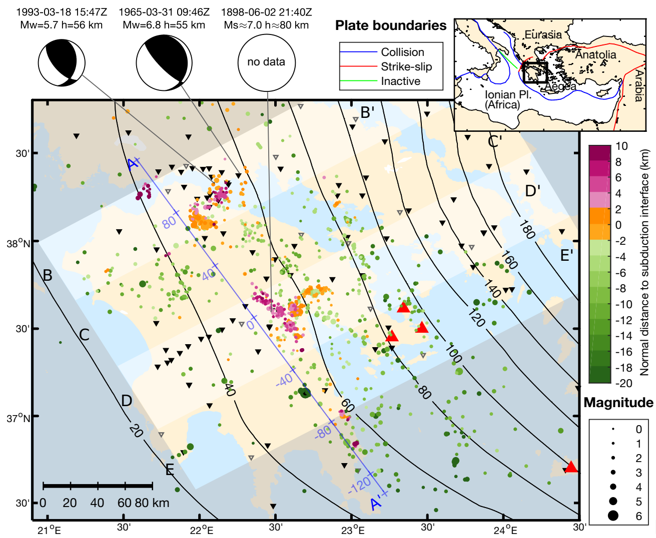
1993-03-18 15:47Z
Mw=5.7 h=56 km
1965-03-31 09:46Z
Mw=6.8 h=55 km
1898-06-02 21:40Z
Ms≈7.0 h≈80 km
no data
Plate boundaries
Collision
Strike-slip
Inactive
Eurasia
Anatolia
Aegea
Arabia
Ionian Pl.
(Africa)
Normal distance to subduction interface (km)
Magnitude
0 20 40 60 80 km
21°E
22°E
23°E
24°E
38°N
37°N
B'
C'
D'
E'
B
C
D
E
A
A'

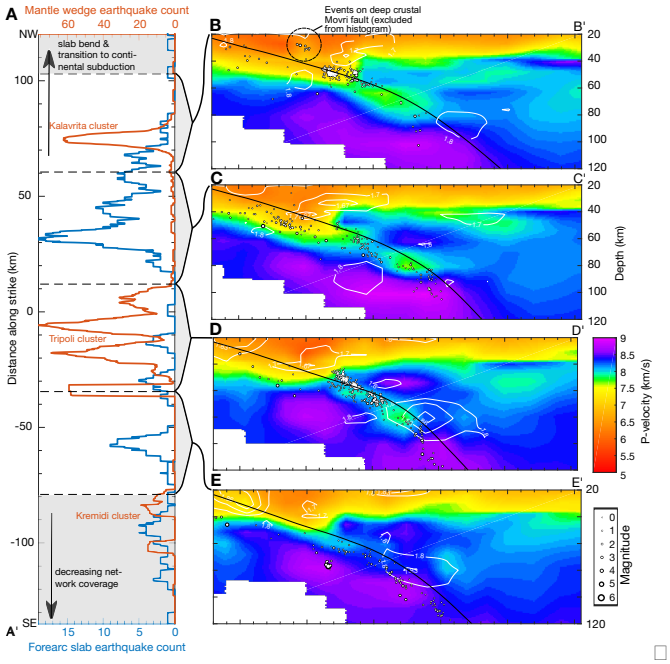

Fig. 2. Distribution of slab earthquakes and seismic velocity structure beneath western Greece.

A [illegible] **B – E** [illegible]

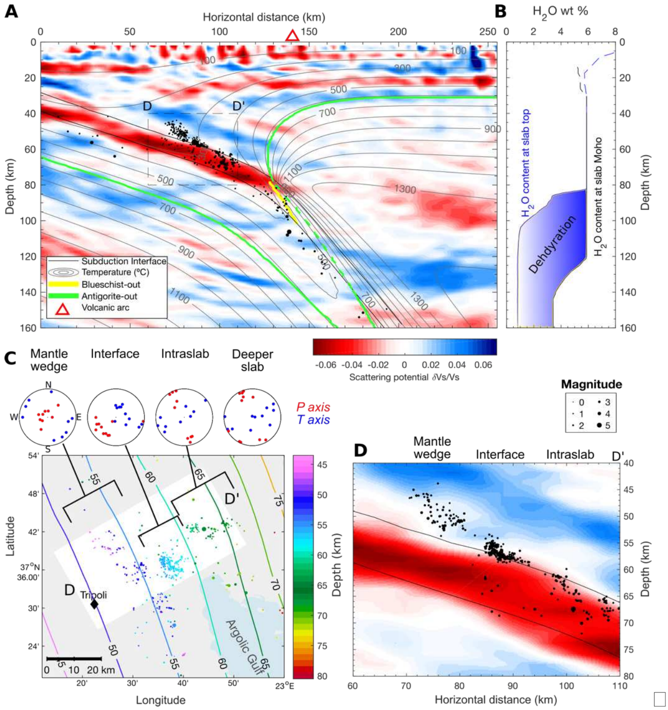
A
Horizontal distance (km)
Depth (km)
D
D'
Subduction Interface
Temperature (°C)
Blueschist-out
Antigorite-out
Volcanic arc
B
H2O wt %
H2O content at slab top
H2O content at slab Moho
Dehydration
Depth (km)
Scattering potential δVs/Vs
C
Mantle wedge
Interface
Intraslab
Deeper slab
P axis
T axis
Latitude
Longitude
Tripoli
Argolic Gulf
Depth (km)
Magnitude
D
Mantle wedge
Interface
Intraslab
D'
Depth (km)
Horizontal distance (km)

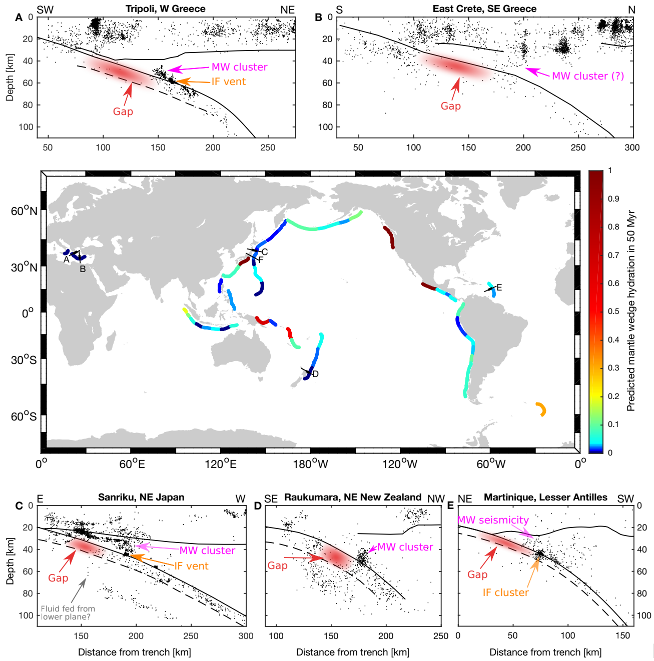
A
Tripoli, W Greece
SW
NE
Depth [km]
MW cluster
IF vent
Gap
B
East Crete, SE Greece
S
N
MW cluster (?)
Gap
60°N
30°N
0°
30°S
60°S
0°
60°E
120°E
180°W
120°W
60°W
0°
Predicted mantle wedge hydration in 50 Myr
C
Sanriku, NE Japan
E
W
MW cluster
IF vent
Gap
Fluid fed from lower plane?
D
SE
Raukumara, NE New Zealand
NW
MW cluster
Gap
E
NE
Martinique, Lesser Antilles
SW
MW seismicity
Gap
IF cluster
Distance from trench [km]

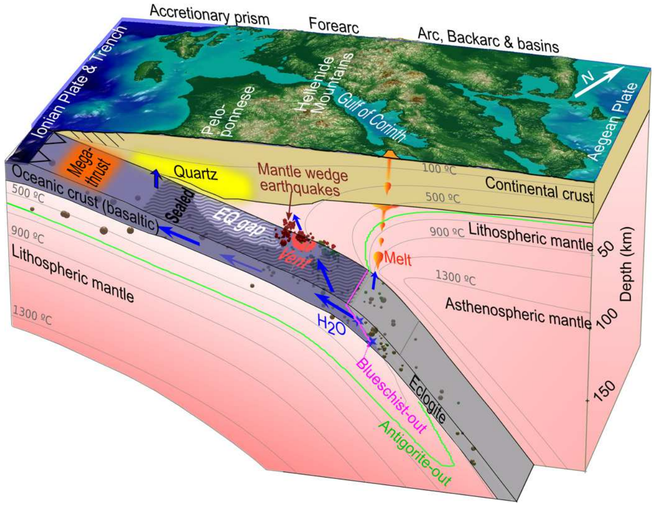

The fluids originate from dehydration reactions in the slab and flow either toward the melting zone in the mantle or updip below a sealed plate interface. Fluids that flow updip trigger earthquakes (EQ, black circles) as they migrate along the slab toward the overriding crust (where they precipitate into quartz) or if they escape via localized vents into the cold mantle wedge corner (where they cause unusual mantle wedge earthquakes). Reduced fluid flow in the subducting crust updip of these vents leads to reduced seismicity. Other subduction zones with cold interfaces and dry mantle wedges (see Fig. 4) exhibit similar fluid migration patterns.

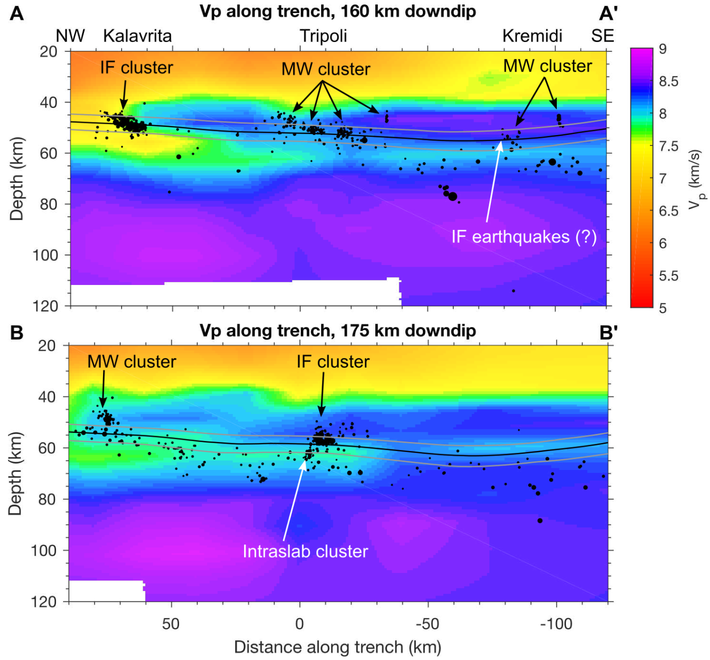
A
Vp along trench, 160 km downdip
A'
NW
Kalavrita
Tripoli
Kremidi
SE
IF cluster
MW cluster
MW cluster
IF earthquakes (?)
Depth (km)
20
40
60
80
100
120
V
p
(km/s)
9
8.5
8
7.5
7
6.5
6
5.5
5
B
Vp along trench, 175 km downdip
B'
MW cluster
IF cluster
Intraslab cluster
Depth (km)
20
40
60
80
100
120
50
0
-50
-100
Distance along trench (km)

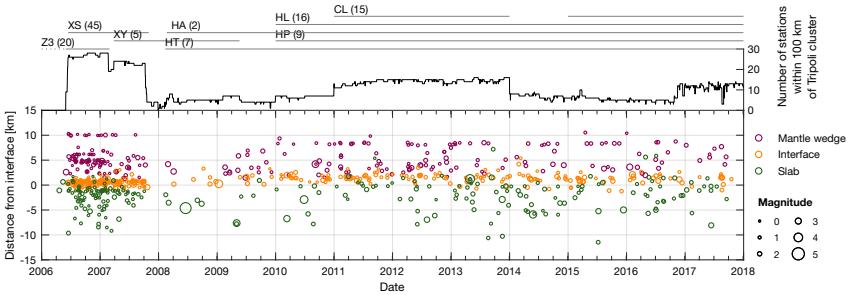

□□□□□□□□□□ □□ □□□□□□□□□□ □□□□□□□□□□□□ □□□□□□□□□□□□□□□□ □□□□□□□□□□ □□□□□The curve on top depicts the number of stations within 100 km radius for which we could download and process waveform data. The apparent periods with more (2006-06 to 2007-10) or less (2007-11 to 2009-02) seismic activity are thus due to differences in network coverage. Hence we detect no apparent cyclic behavior of earthquakes in the mantle wedge (magenta circles), compared to the annual cyclicity observed in Japan (□□). □

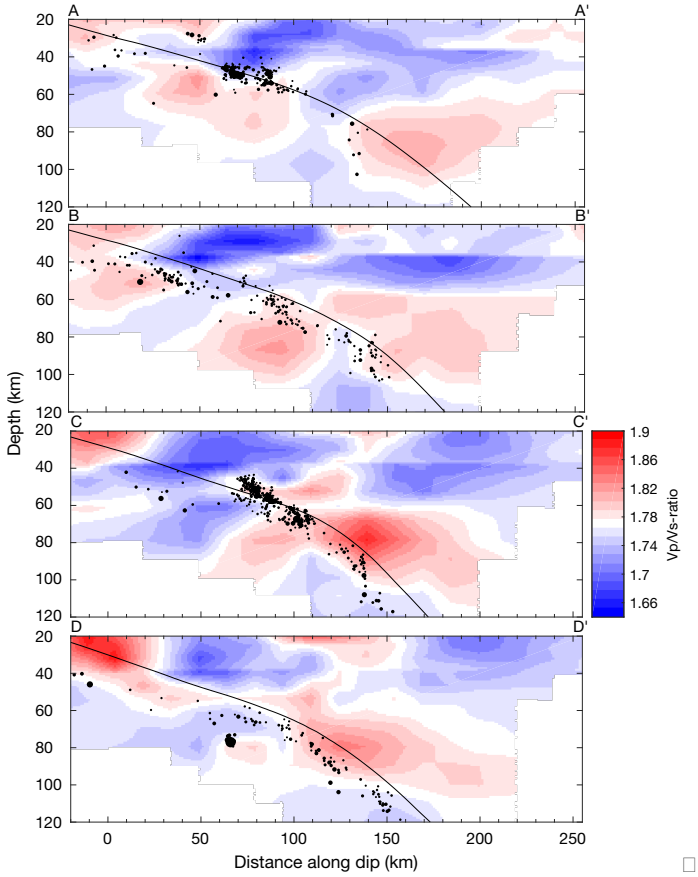

Fig. S3. P-velocity to S-velocity (Vp/Vs) ratio structure beneath western Greece. (A – D)

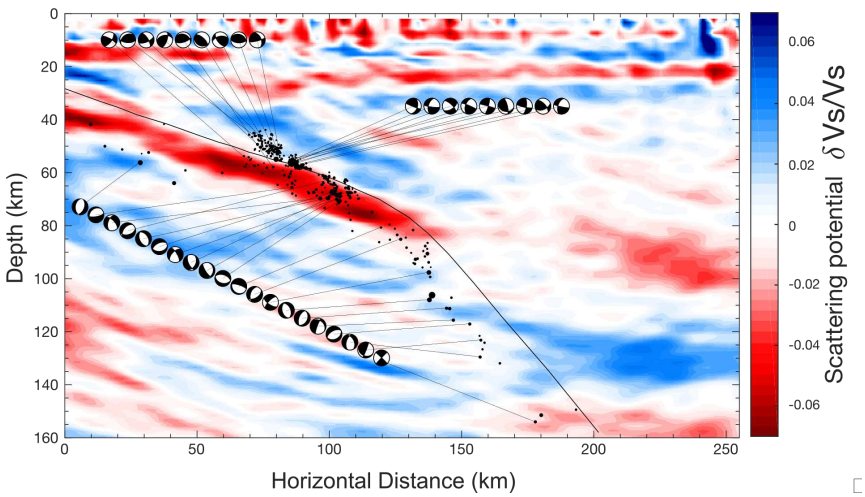
Depth (km)
Horizontal Distance (km)
Scattering potential δVs/Vs
0
20
40
60
80
100
120
140
160
0
50
100
150
200
250
0.06
0.04
0.02
0
-0.02
-0.04
-0.06

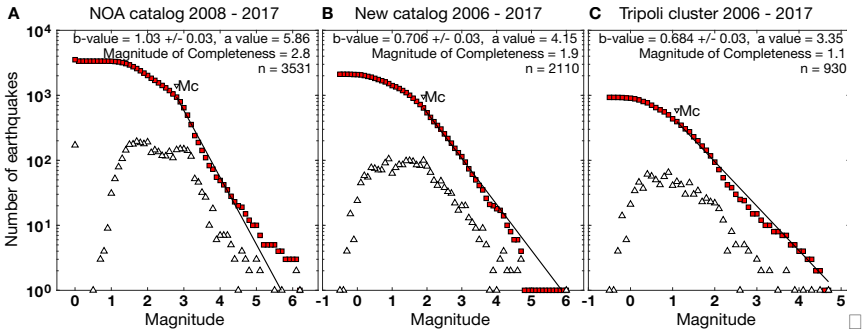
A
NOA catalog 2008 - 2017
b-value = 1.03 +/- 0.03, a value = 5.86
Magnitude of Completeness = 2.8
n = 3531
Mc
B
New catalog 2006 - 2017
b-value = 0.706 +/- 0.03, a value = 4.15
Magnitude of Completeness = 1.9
n = 2110
Mc
C
Tripoli cluster 2006 - 2017
b-value = 0.684 +/- 0.03, a value = 3.35
Magnitude of Completeness = 1.1
n = 930
Mc
Number of earthquakes
Magnitude
Magnitude
Magnitude

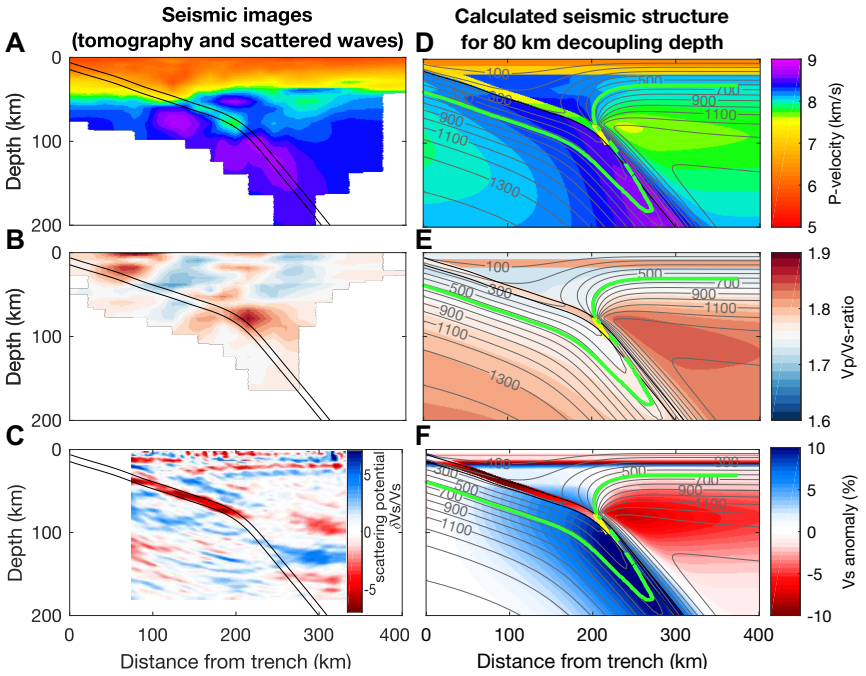

Fig. S6. Comparison of seismic images and calculated seismic structure along the cross section of Fig. 1 D (main text). (**A – C**) [illegible] **A** [illegible] **B** [illegible] **C** [illegible] (**D – F**) [illegible] **D** [illegible] **E** [illegible] **F** [illegible]

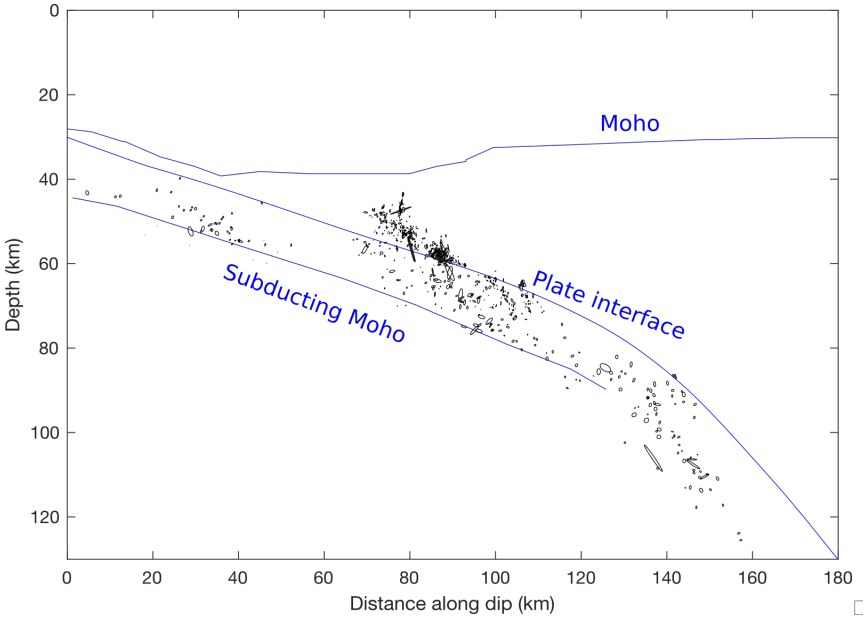

These errors were estimated from n=1000 inversions of jackknife-resampled differential arrival time data. Errors are on average 0.19 km in the horizontal direction [0.20 km in the dip direction (x), 0.17 km in the along-strike direction (y)], and 0.21 km in the vertical direction. The variations in error from one event to another are caused primarily by variations in station coverage at time when the events were recorded.

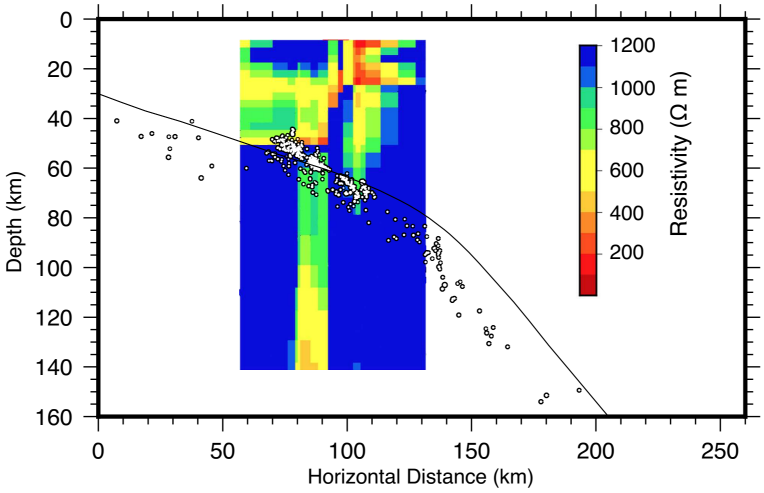

Fig. S8. Eart q ak dis rib tion nd ec ric res s iv ty elow eloponnes
We superimpose the earthquakes from the profile in Fig. 3 A (main text) onto the resistivity image from Tzanis et al. (68), which stems from a magnetotelluric survey of the Peloponnese that was first reported in Galanopoulos et al. (69). The magnetotelluric profile ran parallel to the scattered wave image shown in Fig. 3 A, about 20 km farther southeast. A vertically stretched low-resistivity anomaly coincides precisely with the cluster of interface seismicity, suggesting the presence of highly conductive material, e.g. saline slab fluid at that location. Vertically, the anomaly is likely stretched because depth tends to be poorly constrained in such magnetotelluric images.

Table S1. Seismograph networks from western Greece used in the waveform processing. Here we indicate the time periods that we used for the processing of waveform data from each network. We only used data that were publicly available through data services of the Federation of Digital Seismograph Networks at the time of the study.

Project / Institution	Network	Time period	Number of stations	Reference
Medusa	XS, temporary	2006-06 to 2007-10	46	(□□)
Egelados	Z3, temporary	2006-06 to 2007-04	20	(□□)
Simbaad	XY, temporary	2007 to 2009	5	(□□)
Corinth Rift Laboratory	CL, permanent	2011 to 2013 and 2016 to 2017	15	(□□)
University of Athens	HA, permanent	2008 to 2017	2	(□□)
National Observatory of Athens (NOA)	HL, permanent	2010 to 2017	16	(□□)
University of Patras	HP, permanent	2011 to 2017	9	(□□)
University of Thessaloniki	HT, permanent	2008 to 2017	7	(□□)
Geofon, Deutsches Geoforschungszentrum	GE, permanent	2006 to 2017	3	(□□)

[illegible]	37.90833	23.06027	97.651	291.8	41.4	80.9	t.P.
[illegible]	38.26258	22.13655	48.757	294.8	87.3	-65.0	t.P.
[illegible]	37.81202	22.29213	52.880	155.2	47.5	-79.1	t.P.
[illegible]	38.12738	22.87755	92.357	30.3	72.0	-17.6	t.P.
[illegible]	38.15479	21.96701	47.882	141.0	19.0	-98.0	([illegible])
[illegible]	38.63799	22.05844	68.927	269.2	38.2	-52.7	t.P.
[illegible]	37.67358	21.87896	49.577	244.3	84.3	-70.9	t.P.
[illegible]	37.62747	22.59445	56.446	247.4	57.2	-15.8	t.P.
[illegible]	38.30219	22.11913	53.962	335.4	10.1	84.3	t.P.
[illegible]	38.26491	22.15148	50.641	123.4	9.1	84.7	t.P. , ([illegible])
[illegible]	37.45544	22.63733	54.957	251.5	66.8	-47.9	t.P. , ([illegible])
[illegible]	38.10057	22.05250	49.043	347.2	74.5	-32.9	t.P.
[illegible]	39.38246	22.26299	94.221	335.9	49.8	41.3	t.P.
[illegible]	38.02575	23.48732	152.887	147.1	46.1	85.8	t.P.
[illegible]	37.81068	22.08351	58.671	96.9	63.3	70.9	t.P.
[illegible]	37.95745	22.08488	57.784	63.8	80.5	22.1	t.P. , ([illegible])
[illegible]	38.26439	22.13109	49.165	326.5	41.8	-48.9	t.P.
[illegible]	37.55861	22.81803	69.657	22.9	68.6	18.5	t.P.
[illegible]	38.10071	22.03666	49.772	166.2	86.0	52.9	t.P.
[illegible]	38.10728	22.04878	49.340	237.0	29.4	-43.0	t.P.
[illegible]	39.10487	22.32926	77.040	56.5	89.6	-23.0	t.P.
[illegible]	38.26243	22.11324	54.593	208.9	47.1	84.5	t.P.
[illegible]	38.26505	21.60220	28.293	262.9	57.6	-57.5	t.P.
[illegible]	39.20571	22.20979	82.416	227.4	62.2	66.1	t.P.
[illegible]	38.13694	21.97710	48.424	344.3	78.2	-22.2	t.P. , ([illegible])
[illegible]	38.26150	22.12297	52.811	329.8	11.2	79.6	t.P.
[illegible]	37.59070	22.85322	70.611	40.5	41.7	65.5	t.P.
[illegible]	37.61626	22.60150	55.007	160.0	74.0	90.0	t.P.
[illegible]	38.66357	22.43353	75.630	227.9	56.6	23.4	t.P.
[illegible]	37.62945	22.60436	56.593	132.4	85.2	75.0	t.P.
[illegible]	37.67763	21.89436	50.461	302.0	24.3	80.2	t.P.
[illegible]	37.62473	22.61175	56.422	131.6	65.7	68.0	t.P.
[illegible]	38.12599	21.95401	45.238	294.5	56.0	33.1	t.P.
[illegible]	37.65026	23.81716	156.986	10.0	58.0	-50.0	([illegible])
[illegible]	37.62393	22.59482	65.606	214.7	21.1	47.9	t.P.

3 Synthesis

In this chapter I provide a summary of findings from parts I-III (results chapter) and consolidate these findings in terms of the main research questions: What causes intermediate-depth earthquakes? In the first part of this thesis, I imaged the seismic structure and distribution of intermediate-depth seismicity in the Western Hellenic subduction zone, focusing especially on the location of earthquakes in relation to the main subduction discontinuities (Figs. 3.1, 3.2 I). A surprising result of the study was that earthquakes do not only occur in the subducting crust and slab mantle, but also in the mantle wedge. This phenomenon has not been extensively documented until now. It was found only in three other studies, which came to different conclusions on the cause of mantle wedge seismicity. In the second part, I constrained the mechanism that causes earthquakes in the mantle wedge and derived important new insight into the generation of intermediate-depth earthquakes in the 40-100 km-depth range in general (Fig. 3.2 II). Even though the dense seismograph coverage across Greece yielded high resolution images and hypocenter locations, uncertainties remained too large in some cases to determine precisely where the earthquakes are located relative to the main seismic discontinuities of the subduction system. Improving these relative locations can yield further insights into the processes that act in the system. In the third part, I developed a workflow to deduce whether an earthquake occurred in the mantle wedge, on the interface, in the subducting crust or in the slab mantle (Fig. 3.2 III). In this last chapter, I provide a summary of these three parts and discuss how their results can be integrated. This is followed by an outlook, in which I propose avenues for future research that arise from the findings of this thesis.

3.1 Main findings

The work presented in this thesis has yielded new constraints on the seismic attributes of the Western Hellenic subduction zone. These include new, high-resolution 3-D models of P-velocity, Vp/Vs-ratio and seismic discontinuities, relocated hypocenters (see

Fig. 3.1), a new catalog of focal mechanisms for intermediate-depth earthquakes, and a new model of the subduction zone's thermal structure. With the workflow developed to deduce the earthquakes' locations, I verified independently that earthquakes indeed occur in three separate source regions of the WHSZ: the mantle wedge, the subduction interface and the slab below Tripoli. This information shines a new light on (I) the transition from oceanic subduction in the south of the region to continental subduction in the north; (II) the fate of slab-derived fluids; and (III) the generation of intermediate-depth earthquakes in cold slabs and mantle wedges.

The main results are illustrated in Fig. 3.2 and can be summarized in five points:

1. Intermediate depth seismicity occurs within a single plane throughout the southern part of the WHSZ and is nearly non-existent in the northern part, with an abrupt south-to-north transition occurring at the Kephalonia Transform Fault. This change in seismicity appears to mark the boundary between two subducting domains: oceanic in the south and continental in the north, and reflects their varying composition and fluid content (Fig. 3.1). Slab dehydration seems to be particularly active in the southern part of the system, below the Peloponnese, where there is evidence for partial melting in the subarc mantle. Despite being nearly aseismic, the subducting continental crust in the north exhibits a low-velocity signature to at least 90 km depth (as imaged by P-wave scattering potential $\delta V_P/V_P$). I interpret this low-velocity signature and seismic quiescence as reflecting an absence of fluids, which inhibits metamorphism and seismicity in a metastable continental subducting crust (see Fig. 3.2 II).

2. The transition between oceanic subduction with more rollback in the south to continental subduction with less rollback in the north is marked by a smoothly deformed slab rather than a tear. This slab deformation is accompanied by a gap in deep intraslab seismicity (>60 km depth, Fig. 3.1), probably indicative of a change in thermal regime between south and north. The zone of slab deformation underlies the whole Central Hellenic Shear Zone and seems to affect the deformation in the overriding Aegean plate. I associate both the dextral strike-slip fault system of the 2008 Movri earthquake (M 6.4) and the western extension of the North Anatolian Fault with this area of deformation, which is driven by differential subduction between the south and the north (see Fig. 3.2 I).

3. How fluids interact with the mantle wedge and the overriding crust seems to be affected by the change in subduction style as well as local effects. The results suggest that fluids emanating from the subducted oceanic crust appear to migrate

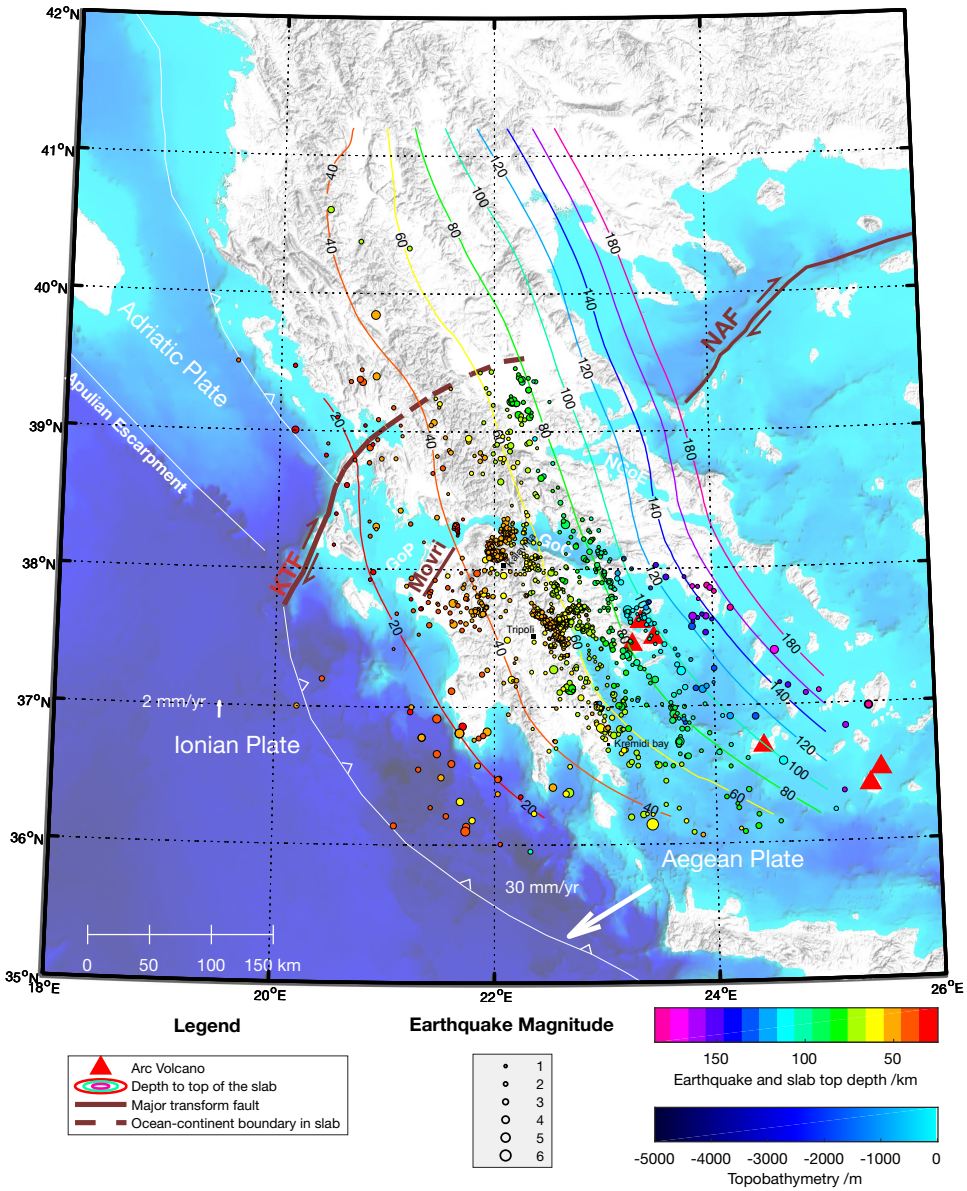

Figure 3.1: Map of mainland Greece and the Western Hellenic Subduction Zone showing relocated hypocenters and the depth of the subduction interface (contour lines). Compared to Figure 5 in *Halpaap et al.* (2018), this figure shows the larger earthquake catalog and updated subduction interface from *Halpaap et al.* (2019). Colored circles represent earthquakes with depths greater than 35 km. The circles are color coded by depth, and their size is proportional to earthquake magnitude. See legend for the description of other symbols and lines. Abbreviations used in the map: KTF: Kephalonia Transform Fault, NAF: North Anatolian Fault; GoC: Gulf of Corinth, GoP: Gulf of Patras, NGoE: Northern Gulf of Evia.

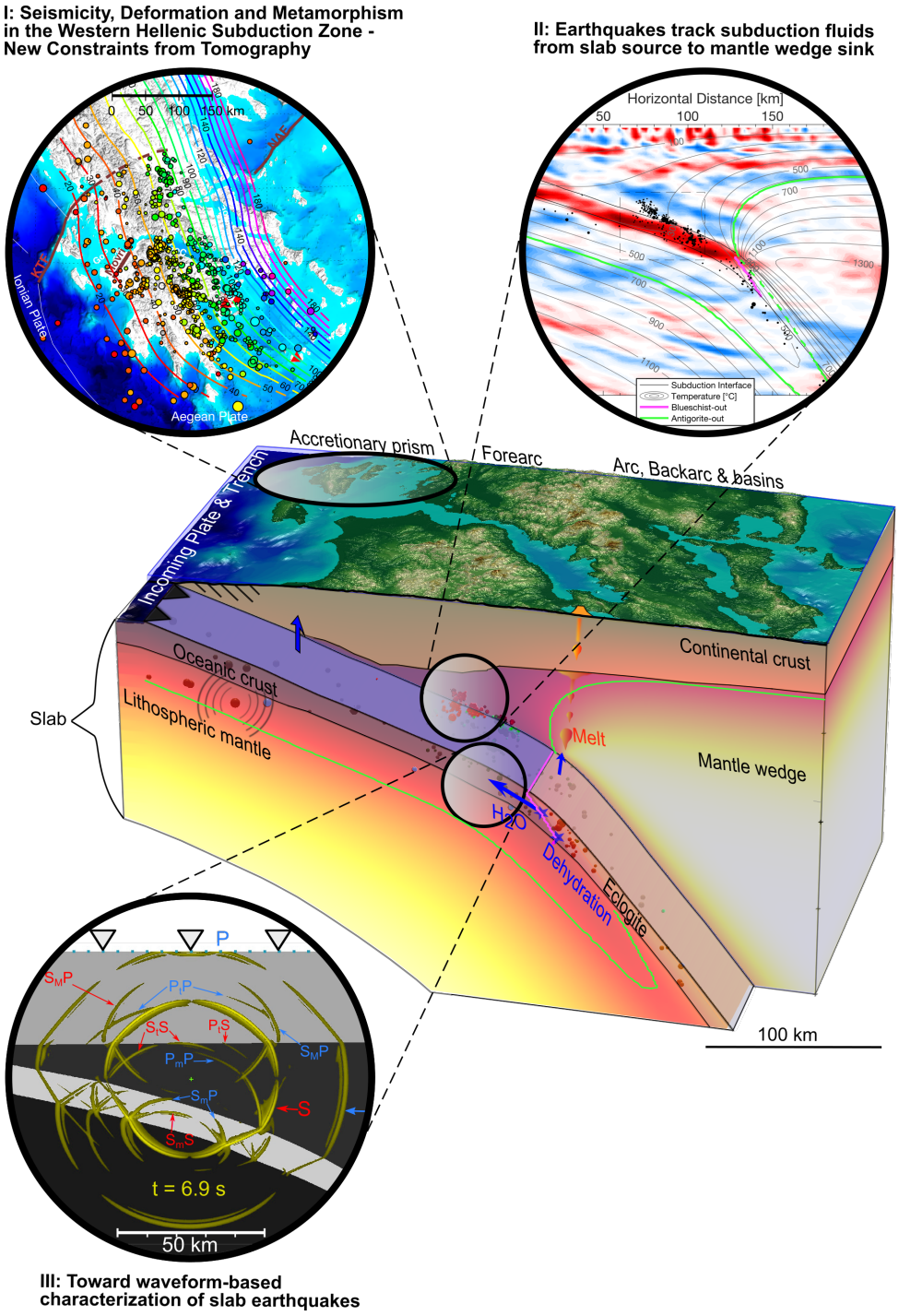

Figure 3.2: Sketch of the subduction system in the Peloponnese-Attica region, and main findings from this thesis (I-III), ordered by appearance in the three papers. **I** Abrupt termination of intermediate-depth seismicity at the transition from oceanic to continental subduction at the Kephalonia Transform Fault. **II** Cluster of mantle wedge seismicity below Tripoli. **III** Waveform simulation of a mantle wedge earthquake.

along three main pathways. One pathway leads directly upward into the hot part of the mantle wedge, where fluids trigger partial melting below the Hellenic arc in the southernmost part of the system. A second pathway, present especially in the central part of the WHSZ, leads fluids updip toward the trench below an intact seal at the plate interface until they reach the lower crust of the overriding plate, where they precipitate quartz. A third pathway exists below Kalavrita, Tripoli, and Kremidi, where local vents within the plate interface seal allow fluids to escape the subducting crust. The fluids migrate into the cold part of the mantle wedge where they trigger earthquakes and, over a time span of 0.1–10 Myr hydrate this part of the wedge. The concentration of fluid at the vents modifies locally the rheology of the subduction interface. This causes not only dense clusters of repeating earthquakes at these sites (see Fig. 3.2 II), but also large, extraordinarily deep interface earthquakes ($\sim$60 km) such as the 1965-03-31 M_w 6.8 event (c.f. *Shaw and Jackson*, 2010).

4. Mantle wedge seismicity and fluid vents on the subduction interface are not unique to Greece, but may be a relatively common feature of cold subduction zones worldwide. However, only a few targeted, high-resolution imaging studies have been able to resolve earthquakes in the mantle wedge until now. In many cases, the resolution afforded by these approaches is not sufficient to distinguish slab earthquakes from mantle wedge earthquakes. As an alternative method, I suggest a workflow to analyze reflected and converted secondary arrivals of deep earthquakes to characterize where these earthquakes occur in relation to the main seismic discontinuities. For mantle wedge earthquakes, reflections from the plate interface and the slab Moho provide evidence of a hypocenter above the slab. In the WHSZ an additional clue comes from the systematic difference in focal mechanisms between earthquakes from different parts of the system. Looking at the global distribution of recognized mantle wedge seismicity, only cold systems appear to host these type of earthquakes. This is likely because seismic failure can only occur in dry mantle wedges - an attribute of cold systems. In warm systems, the mantle wedge contains more hydrated minerals such as serpentine, with levels ranging 10 % to 100 % in the well-studied subduction zones of SE Japan, Cascadia, and Mexico (*Abers et al.*, 2017). Above a concentration of 10 wt% serpentine, the rock is weakened to levels that preclude brittle failure (*Escartín et al.*, 2001). The weakening may explain why there is generally no seismicity in the wedges of warm systems, even though fluid migration into these wedges may occur in some locations. Alternatively, fluid migration into the mantle wedge of

these warm systems may be inhibited by an enhanced seal at the subduction interface, caused by the positive volume change associated with serpentinization (c.f. *Audet et al.*, 2009). A consequence of serpentinization, sealing of the interface, and fluid overpressure in these systems is the occurrence of non-volcanic tremor (e.g., *Schwartz and Rokosky*, 2007). Tremor activity recurs cyclically, which has been interpreted in terms of a process that drains fluid accumulated at the plate interface into the overlying crust (e.g., *Audet et al.*, 2009; *Delph et al.*, 2018), similar to the draining process described for a mantle wedge cluster by *Nakajima and Uchida* (2018).

5. At all sites of mantle wedge seismicity, the subducting crust directly updip from the vent exhibits a region of diminished seismic activity. From this observation, I deduce that in the crust of cold subduction zones, where there is no substantial dehydration in the 40-100 km depth range, the bulk of intermediate-depth earthquakes occurs in response to the updip flow of water-rich fluids. The key implication of this finding is that earthquakes effectively track the flow of fluids from their slab source at >80 km depth to their sink at shallow (<40 km) depth. Between source and sink, the fluids flow updip under a sealed plate interface, facilitating intraslab earthquakes. But where the subducting crust is instead drained of fluids, the generation of intermediate-depth earthquakes is inhibited by the absence of fluid (see main sketch in Fig. 3.2).

3.2 Outlook

Throughout the work that I conducted in this thesis, a number of research questions arose that are yet unanswered, while new potential research targets and avenues have come to light based on some of the results. Here, I provide a perspective on future research, which can be divided into three main categories: (a) better constraining the Hellenic subduction system, (b) improving our understanding of transient behavior in slabs, and (c) advances in high-resolution imaging of subduction systems.

Within the Hellenic subduction zone, the focus of this thesis was the well-instrumented western portion, which has resulted in a comprehensive model of seismic velocities and discontinuities for that region. Simultaneously, scientific advances have been made over the entire subduction zone, for instance with a comprehensive dataset of seismic anisotropy measurements (*Evangelidis*, 2017), subduction interface models along the entire arc (*Bocchini et al.*, 2018a; *Hayes et al.*, 2018), relocated seis-

micity catalogs (*Bocchini et al.*, 2018a; *Mesimeri et al.*, 2018), imaging of a slab tear in the Hellenic slab below 200 km depth (*Hansen et al.*, 2019), and analysis of repeating earthquakes in some areas (*Bocchini et al.*, 2018b; *Mesimeri and Karakostas*, 2018). These results all contribute to a better characterization of the subduction system, but they vary in resolution and can show mismatches. Ideally, the models should be combined into a robust and comprehensive 3-D reference model of the Hellenic subduction zone that may include seismic velocities, anisotropy, density, discontinuities, and high-resolution earthquake locations. Preferably, this model may include the parts of the subduction system that extend toward Albania, Crete, western and southern Turkey, Cyprus, and to depths beyond 200 km, as the slab is believed to penetrate the 660-km discontinuity and reach depths beyond 1000 km in this region (*Zhu et al.*, 2015).

While a combination of existing models would already represent a major advance, there are at least four methods that have proven successful at improving the resolution in other regions or in synthetic models, which have not been applied to Greece yet. First, repeating earthquakes on the plate interface (such as below Tripoli) provide high-resolution information on the location of the interface, and could be used to systematically map the interface location and interplate slip, as it was done below NE Japan (*Uchida et al.*, 2016). Second, other signals that can constrain the location of the plate interface down to depths beyond 400 km are wave conversions from either local earthquakes such as P-to-S or S-to-P (e.g., *Nakajima et al.*, 2002), or the ScS-to-P conversion of core-reflected S-waves from large local earthquakes (e.g., *Osada et al.*, 2010; *Snoke et al.*, 1977). Third, while receiver function studies also use converted phases, they have until recently not been able to suitably account for the complex geometries of rays and amplitude transmission from dipping discontinuities in 3-D. However, suitable migration methods are now available based on the Kirchhoff formulation (e.g., *Hansen and Schmandt*, 2017; *Millet et al.*, 2019), and data coverage in both Greece and Turkey is well-suited for these methods. Fourth, slow earthquake phenomena have not been observed in the Hellenic arc yet, but their ubiquity in various parts of both warm and cold systems suggests that at least some slow phenomena may be observed in Greece. A systematic search should target all subduction-related tremor and low-frequency earthquakes, both in the very shallow trenchward section, and in deeper parts, where I already observed regular earthquakes on the interface.

Recent findings on fluid migration at clusters of mantle wedge seismicity show that these sites are suitable windows to study the transient behavior of the slab, plate interface, and fluid migration in subduction zones in general (c.f. *Nakajima and Uchida*,

2018, and part II). With at least three such clusters located in the Peloponnese region, this part of the subduction zone offers a unique opportunity to study how these processes interact both along dip and along strike of a subduction zone. While comprehensive spatio-temporal constraints on these processes may lead to truly novel insights, the forearc region is well-accessible and confined enough to afford high-quality coverage through targeted 2-D monitoring networks. Other sites that are similarly promising owing to their onshore location, but less due to road accessibility, are located at Raukumara, New Zealand (*Davey and Ristau*, 2011), and in Cauca, Colombia (*Chang et al.*, 2017). The sites offshore Sanriku in NE Japan, and near Martinique in the Lesser Antilles are more difficult to access, because these mantle wedge clusters could only be instrumented effectively with ocean bottom seismometers.

While mantle wedge clusters are being recognized as windows into fluid migration processes, what exactly causes vents to open at the interface and channel fluids from the slab into the mantle wedge remains to be explained. At local scales, *Nakajima and Uchida* (2018) detected periodic changes in seismic attenuation that point to fluids that accumulate under a low-permeability seal at the interface and periodically break through the seal in response to slow-slip events that occur at the base of the locked zone. At regional scales, the somewhat regular spatial distribution (confined depth range of 40–65 km, along-strike spacing of $\sim$70 km) of the seismicity clusters provides additional clues about the origin of the interface vents. This suggests that the location of the fluid vents is not controlled by structural features of the slab making their way down the interface, as this would imply that clusters can occur over a much wider range of depths and with random along-strike spacing. Instead, the exit point of fluids must be controlled by large-scale dynamical, mechanical and geometrical properties of the system. While there are hypotheses regarding what may cause these vents to open, for example preferential focusing due to anisotropic permeability in the slab, to properly understand this behavior we will require comprehensive multidisciplinary efforts besides seismological studies. Valuable insights may be gained from other geophysical methods, geodynamic fluid flow modeling, as well as petrologic and geochemical studies. Future analyses in geophysics may include magnetotellurics, while geodynamic models may provide advances through a combination of brittle rheology and porosity wave propagation such as suggested by *Omlin et al.* (2017). Analyses in petrology and geochemistry would rely on accessible samples in the rock record or in slab-derived fluids that reach the surface.

Further advances to image the internal structure of the slab and mantle wedge

would rely on networks with even higher density coverage than required for monitoring. Besides 3-D receiver function migration, suitable imaging methods that have been suggested or are in development are influenced by reflection seismic processing, interferometric studies, and local earthquake tomography. One such example is found in *Kim et al.* (2018), who introduced a promising method based on the autocorrelation of local earthquake coda to recover the internal structure of the LVL below the plate interface in Alaska. The developments from part III to locate earthquakes relative to discontinuities share some ideas with the autocorrelation method, while the methodology of both works may benefit the location as well as the imaging problem. Applying the imaging method of *Kim et al.* (2018) to Greece would depend on two main factors: (a) A region with continuous intraslab seismicity from the trench toward the arc, such as centrally between Tripoli and Kalvrita, or a region of particularly high seismicity in a confined region, such as below Tripoli. (b) A deployment of seismographs that should provide unprecedented dense coverage along one narrow line, which may include both broadband and short period instruments.

In conjunction with the imaging objectives described above, processing approaches from the field of controlled-source seismics may be applied to local earthquake data to map reflectors and refractors, and to separate signal from noise. Many processing techniques developed in reflection seismics require that the wavefield be recorded without spatial aliasing between traces, which allows 2-D / 3-D Fourier transforms to be applied. However, earthquake monitoring networks usually only produce aliased data at relevant frequencies. This problem could be solved with far denser monitoring networks (whose cost may be acceptable for targeted deployments along a line), or by networks that are only moderately dense but sensitive such that they can detect and record a larger number of deep earthquakes. If neighboring earthquakes occur close enough to one another, then they may be merged into station gathers that would sample the wavefield without aliasing in the vicinity of the slab. Such gathers would allow the application of techniques such as dip-filters to separate phases with negative and positive moveout (i.e., conversions and reflections). Proper signal separation would allow the phase moveout to be corrected properly, which in turn would be critical for stacking and imaging through migration.

The list of methods above provides suggestions for future research targets. Meanwhile, continued earthquake monitoring in the Hellenic subduction zone will provide important data to verify previous findings, and to improve our understanding of the subduction system.

References cited in the synthesis

Abers, G. A., P. E. Van Keken, and B. R. Hacker (2017), The cold and relatively dry nature of mantle forearcs in subduction zones, *Nature Geoscience*, *10*(5), 333–337, doi:10.1038/ngeo2922.

Audet, P., M. G. Bostock, N. I. Christensen, and S. M. Peacock (2009), Seismic evidence for overpressured subducted oceanic crust and megathrust fault sealing, *Nature*, *457*(7225), 76–78, doi:10.1038/nature07650.

Bocchini, G. M., D. Becker, T. Meier, P. E. van Keken, M. Ruscic, G. A. Papadopoulos, M. Rische, and W. Friederich (2018a), Tearing, segmentation, and backstepping of subduction in the Aegean: New insights from seismicity, *Tectonophysics*, *734-735*, 96–118.

Bocchini, G.-M., M. Ruscic, D. Becker, and T. Meier (2018b), Variable spatio-temporal clustering of microseismicity in the Eastern Hellenic Subduction Zone as possible indicator for fluid migration, *Geophysical Research Abstracts*, *20*, 9443.

Chang, Y., L. M. Warren, and G. A. Prieto (2017), Precise locations for intermediate-depth earthquakes in the Cauca Cluster, Colombia, *Bulletin of the Seismological Society of America*, *107*(6), 2649–2663, doi:10.1785/0120170127.

Davey, F. J., and J. Ristau (2011), Fore-arc mantle wedge seismicity under northeast New Zealand, *Tectonophysics*, *509*(3-4), 272–279, doi:10.1016/j.tecto.2011.06.017.

Delph, J. R., A. Levander, and F. Niu (2018), Fluid Controls on the Heterogeneous Seismic Characteristics of the Cascadia Margin, *Geophysical Research Letters*, *45*, 11,021–11,029, doi:10.1029/2018GL079518.

Escartín, J., G. Hirth, and B. Evans (2001), Strength of slightly serpentinized peridotites: Implications for the tectonics of oceanic lithosphere, *Geology*, *29*(11), 1023–1026, doi:10.1130/0091-7613(2001)029<1023:SOSSPI>2.0.CO.

Evangelidis, C. (2017), Seismic anisotropy in the Hellenic subduction zone: Effects of slab segmentation and subslab mantle flow, *Earth and Planetary Science Letters*, *480*, 97–106, doi:10.1016/j.epsl.2017.10.003.

Halpaap, F., S. Rondenay, and L. Ottemöller (2018), Seismicity, deformation, and metamorphism in the Western Hellenic Subduction Zone: New constraints from tomography, *Journal of Geophysical Research: Solid Earth*, *123*(4), 3000–3026, doi:10.1002/2017JB015154.

Halpaap, F., S. Rondenay, A. Perrin, S. Goes, L. Ottemöller, H. Austrheim, R. Shaw, and T. Eeken (2019), Earthquakes track subduction fluids from slab source to mantle

wedge sink, *Science Advances*.

Hansen, S. E., C. P. Evangelidis, and G. A. Papadopoulos (2019), Imaging Slab Detachment within the Western Hellenic Subduction Zone, *Geochemistry, Geophysics, Geosystems*, doi:10.1029/2018GC007810.

Hansen, S. M., and B. Schmandt (2017), P and S Wave Receiver Function Imaging of Subduction With Scattering Kernels, *Geochemistry, Geophysics, Geosystems*, *18*(12), 4487–4502, doi:10.1002/2017GC007120.

Hayes, G. P., G. L. Moore, D. E. Portner, M. Hearne, H. Flamme, M. Furtney, and G. M. Smoczyk (2018), Slab2, a comprehensive subduction zone geometry model, *Science*, *61*(October), 58–61.

Kim, D., K. M. Keranen, G. A. Abers, and L. D. Brown (2018), Enhanced resolution of the subducting plate interface in Central Alaska from autocorrelation of local earthquake coda, *Journal of Geophysical Research: Solid Earth*, doi:10.1029/2018JB016167.

Mesimeri, M., and V. Karakostas (2018), Repeating earthquakes in western Corinth Gulf (Greece): implications for aseismic slip near locked faults, *Geophysical Journal International*, *215*(1), 659–676, doi:10.1093/gji/ggy301.

Mesimeri, M., V. Karakostas, E. Papadimitriou, G. Tsaklidis, and K. Jacobs (2018), Relocation of recent seismicity and seismotectonic properties in the Gulf of Corinth (Greece), *Geophysical Journal International*, *212*, 1123–1142, doi:10.1093/gji/ggx450.

Millet, F., T. Bodin, and S. Rondenay (2019), Multi-Mode 3D Kirchhoff Migration of Receiver Functions at Continental Scale, *Journal of Geophysical Research: Solid Earth*, *submitted*.

Nakajima, J., and N. Uchida (2018), Repeated drainage from megathrusts during episodic slow slip, *Nature Geoscience*, *11*, 351–356, doi:10.1038/s41561-018-0090-z.

Nakajima, J., T. Matsuzawa, and A. Hasegawa (2002), Moho depth variation in the central part of Northeastern Japan estimated from reflected and converted waves, *Physics of the Earth and Planetary Interiors*, *130*(1-2), 31–47, doi:10.1016/S0031-9201(01)00307-7.

Omlin, S., B. Malvoisin, and Y. Y. Podladchikov (2017), Pore fluid extraction by reactive solitary waves in 3-D, *Geophysical Research Letters*, *44*(18), 9267–9275, doi:10.1002/2017GL074293.

Osada, K., K. Yoshizawa, and K. Yomogida (2010), Upper boundary of the pacific plate subducting under Hokkaido, Japan, estimated from ScSp phase, *Physics of the Earth and Planetary Interiors*, *183*, 63–72, doi:10.1016/j.pepi.2010.06.006.

Schwartz, S. Y., and J. M. Rokosky (2007), Slow Slip Events and Seismic Tremor at Circum-Pacific Subduction Zones, *Reviews of Geophysics*, *45*, doi:10.1029/2006RG000208.1.

Shaw, B., and J. Jackson (2010), Earthquake mechanisms and active tectonics of the

Hellenic subduction zone, *Geophysical Journal International*, *181*(2), 966–984, doi: 10.1111/j.1365-246X.2010.04551.x.

Snoke, J. A., I. S. Sacks, and H. Okada (1977), Determintation of the subducting lithosphere boundary by use of converted phases, *Bulletin of the Seismological Society of America*, *67*(4), 1051–1060.

Uchida, N., T. Iinuma, R. M. Nadeau, R. Burgmann, and R. Hino (2016), Periodic slowslip triggers megathrust zone earthquakes in northeastern Japan, *Science*, *351*(6272), 488–492.

Zhu, H., E. Bozdăg, and J. Tromp (2015), Seismic structure of the European upper mantle based on adjoint tomography, *Geophysical Journal International*, *201*(1), 18–52, doi:10.1093/gji/ggu492.

A Common station gathers of subduction zone earthquakes

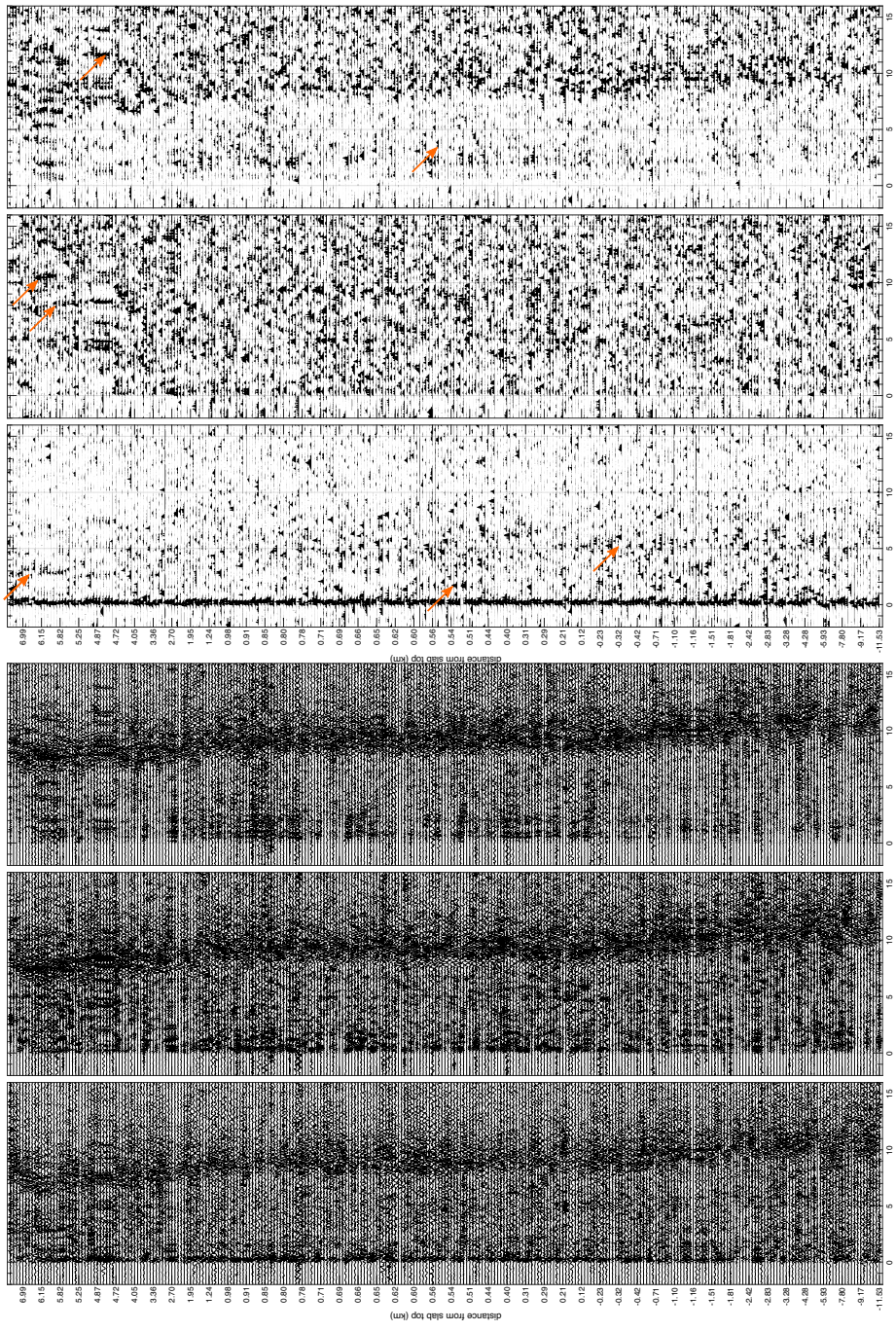
S009.Z
S009.R
S009.T
S009.2p
S009.Rp
S009.Tp
Relative Time,(s)
distance from slab top (km)

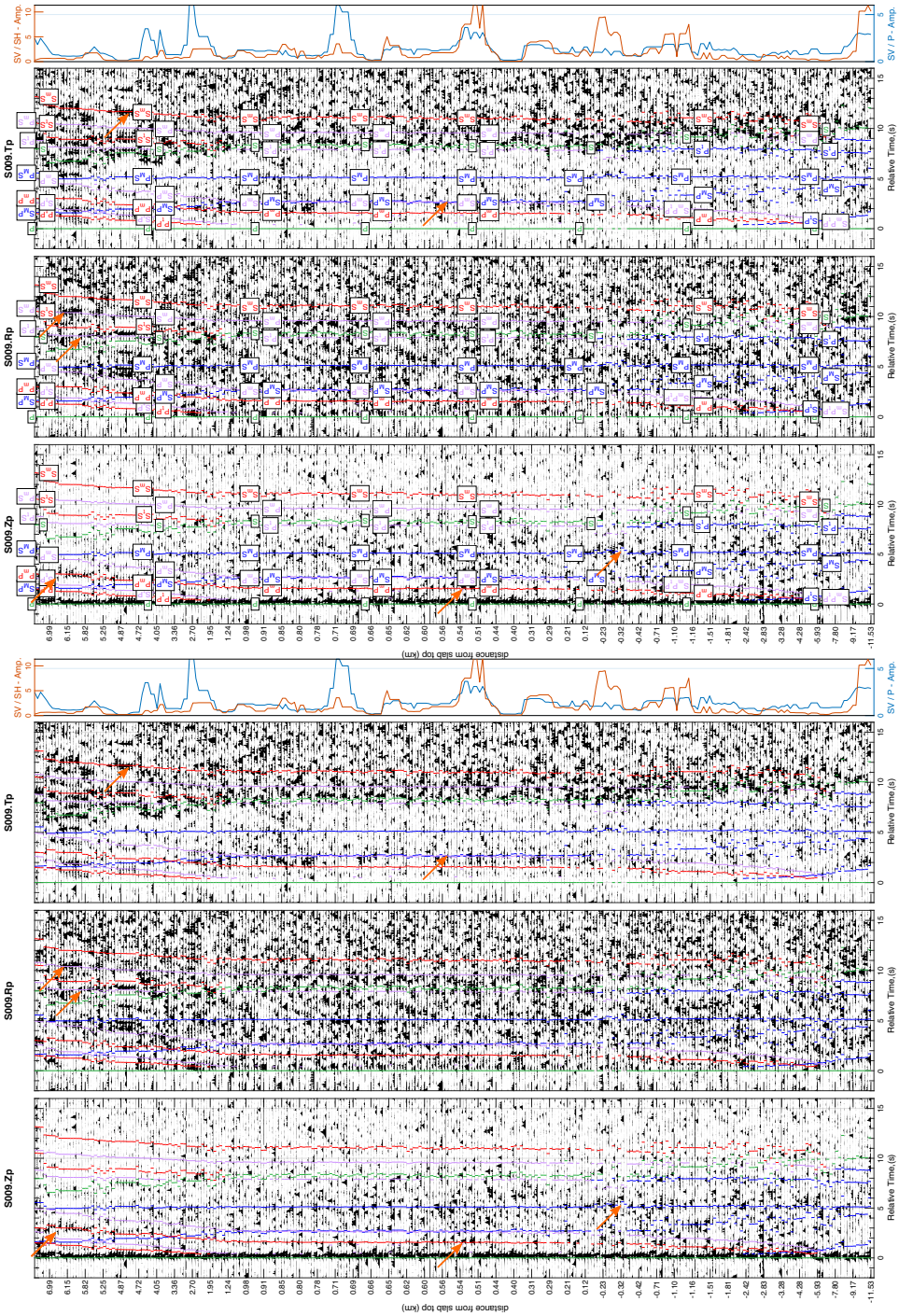
S009.Zp
S009.Rp
S009.Tp
S009.Tp
S009.Rp
S009.Zp
Relative Time,(s)
distance from slab top (km)
SV / SH - Amp.
SV / P - Amp.

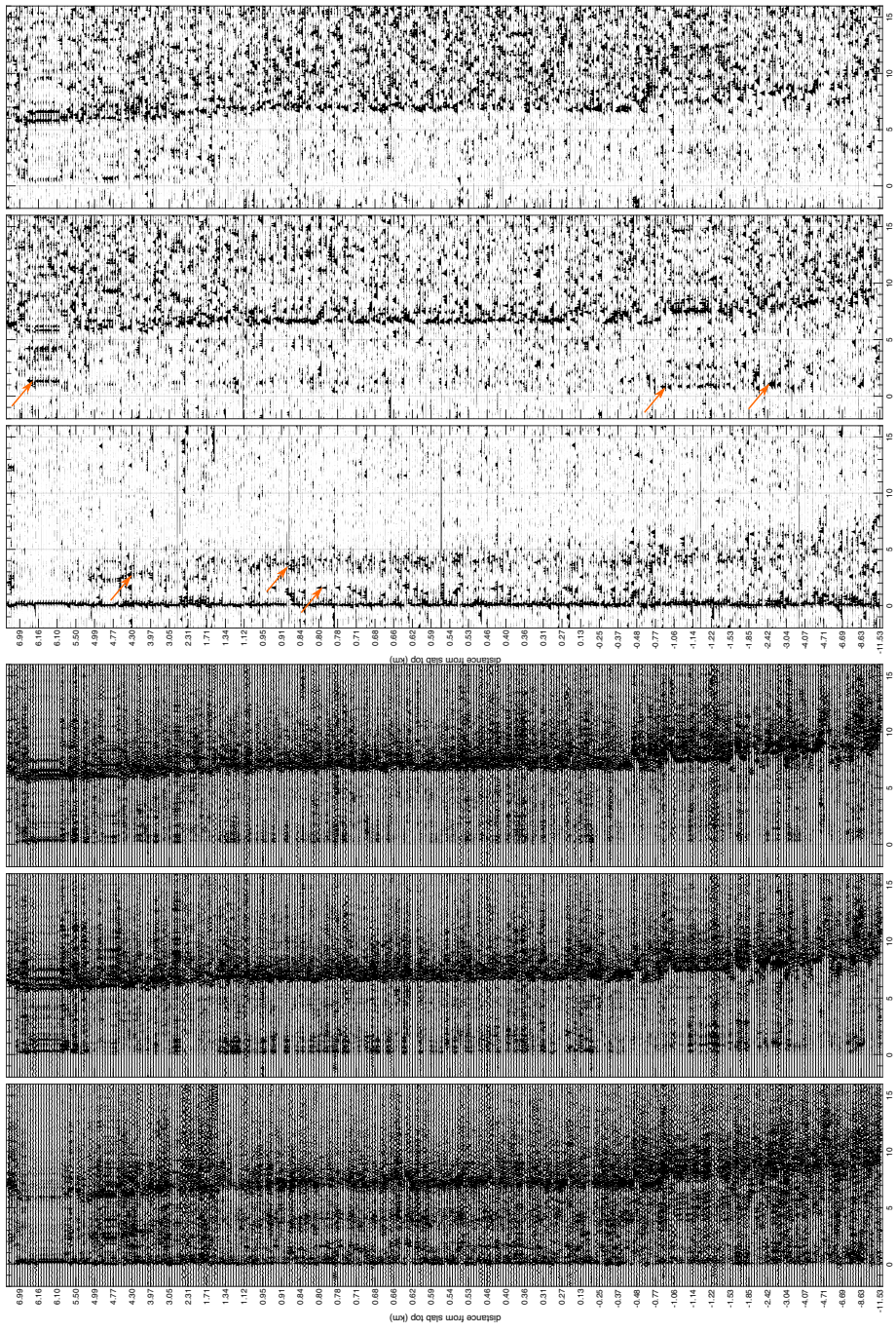
S011.Z
S011.R
S011.T
S011.Zp
S011.Rp
S011.Tp
Relative Time,(s)
distance from slab top (km)
6.99
6.16
6.10
5.50
4.99
4.77
4.30
3.97
3.05
2.31
1.71
1.34
1.12
0.98
0.91
0.84
0.80
0.78
0.71
0.68
0.66
0.62
0.59
0.54
0.53
0.46
0.40
0.36
0.31
0.27
0.13
-0.25
-0.37
-0.48
-0.77
-1.06
-1.14
-1.22
-1.53
-1.85
-2.42
-3.04
-4.07
-4.71
-6.69
-8.63
-11.53

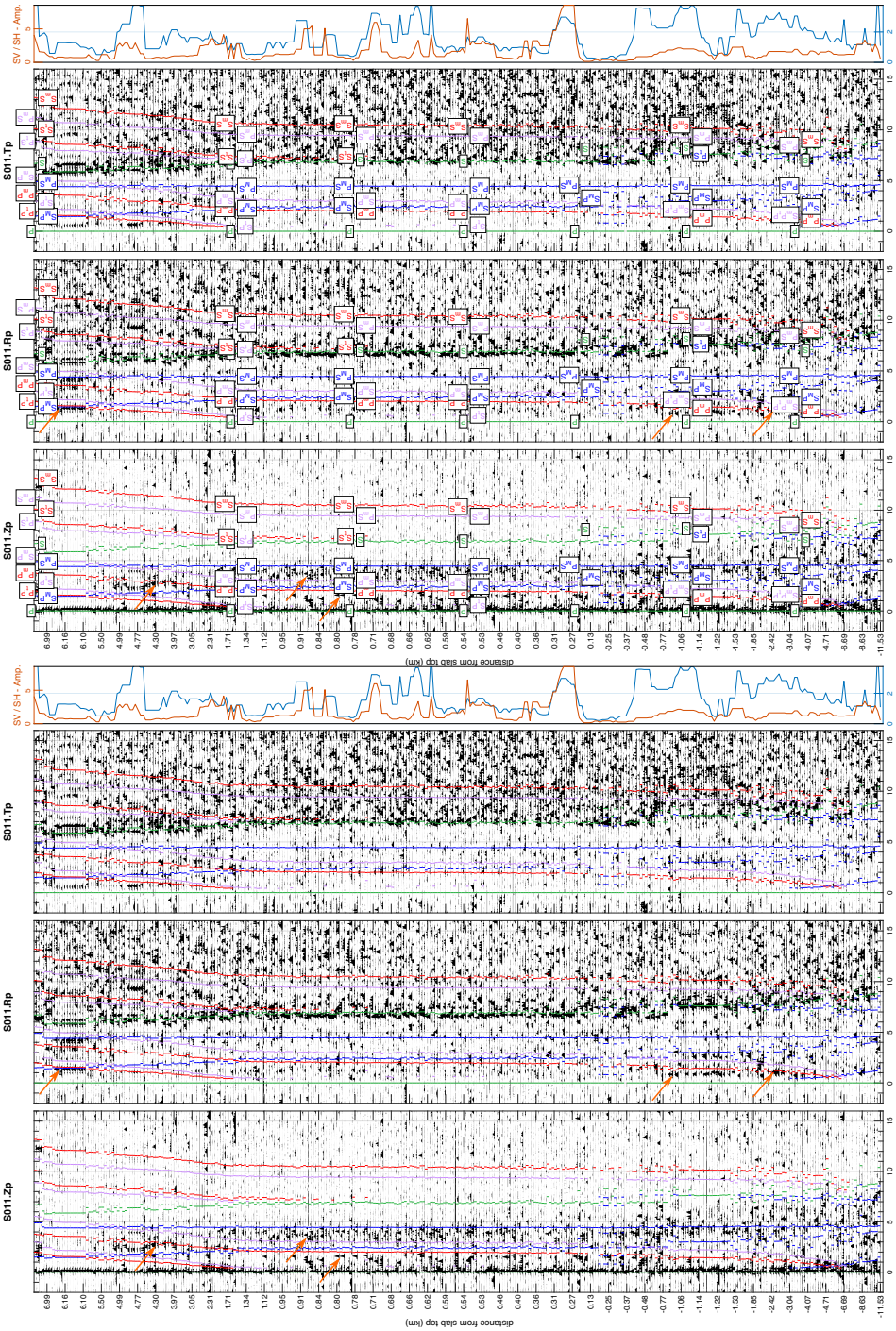
S011.Zp
S011.Rp
S011.Tp
Relative Time,(s)
distance from slab top (km)
SV / SH - Amp.
SV / P - Amp.

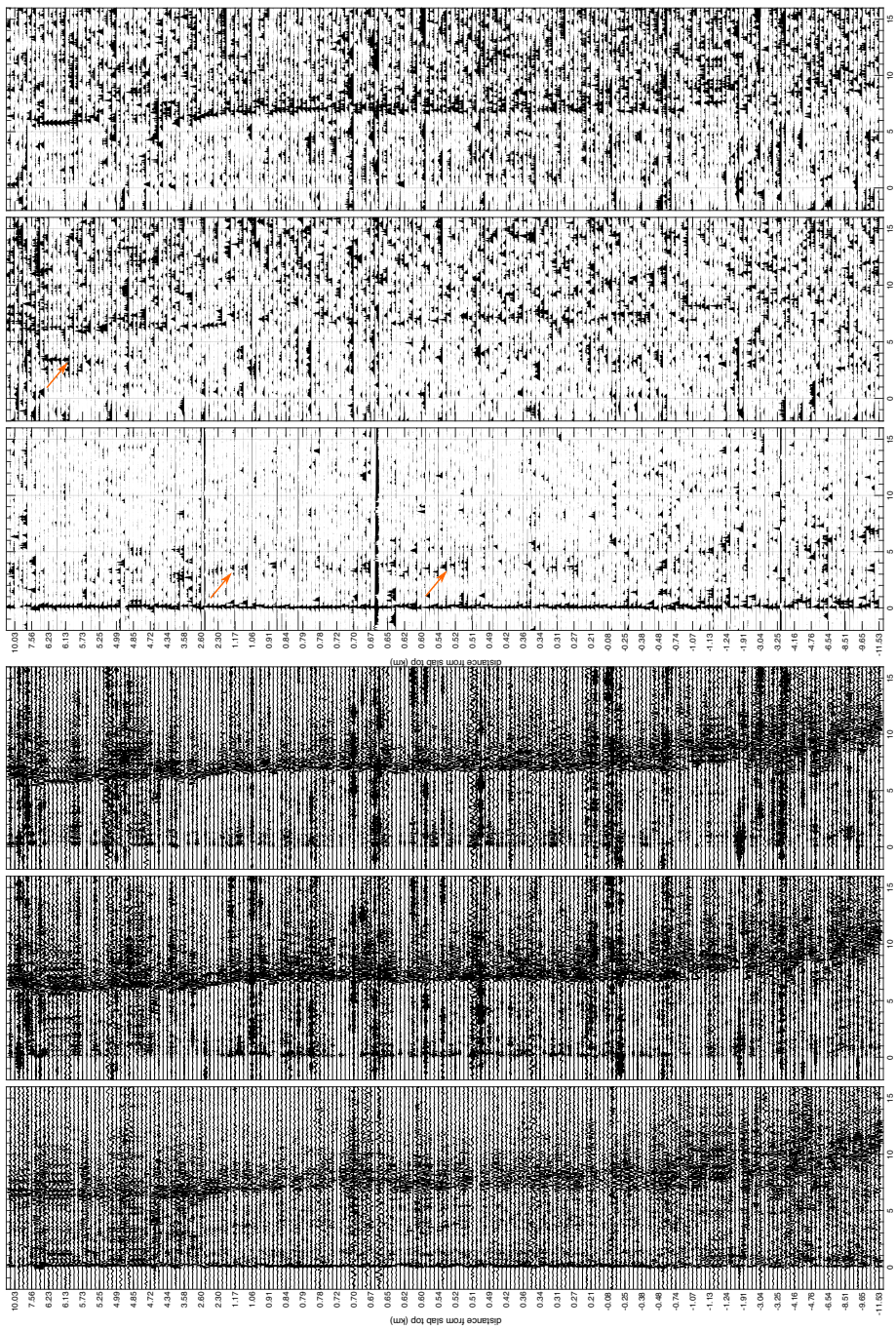
PE05.Z
PE05.R
PE05.T
PE05.2p
PE05.Rp
PE05.Tp
Relative Time,(s)
distance from slab top (km)

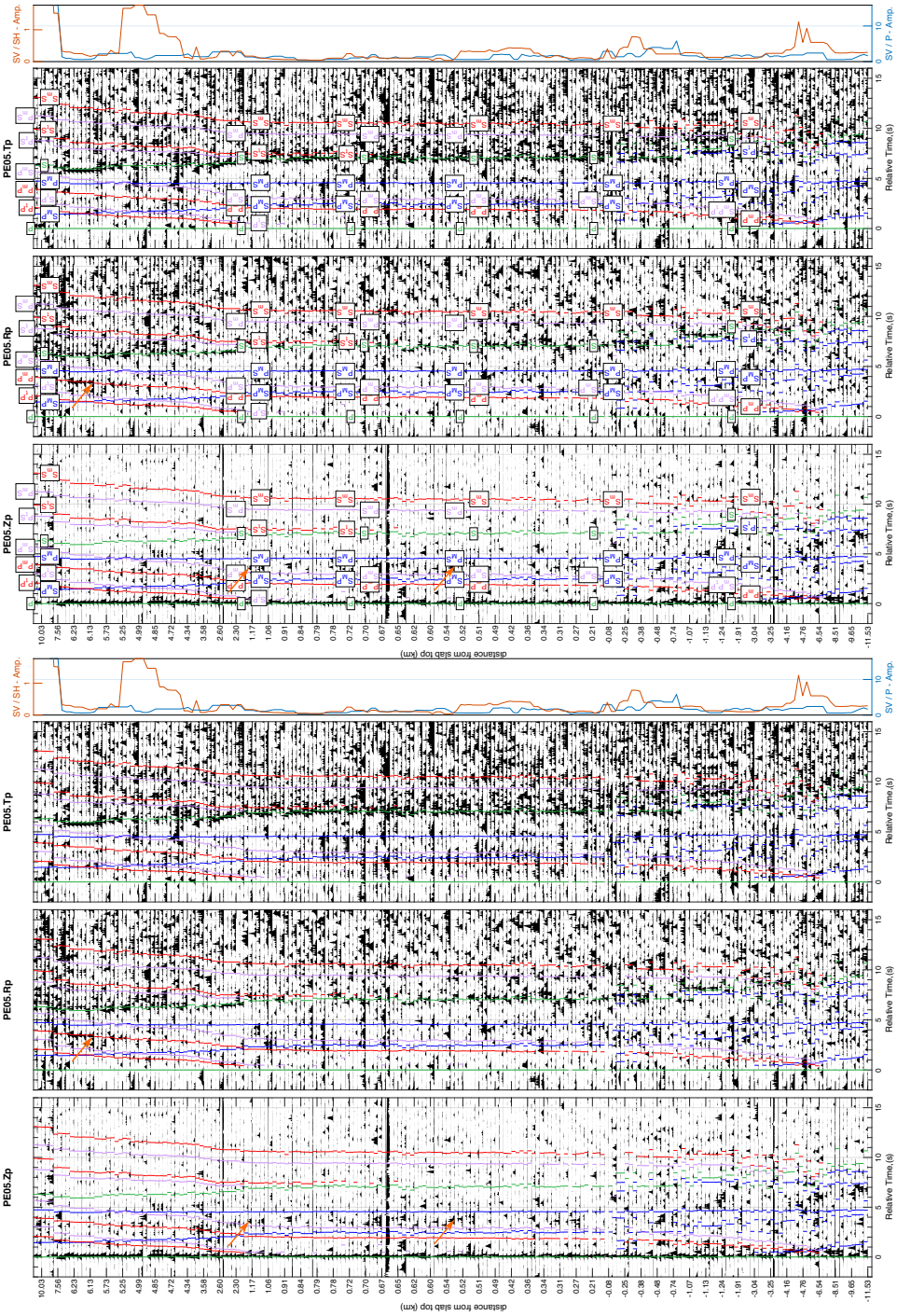
PE05.Zp
PE05.Rp
PE05.Tp
Relative Time,(s)
distance from slab top (km)
SV / SH - Amp.
SV / P - Amp.

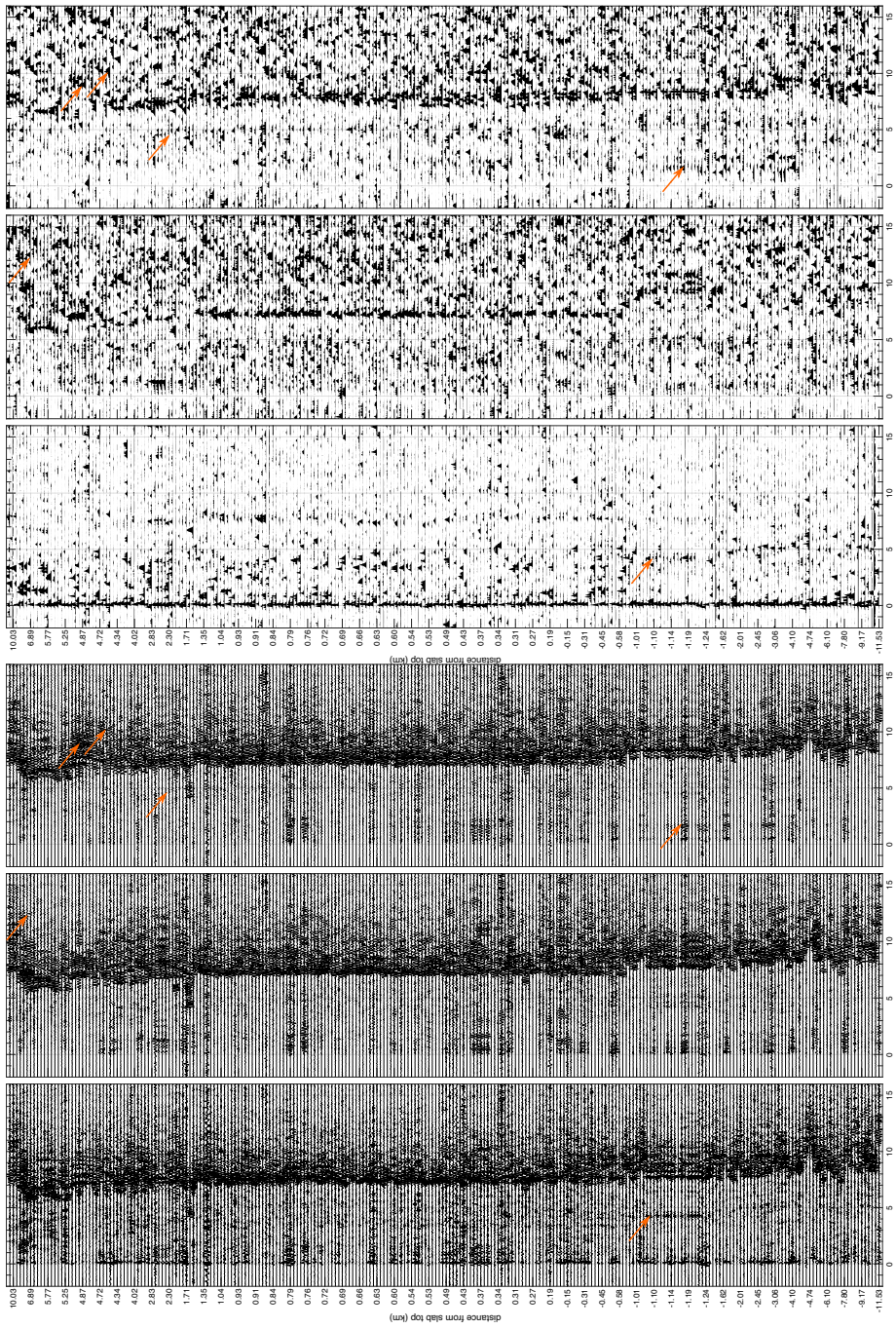
S012.Z
S012.R
S012.T
S012.2p
S012.Rp
S012.Tp
Relative Time,(s)
distance from slab top (km)

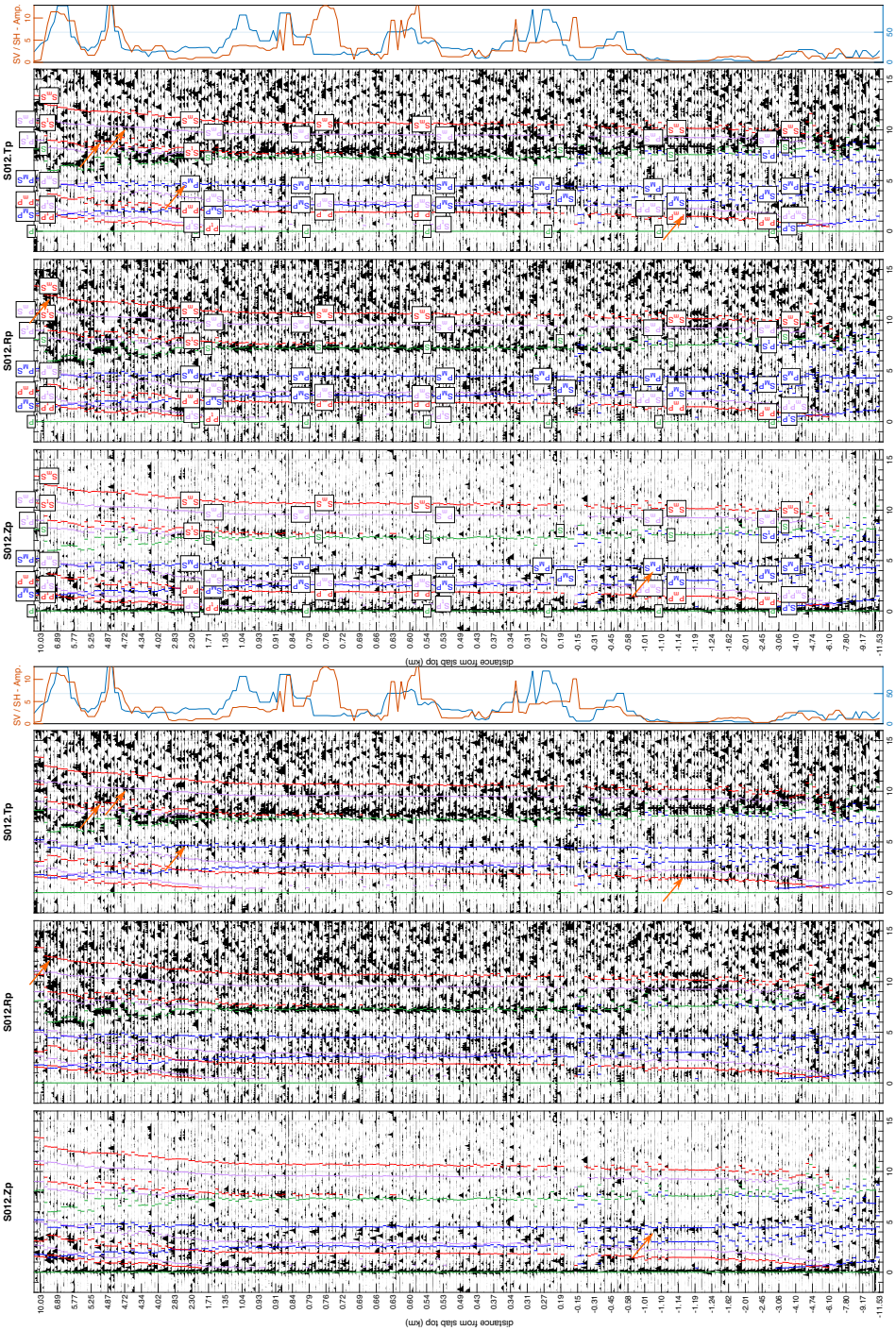
S012.Zp
S012.Rp
S012.Tp
Relative Time,(s)
distance from slab top (km)
SV / SH - Amp.
SV / P - Amp.

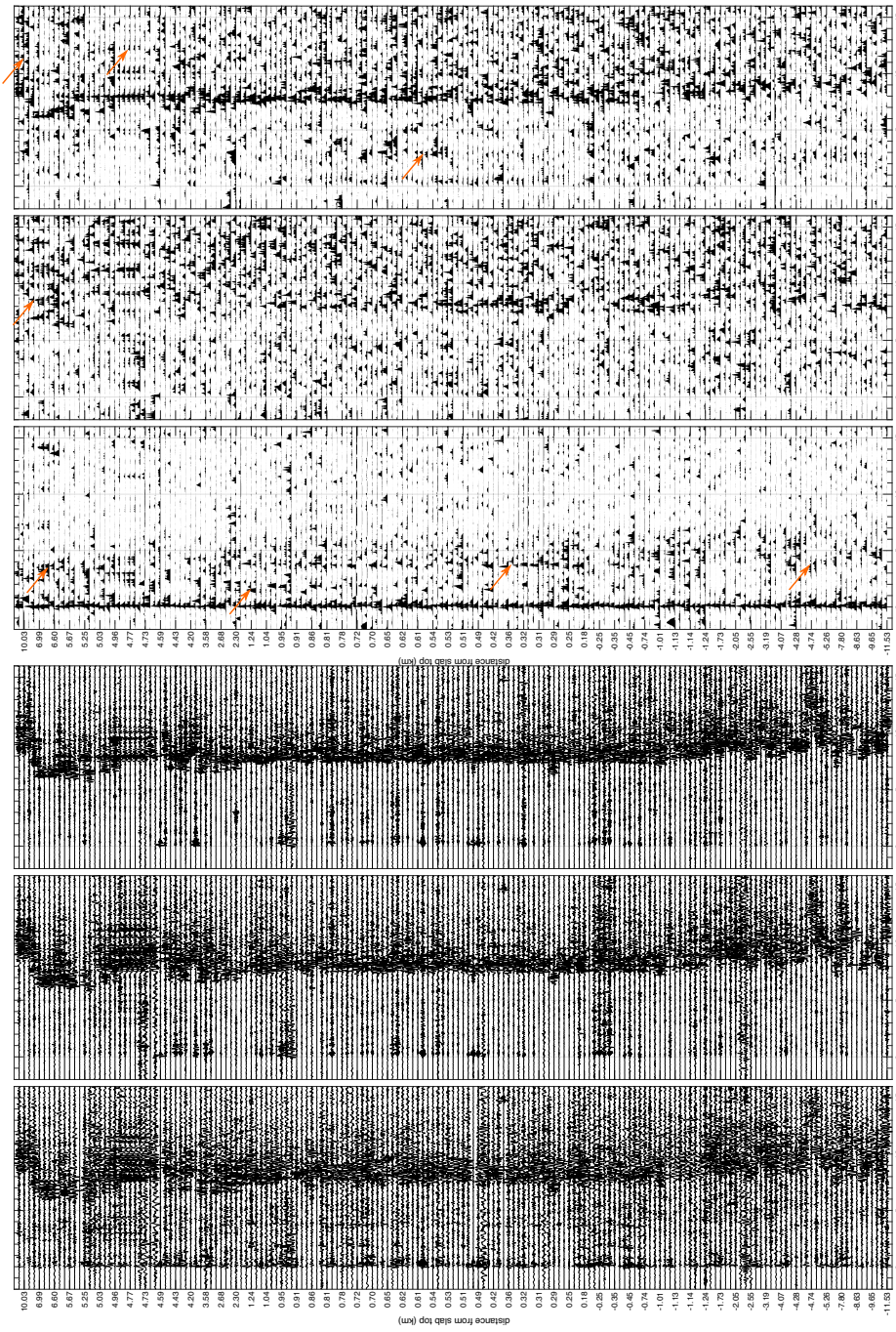
PE02.Z
PE02.R
PE02.T
PE02.2p
PE02.Rp
PE02.Tp
Relative Time,(s)
distance from slab top (km)

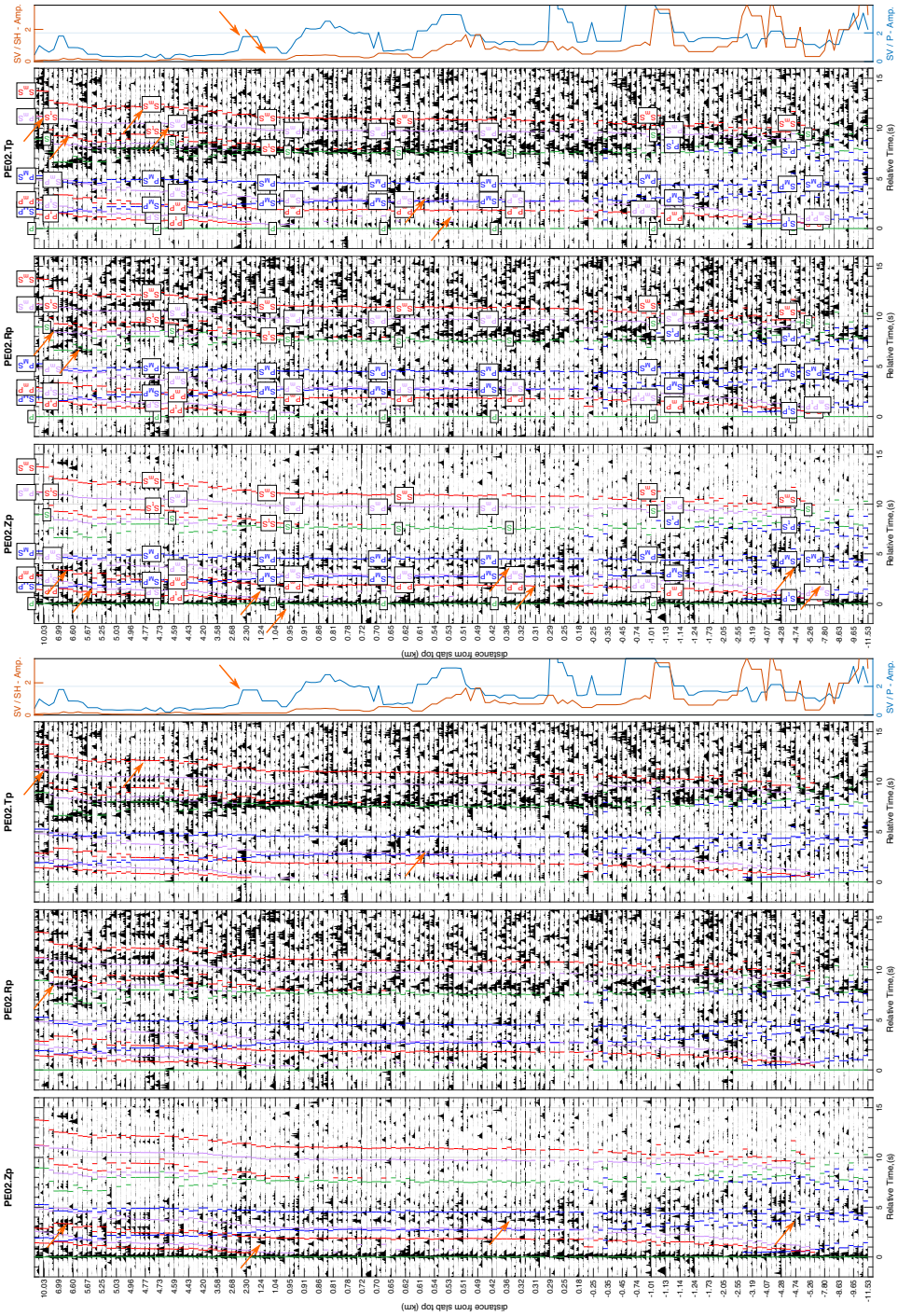
PE02.Zp
PE02.Rp
PE02.Tp
Relative Time,(s)
distance from slab top (km)
SV / SH - Amp.
SV / P - Amp.

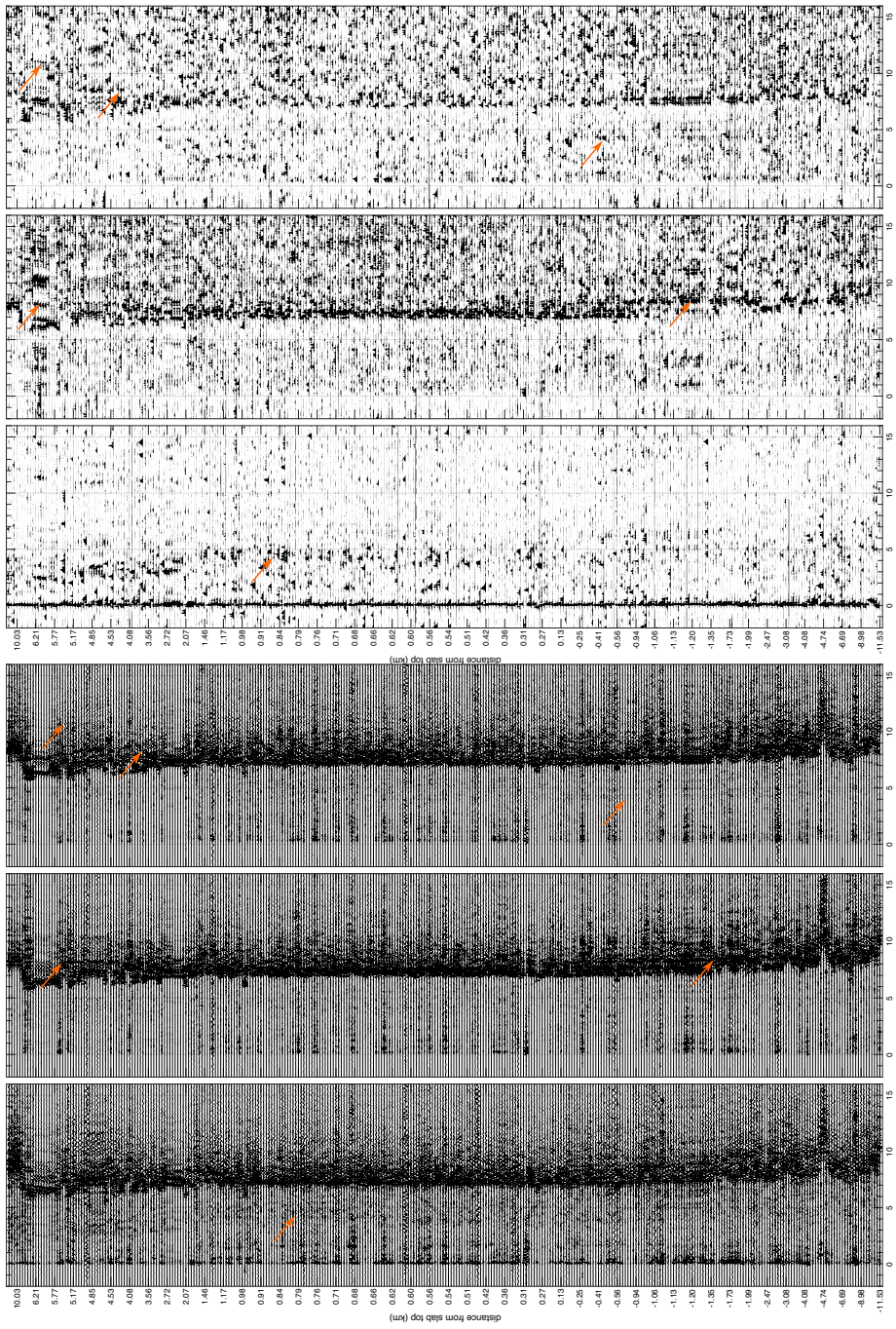
S013.Z
S013.R
S013.T
S013.2p
S013.Rp
S013.Tp
Relative Time,(s)
distance from slab top (km)
10.03
6.21
5.77
5.17
4.85
4.53
4.08
3.56
2.72
2.07
1.46
1.17
0.98
0.91
0.84
0.79
0.76
0.71
0.68
0.66
0.62
0.60
0.58
0.54
0.51
0.42
0.36
0.31
0.27
0.13
-0.25
-0.41
-0.56
-0.94
-1.05
-1.13
-1.20
-1.35
-1.73
-1.99
-2.47
-3.08
-4.09
-4.74
-6.69
-8.98
-11.53

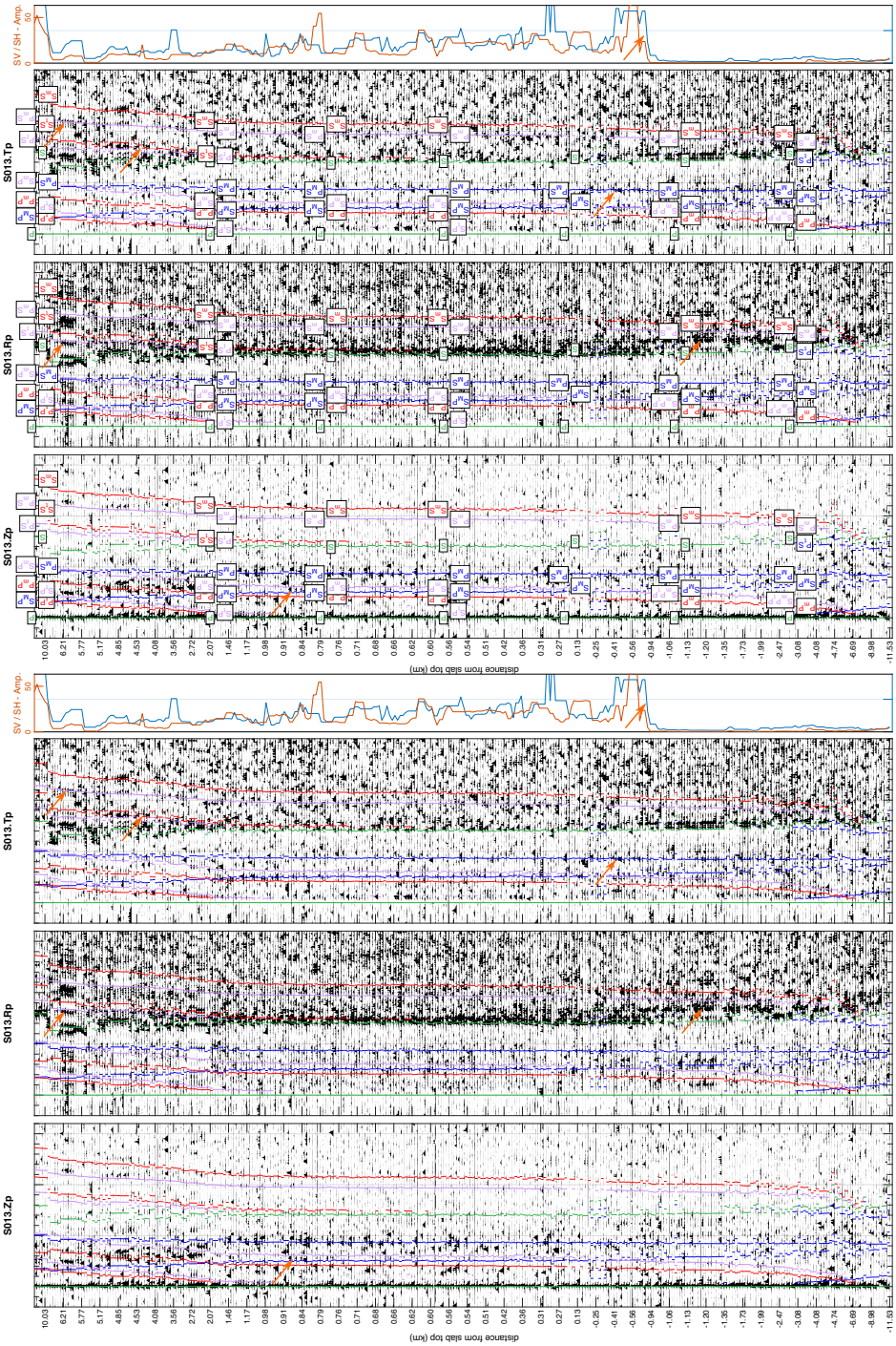
S013.Zp
S013.Rp
S013.Tp
SV / SH - Amp.
SV / P - Amp.
Relative Time (s)
distance from slab top (km)

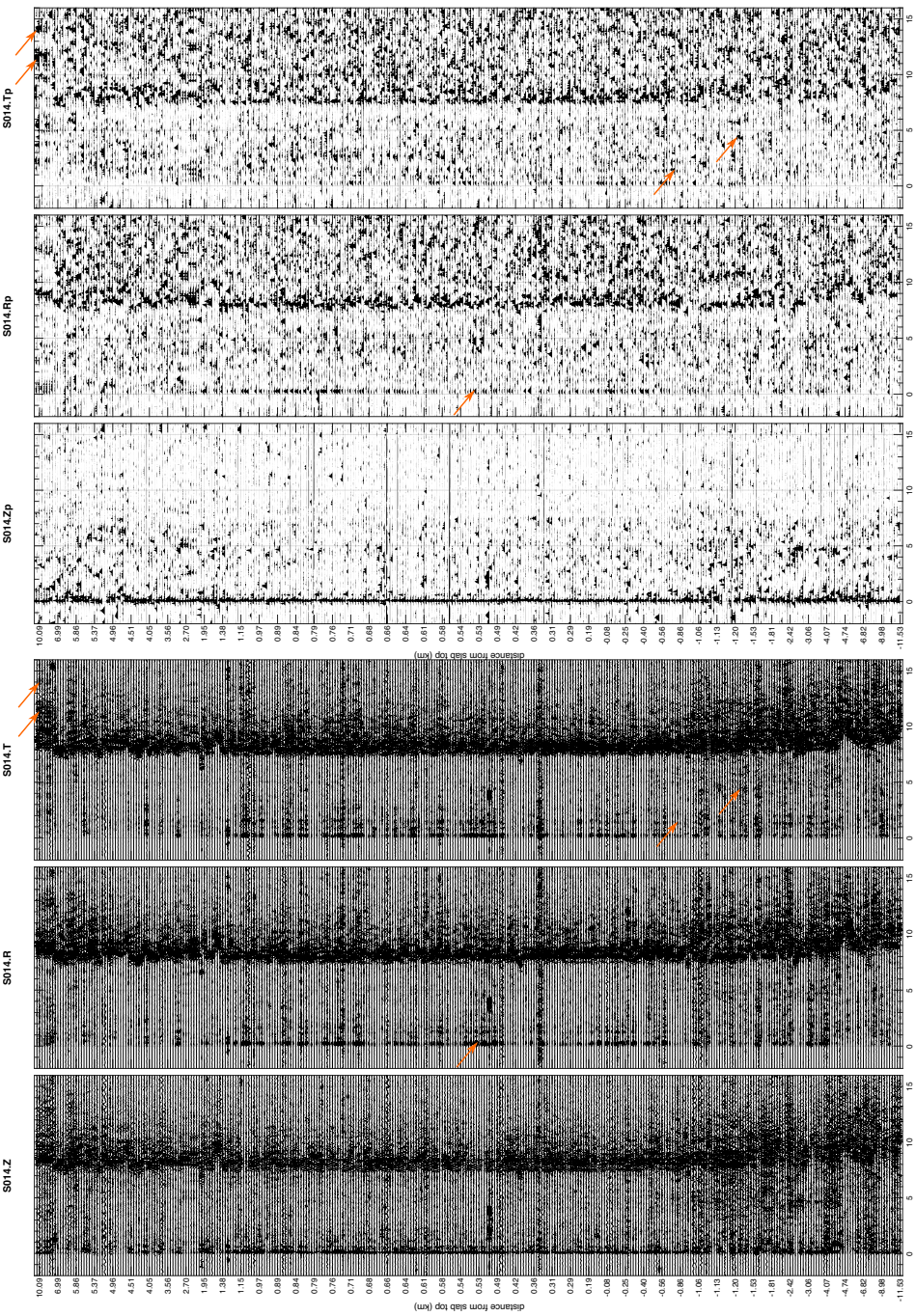
S014.Z
S014.R
S014.T
S014.2p
S014.Rp
S014.Tp
Relative Time,(s)
distance from slab top (km)

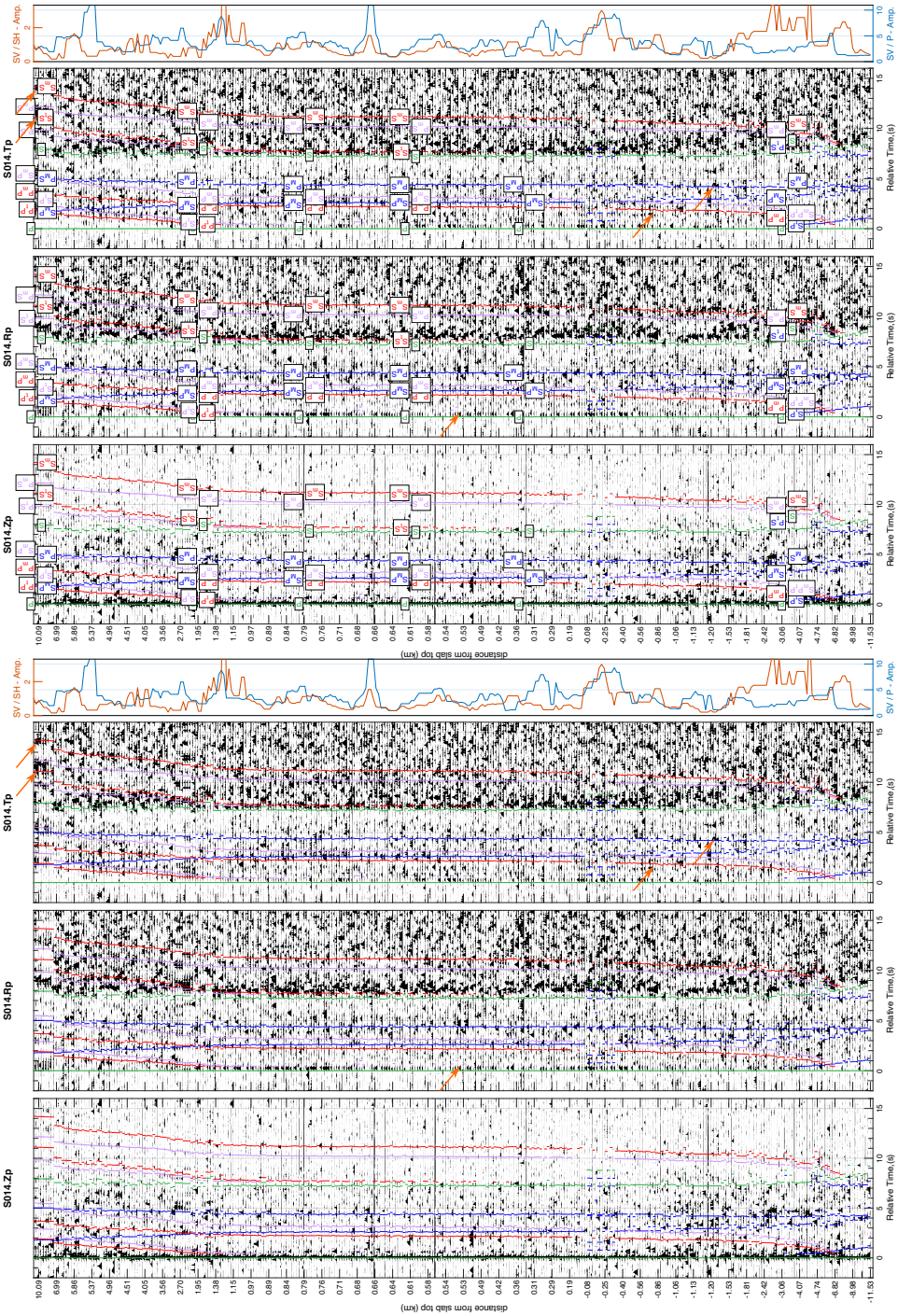
S014.Zp
S014.Rp
S014.Tp
Relative Time (s)
distance from slab top (km)
SV / SH - Amp.
SV / P - Amp.

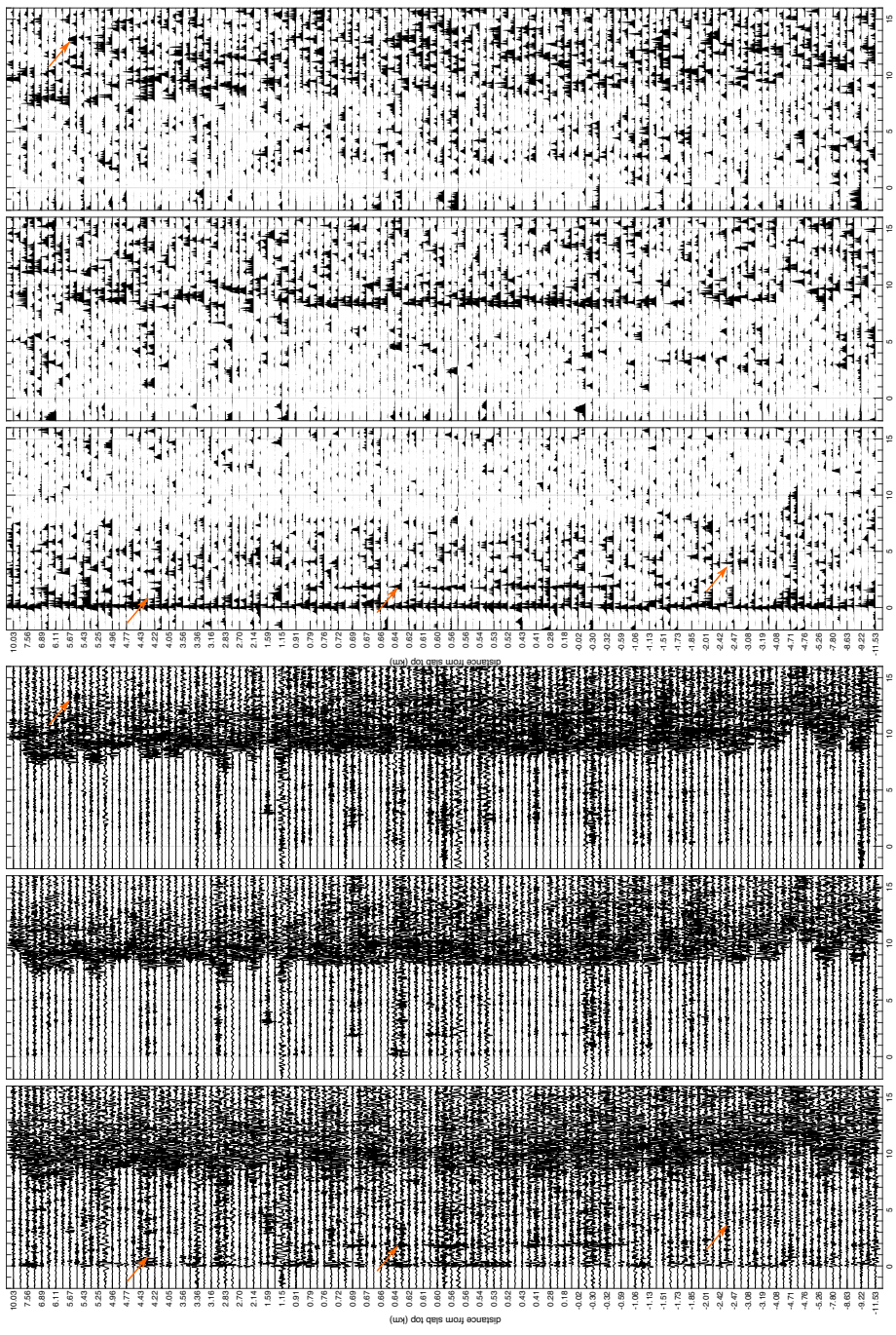
S015.Z
S015.R
S015.T
S015.Zp
S015.Rp
S015.Tp
Relative Time,(s)
distance from slab top (km)

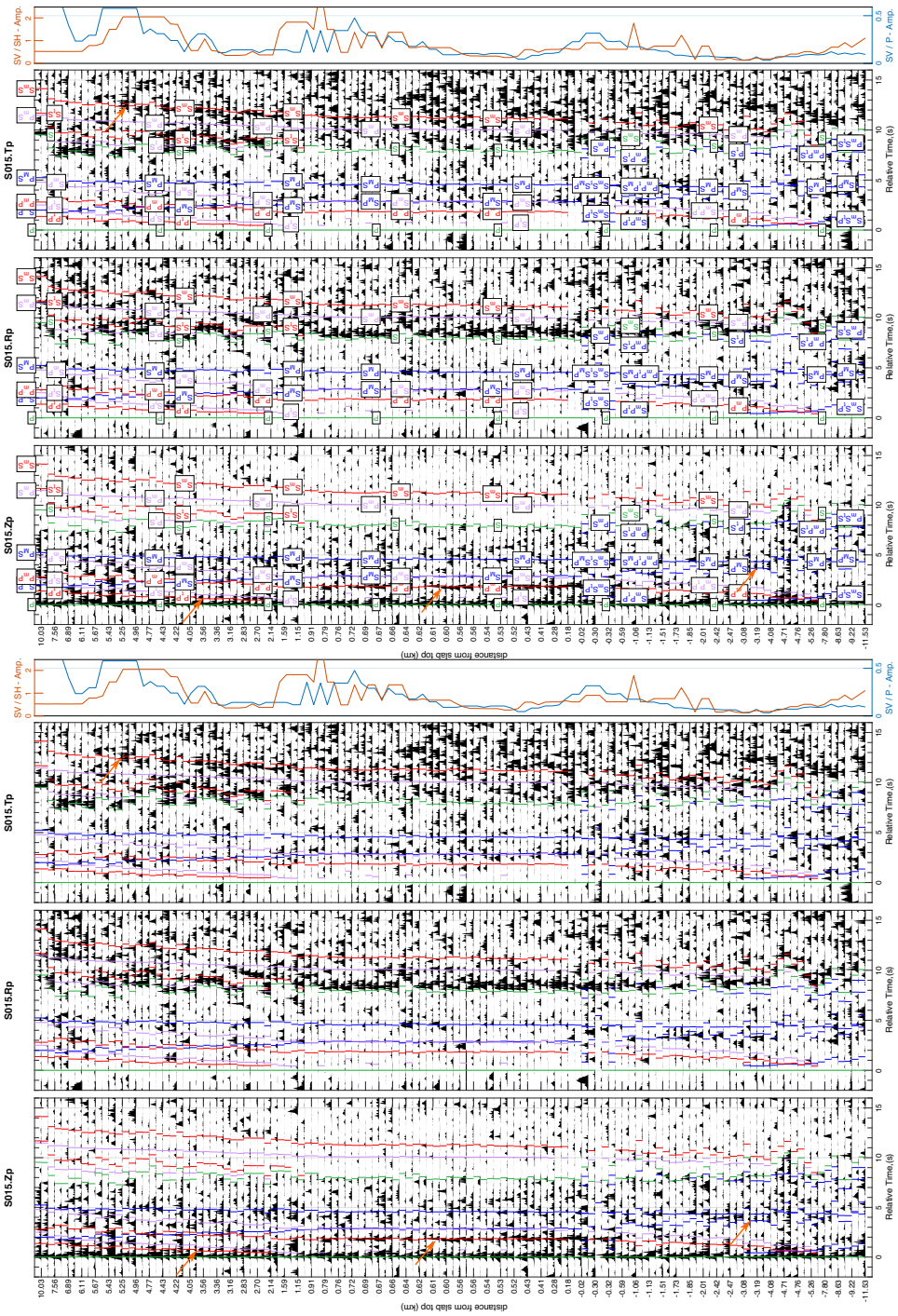
S015.Zp
S015.Rp
S015.Tp
S015.Zp
S015.Rp
S015.Tp
Relative Time,(s)
distance from slab top (km)
SV / SH - Amp.
SV / P - Amp.

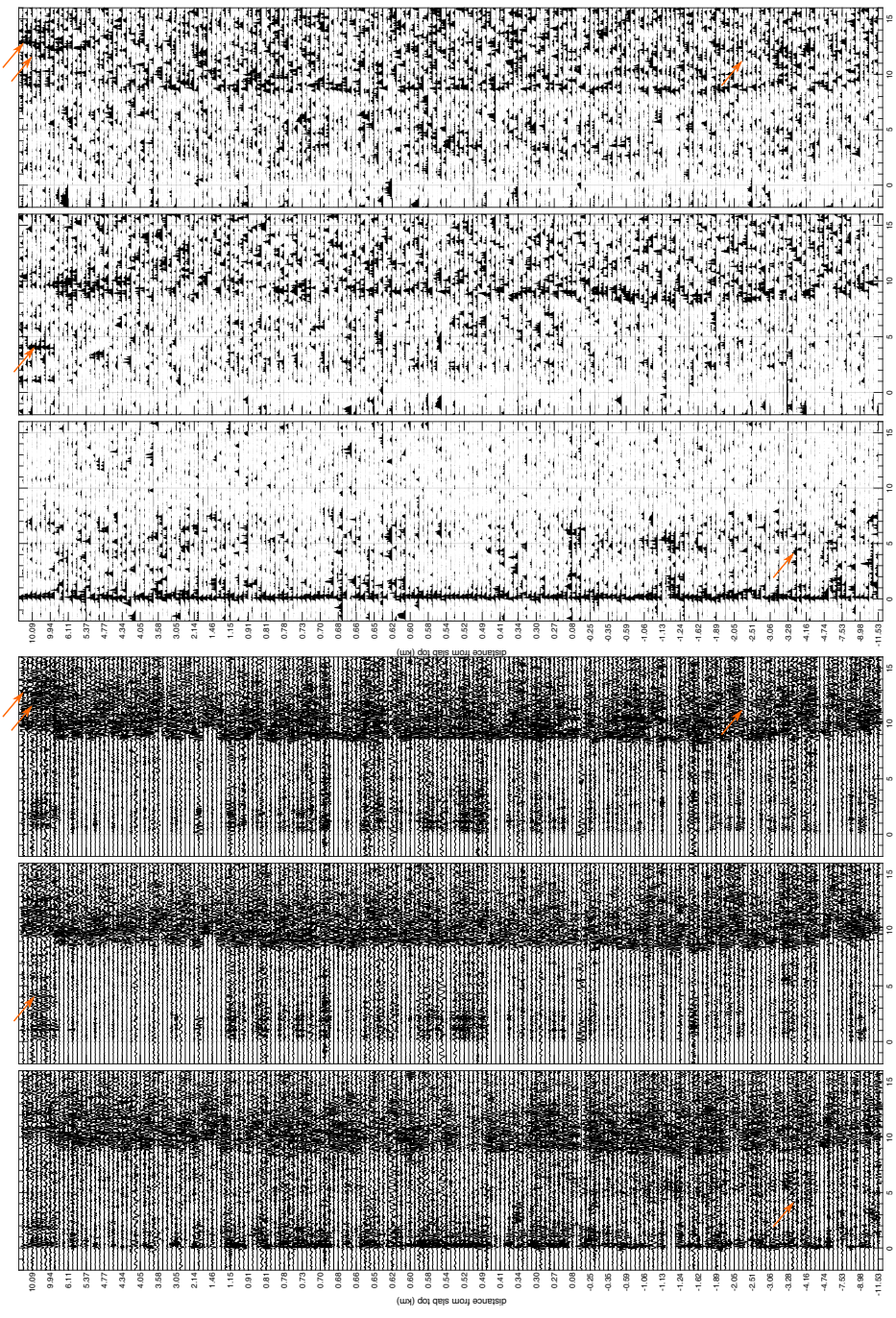
S016.Z
S016.R
S016.T
S016.2p
S016.Rp
S016.Tp
Relative Time,(s)
distance from slab top (km)

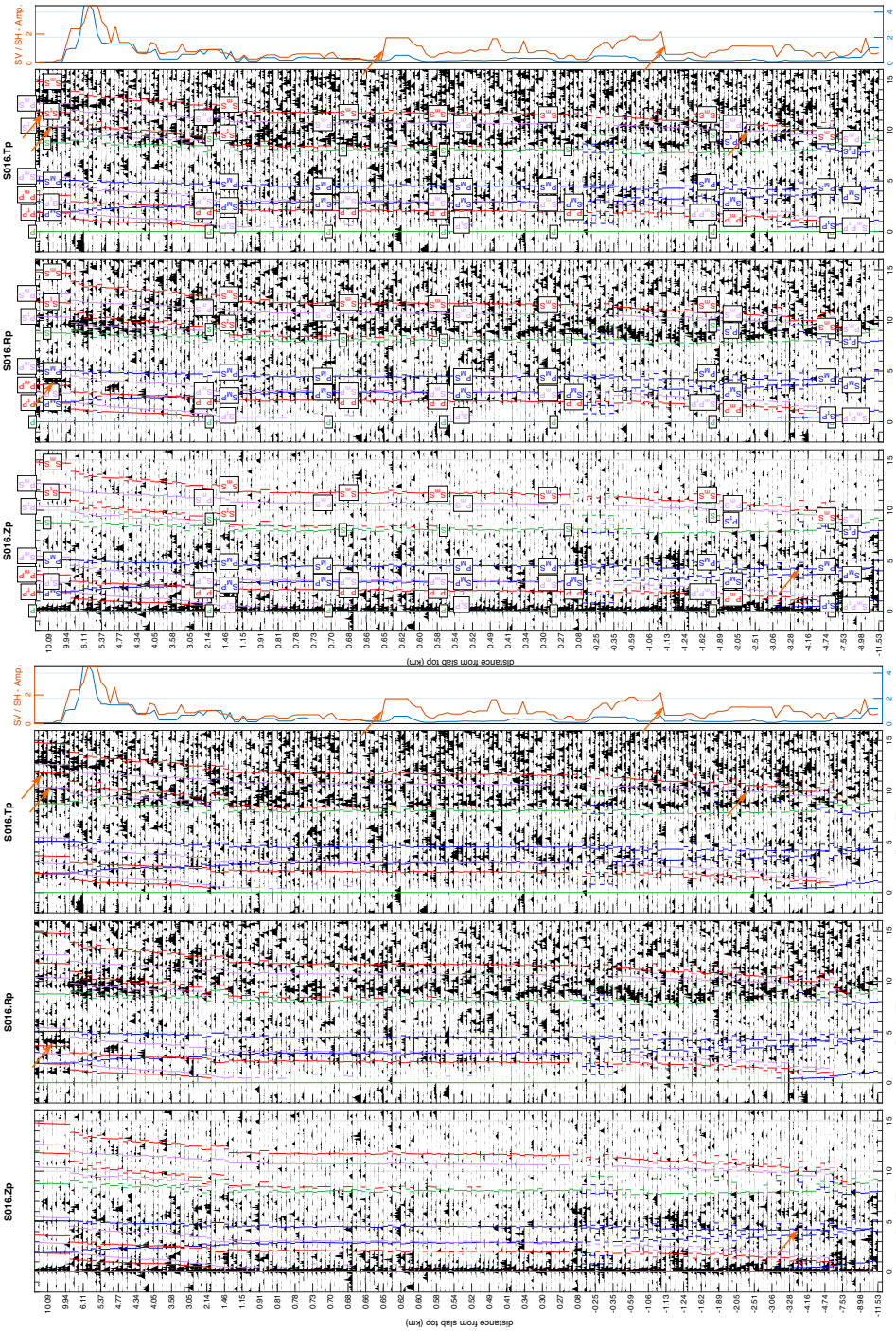
S016.Zp
S016.Rp
S016.Tp
S016.Zp
S016.Rp
S016.Tp
distance from slab top (km)
Relative Time,(s)
SV / SH - Amp.
SV / P - Amp.

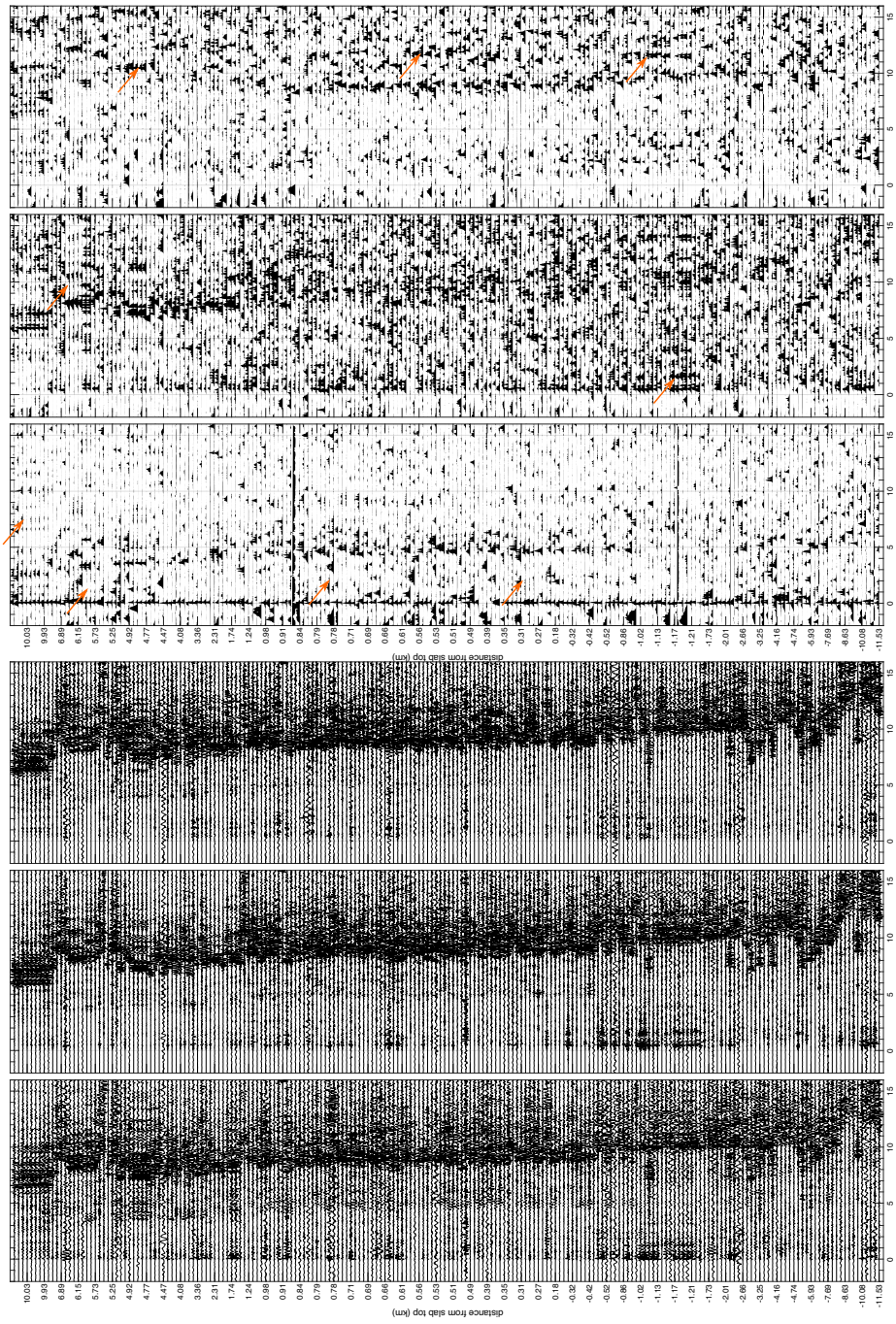
PE07.Z
PE07.R
PE07.T
PE07.2p
PE07.Rp
PE07.Tp
Relative Time,(s)
distance from slab top (km)

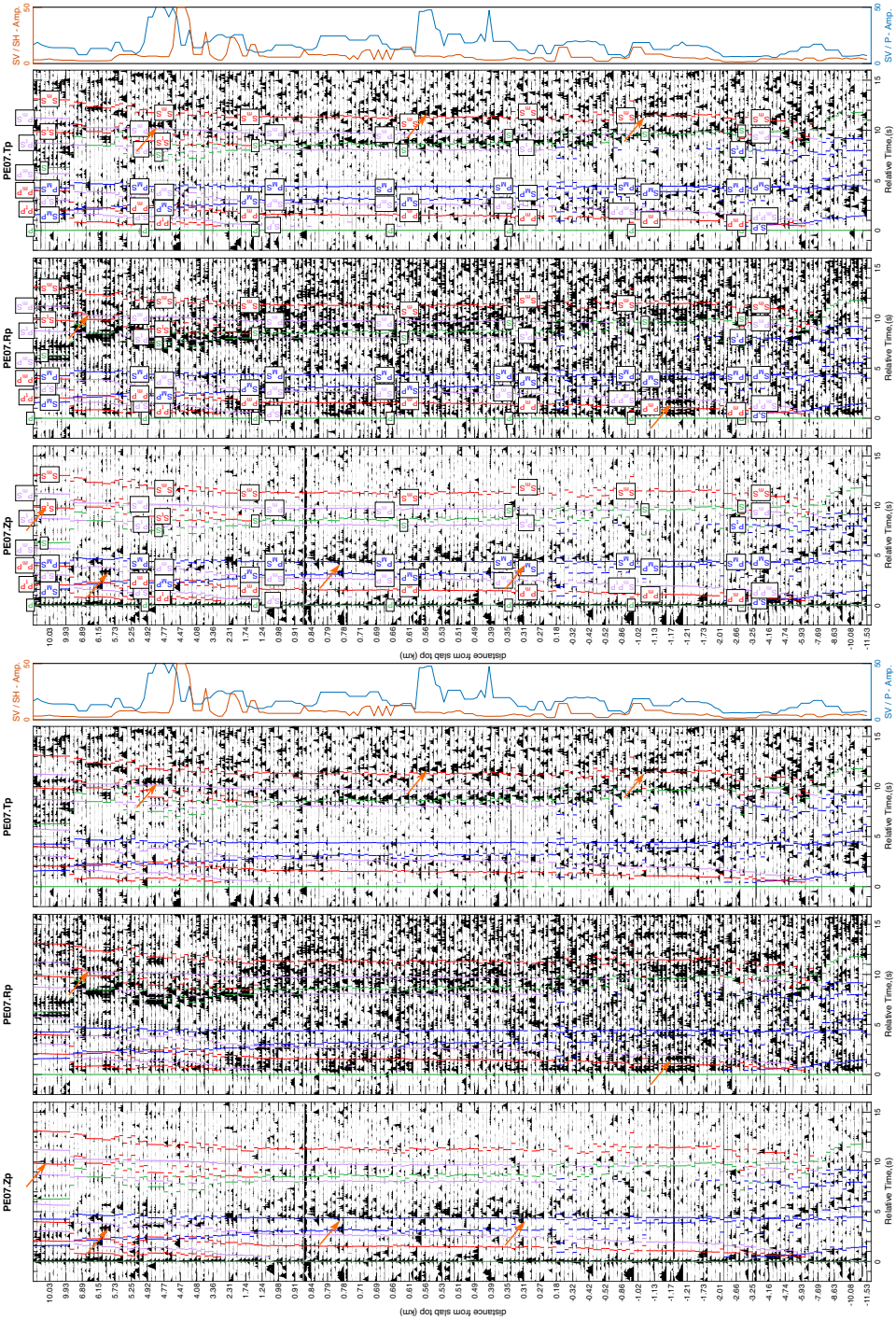
PE07.Zp
PE07.Rp
PE07.Tp
Relative Time,(s)
distance from slab top (km)
SV / SH - Amp.
SV / P - Amp.

Bibliography for chapters 1–3

Abers, G. A. (2005), Seismic low-velocity layer at the top of subducting slabs: Observations, predictions, and systematics, *Physics of the Earth and Planetary Interiors*, *149*(1-2 SPEC. ISS.), 7–29, doi:10.1016/j.pepi.2004.10.002.

Abers, G. A., and B. R. Hacker (2016), A MATLAB toolbox and Excel workbook for calculating the densities, seismic wave speeds, and major element composition of minerals and rocks at pressure and temperature, *Geochemistry, Geophysics, Geosystems*, *17*(2), 616–624, doi:10.1002/2015GC006171.

Abers, G. A., L. S. Mackenzie, S. Rondenay, Z. Zhang, A. G. Wech, and K. C. Creager (2009), Imaging the source region of Cascadia tremor and intermediate-depth earthquakes, *Geology*, *37*(12), 1119–1122, doi:10.1130/G30143A.1.

Abers, G. A., J. Nakajima, P. E. van Keken, S. Kita, and B. R. Hacker (2013), Thermal–petrological controls on the location of earthquakes within subducting plates, *Earth and Planetary Science Letters*, *369-370*, 178–187, doi:10.1016/j.epsl.2013.03.022.

Abers, G. A., P. E. Van Keken, and B. R. Hacker (2017), The cold and relatively dry nature of mantle forearcs in subduction zones, *Nature Geoscience*, *10*(5), 333–337, doi:10.1038/ngeo2922.

Ahrens, J., B. Geveci, and C. Law (2005), ParaView: An end-user tool for large-data visualization, *Visualization Handbook*, *836*, 717–731, doi:10.1016/B978-012387582-2/50038-1.

Amante, C., and B. Eakins (2009), ETOPO1 1 Arc-Minute Global Relief Model: Procedures, Data Sources and Analysis, doi:10.7289/V5C8276M.

Ambraseys, N. N., and J. A. Jackson (1990), Seismicity and associated strain of central Greece between 1890 and 1988, *Geophysical Journal International*, *101*(3), 663–708, doi:10.1111/j.1365-246X.1990.tb05577.x.

Andersen, T. B., H. Austrheim, N. Deseta, P. Silkoset, and L. D. Ashwal (2014), Large subduction earthquakes along the fossil Moho in Alpine Corsica, *Geology*, *42*(5), 395–398, doi:10.1130/G35345.1.

Angiboust, S., P. Agard, H. Raimbourg, P. Yamato, and B. Huet (2011), Subduction interface processes recorded by eclogite-facies shear zones (Monviso, W. Alps), *Lithos*, *127*(1-2), 222–238, doi:10.1016/j.lithos.2011.09.004.

Aristotle University of Thessaloniki Seismological Network (1981), Permanent Regional Seismological Network operated by the Aristotle University of Thessaloniki, International Federation of Digital Seismograph Networks. Other/Seismic Network, doi:10.7914/SN/HT.

Audet, P., and R. Bürgmann (2014), Possible control of subduction zone slow-earthquake periodicity by silica enrichment, *Nature*, *510*, 389–392, doi:10.1038/nature13391.

Audet, P., M. G. Bostock, N. I. Christensen, and S. M. Peacock (2009), Seismic evidence for overpressured subducted oceanic crust and megathrust fault sealing, *Nature*, *457*(7225), 76–78, doi:10.1038/nature07650.

Austrheim, H. (1987), Eclogitization of lower crustal granulites by fluid migration through shear zones, *Earth and Planetary Science Letters*, *81*, 221–232.

Austrheim, H., and T. B. Andersen (2004), Pseudotachylytes from Corsica: Fossil earthquakes from a subduction complex, *Terra Nova*, *16*(4), 193–197, doi:10.1111/j.1365-3121.2004.00551.x.

Austrheim, H., and T. M. Boundy (1994), Pseudotachylytes Generated During Seismic Faulting and Eclogitization of the Deep Crust, *Science*, *265*, 82–83.

Austrheim, H., K. G. Dunkel, O. Plümper, B. Ildefonse, Y. Liu, and B. Jamtveit (2017), Fragmentation of wall rock garnets during deep crustal earthquakes, *Science Advances*, *3*, doi:10.1126/sciadv.1602067.

Baker, C., D. Hatzfeld, H. Lyon-Caen, E. Papadimitriou, and A. Rigo (1997), Earthquake mechanisms of the Adriatic Sea and Western Greece: implications for the oceanic subduction-continental collision transition, *Geophysical Journal International*, *131*(3), 559–594, doi:10.1111/j.1365-246X.1997.tb06600.x.

Beck, S., S. Barrientos, E. Kausel, and M. Reyes (1998), Source characteristics of historic earthquakes along the central Chile subduction zone, *Journal of South American Earth Sciences*, *11*(2), 115–129.

Benetatos, C., a. Kiratzi, C. Papazachos, and G. Karakaisis (2004), Focal mechanisms of shallow and intermediate depth earthquakes along the Hellenic Arc, *Journal of Geodynamics*, *37*(2), 253–296, doi:10.1016/j.jog.2004.02.002.

Beresnev, I. A. (2002), Source parameters observable form the corner frequency of earthquake spectra, *Bulletin of the Seismological Society of America*, *92*(5), 2047–2048, doi:10.1785/0120010266.

Beylkin, G., and R. Burridge (1990), Linearized inverse scattering problems in acoustics and elasticity, *Wave Motion*, *12*(1), 15–52, doi:10.1016/0165-2125(90)90017-X.

Beyreuther, M., R. Barsch, L. Krischer, T. Megies, Y. Behr, and J. Wassermann (2010), ObsPy: A Python toolbox for seismology, *Seismological Research Letters*, *81*(3), 530–533, doi:10.1785/gssrl.81.3.530.

Bijwaard, H., W. Spakman, and E. R. Engdahl (1998), Closing the gap between regional and global travel time tomography, *Journal of Geophysical Research*, *103*(B12), 30,055–30,078, doi:10.1029/98JB02467.

Bleibinhaus, F. (2003), 3D simultaneous refraction and reflection seismic travel time tomography and application to deep seismic TRANSALP wide-angle data, Ph.D. thesis, Ludwig-Maximilians-Universität München.

Bleibinhaus, F., and H. Gebrande (2006), Crustal structure of the Eastern Alps along the TRANSALP profile from wide-angle seismic tomography, *Tectonophysics*, *414*(1-4), 51–69, doi:10.1016/j.tecto.2005.10.028.

Bleibinhaus, F., and S. Hilberg (2012), Shape and structure of the Salzach Valley, Austria, from seismic traveltime tomography and full waveform inversion, *Geophysical Journal International*, *189*(3), 1701–1716, doi:10.1111/j.1365-246X.2012.05447.x.

Bleibinhaus, F., D. Stich, M. Simon, and H. Gebrande (2003), New results from amplitude preserving prestack depth migration of the Münchberg/Vogtland segment of the MVE deep seismic survey, *Journal of Geodynamics*, *35*, 33–43.

Bloch, W., T. John, J. Kummerow, P. Salazar, O. S. Krüger, and S. A. Shapiro (2018), Watching Dehydration: Seismic Indication for Transient Fluid Pathways in the Oceanic Mantle of the Subducting Nazca Slab, *Geochemistry, Geophysics, Geosystems*, pp. 3189–3207, doi:10.1029/2018GC007703.

Bocchini, G. M., D. Becker, T. Meier, P. E. van Keken, M. Ruscic, G. A. Papadopoulos, M. Rische, and W. Friederich (2018a), Tearing, segmentation, and backstepping of subduction in the Aegean: New insights from seismicity, *Tectonophysics*, *734-735*, 96–118.

Bocchini, G.-M., M. Ruscic, D. Becker, and T. Meier (2018b), Variable spatio-temporal clustering of microseismicity in the Eastern Hellenic Subduction Zone as possible indicator for fluid migration, *Geophysical Research Abstracts*, *20*, 9443.

Bock, G., B. Schurr, and G. Asch (2000), High-resolution image of the oceanic Moho in the subducting Nazca plate from P - S converted waves, *Geophysical Research Letters*, *27*(23), 3929–3932, doi:10.1029/2000GL011881.

Bohnhoff, M., J. Makris, D. Papanikolaou, and G. Stavrakakis (2001), Crustal investigations of the Hellenic subduction zone using wide aperture seismic data, *Tectonophysics*, *343*, 239–262.

Bostock, M. G. (2004), Green's functions, source signatures, and the normalization of teleseismic wave fields, *Journal of Geophysical Research*, *109*(B3), B03,303, doi:10.1029/2003JB002783.

Bostock, M. G. (2013), The Moho in subduction zones, *Tectonophysics*, *609*, 547–557, doi:10.1016/j.tecto.2012.07.007.

Bostock, M. G., S. Rondenay, and J. Shragge (2001), Multiparameter two-dimensional inversion of scattered teleseismic body waves 1. Theory for oblique incidence, *Journal of Geophysical Research*, *106*(12), 30,771–30,782.

Bostock, M. G., R. D. Hyndman, S. Rondenay, and S. M. Peacock (2002), An inverted continental Moho and serpentinization of the forearc mantle., *Nature*, *417*(6888), 536–538, doi:10.1038/417536a.

Bozdağ, E., D. Peter, M. Lefebvre, D. Komatitsch, J. Tromp, J. Hill, N. Podhorszki, and D. Pugmire (2016), Global adjoint tomography: first-generation model, *Geophysical Journal International*, *207*(3), 1739–1766, doi:10.1093/gji/ggw356.

Breeding, C. M., and J. J. Ague (2002), Slab-derived fluids and quartz-vein formation in an accretionary prism, Otago Schist, New Zealand, *Geology*, *30*(6), 499–502, doi:10.1130/0091-7613(2002)030<0499:SDFAQV>2.0.CO;2.

Brudzinski, M. R., C. H. Thurber, B. R. Hacker, and E. R. Engdahl (2007), Global Prevalence of Double Benioff Zones, *Science*, *316*(5830), 1472–1474, doi:10.1126/science.1139204.

Brüstle, A. (2012), Seismicity of the eastern Hellenic Subduction Zone, Ph.D. thesis, Ruhr-Universität Bochum.

Cassidy, J. F., and F. Waldhauser (2002), Precise relocations of slab seismicity in the northern Cascadia subduction zone, in *The Cascadia Subduction Zone and Related Subduction Systems*, edited by S. Kirby, K. Wang, and S. Dunlop, pp. 69–74, USGS, Menlo Park, California.

Cerpa, N. G., I. Wada, and C. R. Wilson (2017), Fluid migration in the mantle wedge: Influence of mineral grain size and mantle compaction, *Journal of Geophysical Research: Solid Earth*, *122*(8), 6247–6268, doi:10.1002/2017JB014046.

Chakraborty, S. (2017), A New Mechanism for Upper Crustal Fluid Flow Driven by Solitary Porosity Waves in Rigid Reactive Media?, *Geophysical Research Letters*, *44*(20), 10,324–10,327, doi:10.1002/2017GL075798.

Chamberlain, C. J., C. J. Hopp, C. M. Boese, E. Warren-Smith, D. Chambers, S. X. Chu, K. Michailos, and J. Townend (2017), EQcorrscan: Repeating and near-repeating earthquake detection and analysis in Python, *Seismological Research Letters*, doi:10.1785/0220170151.

Chang, Y., L. M. Warren, and G. A. Prieto (2017), Precise locations for intermediate-depth earthquakes in the Cauca Cluster, Colombia, *Bulletin of the Seismological Society of America*, *107*(6), 2649–2663, doi:10.1785/0120170127.

Christeson, G. L., K. D. McIntosh, and J. A. Karson (2007), Inconsistent correlation of seismic layer 2a and lava layer thickness in oceanic crust, *Nature*, *445*(7126), 418–421, doi:10.1038/nature05517.

Christos, K., K. Kyriaki, L. Vasilios, M. Konstantia, M. Basil, M. Konstantinos, P. Christos, Rovithis Emmanouil, S. Thomas, and T. Nikolaos (2018), S. Ionian sea earthquake M 6.8 on 25/10/2018, *Tech. rep.*, Ministry of Infrastructures and Transportation, Thessaloniki.

Chuang, L., M. Bostock, A. Wech, and A. Plourde (2017), Plateau subduction, intraslab seismicity, and the Denali (Alaska) volcanic gap, *Geology*, *45*(7), doi:10.1130/G38867.1.

Clift, P., and P. Vannucchi (2004), Controls on Tectonic Accretion Versus Erosion in Subduction Zones: Implications for the Origin and Recycling of the Continental Crust, *Reviews of Geophysics*, *42*, doi:10.1029/2003RG000127.

Connolly, J. A., and Y. Y. Podladchikov (2016), An analytical solution for solitary porosity waves: Dynamic permeability and fluidization of nonlinear viscous and viscoplastic rock, *Geofluids*, *15*, 269–292, doi:10.1002/9781119166573.ch23.

Connolly, J. a. D. (2005), Computation of phase equilibria by linear programming: A tool for geody-

namic modeling and its application to subduction zone decarbonation, *Earth and Planetary Science Letters*, *236*(1-2), 524–541, doi:10.1016/j.epsl.2005.04.033.

Corinth Rift Laboratory Team And RESIF Datacenter (2013), CL - Corinth Rift Laboratory Seismological Network (CRLNET), doi:https://doi.org/10.15778/resif.cl.

Davey, F. J., and J. Ristau (2011), Fore-arc mantle wedge seismicity under northeast New Zealand, *Tectonophysics*, *509*(3-4), 272–279, doi:10.1016/j.tecto.2011.06.017.

Davies, D. R., C. R. Wilson, and S. C. Kramer (2011), Fluidity: A fully unstructured anisotropic adaptive mesh computational modeling framework for geodynamics, *Geochemistry, Geophysics, Geosystems*, *12*(6), doi:10.1029/2011GC003551.

de Kool, M., N. Rawlinson, and M. Sambridge (2006), A practical grid-based method for tracking multiple refraction and reflection phases in three-dimensional heterogeneous media, *Geophysical Journal International*, *167*(1), 253–270, doi:10.1111/j.1365-246X.2006.03078.x.

Del Ben, A., A. Mocnik, V. Volpi, and P. Karvelis (2015), Old domains in the South Adria plate and their relationship with the West Hellenic front, *Journal of Geodynamics*, *89*, 15–28, doi:10.1016/j.jog.2015.06.003.

Delph, J. R., A. Levander, and F. Niu (2018), Fluid Controls on the Heterogeneous Seismic Characteristics of the Cascadia Margin, *Geophysical Research Letters*, *45*, 11,021–11,029, doi:10.1029/2018GL079518.

DeMets, C., R. G. Gordon, D. F. Argus, and S. Stein (1994), Effect of recent revisions to the geomagnetic reversal time scale on estimates of current plate motions, *Geophysical Research Letters*, *21*(20), 2191, doi:10.1029/94GL02118.

Diehl, T., E. Kissling, and P. Bormann (2002), Tutorial for consistent phase picking at local to regional distances, in *New Manual of Seismological Observatory Practice (NMSOP-2)*, edited by P. Bormann, chap. IS 11.4, pp. 1–21, IASPEI, GFZ German Research Centre for Geosciences, Potsdam, doi:10.2312/GFZ.NMSOP-2_IS_11.4.

Dinc, A. N., I. Koulakov, M. Thorwart, W. Rabbel, E. R. Flueh, I. Arroyo, W. Taylor, and G. Alvarado (2010), Local earthquake tomography of central Costa Rica: Transition from seamount to ridge subduction, *Geophysical Journal International*, *183*(1), 286–302, doi:10.1111/j.1365-246X.2010.04717.x.

Durand, V., M. Bouchon, M. A. Floyd, N. Theodulidis, D. Marsan, H. Karabulut, and J. Schmittbuhl (2014), Observation of the spread of slow deformation in Greece following the breakup of the slab, *Geophysical Research Letters*, *41*(20), 7129–7134, doi:10.1002/2014GL061408.

Eberhart-Phillips, D. (1990), Three-dimensional P and S velocity structure in the Coalinga region, California, *Journal of Geophysical Research*, *95*(B10), 15,343–15,363, doi:10.1029/JB095iB10p15343.

Eberhart-Phillips, D., and S. Bannister (2010), 3-D imaging of Marlborough, New Zealand, subducted plate and strike-slip fault systems, *Geophysical Journal International*, *182*(1), 73–96, doi:10.1111/j.1365-246X.2010.04621.x.

Eberhart-Phillips, D., and M. Reyners (1999), Plate interface properties in the northeast Hikurangi subduction zone, New Zealand, from converted seismic waves, *Geophysical Research Letters*, *26*(16), 2565–2568, doi:10.1029/1999GL900567.

Eberhart-Phillips, D., and M. Reyners (2009), Three-dimensional distribution of seismic anisotropy in the Hikurangi subduction zone beneath the central North Island, New Zealand, *Journal of Geophysical Research: Solid Earth*, *114*(6), doi:10.1029/2008JB005947.

Eberhart-Phillips, D., and M. Reyners (2012), Imaging the Hikurangi Plate interface region, with improved local-earthquake tomography, *Geophysical Journal International*, *190*(2), 1221–1242, doi:10.1111/j.1365-246X.2012.05553.x.

Eberhart-Phillips, D., D. H. Christensen, T. M. Brocher, R. Hansen, N. A. Ruppert, P. J. Haeussler, and G. A. Abers (2006), Imaging the transition from Aleutian subduction to Yakutat collision in central Alaska , with local earthquakes and active source data, *Journal of Geophysical Research*, *111*, doi:

10.1029/2005JB004240.

Eberhart-Phillips, D., M. Reyners, M. Faccenda, and J. Naliboff (2013), Along-strike variation in subducting plate seismicity and mantle wedge attenuation related to fluid release beneath the North Island, New Zealand, *Physics of the Earth and Planetary Interiors*, *225*, 12–27, doi:10.1016/j.pepi.2013.10.002.

Eeken, T., S. Goes, H. A. Pedersen, N. T. Arndt, and P. Bouilhol (2018), Seismic evidence for depth-dependent metasomatism in cratons, *Earth and Planetary Science Letters*, *491*, 148–159, doi:10.1016/j.epsl.2018.03.018.

Escartín, J., G. Hirth, and B. Evans (2001), Strength of slightly serpentinized peridotites: Implications for the tectonics of oceanic lithosphere, *Geology*, *29*(11), 1023–1026, doi:10.1130/0091-7613(2001)029<1023:SOSSPI>2.0.CO.

Evangelidis, C. (2017), Seismic anisotropy in the Hellenic subduction zone: Effects of slab segmentation and subslab mantle flow, *Earth and Planetary Science Letters*, *480*, 97–106, doi:10.1016/j.epsl.2017.10.003.

Evans, J. R., D. Eberhart-Phillips, and C. H. Thurber (1999), User's manual for SIMULPS12 for imaging Vp and Vp/Vs: A derivative of the "Thurber" tomographic inversion SIMUL3 for local earthquakes and explosions, *Tech. rep.*, U.S. Geological Survey, Menlo Park.

Faccenda, M., T. Gerya, and L. Burlini (2009), Deep slab hydration induced by bending-related variations in tectonic pressure, *Nature Geoscience*, *2*(11), 790–793, doi:10.1038/ngeo656.

Faccenda, M., T. V. Gerya, N. S. Mancktelow, and L. Moresi (2012), Fluid flow during slab unbending and dehydration: Implications for intermediate-depth seismicity, slab weakening and deep water recycling, *Geochemistry, Geophysics, Geosystems*, *13*(1), doi:10.1029/2011GC003860.

Farr, T. G., P. A. Rosen, E. Caro, R. Crippen, R. Duren, S. Hensley, M. Kobrick, M. Paller, E. Rodriguez, L. Roth, D. Seal, S. Shaffer, J. Shimada, J. Umland, M. Werner, M. Oskin, D. Burbank, and D. Alsdorf (2007), The Shuttle Radar Topography Mission, *Reviews of Geophysics*, *45*, doi:10.1029/2005RG000183.

Finetti, I. R., and A. Del Ben (2005), Crustal Tectono-Stratigraphic Setting of the Adriatic Sea from New CROP Seismic Data, in *Deep Seismic Exploration of the Central Mediterranean and Italy*, edited by I. R. Finelli, 1 ed., chap. 23, Elsevier, Amsterdam.

Flerit, F., R. Armijo, G. King, and B. Meyer (2004), The mechanical interaction between the propagating North Anatolian Fault and the back-arc extension in the Aegean, *Earth and Planetary Science Letters*, *224*(3-4), 347–362, doi:10.1016/j.epsl.2004.05.028.

Frankel, A., and H. Kanamori (1983), Determination of Rupture Duration and Stress Drop for Earthquakes in Southern California, *Bulletin of the Seismological Society of America*, *73*(6), 1527–1551, doi:10.1785/gssrl.67.1.38.

Friederich, W., and T. Meier (2005), Egelados project 2005/07, International Federation of Digital Seismograph Networks. Other/Seismic Network, doi:10.14470/M87550267382.

Friederich, W., and T. Meier (2008), Temporary Seismic Broadband Network Acquired Data on Hellenic Subduction Zone, *Eos, Transactions American Geophysical Union*, *89*(40), 378, doi:10.1029/2008EO400002.

Frohlich, C. (2006), *Deep Earthquakes*, Cambridge University Press, Cambridge.

Galanis, O., C. Papazachos, E. Scordilis, and P. Hatzidimitriou (2006), Improved earthquake locations in Greece using the DD algorithm and a 3D velocity model, *First European Conference on Earthquake Engineering and Seismology*, p. 810.

Galanopoulos, D., V. Sakkas, D. Kosmatos, and E. Lagios (2005), Geoelectric investigation of the Hellenic subduction zone using long period magnetotelluric data, *Tectonophysics*, *409*(1-4), 73–84, doi:10.1016/j.tecto.2005.08.010.

Gallovič, F., J. Zahradník, D. Křížová, V. Plicka, E. Sokos, A. Serpetsidaki, and G. A. Tselentis (2009),

From earthquake centroid to spatial-temporal rupture evolution: Mw 6.3 Movri Mountain earthquake, June 8, 2008, Greece, *Geophysical Research Letters*, *36*(21), doi:10.1029/2009GL040283.

Garth, T., and A. Rietbrock (2014), Downdip velocity changes in subducted oceanic crust beneath Northern Japan-insights from guided waves, *Geophysical Journal International*, *198*(3), 1342–1358, doi:10.1093/gji/ggu206.

GEOFON Data Centre (1993), GEOFON Seismic Network, doi:https://doi.org/10.14470/tr560404.

Gesret, A., M. Laigle, J. Diaz, M. Sachpazi, M. Charalampakis, and A. Hirn (2011), Slab top dips resolved by teleseismic converted waves in the Hellenic subduction zone, *Geophysical Research Letters*, *38*(20), doi:10.1029/2011GL048996.

Goes, S., J. Armitage, N. Harmon, H. Smith, and R. Huismans (2012), Low seismic velocities below mid-ocean ridges: Attenuation versus melt retention, *Journal of Geophysical Research*, *117*, doi:10.1029/2012JB009637.

Govers, R., and M. J. R. Wortel (2005), Lithosphere tearing at STEP faults: Response to edges of subduction zones, *Earth and Planetary Science Letters*, *236*(1-2), 505–523, doi:10.1016/j.epsl.2005.03.022.

Grad, M., T. Tiira, M. Behm, A. A. Belinsky, D. C. Booth, E. Brückl, R. Cassinis, R. A. Chadwick, W. Czuba, A. V. Egorkin, R. W. England, Y. M. Erinchek, G. R. Fougler, E. Gaczyński, A. Gosar, A. Guterch, E. Hegedüs, P. Hrubcová, T. Janik, W. Jokat, E. E. Karagianni, G. R. Keller, A. Kelly, K. Komminaho, T. Korja, J. Kortström, S. L. Kostyuchenko, E. Kozlovskaya, G. Laske, L. Lenkey, U. Luosto, P. K. Maguire, M. Majdański, M. Malinowski, F. Marone, J. Mechie, E. D. Milshtein, G. Motuza, S. Nikolova, S. Olsson, M. Pasyanos, O. V. Petrov, V. E. Rakitov, R. Raykova, O. Ritzmann, R. Roberts, M. Sachpazi, I. A. Sanina, M. C. Schmidt-Aursch, I. Serrano, A. Špičák, P. Środa, F. Šumanovac, B. Taylor, A. G. Vedrentsev, J. Vozár, Z. Weber, M. Wilde-Piórko, T. P. Yegorova, J. Yliniemi, B. Zelt, and E. E. Zolotov (2009), The Moho depth map of the European Plate, *Geophysical Journal International*, *176*(1), 279–292, doi:10.1111/j.1365-246X.2008.03919.x.

Green II, H. W., and H. Houston (1995), The Mechanics of Deep Earthquakes, *Annual Review of Earth and Planetary Sciences*, *23*, 169–213.

Grevemeyer, I., C. R. Ranero, and M. Ivandic (2018), Structure of oceanic crust and serpentinization at subduction trenches, *Geosphere*, *14*(2), 395–418, doi:10.1130/GES01537.1.

Hacker, B. R. (2003), Subduction factory 1. Theoretical mineralogy, densities, seismic wave speeds, and H 2 O contents, *Journal of Geophysical Research*, *108*(B1), 2029, doi:10.1029/2001JB001127.

Hacker, B. R., and G. A. Abers (2004), Subduction Factory 3: An Excel worksheet and macro for calculating the densities, seismic wave speeds, and H2O contents of minerals and rocks at pressure and temperature, *Geochemistry, Geophysics, Geosystems*, *5*, doi:10.1029/2003GC000614.

Hacker, B. R., S. M. Peacock, G. A. Abers, and S. D. Holloway (2003), Subduction factory 2. Are intermediate-depth earthquakes in subducting slabs linked to metamorphic dehydration reactions?, *Journal of Geophysical Research*, *108*(B1), 2030, doi:10.1029/2001JB001129.

Halpaap, F., S. Rondenay, and L. Ottemöller (2018), Seismicity, deformation, and metamorphism in the Western Hellenic Subduction Zone: New constraints from tomography, *Journal of Geophysical Research: Solid Earth*, *123*(4), 3000–3026, doi:10.1002/2017JB015154.

Halpaap, F., S. Rondenay, A. Perrin, S. Goes, L. Ottemöller, H. Austrheim, R. Shaw, and T. Eeken (2019), Earthquakes track subduction fluids from slab source to mantle wedge sink, *Science Advances*.

Hanks, T. C., and H. Kanamori (1979), A moment magnitude scale, doi:10.1029/JB084iB05p02348.

Hansen, S. E., C. P. Evangelidis, and G. A. Papadopoulos (2019), Imaging Slab Detachment within the Western Hellenic Subduction Zone, *Geochemistry, Geophysics, Geosystems*, doi:10.1029/2018GC007810.

Hansen, S. M., and B. Schmandt (2017), P and S Wave Receiver Function Imaging of Subduction With Scattering Kernels, *Geochemistry, Geophysics, Geosystems*, *18*(12), 4487–4502, doi:10.1002/2017GC007120.

Hasegawa, A., and J. Nakajima (2017), Seismic imaging of slab metamorphism and genesis of intermediate-depth intraslab earthquakes, *Progress in Earth and Planetary Science*, *4*(1), 12, doi:10.1186/s40645-017-0126-9.

Hasegawa, A., J. Nakajima, N. Uchida, T. Okada, D. Zhao, T. Matsuzawa, and N. Umino (2009), Plate subduction, and generation of earthquakes and magmas in Japan as inferred from seismic observations: An overview, *Gondwana Research*, *16*(3-4), 370–400, doi:10.1016/j.gr.2009.03.007.

Haslinger, F., and E. Kissling (2001), Investigating effects of 3-D ray tracing methods in local earthquake tomography, *Physics of the Earth and Planetary Interiors*, *123*(2-4), 103–114, doi:10.1016/S0031-9201(00)00204-1.

Haslinger, F., E. Kissling, J. Ansorge, D. Hatzfeld, E. E. Papadimitriou, V. Karakostas, K. C. Makropoulos, H. G. Kahle, and Y. Peter (1999), 3D Crustal structure from local earthquake tomography around Gulf of Arta, *Tectonophysics*, *304*, 210–218.

Hatzfeld, D. (1994), On the shape of the subducting slab beneath the Peloponnese, Greece, *Geophysical Research Letters*, *21*(3), 173–176, doi:10.1029/93GL03079.

Hatzfeld, D., and C. Martin (1992), Intermediate depth seismicity in the Aegean defined by teleseismic data, *Earth and Planetary Science Letters*, *113*(1-2), 267–275, doi:10.1016/0012-821X(92)90224-J.

Havskov, J., and L. Ottemöller (1999), SeisAn Earthquake Analysis Software, *Seismological Research Letters*, *70*(5), 532–534.

Hayashida, T., F. Tajima, J. Nakajima, and J. Mori (2012), A three-dimensional seismic wave speed model in southwestern Japan from combined use of waveform modeling and travel-time tomography, *Journal of Geophysical Research B: Solid Earth*, *117*(11), doi:10.1029/2012JB009345.

Hayes, G. P., G. L. Moore, D. E. Portner, M. Hearne, H. Flamme, M. Furtney, and G. M. Smoczyk (2018), Slab2, a comprehensive subduction zone geometry model, *Science*, *61*(October), 58–61.

Helffrich, G., and G. A. Abers (1997), Slab low-velocity layer in the eastern Aleutian subduction zone, *Geophysical Journal International*, *130*(3), 640–648, doi:10.1111/j.1365-246X.1997.tb01858.x.

Helffrich, G. R. (1996), Subducted Lithospheric Slab Velocity Structure: Observations and Mineralogical Inferences, *Subduction: Top to Bottom*, *96*, 215–222.

Hiramatsu, Y., H. Yamanaka, K. Tadokoro, K. Nishigami, and S. Ohmi (2002), Scaling law between corner frequency and seismic moment of microearthquakes: Is the breakdown of the cube law a nature of earthquakes?, *Geophysical Research Letters*, *29*(8), 8–11, doi:10.1029/2001GL013894.

Hirose, F., J. Nakajima, and A. Hasegawa (2008), Three-dimensional seismic velocity structure and configuration of the Philippine Sea slab in southwestern Japan estimated by double-difference tomography, *Journal of Geophysical Research: Solid Earth*, *113*(9), doi:10.1029/2007JB005274.

Holland, T. J. B., and R. Powell (1998), An internally consistent thermodynamic data set for phases of petrological interest, *Journal of Metamorphic Geology*, *16*, 309–343, doi:10.1111/j.1525-1314.1998.00140.x.

Horleston, A. C., and G. R. Helffrich (2012), Constraining sediment subduction: A converted phase study of the Aleutians and Marianas, *Earth and Planetary Science Letters*, *359-360*, 141–151, doi:10.1016/j.epsl.2012.10.019.

Hyndman, R. D., P. A. McCrory, A. Wech, H. Kao, and J. Ague (2015), Cascadia subducting plate fluids channelled to fore-arc mantle corner: ETS and silica deposition, *Journal of Geophysical Research: Solid Earth*, *120*, 4344–4358, doi:10.1002/2015JB011920.

International Seismological Centre (2017a), On-line Bulletin, Internatl. Seismol. Cent., Thatcham, United Kingdom, doi:http://doi.org/10.31905/D808B830.

International Seismological Centre (2017b), EHB Bulletin, Internatl. Seismol. Cent., Thatcham, United Kingdom, doi:http://doi.org/10.31905/D808B830.

Jackson, J., and D. McKenzie (1988), The relationship between plate motions and seismic moment tensors, and the rates of active deformation in the Mediterranean and Middle East, *Geophysical Journal*

International, *93*(1), 45–73, doi:10.1111/j.1365-246X.1988.tb01387.x.

Jamtveit, B., Y. Ben-Zion, F. Renard, and H. Austrheim (2018), Earthquake-induced transformation of the lower crust, *Nature*, *556*(7702), 487–491, doi:10.1038/s41586-018-0045-y.

John, T., S. Medvedev, L. H. Rüpke, T. B. Andersen, Y. Y. Podladchikov, and H. Austrheim (2009), Generation of intermediate-depth earthquakes by self-localizing thermal runaway, *Nature Geoscience*, *2*, 137–140, doi:10.1038/ngeo419.

Jung, H., H. W. Green II, and L. F. Dobrzhinetskaya (2004), Intermediate-depth earthquake faulting by dehydration embrittlement with negative volume change., *Nature*, *428*, 545–549, doi:10.1038/nature02412.

Karakonstantis, A., and P. Papadimitriou (2010), Earthquake Relocation in Greece Using a Unified and Homogenized Seismological Catalogue, *Bulletin of the Geological Society of Greece*, *43*(4), 2043–2052.

Karastathis, V. K., E. Mouzakiotis, A. Ganas, and G. A. Papadopoulos (2015), High-precision relocation of seismic sequences above a dipping Moho: the case of the January–February 2014 seismic sequence on Cephalonia island (Greece), *Solid Earth*, *6*, 173–184, doi:10.5194/se-6-173-2015.

Kaus, B. J. P., and Y. Y. Podladchikov (2006), Initiation of localized shear zones in vizcoelastoplastic rocks, *Journal of Geophysical Research: Solid Earth*, *111*(B04), doi:10.1029/2005JB003652.

Kawakatsu, H., and T. Seno (1983), Triple seismic zone and the regional variation of seismicity along the northern Honshu arc (Japan)., *Journal of Geophysical Research*, *88*(B5), 4215–4230, doi:10.1029/JB088iB05p04215.

Kawakatsu, H., and S. Watada (2007), Seismic Evidence for Deep-Water Transportation in the Mantle, *Science*, *316*, 1468–1471, doi:10.1126/science.1140855.

Kawakatsu, H., P. Kumar, Y. Takei, M. Shinohara, T. Kanazawa, E. Araki, and K. Suyehiro (2009), Seismic evidence for sharp lithosphere-asthenosphere boundaries of oceanic plates., *Science*, *324*(5926), 499–502, doi:10.1126/science.1169499.

Kelemen, P. B., and G. Hirth (2007), A periodic shear-heating mechanism for intermediate-depth earthquakes in the mantle, *Nature*, *446*(7137), 787–790, doi:10.1038/nature05717.

Kennett, B. L. N., E. R. Engdahl, and R. Buland (1995), Constraints on seismic velocities in the Earth from traveltimes, *Geophys. J. Int*, *122*, 108–124, doi:10.1111/j.1365-246X.1995.tb03540.x.

Kim, D., K. M. Keranen, G. A. Abers, and L. D. Brown (2018), Enhanced resolution of the subducting plate interface in Central Alaska from autocorrelation of local earthquake coda, *Journal of Geophysical Research: Solid Earth*, doi:10.1029/2018JB016167.

Kim, D., K. M. Keranen, G. A. Abers, and L. D. Brown (2019), Enhanced Resolution of the Subducting Plate Interface in Central Alaska From Autocorrelation of Local Earthquake Coda, *Journal of Geophysical Research: Soild Earth*, *124*, doi:10.1029/2018JB016167.

Kim, Y., M. S. Miller, F. D. Pearce, and R. W. Clayton (2012), Seismic imaging of the Cocos plate subduction zone system in central Mexico, *Geochemistry, Geophysics, Geosystems*, *13*(7), doi:10.1029/2012GC004033.

Kim, Y., G. A. Abers, J. Li, D. Christensen, J. Calkins, and S. Rondenay (2014), Alaska Megathrust 2: Imaging the megathrust zone and Yakutat/Pacific plate interface in the Alaska subduction zone, *Journal of Geophysical research : Soild Earth*, *119*, 1924–1941, doi:10.1002/jgrb.50358.Alaska.

Kirby, S. H., E. Engdahl, and R. Denlinger (1996), Intermediate depth intraslab earthquakes and arc volcanism as physical expressions of crustal and uppermost mantle metamorphism in subducting slabs, in *Subduction from top to bottom*, edited by G. Bebout, D. Scholl, S. Kirby, and J. Platt, pp. 195–214, AGU Geophys. Mono. No. 96.

Kissling, E., W. L. Ellsworth, D. Eberhart-Phillips, and U. Kradolfer (1994), Initial reference models in local earthquake tomography, *Journal of Geophysical Research*, *99*(B10), 19,635–19,646.

Kita, S., and T. P. Ferrand (2018), Physical mechanisms of oceanic mantle earthquakes: Comparison of

natural and experimental events, *Scientific Reports*, *8*, doi:10.1038/s41598-018-35290-x.

Kita, S., T. Okada, J. Nakajima, T. Matsuzawa, and A. Hasegawa (2006), Existence of a seismic belt in the upper plane of the double seismic zone extending in the along-arc direction at depths of 70 – 100 km beneath NE Japan, *Geophysical Research Letters*, *33*, doi:10.1029/2006GL028239.

Kita, S., T. Okada, A. Hasegawa, J. Nakajima, and T. Matsuzawa (2010), Anomalous deepening of a seismic belt in the upper-plane of the double seismic zone in the Paci fi c slab beneath the Hokkaido corner : Possible evidence for thermal shielding caused by subducted forearc crust materials, *Earth and Planetary Science Letters*, *290*, 415–426, doi:10.1016/j.epsl.2009.12.038.

Klein, F. W. (2002), User's Guide to HYPOINVERSE-2000, a Fortran Program to Solve for Earthquake Locations and Magnitudes, *Tech. rep.*, U.S. Geol. Surv., doi:http://geopubs.wr.usgs.gov/open-file/of02-171/.

Klemd, R., T. John, E. E. Scherer, S. Rondenay, and J. Gao (2011), Changes in dip of subducted slabs at depth: Petrological and geochronological evidence from HP-UHP rocks (Tianshan, NW-China), *Earth and Planetary Science Letters*, *310*(1-2), 9–20, doi:10.1016/j.epsl.2011.07.022.

Kokinou, E., E. Kamberis, A. Vafidis, D. Monopolis, G. Ananiadis, and A. Zelilidis (2005), Deep seismic reflection data from offshore Western Greece: A new crustal model for the Ionian Sea, *Journal of Petroleum Geology*, *28*(2), 185–202, doi:10.1111/j.1747-5457.2005.tb00079.x.

Kokinou, E., E. Papadimitriou, V. Karakostas, E. Kamberis, and F. Vallianatos (2006), The Kefalonia Transform Zone (offshore Western Greece) with special emphasis to its prolongation towards the Ionian Abyssal Plain, *Marine Geophysical Researches*, *27*(4), 241–252, doi:10.1007/s11001-006-9005-2.

Komatitsch, D. (2005), The spectral-element method in seismology, *Geophysical Monograph Series*, *157*, 205–227, doi:10.1029/157GM13.

Komatitsch, D., and J. Tromp (2003), A perfectly matched layer absorbing boundary condition for the second-order seismic wave equation, *Geophysical Journal International*, *154*, 146–153, doi:10.1017/CBO9781107415324.004.

Konstantinou, K. I., N. S. Melis, and K. Boukouras (2010), Routine regional moment tensor inversion for earthquakes in the Greek region: The National Observatory of Athens (NOA) database (2001–2006), *Seismological Research Letters*, *81*(5), 750–760, doi:10.1785/gssrl.

Koulakov, I., M. K. Kaban, M. Tesauro, and S. Cloetingh (2009), P- and S-velocity anomalies in the upper mantle beneath Europe from tomographic inversion of ISC data, *Geophysical Journal International*, *179*(1), 345–366, doi:10.1111/j.1365-246X.2009.04279.x.

Kühn, A., J. Glodny, H. Austrheim, and A. Råheim (2000), The Caledonian tectono-metamorphic evolution of the Lindås Nappe: Constraints from U-Pb, Sm-Nd and Rb-Sr ages of granitoid dykes, *Norwegian Journal of Geology*, *82*, 45–57.

Kumar, P., and H. Kawakatsu (2011), Imaging the seismic lithosphere-asthenosphere boundary of the oceanic plate, *Geochemistry, Geophysics, Geosystems*, *12*(1), doi:10.1029/2010GC003358.

Kyriakopoulos, C., A. V. Newman, A. M. Thomas, M. Moore-Driskell, and G. T. Farmer (2015), A new seismically constrained subduction interface model for Central America, *Journal*, pp. 5535–5548, doi:10.1002/2014JB011859.

Laigle, M., A. Hirn, M. Sachpazi, and C. Clément (2002), Seismic coupling and structure of the Hellenic subduction zone in the Ionian Islands region, *Earth and Planetary Science Letters*, *200*(3-4), 243–253, doi:10.1016/S0012-821X(02)00654-4.

Laigle, M., A. Hirn, M. Sapin, A. Bécel, P. Charvis, E. Flueh, J. Diaz, J. F. Lebrun, A. Gesret, R. Raffaele, A. Galvé, M. Evain, M. Ruiz, H. Kopp, G. Bayrakci, W. Weinzierl, Y. Hello, J. C. Lépine, J. P. Viodé, M. Sachpazi, J. Gallart, E. Kissling, and R. Nicolich (2013), Seismic structure and activity of the north-central Lesser Antilles subduction zone from an integrated approach: Similarities with the Tohoku forearc, *Tectonophysics*, *603*, doi:10.1016/j.tecto.2013.05.043.

Lamara, S. (2015), 3D Waveform Tomography of the Hellenic Subduction Zone, Ph.D. thesis, Ruhr-

Universität Bochum.

Laske, G., A. Dziewonski, and G. Masters (2013), Reference Earth Model, https://igppweb.ucsd.edu/~gabi/rem.html.

Lay, T. (1994), The Fate of Descending Slabs, *Annual Review of Earth and Planetary Sciences*, *22*, 33–61, doi:10.1146/annurev.earth.22.1.33.

Lay, T., and T. C. Wallace (1995), *Modern Global Seismology*, Academic Press, San Diego, doi:10.1016/S0074-6142(05)80009-9.

Lay, T., H. Kanamori, C. J. Ammon, A. R. Hutko, K. Furlong, and L. Rivera (2009), The 2006-2007 Kuril Islands great earthquake sequence, *Journal of Geophysical Research: Solid Earth*, *114*(11), doi:10.1029/2008JB006280.

Li, J., G. A. Abers, Y. Kim, and D. Christensen (2013), Alaska megathrust 1: Seismicity 43 years after the great 1964 Alaska megathrust earthquake, *Journal of Geophysical Research: Solid Earth*, *118*(9), 4861–4871, doi:10.1002/jgrb.50358.

Li, X., G. Bock, A. Vafidis, R. Kind, H. P. Harjes, W. Hanka, K. Wylegalla, M. van der Meijde, and X. Yuan (2003), Receiver function study of the Hellenic subduction zone: Imaging crustal thickness variations and the oceanic Moho of the descending African lithosphere, *Geophysical Journal International*, *155*(2), 733–748, doi:10.1046/j.1365-246X.2003.02100.x.

Lienert, B. R., and J. Havskov (1995), A computer program for locating earthquakes both locally and globally, *Seismological Research Letters*, *66*(5), 26–36, doi:10.1785/gssrl.66.5.26.

Lomax, A., A. Michelini, and A. Curtis (2009), Earthquake Location, Direct, Global-Search Methods, doi:10.1007/978-0-387-30440-3.

Lücke, O. H., and I. G. Arroyo (2015), Density structure and geometry of the Costa Rican subduction zone from 3-D gravity modeling and local earthquake data, *Solid Earth*, *6*(4), 1169–1183, doi:10.5194/se-6-1169-2015.

MacKenzie, L. S., G. A. Abers, S. Rondenay, and K. M. Fischer (2010), Imaging a steeply dipping subducting slab in Southern Central America, *Earth and Planetary Science Letters*, *296*(3-4), 459–468, doi:10.1016/j.epsl.2010.05.033.

Makropoulos, K., G. Kaviris, and V. Kouskouna (2012), An updated and extended earthquake catalogue for Greece and adjacent areas since 1900, *Natural Hazards and Earth System Science*, *12*(5), 1425–1430, doi:10.5194/nhess-12-1425-2012.

Malagnini, L., K. Mayeda, S. Nielsen, S. H. Yoo, I. Munafo', C. Rawles, and E. Boschi (2013), Scaling Transition in Earthquake Sources: A Possible Link Between Seismic and Laboratory Measurements, *Pure and Applied Geophysics*, *171*(10), 2685–2707, doi:10.1007/s00024-013-0749-8.

Manning, C. E. (1994), The solubility of quartz in H2O in the lower crust and upper mantle, *Geochimica et Cosmochimica Acta*, *58*(22), 4831–4839.

Martin, S., and A. Rietbrock (2006), Guided waves at subduction zones: Dependencies on slab geometry, receiver locations and earthquake sources, *Geophysical Journal International*, *167*(2), 693–704, doi:10.1111/j.1365-246X.2006.02963.x.

Matsuzawa, T., T. Kono, A. Hasegawa, and A. Takagi (1990), Subducting plate boundary beneath the northeastern Japan arc estimated from SP converted waves, *Tectonophysics*, *181*(1-4), 123–133, doi:10.1016/0040-1951(90)90012-W.

McClusky, S., S. Balassanian, A. Barka, C. Demir, S. Ergintav, I. Georgiev, O. Gurkan, M. Hamburger, K. Hurst, H. Kahle, K. Kastens, G. Kekelidze, R. King, V. Kotzev, O. Lenk, S. Mahmoud, A. Mishin, M. Nadariya, A. Ouzounis, D. Paradissis, Y. Peter, M. Prilepin, R. Reilinger, I. Sanli, H. Seeger, A. Tealeb, M. N. Toksöz, and G. Veis (2000), Global Positioning System constraints on plate kinematics and dynamics in the eastern Mediterranean and Caucasus, *Journal of Geophysical Research*, *105*(B3), 5695, doi:10.1029/1999JB900351.

McCrory, P. A., J. L. Blair, F. Waldhauser, and D. H. Oppenheimer (2012), Juan de Fuca slab geometry

and its relation to Wadati-Benioff zone seismicity, *Journal of Geophysical Research: Solid Earth*, *117*(9), doi:10.1029/2012JB009407.

McGary, R. S., R. L. Evans, P. E. Wannamaker, J. Elsenbeck, and S. Rondenay (2014), Pathway from subducting slab to surface for melt and fluids beneath Mount Rainier., *Nature*, *511*, 338–40, doi:10.1038/nature13493.

McKenzie, D. (1972), Active tectonics of the Mediterranean region, *Geophys. J. R. Astron. Soc.*, *30*, 109–185.

Meighan, H. E., U. Ten Brink, and J. Pulliam (2013), Slab tears and intermediate-depth seismicity, *Geophysical Research Letters*, *40*(16), 4244–4248, doi:10.1002/grl.50830.

Melgar, D., A. Ganas, J. Geng, C. Liang, E. J. Fielding, and I. Kassaras (2017), Source characteristics of the 2015 Mw 6.5 Lefkada, Greece, strike-slip earthquake, *Journal of Geophysical Research: Solid Earth*, pp. 2260–2273, doi:10.1002/2016JB013452.

Mesimeri, M., and V. Karakostas (2018), Repeating earthquakes in western Corinth Gulf (Greece): implications for aseismic slip near locked faults, *Geophysical Journal International*, *215*(1), 659–676, doi:10.1093/gji/ggy301.

Mesimeri, M., V. Karakostas, E. Papadimitriou, G. Tsaklidis, and K. Jacobs (2018), Relocation of recent seismicity and seismotectonic properties in the Gulf of Corinth (Greece), *Geophysical Journal International*, *212*, 1123–1142, doi:10.1093/gji/ggx450.

Millet, F., T. Bodin, and S. Rondenay (2019), Multi-Mode 3D Kirchhoff Migration of Receiver Functions at Continental Scale, *Journal of Geophysical Research: Solid Earth*, *submitted*.

Montabetti, J. F., and E. R. Kanasewich (1970), Enhancement of teleseismic body wave phases with a polarisation analysis, *Geophys. J. R. Astron. Soc.*, *21*(July), 119–129.

Monteiller, V., S. Chevrot, D. Komatitsch, and Y. Wang (2015), Three-dimensional full waveform inversion of short-period teleseismic wavefields based upon the SEM-DSM hybrid method, *Geophysical Journal International*, *202*(2), 811–827, doi:10.1093/gji/ggv189.

Morishige, M., and P. E. van Keken (2018), Fluid migration in a subducting viscoelastic slab, *Geochemistry, Geophysics, Geosystems*, *19*, doi:10.1002/2017GC007236.

Nadeau, R. M., and L. R. Johnson (1998), Seismological studies at Parkfield VI: moment release rates and estimates of source parameters for small repeating earthquakes, *Bulletin of the Seismological Society of America*, *88*(3), 790–814.

Nakajima, J., and N. Uchida (2018), Repeated drainage from megathrusts during episodic slow slip, *Nature Geoscience*, *11*, 351–356, doi:10.1038/s41561-018-0090-z.

Nakajima, J., T. Matsuzawa, and A. Hasegawa (2002), Moho depth variation in the central part of Northeastern Japan estimated from reflected and converted waves, *Physics of the Earth and Planetary Interiors*, *130*(1-2), 31–47, doi:10.1016/S0031-9201(01)00307-7.

Nakajima, J., Y. Tsuji, A. Hasegawa, S. Kita, T. Okada, and T. Matsuzawa (2009), Tomographic imaging of hydrated crust and mantle in the subducting Pacific slab beneath Hokkaido, Japan: Evidence for dehydration embrittlement as a cause of intraslab earthquakes, *Gondwana Research*, *16*(3-4), 470–481, doi:10.1016/j.gr.2008.12.010.

Nakajima, J., N. Uchida, T. Shiina, A. Hasegawa, B. R. Hacker, and S. H. Kirby (2013), Intermediate-depth earthquakes facilitated by eclogitization-related stresses, *Geology*, *41*(6), 659–662, doi:10.1130/G33796.1.

National Observatory of Athens; Institute of Geodynamics (1997), National Observatory of Athens Seismic Network, International Federation of Digital Seismograph Networks. Other/Seismic Network, doi:10.7914/SN/HL.

National Observatory of Athens; Institute of Geodynamics (2018), Database of revised events, http://bbnet.gein.noa.gr/HL/databases/database.

Nicholson, T., M. Bostock, and J. F. Cassidy (2005), New constraints on subduction zone structure in

northern Cascadia, *Geophysical Journal International*, *161*(3), 849–859, doi:10.1111/j.1365-246X.2005.02605.x.

Nixon, C. W., L. C. McNeill, J. M. Bull, R. E. Bell, R. L. Gawthorpe, T. J. Henstock, D. Christodoulou, M. Ford, B. Taylor, D. Sakellariou, G. Ferentinos, G. Papatheodorou, M. R. Leeder, R. E. Collier, A. M. Goodliffe, M. Sachpazi, and H. Kranis (2016), Rapid spatiotemporal variations in rift structure during development of the Corinth Rift, central Greece, *Tectonics*, doi:10.1002/2015TC004026.

Olive, J. A., F. Pearce, S. Rondenay, and M. D. Behn (2014), Pronounced zonation of seismic anisotropy in the Western Hellenic subduction zone and its geodynamic significance, *Earth and Planetary Science Letters*, *391*, 100–109, doi:10.1016/j.epsl.2014.01.029.

Omlin, S., B. Malvoisin, and Y. Y. Podladchikov (2017), Pore fluid extraction by reactive solitary waves in 3-D, *Geophysical Research Letters*, *44*(18), 9267–9275, doi:10.1002/2017GL074293.

Osada, K., K. Yoshizawa, and K. Yomogida (2010), Upper boundary of the pacific plate subducting under Hokkaido, Japan, estimated from ScSp phase, *Physics of the Earth and Planetary Interiors*, *183*, 63–72, doi:10.1016/j.pepi.2010.06.006.

Ottemöller, L., P. Voss, and J. Havskov (2016), Seisan Earthquake Analysis Software Manual, *Tech. rep.*, Department of Earth Science, University of Bergen, Bergen.

Papadopoulos, G. A. (2003), Tsunami hazard in the Eastern Mediterranean: Strong earthquakes and tsunamis in the Corinth Gulf, Central Greece, *Natural Hazards*, *29*, 437–464.

Papadopoulos, G. A., V. Karastathis, C. Kontoes, M. Charalampakis, A. Fokaefs, and I. Papoutsis (2010), Crustal deformation associated with east Mediterranean strike-slip earthquakes: The 8 June 2008 Movri (NW Peloponnese), Greece, earthquake (Mw6.4), *Tectonophysics*, *492*(1-4), 201–212, doi:10.1016/j.tecto.2010.06.012.

Papanikolaou, D. J., and L. H. Royden (2007), Disruption of the Hellenic arc: Late Miocene extensional detachment faults and steep Pliocene-Quaternary normal faults - Or what happened at Corinth?, *Tectonics*, *26*(5), doi:10.1029/2006TC002007.

Papazachos, B. C., V. G. Karakostas, C. B. Papazachos, and E. M. Scordilis (2000), The geometry of the Wadati-Benioff zone and lithospheric kinematics in the Hellenic arc, *Tectonophysics*, *319*(4), 275–300, doi:10.1016/S0040-1951(99)00299-1.

Papazachos, C., and G. Nolet (1997), P and S deep velocity structure of the Hellenic area obtained by robust nonlinear inversion of travel times, *Journal of Geophysical Research*, *102*, 8349–8367, doi:10.1029/96JB03730.

Paul, A., H. Karabulut, and RESIF (2013), Seismic network XY:SIMBAAD temporary experiment - Backbone of broadband stations. RESIF - Réseau Sismologique et géodésique Français., doi:https://doi.org/10.15778/resif.xy2007.

Paulatto, M., M. Laigle, A. Galve, P. Charvis, M. Sapin, G. Bayrakci, M. Evain, and H. Kopp (2017), Dehydration of subducting slow-spread oceanic lithosphere in the Lesser Antilles, *Nature Communications*, doi:10.1038/ncomms15980.

Pe-Piper, G., and D. J. W. Piper (2007), Neogene backarc volcanism of the Aegean: New insights into the relationship between magmatism and tectonics, *Geological Society of America Special Papers*, *418*(02), 17–31, doi:10.1130/2007.2418(02).

Peacock, S. M. (1993), The importance of blueschist -> eclogite dehydration reactions in subducting oceanic crust, *Geological Society of America Bulletin*, *105*(5), 684–694, doi:10.1130/0016-7606(1993)105<0684:TIOBED>2.3.CO;2.

Pearce, F. D. (2015), Seismic imaging of the western Hellenic subduction zone: The relationship between slab composition, retreat rate, and overriding lithosphere genesis, Ph.D. thesis, Massachusetts Institute of Technology.

Pearce, F. D., S. Rondenay, M. Sachpazi, M. Charalampakis, and L. H. Royden (2012), Seismic investigation of the transition from continental to oceanic subduction along the western Hellenic subduction Zone, *Journal of Geophysical Research: Solid Earth*, *117*, doi:10.1029/2011JB009023.

Perrin, A., S. Goes, J. Prytulak, D. R. Davies, C. Wilson, and S. Kramer (2016), Reconciling mantle wedge thermal structure with arc lava thermobarometric determinations in oceanic subduction zones, *Geochemistry, Geophysics, Geosystems*, *17*, 4105–4127, doi:10.1002/2016GC006527.

Piromallo, C., and A. Morelli (2003), P wave tomography of the mantle under the Alpine-Mediterranean area, *Journal of Geophysical Research*, *108*(B2), doi:10.1029/2002JB001757.

Poli, S., and M. W. Schmidt (2002), Petrology of Subducted Slabs, *Annual Review of Earth and Planetary Sciences*, *30*, 207–235, doi:10.1146/annurev.earth.30.091201.140550.

Poliannikov, O. V., S. Rondenay, and L. Chen (2012), Interferometric imaging of the underside of a subducting crust, *Geophysical Journal International*, *189*(1), 681–690, doi:10.1111/j.1365-246X.2012.05389.x.

Prieto, G. A., P. M. Shearer, F. L. Vernon, and D. Kilb (2004), Earthquake source scaling and self-similarity estimation from stacking P and S spectra, *Journal of Geophysical Research B: Solid Earth*, *109*(8), 1–13, doi:10.1029/2004JB003084.

Prieto, G. A., G. C. Beroza, S. A. Barrett, G. A. López, and M. Florez (2012), Earthquake nests as natural laboratories for the study of intermediate-depth earthquake mechanics, *Tectonophysics*, *570-571*, 42–56, doi:10.1016/j.tecto.2012.07.019.

Prieto, G. a., M. Florez, S. a. Barrett, G. C. Beroza, P. Pedraza, J. F. Blanco, and E. Poveda (2013), Seismic evidence for thermal runaway during intermediate-depth earthquake rupture, *Geophysical Research Letters*, *40*, 6064–6068, doi:10.1002/2013GL058109.

Ramachandran, K., and R. D. Hyndman (2012), The fate of fluids released from subducting slab in northern Cascadia, *Solid Earth*, *3*(1), 121–129, doi:10.5194/se-3-121-2012.

Ranero, C. R., J. P. Morgan, K. McIntosh, and C. Reichert (2003), Bending-related faulting and mantle serpentinization at the Middle America trench., *Nature*, *425*(6956), 367–373, doi:10.1038/nature01961.

Rawlinson, N., and M. Sambridge (2004), Multiple reflection and transmission phases in complex layered media using a multistage fast marching method, *Geophysics*, *69*(5), 1338–1350, doi:10.1190/1.1801950.

Reading, A. M., D. Gubbins, and W. Mao (2001a), A multiphase seismic investigation of the shallow subduction zone, southern North Island, New Zealand, *Geophys. J. Int*, *147*, 215–226.

Reading, A. M., W. Mao, and D. Gubbins (2001b), Polarization filtering for automatic pickking of seismic data and improved converted phase detection, *Geophysical Journal International*, *147*, 227–234, doi:10.1046/j.1365-246X.2001.00501.x.

Regnier, M., J. Chiu, R. F. Smalley Jr., B. L. Isacks, and M. Araujo (1994), Crustal thickness variation in the Andean foreland, Argentina, from converted waves, *Bulletin of the Seismological Society of America*, *84*(4200106,), 1097–1111.

Reilinger, R., S. McClusky, P. Vernant, S. Lawrence, S. Ergintav, R. Cakmak, H. Ozener, F. Kadirov, I. Guliev, R. Stepanyan, M. Nadariya, G. Hahubia, S. Mahmoud, K. Sakr, A. ArRajehi, D. Paradissis, A. Al-Aydrus, M. Prilepin, T. Guseva, E. Evren, A. Dmitrotsa, S. V. Filikov, F. Gomez, R. Al-Ghazzi, and G. Karam (2006), GPS constraints on continental deformation in the Africa-Arabia-Eurasia continental collision zone and implications for the dynamics of plate interactions, *Journal of Geophysical Research: Solid Earth*, *111*(5), doi:10.1029/2005JB004051.

Reyes, C. G., and M. E. West (2011), The Waveform Suite: A Robust Platform for Manipulating Waveforms in MATLAB, *Seismological Research Letters*, *82*(1), 104–110, doi:10.1785/gssrl.

Reyners, M., D. Eberhart-Phillips, G. Stuart, and Y. Nishimura (2006), Imaging subduction from the trench to 300 km depth beneath the central North Island, New Zealand, with Vp and Vp/Vs, *Geophysical Journal International*, *165*(2), 565–583, doi:10.1111/j.1365-246X.2006.02897.x.

Rizzo, A. L., A. Caracausi, V. Chavagnac, P. Nomikou, P. N. Polymenakou, M. Mandalakis, G. Kotoulas, A. Magoulas, A. Castillo, and D. Lampridou (2016), Kolumbo submarine volcano (Greece): An active window into the Aegean subduction system, *Scientific Reports*, *6*(February), 28,013, doi:10.1038/

srep28013.

Rogers, G., and H. Dragert (2003), Episodic Tremor and Slip on the Cascadia Subduction Zone: The Chatter of Silent Slip, *Science*, *300*(5627), 1942–1943, doi:10.1126/science.1084783.

Rondenay, S. (2006), Multi-disciplinary Experiments for Dynamic Understanding of Subduction under the Aegean Sea, International Federation of Digital Seismograph Networks. Other/Seismic Network, doi:10.7914/SN/XS_2006.

Rondenay, S. (2009), Upper Mantle Imaging with Array Recordings of Converted and Scattered Teleseismic Waves, *Surveys in Geophysics*, *30*(4-5), 377–405, doi:10.1007/s10712-009-9071-5.

Rondenay, S., M. G. Bostock, and J. Shragge (2001), Multiparameter two-dimensional inversion of scattered teleseismic body waves 3. Application to the Cascadia 1993 data set, *Journal of Geophysical Research*, *106*(12), 30,795–30,807.

Rondenay, S., G. A. Abers, and P. E. van Keken (2008), Seismic imaging of subduction zone metamorphism, *Geology*, *36*(4), 275–278, doi:10.1130/G24112A.1.

Rondenay, S., L. G. J. Montési, and G. A. Abers (2010), New geophysical insight into the origin of the Denali volcanic gap, *Geophysical Journal International*, *182*(2), 613–630, doi:10.1111/j.1365-246X.2010.04659.x.

Rontogianni, S., N. S. Konstantinou, C. P. Melis, and Evangelidis (2011), Slab stress field in the Hellenic subduction zone as inferred from intermediate-depth earthquakes, *Earth, Planets and Space*, *63*(2), 139–144, doi:10.5047/eps.2010.11.011.

Royden, L. H., and D. J. Papanikolaou (2011), Slab segmentation and late Cenozoic disruption of the Hellenic arc, *Geochemistry, Geophysics, Geosystems*, *12*(3), doi:10.1029/2010GC003280.

Sachpazi, M., A. Hirn, C. Clément, F. Haslinger, M. Laigle, E. Kissling, P. Charvis, Y. Hello, J. C. Lépine, M. Sapin, and J. Ansorge (2000), Western Hellenic subduction and Cephalonia Transform: Local earthquakes and plate transport and strain, *Tectonophysics*, *319*(4), 301–319, doi:10.1016/S0040-1951(99)00300-5.

Sachpazi, M., A. Galvé, M. Laigle, A. Hirn, E. Sokos, A. Serpetsidaki, J. M. Marthelot, J. M. Pi Alperin, B. Zelt, and B. Taylor (2007), Moho topography under central Greece and its compensation by Pn time-terms for the accurate location of hypocenters: The example of the Gulf of Corinth 1995 Aigion earthquake, *Tectonophysics*, *440*(1-4), 53–65, doi:10.1016/j.tecto.2007.01.009.

Sachpazi, M., M. Laigle, M. Charalampakis, J. Diaz, E. Kissling, A. Gesret, A. Becel, E. Flueh, P. Miles, and A. Hirn (2016a), Segmented Hellenic slab rollback driving Aegean deformation and seismicity, *Geophysical Research Letters*, pp. 651–658, doi:10.1002/2015GL066818.

Sachpazi, M., M. Laigle, M. Charalampakis, D. Sakellariou, E. Flueh, E. Sokos, E. Daskalaki, A. Galvé, P. Petrou, and A. Hirn (2016b), Slab segmentation controls the interplate slip motion in the SW Hellenic subduction: New insight from the 2008 Mw 6.8 Methoni interplate earthquake, *Geophysical Research Letters*, *43*(18), 9619–9626, doi:10.1002/2016GL070447.

Samson, J. C., and J. Olson (1981), Data-adaptive polarization filters for multichannel geophysical data, *Geophysics*, *46*(10), 1423, doi:10.1190/1.1441149.

Savard, G., M. G. Bostock, and N. I. Christensen (2018), Seismicity, Metamorphism, and Fluid Evolution Across the Northern Cascadia Fore Arc, *Geochemistry, Geophysics, Geosystems*, *19*(6), 1881–1897, doi:10.1029/2017GC007417.

Schmidt, M. W., and S. Poli (1998), Experimentally based water budgets for dehydrating slabs and consequences for arc magma generation, *Earth and Planetary Science Letters*, *163*, 361–379, doi:10.1016/S0012-821X(98)00142-3.

Schoenberg, M., and J. Protazio (1992), "Zoeppritz" rationalized and generalized to anisotropy, *Journal of Seismic Exploration*, *1*, 125–144.

Schorlemmer, D., F. Euchner, P. Kästli, and J. Saul (2011), QuakeML: Status of the XML-based seismological data exchange format, *Annals of Geophysics*, *54*(1), 59–65, doi:10.4401/ag-4874.

Schwartz, S. Y., and J. M. Rokosky (2007), Slow Slip Events and Seismic Tremor at Circum-Pacific Subduction Zones, *Reviews of Geophysics*, *45*, doi:10.1029/2006RG000208.1.

Scordilis, E. M., D. Kementzetzidou, and B. C. Papazachos (2016), Local magnitude calibration of the Hellenic Unified Seismic Network, *Journal of Seismology*, *20*(1), 319–332, doi:10.1007/s10950-015-9529-5.

Serpetsidaki, A., P. Elias, M. Ilieva, P. Bernard, P. Briole, A. Deschamps, S. Lambotte, H. Lyon-Caen, E. Sokos, and G. A. Tselentis (2014), New constraints from seismology and geodesy on the Mw = 6.4 2008 Movri (Greece) earthquake: Evidence for a growing strike-slip fault system, *Geophysical Journal International*, *198*(3), 1373–1386, doi:10.1093/gji/ggu212.

Serpetsidaki, A., E. Sokos, and G.-A. Tselentis (2016), A ten year Moment Tensor database for Western Greece, *Physics and Chemistry of the Earth, Parts A/B/C*, doi:10.1016/j.pce.2016.04.007.

Shaw, B., and J. Jackson (2010), Earthquake mechanisms and active tectonics of the Hellenic subduction zone, *Geophysical Journal International*, *181*(2), 966–984, doi:10.1111/j.1365-246X.2010.04551.x.

Shiina, T., J. Nakajima, T. Matsuzawa, G. Toyokuni, and S. Kita (2017), Depth variations in seismic velocity in the subducting crust: Evidence for fluid-related embrittlement for intermediate-depth earthquakes, *Geophysical Research Letters*, pp. 810–817, doi:10.1002/2016GL071798.

Shillington, D. J., A. Bécel, M. R. Nedimović, H. Kuehn, S. C. Webb, G. A. Abers, K. M. Keranen, J. Li, M. Delescluse, and G. A. Mattei-Salicrup (2015), Link between plate fabric, hydration and subduction zone seismicity in Alaska, *Nature Geoscience*, *8*(December), 961 – 964, doi:10.1038/ngeo2586.

Shimamura, K., T. Matsuzawa, T. Okada, N. Uchida, T. Kono, and A. Hasegawa (2011), Similarities and differences in the rupture process of the M ˜ 4.8 repeating-earthquake sequence off Kamaishi, northeast Japan: Comparison between the 2001 and 2008 events, *Bulletin of the Seismological Society of America*, *101*(5), 2355–2368, doi:10.1785/0120100295.

Shragge, J., M. G. Bostock, and S. Rondenay (2001), Multiparameter two-dimensional inversion of scattered teleseismic body waves 2. Numerical examples, *Journal of Geophysical Research*, *106*(12), 30,783–30,793.

Shuey, R. T. (1985), A simplification of the Zoeppritz equations, *Geophysics*, *50*(4), 609–614, doi:10.1190/1.1441936.

Smith, W. H. F., and D. T. Sandwell (1997), Global sea floor topography from satellite altimetry and ship depth soundings, *Science*, *277*(5334), 1956–1962, doi:10.1126/science.277.5334.1956.

Snoke, J. A., I. S. Sacks, and H. Okada (1974), A model not requiring continuous lithosphere for anomalous high-frequency arrivals from deep-focus South American earthquakes, *Physics of the Earth and Planetary Interiors*, *9*(3), 199–206, doi:10.1016/0031-9201(74)90137-X.

Snoke, J. A., I. S. Sacks, and H. Okada (1977), Determintation of the subducting lithosphere boundary by use of converted phases, *Bulletin of the Seismological Society of America*, *67*(4), 1051–1060.

Snoke, J. A., J. W. Munsey, A. G. Teague, and G. A. Bollinger (1984), Program for focal mechanism determination by combined use of polarity and SV-P amplitude ratio data, *Earthquake Notes*, *55*(3), 15.

Sodoudi, F., A. Brüstle, T. Meier, R. Kind, W. Friederich, and E. working group (2015), Receiver function images of the Hellenic subduction zone and comparison to microseismicity, *Solid Earth*, *6*(1), 135–151, doi:10.5194/se-6-135-2015.

Song, T.-r. A., D. V. Helmberger, M. R. Brudzinski, R. W. Clayton, P. Davis, X. Pérez-campos, and S. K. Singh (2009), Subducting slab ultra-slow velocity layer coincident with silent earthquakes in southern Mexico, *Science*, *502*(April), 502–507, doi:10.1126/science.1167595.

Spakman, W., M. J. R. Wortel, and N. J. Vlaar (1988), The Hellenic Subduction Zone: A tomographic image and its geodynamic implications, *Geophysical Research Letters*, *15*(1), 60–63, doi:10.1029/GL015i001p00060.

Speranza, F., L. Minelli, A. Pignatelli, and M. Chiappini (2012), The Ionian Sea: The oldest in situ

ocean fragment of the world?, *Journal of Geophysical Research B: Solid Earth*, *117*(12), doi:10.1029/2012JB009475.

Stark, P. B., and C. Frohlich (1985), The depths of the deepest deep earthquakes, *Journal of Geophysical Research*, *90*(B2), 1859–1869.

Suckale, J., S. Rondenay, M. Sachpazi, M. Charalampakis, A. Hosa, and L. H. Royden (2009), High-resolution seismic imaging of the western Hellenic subduction zone using teleseismic scattered waves, *Geophysical Journal International*, *178*(2), 775–791, doi:10.1111/j.1365-246X.2009.04170.x.

Syracuse, E. M., G. A. Abers, K. Fischer, L. MacKenzie, C. Rychert, M. Protti, V. Gonzalez, and W. Strauch (2008), Seismic tomography and earthquake locations in the Nicaraguan and Costa Rican upper mantle, *Geochemistry, Geophysics, Geosystems*, *9*(7), doi:10.1029/2008GC001963.

Syracuse, E. M., P. E. van Keken, G. A. Abers, D. Suetsugu, C. Bina, T. Inoue, D. A. Wiens, and M. Jellinek (2010), The global range of subduction zone thermal models, *Physics of the Earth and Planetary Interiors*, *183*, 73–90, doi:10.1016/j.pepi.2010.02.004.

Tape, C., Q. Liu, A. Maggi, and J. Tromp (2009), Adjoint tomography of the southern california crust, *Science*, *325*(5943), 988–992, doi:10.1126/science.1175298.

The Ancorp Working Group, O. Oncken, E. Lüschen, J. Mechie, S. Sobolev, A. Schulze, C. Gaedicke, S. Grunewald, J. Bribach, G. Asch, P. Giese, P. Wigger, M. Schmitz, S. Lueth, E. Scheuber, C. Haberland, A. Rietbrock, H. Götze, H. Brasse, R. Patzwahl, G. Chong, H. Wilke, G. González, A. Jensen, M. Araneda, H. Vieytes, G. Behn, E. Martínez, R. Rössling, J. Amador, E. Ricaldi, H. Chumacero, and R. Luterstein (1999), Seismic reflection image revealing offset of Andean subduction-zone earthquake locations into oceanic mantle, *Nature*, *397*(January), 341–344, doi:10.1038/16909.

Theunissen, T., S. Chevrot, M. Sylvander, V. Monteiller, M. Calvet, A. Villasenor, S. Benahmed, H. Pauchet, and F. Grimaud (2018), Absolute earthquake locations using 3-D versus 1-D velocity models below a local seismic network: example from the Pyrenees, *Geophysical Journal International*, *212*, 1806–1828, doi:10.1093/gji/ggx472.

Thompson, G., and C. Reyes (2017), GISMO - a seismic data analysis toolbox for MATLAB.

Thurber, C. H. (1983), Earthquake locations and three-dimensional crustal structure in the Coyote Lake Area, central California, *Journal of Geophysical Research*, *88*(B10), 8226, doi:10.1029/JB088iB10p08226.

Thurber, C. H., and D. Eberhart-Phillips (1999), Local earthquake tomography with flexible gridding, *Computers and Geosciences*, *25*(7), 809–818, doi:10.1016/S0098-3004(99)00007-2.

Tichelaar, B. W., and L. J. Ruff (1989), How Good Are Our Best Models?, *EOS*, *70*(20), 593, 605–606.

Tong, P., C.-W. Chen, D. Komatitsch, P. Basini, and Q. Liu (2014), High-resolution seismic array imaging based on an SEM-FK hybrid method, *Geophysical Journal International*, *197*, 369–395, doi:10.1093/gji/ggt508.

Tzanis, A., A. Efstathiou, S. Chailas, and M. Stamatakis (2018), Evidence of recent plutonic magmatism beneath Northeast Peloponnesus (Greece) and its relationship to regional tectonics, *Geophysical Journal International*, *212*(3), 1600–1626, doi:10.1093/gji/ggx486.

Uchida, N., T. Matsuzawa, A. Hasegawa, and T. Igarashi (2005), Recurrence intervals of characteristic M4.8 \pm 0.1 earthquakes off-Kamaishi , NE Japan — Comparison with creep rate estimated from small repeating earthquake data, *Earth and Planetary Science Letters*, *233*, 155–165, doi:10.1016/j.epsl.2005.01.022.

Uchida, N., T. Matsuzawa, W. L. Ellsworth, K. Imanishi, T. Okada, and A. Hasegawa (2007), Source parameters of a M4.8 and its accompanying repeating earthquakes off Kamaishi, NE Japan: Implications for the hierarchical structure of asperities and earthquake cycle, *Geophysical Research Letters*, *34*, 3–7, doi:10.1029/2007GL031263.

Uchida, N., S. H. Kirby, T. Okada, R. Hino, and A. Hasegawa (2010), Supraslab earthquake clusters above the subduction plate boundary offshore Sanriku, northeastern Japan: Seismogenesis in a graveyard of detached seamounts?, *Journal of Geophysical Research: Solid Earth*, *115*(9), doi:

10.1029/2009JB006797.

Uchida, N., T. Matsuzawa, W. L. Ellsworth, K. Imanishi, K. Shimamura, and A. Hasegawa (2012), Source parameters of microearthquakes on an interplate asperity off Kamaishi, NE Japan over two earthquake cycles, *Geophysical Journal International*, *189*(2), 999–1014, doi:10.1111/j.1365-246X.2012.05377.x.

Uchida, N., T. Iinuma, R. M. Nadeau, R. Burgmann, and R. Hino (2016), Periodic slowslip triggers megathrust zone earthquakes in northeastern Japan, *Science*, *351*(6272), 488–492.

Um, J., and C. H. Thurber (1987), A fast algorithm for two-point ray tracing, *Bulletin of the Seismological Society of America*, *77*(June), 972–986.

Umino, N., A. Hasegawa, and T. Matsuzawa (1995), sP depth phase at small epicentral distances and estimated subducting plate boundary, *Geophysical Journal International*, *120*(2), 356–366, doi:10.1111/j.1365-246X.1995.tb01824.x.

University of Athens (2008), University of Athens, Seismological Laboratory, International Federation of Digital Seismograph Networks. Other/Seismic Network, doi:10.7914/SN/HA.

University of Patras; Geology Department; Seismological Laboratory (2000), PSLNET, permanent seismic network operated by the University of Patras, Greece, International Federation of Digital Seismograph Networks. Other/Seismic Network, doi:10.7914/SN/HP.

Unsworth, M., and S. Rondenay (2013), Mapping the Distribution of Fluids in the Crust and Lithospheric Mantle Utilizing Geophysical Methods, in *Metasomatism and the Chemical Transformation of Rock, Lecture Notes in Earth System Sciences*, edited by D. E. Harlov and H. Austrheim, pp. 535–598, Springer-Verlag Berlin Heidelberg, doi:10.1007/978-3-642-28394-9_13.

Van Keken, P. E., B. R. Hacker, E. M. Syracuse, and G. A. Abers (2011), Subduction factory: 4. Depth-dependent flux of H<inf>2</inf>O from subducting slabs worldwide, *Journal of Geophysical Research: Solid Earth*, *116*(1), doi:10.1029/2010JB007922.

van Keken, P. E., S. Kita, and J. Nakajima (2012), Thermal structure and intermediate-depth seismicity in the Tohoku-Hokkaido subduction zones, *Solid Earth*, *3*(2), 355–364, doi:10.5194/se-3-355-2012.

Vassilakis, E., L. H. Royden, and D. Papanikolaou (2011), Kinematic links between subduction along the Hellenic trench and extension in the Gulf of Corinth, Greece: A multidisciplinary analysis, *Earth and Planetary Science Letters*, *303*(1-2), 108–120, doi:10.1016/j.epsl.2010.12.054.

Vidale, J. E., D.A.Schmidt, S. Malone, A. J. Hotovec-Ellis, S. Moran, K. C. Creager, and H. Houston (2014), Deep long-period earthquakes west of the volcanic arc in Oregon: Evidence of serpentine dehydration in the fore-arc mantle wedge, *Geophysical Research Letters*, *41*, 370–376, doi:10.1002/2013GL059118.

von Huene, R., T. Reston, N. Kukowski, G. Dehghani, and W. Weinrebe (1997), A subducting seamount beneath the Mediterranean Ridge, *Tectonophysics*, *271*(3-4), 249–261, doi:10.1016/S0040-1951(96)00241-7.

Waldhauser, F. (2012), User Guide to HypoDD Version 2.1b, *Tech. rep.*, Lamont-Doherty Earth Observatory, Palisades, New York.

Waldhauser, F., and W. L. Ellsworth (2000), A double-difference earthquake location algorithm: Method and application to the northern Hayward fault, California, *Bulletin of the Seismological Society of America*, *6*, 1353–1368.

Wang, K. (2002), Unbending combined with dehydration embrittlement as a cause for double and triple seismic zones, *Geophysical Research Letters*, *29*(18), 36–1–36–4, doi:10.1029/2002GL015441.

Wang, K., and A. M. Tréhu (2016), Invited review paper: Some outstanding issues in the study of great megathrust earthquakes—The Cascadia example, *Journal of Geodynamics*, *98*, doi:10.1016/j.jog.2016.03.010.

Wang, X., D. Zhao, and J. Li (2016), The 2013 Wyoming upper mantle earthquakes: Tomography and tectonic implications, *Journal of Geophysical Research: Soild Earth*, *121*, 6797–6808, doi:10.1002/

2016JB013118.

Wannamaker, P. E., R. L. Evans, P. A. Bedrosian, M. J. Unsworth, V. Maris, and R. S. McGary (2014), Segmentation of plate coupling, fate of subduction fluids, and modes of arc magmatism in Cascadia, inferred from magnetotelluric resistivity, *Geochemistry, Geophysics, Geosystems*, *15*, 4692–4711, doi:10.1002/2015GC00591.

Wei, S. S., D. A. Wiens, P. E. van Keken, and C. Cai (2017), Slab temperature controls on the Tonga double seismic zone and slab mantle dehydration, *Science Advances*, *3*, doi:10.1126/sciadv.1601755.

Wells, R. E., R. J. Blakely, and C. S. Weaver (2002), Cascadia microplate models and within-slab earthquakes, in *The Cascadia Subduction Zone and Related Subduction Systems—Seismic Structure, Intraslab Earthquakes and Processes, and Earthquake Hazards*, edited by S. Kirby, K. Wang, and S. Dunlop, pp. 17–23, U.S. Geological Survey, Menlo Park, California.

Wessel, P., and W. H. F. Smith (1996), A global, self-consistent, hierarchical, high-resolution shoreline, *Journal of Geophysical Research*, *101*(B4), 8741–8743.

Wilson, C. R., M. Spiegelman, P. E. van Keken, and B. R. Hacker (2014), Fluid flow in subduction zones: The role of solid rheology and compaction pressure, *Earth and Planetary Science Letters*, *401*, 261–274, doi:10.1016/j.epsl.2014.05.052.

Wortel, M. J. R., and Spakman (2000), Subduction and Slab Detachment in the Mediterranean-Carpathian Region, *Science*, *290*(5498), 1910–1917, doi:10.1126/science.290.5498.1910.

Xu, W., C. Lithgow-Bertelloni, L. Stixrude, and J. Ritsema (2008), The effect of bulk composition and temperature on mantle seismic structure, *Earth and Planetary Science Letters*, *275*(1-2), 70–79, doi:10.1016/j.epsl.2008.08.012.

Yamasaki, T. (2003), Double seismic zone and dehydration embrittlement of the subducting slab, *Journal of Geophysical Research*, *108*(B4), 2212, doi:10.1029/2002JB001918.

Ye, L., T. Lay, Z. Zhan, H. Kanamori, and J.-l. Hao (2016), The isolated 680 km deep 30 May 2015 MW 7.9 Ogasawara (Bonin) Islands earthquake, *Earth and Planetary Science Letters*, *433*(June 1994), 169–179, doi:10.1016/j.epsl.2015.10.049.

Zelt, B. C., B. Taylor, M. Sachpazi, and A. Hirn (2005), Crustal velocity and Moho structure beneath the Gulf of Corinth, Greece, *Geophysical Journal International*, *162*(1), 257–268, doi:10.1111/j.1365-246X.2005.02640.x.

Zhang, H., and C. H. Thurber (2003), User's manual for tomoDD1.1 for determining event locations and velocity structure from local earthquakes and explosions, *Tech. rep.*, Department of Geology and Geophysics, University of Wisconsin-Madison, Madison.

Zhang, H., C. H. Thurber, D. Shelly, S. Ide, G. C. Beroza, and A. Hasegawa (2004), High-resolution subducting-slab structure beneath northern Honshu, Japan, revealed by double-difference tomography, *Geology*, *32*(4), 361–364, doi:10.1130/G20261.2.

Zhao, D., T. Matsuzawa, and A. Hasegawa (1997), Morphology of the subducting slab boundary in the northeastern Japan arc, *Physics of the Earth and Planetary Interiors*, *102*(96), 89–104, doi:10.1016/S0031-9201(96)03258-X.

Zhu, H., E. Bozdăg, D. Peter, and J. Tromp (2012), Structure of the European upper mantle revealed by adjoint tomography, *Nature Geoscience*, *5*, 493–498, doi:10.1093/gji/ggu492.

Zhu, H., E. Bozdăg, and J. Tromp (2015), Seismic structure of the European upper mantle based on adjoint tomography, *Geophysical Journal International*, *201*(1), 18–52, doi:10.1093/gji/ggu492.

Zoeppritz, K. (1919), VII b. Über Reflexion und Durchgang seismischer Wellen durch Unstetigkeitsflächen, *Nachrichten von der Gesellschaft der Wissenschaften zu Göttingen, mamthematisch-physikalische Klasse*, *1919*, 66–84.

Graphic design: Communication Division, UiB / Print: Skipnes Kommunikasjon AS

uib.no

ISBN: 9788230867921 (print)
9788230856796 (PDF)